AXIAL COMPRESSOR STALL

BY

IVOR JOHN DAY

CHRIST'S COLLEGE

CAMBRIDGE

DISSERTATION SUBMITTED TO THE UNIVERSITY OF CAMBRIDGE
FOR THE DEGREE OF DOCTOR OF PHILOSOPHY

JUNE 1976

PREFACE

The author wishes to express his sincerest appreciation for the assistance received, both academic and administrative, from Dr. N.A. Cumpsty who has so willingly supervised this work over the last two years. Further special thanks are extended to Professor J.H. Horlock, for his initial supervision of the project and his continuing interest and encouragement.

The experimental work would not have been possible without the generous loan of the four stage compressor rig by the Derby College of Arts and Technology. The co-operation of Mr. M.J.C.B. Sharvell in this respect, is greatly appreciated.

The help and advice received from Dr. E.M. Greitzer over the past twelve months is gratefully acknowledged, as is the interest in the work and the hospitality shown during my visit to ONERA by M. J. Fabri. Thanks are also extended to Mr. E. Deverson and the other members of the Whittle Laboratory staff, especially Mrs. B. Roe, Mr. K. Bryant, Mr. R. Lawrence and Mr. R. Parfey, whose help has been invaluable over the past three and a half years. I would also like to acknowledge the tireless assistance of my wife, who is as much part of the work as I am, and to thank Mrs. P. Lister for typing the thesis.

Grateful acknowledgements are made to the Ministry of Defence, Procurement Executive, for their financial support of the research project, and to the Charles Rylott Foster Scholarship of South Africa for the assistance given to the author. In the latter respect, special thanks are due to Major C. Cowley, trustee of the scholarship, for his understanding and encouragement.

Declaration

The contents of this thesis has not been submitted to any other university and, with the exception of Chapter 6, is the sole work of the author. Chapter 6 was derived from the first draft of a paper to be submitted for publication by Day, Greitzer and Cumpsty. Although the draft of the paper was not prepared by the author, the principal ideas expressed in it are those of the author alone and are documented in several unpublished reports written over the past two years.

I. J. Day.

30/6/76.

SUMMARY

This dissertation describes the experimental investigation of rotating stall in compressors of high hub-tip ratio. Measurements were obtained in builds of one to four stages, covering a wide range of design flow rates and also a change in design reaction. The purpose of the experimental work has been to gain a better understanding of the details of the flow in the stall cell, so as to make possible the prediction of the in-stall performance of axial flow compressors.

A new, on-line, phase-lock sampling technique has been developed, which, for the first time, allows the quasi-continuous recording of instantaneous velocity, pressure and flow direction measurements from within the stall cell. The technique provides results of superior quality to any hitherto available, and has been used to study the details of the flow under various test conditions. In particular, the axial and radial profiles of the stall cells in multi-stage compressors of different design flow rates were considered. The effects of changes in design reaction, blade row spacing and the influence of the number of stages in the compressor were also investigated. Finally, measurements were obtained to try to determine the differences between full-span and part-span stall.

From a study of the results obtained, a fundamentally new picture of the flow in the stall cell has been built up, which shows features that are at variance with conventional ideas about stall cell structure. It has been shown that within the compressor itself, the edges of the cell do not follow streamlines in the unstalled flow, as might be expected of a dead wake, but rather assume an attitude implying tangential flow across the cell. The presence of this tangential flow is easily detectable from the measurements obtained

within the cell, and is supported by the observation of extremely high whirl velocities just upstream of the rotor blades. Comparatively little flow is shown to pass axially through the stalled region, but, because of the opposing accelerating and decelerating influences of the rotor and stator blades, the axial movement of this small amount of fluid has been shown to lead to the dissipation of large amounts of mechanical energy. This results in the overheating of the compressor during stall.

Centrifugal effects in the swirling flow ahead of the rotor blades are shown to contribute to strong radial pressure gradients in the stall cell, and are thought to be responsible for the fact that the pressure rise across a stage in the stalled region occurs ahead of the rotor blades. This observation is included in an overall model of compressor performance which is then used to explain the observed relationships between the various time-averaged compressor characteristics. This performance model is also used to provide some explanation of the observation (first made by McKenzie) that the total-to-static pressure rise across a stalled compressor appears to be independent of the blading used, but increases by a fixed amount for each stage in the compressor.

Time-averaged measurements were obtained from all the compressor builds tested, and were used in conjunction with the overall flow model to formulate a new correlation for predicting the performance of a stalled compressor. The correlation makes use of the above idea that the pressure rise during stall is independent of the blading used, for both part-span and full-span stall, and relies on the concept of a critical level of cell blockage to distinguish between operation in either of these two modes. The work reveals the effect of the number of stages and the design flow coefficient on the behaviour of the compressor, and demonstrates the unexpected influence of system parameters (such as

throttle line slope) on the stalling performance. The correlation also makes it possible to predict the occurrence of either full-span or part-span stall at stall inception from a knowledge of the unstalled characteristic, and allows estimates to be made of the size of the stall/unstall hysteresis loop. Data obtained from the literature are successfully correlated by this approach, and a new basis is therefore established from which to view the stalling behaviour of all axial flow compressors.

CONTENTS

NOTATION

All symbols are defined locally in the text, but for ease of reference, the more important ones are listed here.

P	total or static pressure according to context (referenced to atmospheric pressure)
$\bar{P}$	time-averaged pressure of flow in stalled and unstalled parts of annulus
Ψ	pressure rise coefficient; denominator $\rho\bar{U}^2$ unless specifically stated to the contrary
Ψ_{T-S}	$(P_{\text{exit static}} - P_{\text{inlet total}})/\rho\bar{U}^2$
Ψ_{S-S}	$(P_{\text{exit static}} - P_{\text{inlet static}})/\rho\bar{U}^2$
ϕ	flow coefficient, $C_x/\bar{U}$
ϕ^*	design flow coefficient (after Howell)
ϕ_{us}	local flow coefficient in unstalled flow
ϕ_s	local flow coefficient in stall cell
$\bar{\phi}$	averaged flow coefficient of flow in stalled and unstalled parts of annulus
λ	portion of annulus occupied by stall cell, expressed as a fraction or a percentage
$1-\lambda$	portion of annulus unstalled
C	absolute velocity
C_x	axial component of velocity, positive from inlet to exit
C_θ	tangential component of velocity, positive in direction of rotation
A_x	annulus cross-sectional area
A_θ	cross-sectional flow area in meridional plane
$\bar{U}$	blade speed at mid-height
R	compressor radius
N	number of stages

CHAPTER 1

Introduction

Rotating stall was first observed in the 1940's, but only became of real interest to the engineering world during the early stages of the development of the jet engine. It was immediately recognized as the source of blade vibrations leading to spectacular failures and therefore became a problem in urgent need of a solution. The first academic work on rotating stall appeared in the early 1950's and continued energetically for almost a decade. However, by 1960 some of the problems of blade vibration had been overcome by mechanical means, and as no adequate description of the phenomenon had emerged from either theory or experiment, work in this field slowed down.

In the last five years interest in rotating stall has been revived. This has been partly due to improvements in analytic methods made possible by the advent of the electronic computer and partly due to new requirements from industry. In the latter respect, emphasis has shifted from blade vibration problems to a need for design information on the performance of compressors operating in stall. The present work began in response to this request, but it is hoped that the results obtained will be of wider interest, since entirely new light is shed on some aspects of the phenomenon.

A rotating stall cell can be described as a propagating disturbance which moves from blade to blade around the compressor annulus. Stall cells will form when the compressor is throttled beyond the stall limit and may appear in any number from 1 to perhaps 16 or more, depending on the compressor configuration. The phenomenon is not limited to compressors, but also occurs in stationary blade rows, both annular and linear. The classical explanation for the propagation

of the cells can be described as follows: the cell, being an area of retarded flow, will divert the oncoming fluid about itself in such a way that the angle of incidence on the blades to one side of the cell will be increased, while that on the other side will be decreased. The blades subject to the increased incidence will stall and those on the other side will unstall, thus the cell moves from blade to blade. In absolute terms, the direction of propagation in a compressor will be the same as that of the rotor, while the velocity will commonly be between one-tenth and two-thirds of the rotor speed.

In order to guard against blade vibrations caused by rotating stall, it is necessary to know the number of cells and the speed of rotation. The greater part of the early theoretical work was therefore concerned with the prediction of these quantities. In most cases the cell number and speed of rotation were regarded as being functions of the blading characteristics only. The results obtained were not conclusive and thus later theories have attempted to introduce interactive effects between various blade rows. All in all, however, it must be concluded that the theoretical predictions have been rather disappointing, especially in terms of useful results for single stage and multi-stage compressors. The work reported here suggests that the failure of these methods is partly due to unrealistic assumptions about the behaviour of the fluid in the stall cells.

There has also been a large amount of experimental research aimed at understanding rotating stall. The experimental techniques have been many and varied. High response instruments have been employed to record the velocities and pressures in the stall cell and to monitor the changes which take place when the blading configurations are altered. Smoke tests and Schlieren photography have also been used to study the details of the flow. The measurements have shown that the

explanation of stall propagation is not as simple as suggested by the classical idea of stalling and unstalling of blades due to changes in incidence angles. However, the complexity of the phenomenon has meant that the results from various sources have remained as isolated observations, they have not been drawn together to produce a unified picture of stall behaviour. The new phase-lock sampling technique described in this thesis has improved the understanding of rotating stall to the point where certain commonly observed phenomena can now be explained in terms of an overall model of the flow.

It was mentioned previously that part of the motivation behind the present work is due to the interest of gas turbine manufacturers in the stalled performance of an axial flow compressor. This interest has arisen from design proposals in which a short axial compressor is mounted ahead of a centrifugal impeller. In order to match the two components, it is desirable to be able to predict the performance of the axial unit over the entire operating range.

Another situation in which an understanding of stalled performance has recently become significant is in the analysis of the dynamic behaviour of the compression system as a whole. A successful method of predicting compression system surge cycles has recently been published by Greitzer (1 & 2), but the analysis depends on prior knowledge of the stalled pressure rise characteristic of the compressor. The new semi-empirical model presented in this thesis can be used to provide this information, and to satisfy the requirements of the engine manufacturers.

Experimental work on rotating stall suggests that the type of stall cell present in the compressor influences the stalled performance. In this respect stall cells can be divided into two types, full-span or part-span, according to the radial extent of the disturbance. It

has been observed that when a compressor is throttled beyond the stall limit, the first stall cells to form may be either full-span or part-span depending on the compressor configuration. In the case of the former type, the pressure rise frequently falls abruptly at stall, but if part-span cells are present the pressure is more likely to decrease progressively as the throttle is closed. If, in the case of part-span stall, the compressor flow rate is sufficiently reduced, this configuration will give way to full-span stall with an accompanying drop in pressure rise. Full-span stall is thus the end result of severe throttling. Some exceptions to this rule have been noted, but only in compressors of relatively low hub-tip ratio. These observations form the basis of the performance correlation described in Chapter 6.

The work presented in this thesis can be divided into two parts, one concerned with the details of the flow in the stall cell and the other with the time-averaged performance during stall. The study of the flow in the stall cell makes use of detailed measurements obtained from a new phase-lock sampling technique. The results are more comprehensive than any hitherto available and cover a wide range of compressor designs. From these, a model of the flow in the stall cell has been built up, which shows the cell to be a highly active region rather than a passive region of dead fluid as has often been assumed in the past. In spite of the improved measurements and cell model, there are still certain aspects of the flow which remain unexplained and it has therefore not been possible to predict the pressure rise of the compressor from first principles.

With regard to the time-averaged performance, an analysis of the pressure rise characteristics of the various compressor builds has led to the formulation of a new semi-empirical correlation from

which the overall performance can be calculated. In this work, use is made of the parallel compressor hypothesis and of the behavioural characteristic of full-span and part-span stall. The correlation is not only useful in its own right, but its formulation has provided a unifying basis from which to view all other stall performance results. It has been shown for the first time that the design flow rate, the number of stages and the slope of the throttle line, all influence the type of stall cell present and affect the size of the stall/unstall hysteresis loop. It has also been shown that the rules usually assumed to relate the static-to-static and total-to-static characteristics in unstalled flow cannot be applied during stalled operation, so that the way in which the compressor performance is measured in stall is of vital importance. These observations help to explain the diversity of some of the results obtained in the past.

A background to the present work is given in Chapter 2 in the form of a broadly based literature review. The experimental apparatus and instrumentation, including the phase-lock sampling technique, are described in Chapter 3. Both time-averaged and unsteady results are presented in Chapter 4, while the details of the flow in the stall cell are discussed in Chapter 5. In Chapter 6 the model for the stalled performance prediction is considered. The conclusions drawn from all of the work are summarised in Chapter 7.

CHAPTER 2

Review of Previous Work

The literature on rotating stall can be divided into theoretical and experimental categories. Certain aspects of the work in both these fields will be considered so as to provide a general background to the current project.

The majority of theoretical papers set out to provide information on stall inception and to predict the number and rotational speed of the stall cells. A much smaller portion of the literature is concerned with the performance of a compressor once rotating stall has been established. The latter work is of greatest importance here, however, some discussion of the inception and propagation theories will be included in the literature review because of the relevance of the present work to the flow models employed in these theories. Surge analysis and stage stacking procedures will also be discussed for similar reasons.

The experimental papers, on the other hand, are generally concerned with attempts of one form or another to determine the factors controlling rotating stall. The earlier papers concentrate on the behavioural details of the stall cells, while some of the later papers are concerned with compressor performance during stall and with the detailed measurement of the unsteady flow. The work reported in this thesis is concerned with both performance and unsteady measurements and so the later papers will be considered in greater detail.

2.1 Theoretical Literature

When rotating stall was first discovered in the early 1940's, it was immediately held to be the source of vibrations causing fatigue failure of compressor blades. It was therefore of great importance to the engine designers to be able to predict the rotational speed and the number of stall cells which may occur in a particular compressor. With this practical problem as the prime motivation, numerous rotating stall models were proposed during the 1950's, nearly all of which were based on small perturbation analyses. It soon became clear, however, that the accurate prediction of stall cell frequencies was a difficult problem and through lack of success, work in this direction slowed down. In recent years numerical techniques made possible by the advent of the digital computer have re-awoken interest in this field, especially in Japan where most of the latest work has been done.

The practical interest in propagation frequencies meant that little attention was given to the problem of predicting the performance of a compressor operating in stall. Even at the present time there are only a few theories concerned with this problem. It may be thought that this branch of the analysis would have followed directly from the rotating stall theories, as any accurate description of the flow field would provide information on the time-averaged pressure rise to be expected. However, since none of the rotating stall theories were found to be really successful, no attempts were made to pursue the analyses further. Another point to be noted here is that most of the rotating stall theories were limited to the simple case of an isolated blade row and, therefore, were not expected to be very useful for predicting the behaviour of multi-stage compressors. For these reasons, the performance theories which are available have developed independently of the rotating stall analyses (except in one case) and

are not based on a detailed description of the flow field. Instead, the use of the parallel compressor model has been invoked in order to simplify the analysis and to allow it to be applied to multi-stage compressors.

In the discussion of the theoretical work which follows, the rotating stall theories are considered first, after which the performance models will be reviewed. Part of the present experimental work is intended to provide a better understanding of the details of the stall cell, and therefore particular attention will be given to the physical assumptions made in the rotating stall theories. The performance theories, on the other hand, are of interest in themselves as they provide a background to the performance correlation proposed in this thesis.

2.1.1 Rotating Stall Theories

The objectives of rotating stall theories are usually three-fold: to provide some sort of stall inception criteria, to predict the number of stall cells and to estimate the speed of rotation. In some cases, only one or two of these objectives are attained depending on the way in which the mathematical model of the flow is set up. The greater number of these theories are limited to small perturbations and cannot be expected to provide useful information once the stall cell disturbance has increased to a finite size. In view of this restriction, a few models have been proposed in which finite disturbances are admissible. The stall theories are therefore divided into two groups depending on the restrictions placed on the size of the stall cells. The larger group will be considered first.

1) Small Perturbation Theories

Small perturbation analyses can usually be regarded as

consisting of three parts: an upstream potential flow field, a linearized downstream field in which all disturbances are small and the static pressure satisfies Laplace's equation, and a set of matching conditions relating these two flow fields through the performance characteristics of the blade row. Expressing the system in this way, the stall cell details can be found by perturbing the flow and observing the wave number and frequency at which the disturbance first tends to stabilise.

It should be noted that not all small perturbation analyses are able to determine the number of stall cells. This ability depends mainly on the way in which the cascade parameters are introduced into the analysis. It was suggested by Emmons, Kronauer and Rockett (3), that a full solution is only possible if the equations are set up in the absolute reference frame and if the cascade performance characteristics are nonlinear and include a boundary layer response time of some sort. These requirements will ensure that the boundary condition placed on the upstream flow field will contain terms of sufficient dimensional variety to permit the determination of both stall velocity and wave length.

Reviews of small perturbation theories have been given by Emmons, Kronauer and Rockett (3), Dunham (4), Takata and Nagano (5), Horlock (6) and in the NASA compressor manual, SP-36. For this reason detailed descriptions of the theories will not be given here, however, a survey will be undertaken of the various physical assumptions and cascade details used in the analyses. It will thus be possible to compare the physical concept of the stall cell embodied in the theories with the detailed flow measurements presented in Chapter 4. The physical assumptions can be listed as follows:

a) Constant exit plane static pressure. This assumption was made by

Emmons, Pearson and Grant (7), Stenning and Krieble (8), and Fabri and Siestrunck (9). It avoids the necessity for a linearized solution of the downstream flow field as used by the other small perturbation theories. It was pointed out by Dunham (4) that this assumption is not expected to be true for isolated blade rows and is certainly not true for single or multi-stage compressors.

b) Constant blade leaving angle. This was assumed by Emmons, Pearson and Grant (7), Stenning and Krieble (8), Marble (10), Dunham (4), and Fabri and Siestrunck (9). Emmons, Kronauer and Rockett (3) also made this assumption, saying that it is experimentally fairly good, but do not refer to any specific experiment. The present work, although not for an isolated blade row, suggests that this is not true even for small stall cells. The experimental work of Nagano, Takata and Machida (11) also shows that under unsteady conditions the outlet flow angle is a definite function of the inlet angle. Ludwig, Nenni and Arendt (12) in their analysis make use of a measured relationship between inlet and outlet angles.

c) Channel exit area as a function of inlet angle. This assumption was made in conjunction with that of constant exit plane pressure by Emmons, Pearson and Grant (3), and Stenning and Krieble (8). The cascade blades are represented as channels of finite length in which the exit flow area is taken to be a linear function of inlet angle. By expressing blockage in terms of an area ratio in this way, the pressure rise across the blade row can be related to the velocity perturbation in the upstream flow field.

This picture of the flow may be a good representation of blades on the verge of stalling, but the present experiments suggest that it is unrealistic for even the smallest of stall cells.

d) Stagnation pressure loss as a function of inlet angle. Here the stagnation pressure loss coefficient is defined as a linear, or

nonlinear , function of inlet angle. Stenning and Krieble (8), Emmons, Kronauer and Rockett (3) and Dunham (4) all assume a nonlinear continuous relationship between loss coefficient and inlet angle for all possible angles. Marble (10) and Fabri and Siestrunck (9), on the other hand, assume the relationship to be discontinuous at a critical stalling angle.

Recent experimental work by Nagano et al. (11) suggests the relationship to be nonlinear and continuous.

e) Boundary layer time delay. The two methods of relating pressure rise to inlet flow angle considered in c) and d) above were for steady state conditions. In unsteady flow, the blades cannot be expected to respond instantaneously to changes in inlet angle. To estimate the dynamic response from the steady performance, a boundary layer time delay is introduced. Most of the theories make use of a time delay except Marble (10) and Dunham (4). Ludwig et al. (12) include a time delay in their analysis, but then assume it to be negligible.

Nagano et al. (11) attempted to obtain an accurate measurement of the boundary layer response time. This work will be considered further in the section on experimental papers.

f) Constant mass flow rate. This is an assumption which is tacitly made in all small perturbation analyses and is tantamount to assuming a throttle of infinite impedance. If a more realistic throttle line were to be assumed, the boundary conditions at upstream infinity would have to be changed as the flow becomes unstable and the pressure rise falls.

It will be shown in Chapter 6 that in reality the throttle line plays a significant part in the stalled behaviour of the compressor.

The physical picture of the flow introduced into the small perturbation theories by the above assumptions cannot be checked by experimental results obtained from fully developed stall cells, as under these circumstances the disturbances are always large. Nevertheless, if useful propagation velocities are to be predicted by these methods, then the flow picture should at least be representative of the true situation in the actual compressor.

2) Nonlinear Finite Disturbance Theories

Only three rotating stall theories will be considered in this section; namely those of Takata and Nagano (5), Stenning and Krieble (8) and Fabri and Siestrunck (9). The approach adopted is different in each case and so the papers will be reviewed separately.

a) Takata and Nagano give a perturbation analysis in which the equations of motion are not linearized in the downstream field, and finite disturbances are admissible. The analysis is the most advanced to date and is used in a qualitative manner to try to determine the factors influencing the number of cells and speed of rotation.

The analysis considers an irrotational upstream flow field, and a downstream field in which the static pressure can be assumed constant, either at the blade row exit or at downstream infinity. The two flow fields are connected across an actuator plane by a continuity condition and the unsteady blade row characteristics. These characteristics are expressed in terms of a total pressure loss coefficient and an outlet flow angle, both of which are nonlinear functions of the inlet flow angle and include the boundary layer time delay measured by Nagano et al. (11). The solution is achieved numerically by means of a successive over-relaxation technique applied to finite difference versions of the equations in which both time and

space have been segmented in the downstream flow field.

The steps involved in obtaining a solution can be summarized in the following way: the inlet flow angle is fixed and an arbitrary disturbance fed into the equations. If the disturbance dies away after a set number of time steps, rotating stall will not take place. The inlet angle is then increased fractionally and the process repeated until a stable solution with a propagating disturbance is obtained. The speed of rotation can then be calculated from the distance moved in a given time. Further throttling of the flow can be represented by increasing the inlet flow angle and using the previous solution as an initial disturbance.

The analysis was used in a qualitative way to try to determine the factors influencing the number of cells and the speed of rotation. Two examples of isolated blade rows were considered, one for two-dimensional flow and the other for three-dimensional flow; the latter using three different sets of blade row characteristics to represent changing conditions over the blade height. In both cases it was found that the number of cells could not be uniquely determined. The same was true for two blade rows of infinitesimal spacing. The number of cells was however uniquely determined in the case of an inlet guide vane row followed by a rotor row. Here, the number of cells and the speed of rotation were shown to depend on the spacing between the two blade rows, and thus it was suggested that the inertial effect of the fluid between the blade rows plays an important part in selecting the number of cells.

The quantitative results obtained were reasonable, but, although the analysis represents a considerable advance on any of the small perturbation theories, unique solutions for the important cases of an isolated blade row and a rotor-stator combination are still

not possible.

b) Stenning and Krieble - Vortex Theory (8). After observing interferograms of the stalling process in a cascade of aerofoils, Stenning and Krieble proposed a vortex shedding model of rotating stall from which plausible propagation velocities can be obtained.

A picture of the stall cell wake is built up by assuming that each aerofoil entering the stall cell sheds a discrete potential vortex and, similarly, each aerofoil leaving the stalled area sheds another vortex, but of opposite sign. These vortices then move in such a way as to form two parallel sheets which translate tangentially at the speed of the cell. In the wake, the vortices are positioned so that the velocities they induce can be matched with the velocity of the unstalled flow surrounding the cell. If the induced velocity between the vortex sheets is held near zero, and if the strength of the shed vorticity is assumed equal to the bound vorticity of the unstalled blades, then the propagation velocity of the cell can be determined in terms of the velocity of the unstalled flow. This velocity can in turn be related to a loss free pressure rise coefficient to give the cell speed as a function of the cascade performance.

Although the analysis is not restricted to cells of small size, the authors suggest that if the distance between the two vortex sheets becomes too great, the requirement of zero axial flow in the cell will not be upheld. In this case, the cell will split as the aerofoils at the centre of the cell unstall. The number of cells will therefore increase as the mean compressor flow rate decreases, which, by experimental observation, is not usually the case. A further limitation of the model is that it is clearly restricted to isolated blade rows and cannot be used to explain stall in more complex configurations.

c) Fabri and Siestrunck (9). In this work the results of a small perturbation theory (mentioned previously) are generalised to apply to finite disturbances. An argument based on a critical angle of attack and the duality of conditions in the stalled and unstalled flow on the cell boundaries, is used to show that the propagation velocity for a finite disturbance will be the same as that for a small perturbation. The paper goes on to develop a one-dimensional model of stall in which the angle of attack of the unstalled flow remains at the critical value. The cell size is then directly related to the overall mass flow rate of the compressor. These ideas were extended by Fabri in a more recent paper which will be considered below.

2.1.2 Stalled Performance Models

In this section, the models and theories for predicting the performance of a compressor operating in stall will be considered. These models are of primary interest to the present work as they provide a background to the new performance correlation presented in Chapter 6.

The difficulties involved in obtaining an adequate description of the flow field in an isolated blade row have been demonstrated in the preceding section. When attempting to predict the performance of a multi-stage compressor therefore, a more general approach has been necessary in which the precise details of the flow in the blade row are not considered. Instead, use is made of the parallel compressor hypothesis in which the compressor is viewed as a unit, irrespective of the number of stages. The stalled and unstalled parts of the annulus are assumed to operate as separate compressors in parallel, discharging into the same exit ducting. The various conditions under

which this model of the flow is applied distinguishes one performance theory from another.

a) Smith and Fletcher (15). The earliest work on stalled performance was done by Smith and Fletcher in 1954. They observed the stalling behaviour of six compressors of different designs and types and then attempted to explain the shapes of the characteristics obtained. Because their measurements did not show any consistent change in cell size with change in overall flow rate, a model was proposed in which the flow rate through the cell was allowed to change, but the cell size was held equal to half the compressor annulus. Thus, as the throttle was closed the flow rate in the stalled and unstalled areas changed until, at shut-off, the reversed flow velocity was equal to that of the through-flow. The average pressure rise was allowed to increase during this process.

Models much like those of Gray and Dunham below were also proposed, but were not accepted because of the necessity of the idea of a change in cell size with a change in overall flow rate. Subsequent measurements have, however, shown this idea to be valid.

b) McKenzie (16). Of the three fairly similar models proposed by Dunham, Gray and McKenzie, the McKenzie model is the simplest and most practical and will therefore be considered first.

In accordance with the parallel compressor hypothesis, the stalled and unstalled areas of the annulus are considered to operate separately, like two compressors in parallel. The assumption is then made that there is zero flow through the stalled area, while the unstalled flow operates as it would do under steady conditions, but at a flow rate such that the pressure rise will be equal to that generated in the stall cell. Constant exit plane static pressure is thus assumed. In terms of the compressor characteristic, the operating

which this model of the flow is applied distinguishes one performance theory from another.

a) Smith and Fletcher (15). The earliest work on stalled performance was done by Smith and Fletcher in 1954. They observed the stalling behaviour of six compressors of different designs and types and then attempted to explain the shapes of the characteristics obtained. Because their measurements did not show any consistent change in cell size with change in overall flow rate, a model was proposed in which the flow rate through the cell was allowed to change, but the cell size was held equal to half the compressor annulus. Thus, as the throttle was closed the flow rate in the stalled and unstalled areas changed until, at shut-off, the reversed flow velocity was equal to that of the through-flow. The average pressure rise was allowed to increase during this process.

Models much like those of Gray and Dunham below were also proposed, but were not accepted because of the necessity of the idea of a change in cell size with a change in overall flow rate. Subsequent measurements have, however, shown this idea to be valid.

b) McKenzie (16). Of the three fairly similar models proposed by Dunham, Gray and McKenzie, the McKenzie model is the simplest and most practical and will therefore be considered first.

In accordance with the parallel compressor hypothesis, the stalled and unstalled areas of the annulus are considered to operate separately, like two compressors in parallel. The assumption is then made that there is zero flow through the stalled area, while the unstalled flow operates as it would do under steady conditions, but at a flow rate such that the pressure rise will be equal to that generated in the stall cell. Constant exit plane static pressure is thus assumed. In terms of the compressor characteristic, the operating

points of the two flow regions can be illustrated as follows:

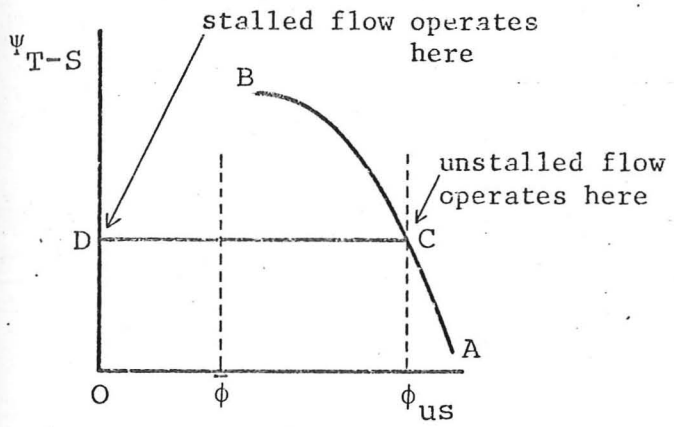

AB - unstalled characteristic
CD - rotating stall chic.
$\bar{\phi}$ - mean flow coefficient
ϕ_{us} - unstalled flow coef.

The assumption of constant exit plane static pressure implies that on a total-to-static plot as shown, the stalled branch of the characteristic will simply be a horizontal line. Thus, if the compressor flow rate is reduced the pressure rise will remain the same, but the stalled and unstalled areas will change in size. The fraction of the annulus occupied by the stall cell can be related to the mean flow rate, $\bar{\phi}$, by the expression:

$$\text{fraction stalled} = \lambda = \frac{\phi_{us} - \bar{\phi}}{\phi_{us}}$$

where ϕ_{us} is the flow coefficient of the unstalled flow. The idea of determining the size of the stall cell in this way is extremely useful and will be used extensively in Chapter 6.

In this model the vertical position of the stalled branch of the characteristic is fixed empirically. It was noted by McKenzie that the shut-off pressure rise of most compressors is independent of the compressor design, and usually falls between the limits of $\Psi_{T-S} = .1$ and $\Psi_{T-S} = .15$, per stage. The stalled branch of the characteristic is therefore just a horizontal line with a zero-flow intercept somewhere between these two limits.

Having outlined this model of the flow, McKenzie suggests that it can be used to explain the phenomenon of abrupt or progressive

stall. If, in a high hub-tip ratio compressor, the peak unstalled pressure rise is above the shut-off pressure rise the pressure will fall abruptly at stall. On the other hand, if the maximum unstalled pressure rise is less than the shut-off value, as may happen in a lightly loaded machine, the pressure rise will continue to increase progressively as the flow rate is reduced to zero. A more detailed argument, based on local blade characteristics, is used for low hub-tip ratio compressors.

The model is simple and practical and gives realistic results in the majority of cases, however, it makes no distinction between full-span and part-span stall and says nothing about the size of the hysteresis loop.

c) Gray (17). The experimental work of Turner and Sparks (18) shows that a unique characteristic can be defined for a blade row forced to operate under conditions of negative flow. Gray proposed that such a characteristic should be incorporated into the McKenzie model to take account of reversed flow in the stall cell. A sketch illustrating this idea is shown below.

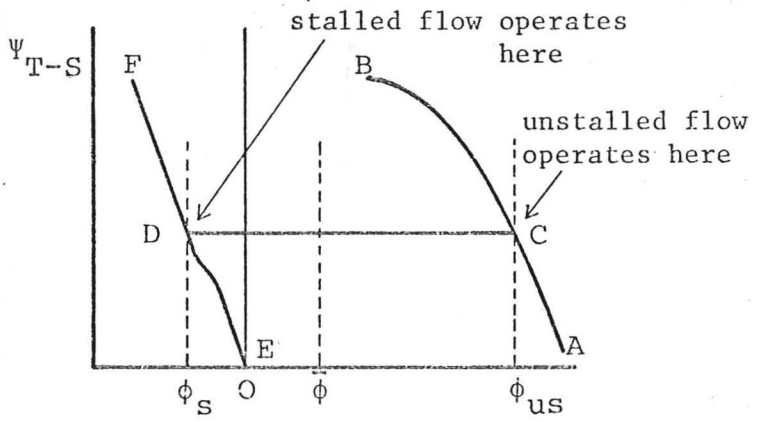

AB - unstalled characteristics
CD - rotating stall chic.
EF - reversed flow chic.
$\bar{\phi}$ - mean flow coefficient
ϕ_{us} - unstalled flow coef.
ϕ_s - reversed flow coef.

The negative flow characteristic represents, of course, a pressure loss between exit and inlet rather than a pressure rise between inlet and exit. In this model the fraction of the annulus occupied by the stall cell is given by:

$$\lambda = \frac{\phi_{us} - \bar{\phi}}{\phi_{us} - \phi_s}$$

This model would explain the experimental observation made by Iura and Rannie (19) that the annulus is not completely stalled at shut-off, i.e. at $\bar{\phi} = 0$.

d) Dunham (4 and 14). Dunham postulated the existence of a fully stalled characteristic to represent the performance of the blades operating under stalled conditions. This idea is supported by the work of Cornell (20) who analysed the performance of a cascade of flat plates with flow separation from one surface. The analysis suggested a characteristic of negative slope, as shown in the sketch below. In accordance with the parallel compressor hypothesis, the stalled flow in the annulus is expected to operate on this fully stalled characteristic, while the unstalled flow will operate on the steady-state branch.

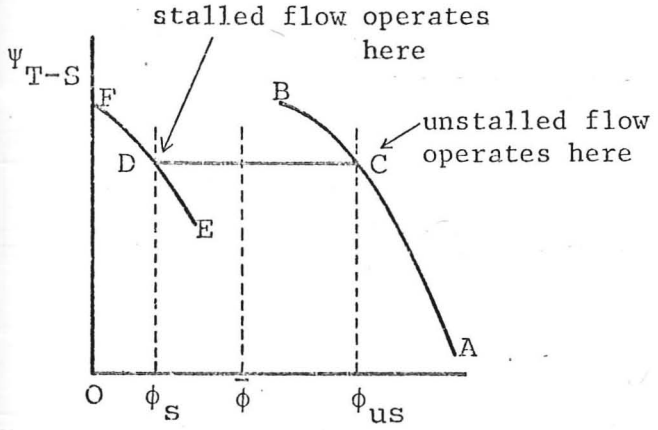

AB - unstalled characteristic
CD - rotating stall chic.
EF - fully stalled chic.
$\bar{\phi}$ - mean flow coefficient
ϕ_{us} - unstalled flow coef.
ϕ_s - stalled flow coef.

Dunham did not make the direct assumption of constant exit plane static pressure, but made use of a constant pressure rise throughout the rotating stall regime. In reference (4) Dunham shows that the exit plane static pressure will not be constant, but that the circumferential average of the pressure in the stalled and unstalled part of the annulus will be equal. The use of a horizontal line joining the two characteristics is therefore acceptable.

The throttle position in itself is not sufficient to fix the operating pressure level in a two-part flow system such as that shown here, and so some further condition is required. In the McKenzie model the condition was satisfied by empirical information, however, Dunham suggested that the level is dictated by a stability requirement. In reference (4), an analysis of cell stability was undertaken leading to the conclusion that the slopes of the stalled and unstalled characteristics should be equal at the operating level. The compressor characteristic is thus completely defined, but only if the shape of the fully stalled characteristic is known. No measurements of such a characteristic are available and these ideas remain unchecked.

An alternative stability criterion was proposed by Yerskov (21) based on a principle of maximum flow of energy, i.e. the integral of pressure rise times flow rate. The arguments in favour of this principle were not accepted by Dunham. Also, from reference (21) it would appear that the stability argument can only be applied if the stagnation pressure rise at zero flow is at least comparable with that of the unstalled flow. If this were not so, then rotating stall would only be possible at one isolated point on the entire characteristic.

In the Dunham model, the fraction of the annulus which is stalled is given by:

$$\lambda = \frac{\phi_{us} - \bar{\phi}}{\phi_{us} - \phi_s}$$

The annulus will thus be fully stalled before the shut-off condition is reached.

e) Fabri (22). The one-dimensional model used by Fabri is much like that of McKenzie. Zero flow is assumed in the stall cell and the static pressure is taken as constant in the exit plane. The

model is, however, significantly different from the preceding works in that the stall limit and the stall operating level are obtained from an analysis of the flow field downstream of an isolated rotor. In this sense the model is restricted to a single blade row.

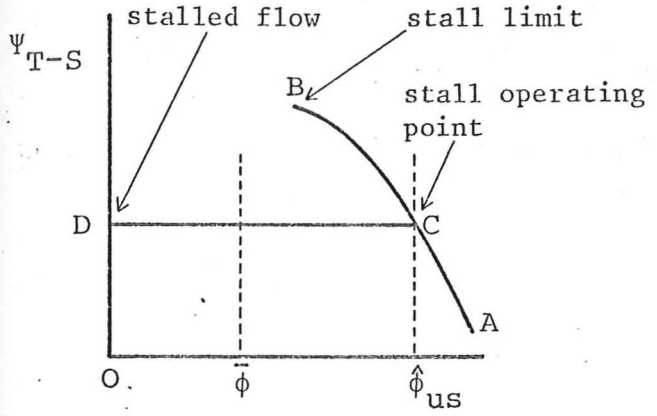

AB - unstalled characteristic
CD - rotating stall chic.
$\bar{\phi}$ - mean flow coefficient
$\hat{\phi}_{us}$ - unstalled flow coef., for solid body rotation downstream of rotor

The analytic determination of the stall operating level rests on the requirement that the radial pressure gradients in and out of the stalled flow downstream of the blade row should be equal. Since the stall cell wake is assumed to consist of dead fluid which rotates as a solid body to retain its identity, the unstalled flow surrounding the cell should also rotate as a solid body. Only in this way can the pressures in the stalled and unstalled flow be in equilibrium. The level of the pressure rise during stall is thus fixed by the flow coefficient, $\hat{\phi}_{us}$, at which the unstalled flow downstream of the rotor will rotate as a solid body.

To find the unstalled flow coefficient corresponding to solid body rotation, use is made of the expression for the cell speed derived in an earlier paper by Fabri and Siestrunck (9). The expression gives the stall frequency coefficient, c , at any radius, r , as a function of the local pressure rise coefficient:

$$c = \frac{V_{cell}}{U_r} = \frac{1 + \Psi_{T-S}}{2}$$

where Ψ_{T-S} is the total-to-static pressure rise divided by $\frac{1}{2}\rho U_r^2$, where U_r is the local blade speed. If the stalled

and unstalled flow downstream of the rotor is to rotate as a solid body, then the stall frequency coefficient must be the same at all radii, i.e. $dc/dr = 0$. This requirement fixes the radial variation in pressure rise coefficient across the blade row, and can be used in conjunction with a knowledge of the local blade row characteristics to determine the flow coefficient at which solid body rotation occurs. In the experimental case quoted by Fabri, the predicted stall performance level was in good agreement with the experimental results.

The possibility that the requirement of solid body rotation might not be met anywhere on the unstalled characteristic was investigated by Le Bot (23). He suggested that, in such a case, rotating stall would not be possible and so axisymmetric stall would be necessary. Experiments conducted in connection with the present work were not entirely in support of this idea. Wall stall may have been present, but was soon replaced by rotating stall on further throttling.

The arguments presented by Fabri are restricted to an isolated blade row and rely heavily on the accuracy of the cell speed equation. The model as a whole is also difficult to apply due to the necessity of a prior knowledge of the blade row characteristics, i.e. the local friction and off-design losses.

It can be seen that the performance models presented here are all very similar in essence, each one making use of the parallel compressor hypothesis, but under slightly different boundary conditions. The Gray, McKenzie and Dunham models respectively make provision for reversed flow, zero flow, and through flow in the stall cell. The experimental results of Chapter 4 show that these three assumptions are only idealised cases of a more complex situation in which reversed flow and through flow can exist simultaneously in

the stall cell. In Chapter 6, a new performance model is proposed which takes account of differences between full-span and part-span stall and is able to predict the size of the hysteresis loop.

2.1.3 Stage Stacking Procedures

Stage stacking procedures are not directly relevant to the present work, as they are intended to predict the performance of multi-stage compressors in which compressibility effects play an important part. These procedures are, however, of interest in terms of the assumptions they make about rotating stall performance.

Three papers were consulted: those of Huppert and Benser (24), Benser (25), and Doyle and Dixon (26). In each case, performance characteristics were assumed for various groups of stages and then used to compute a performance map for the compressor as a whole. Through the use of abrupt or progressive characteristics and the introduction of hysteresis loops, the computed maps were made to look like those obtained in practice. Stage interaction effects were also simulated in the model by linking certain groups of stages in such a way that the stalling of one of the stages would force the premature stalling of the remaining stages in the group. By simulating the compressor performance in this way, the effect of various stage characteristics on the compressor map could be determined and suggestions made for improvements in performance.

It should be noted that in all three papers considered, the performance of any stage in the compressor was assumed to be predetermined and invariable. It will be shown in Chapter 6 that this assumption is not true. The stalling performance of a compressor stage is not unique, but depends on the conditions under which it operates. The exit plane conditions of a stage may be modified by a

following unstalled stage, in which case a stage normally exhibiting abrupt stall may be forced to stall progressively and vice versa. This point was also made by Dunham in reference (14), but without experimental examples.

2.1.4 Compressor Surge

Although the problem of surge does not fall within the scope of this thesis, it is often allied with rotating stall in the literature. In broad terms, surge may be regarded as a compression system instability rather than an instability of the compressor itself. Linear analyses have been presented by Emmons, Pearson and Grant (7), Huppert and Renser (24) and others, but with regard to the quantitative prediction of the type of instability which will occur, either stall or surge, the nonlinear work of Greitzer is the most important.

Grietzer has presented two papers (1 and 2); the first setting out the stability analysis and the second providing the experimental support. In the analytic paper, the transient response of a compressor system subject to an initial disturbance was analysed using the non-linear equations of motion and the measured steady characteristic of the compressor. A time constant was introduced to relate the dynamic performance of the compressor to the steady state performance. The analysis shows that a critical value of a nondimensionalized parameter, B , can be defined above which the compressor will surge and below which rotating stall will be found. The parameter B is primarily a function of compressor speed, plenum volume, and ducting length. In the experimental paper it was verified that if these parameters are varied, but keeping B constant, the system performance will remain unchanged. The existence of a critical value of B, dividing stall and surge, was also proved.

2.2 Experimental Literature

Numerous experimental reports have been published over the last 30 years, but only those most pertinent to the present work will be considered here. In this respect, attention has been focussed on papers dealing with general behaviour of rotating stall cells, the performance of compressors operating in stall and the detailed measurement of the flow in a stalled blade row. The latter category is considered to be of greatest interest here. A more general view of the experimental work on rotating stall can be obtained from reviews such as those published by Emmons, Kronauer and Rockett (3), Rannie (27), Horlock (6) and from the NASA Compressor manual, SP-36. A comprehensive review of all rotating stall literature, both theoretical and experimental, has also been compiled by Yershov (21). This work was found very useful, however, it was not easy to follow as the available translation was unedited and the Russian technological symbols had been retained.

2.2.1 General Studies of Rotating Stall

Three early papers are grouped under this heading: those of Rockett (28), Valensi (29) and Iura and Rannie (19). All are concerned with the behavioural details of rotating stall cells.

Iura and Rannie worked mainly with a three stage free vortex compressor of 0.6 hub-tip ratio. Single stage builds of both free vortex and solid body blading were also studied. The three stage work is considered more important as this is one of the very few papers giving stall details in a multi-stage compressor. Hot wires were used to count the number of cells and to distinguish between part-span and full-span stall. The effect of these different stall types on the compressor performance was illustrated through the

pressure rise and torque characteristics. By careful measurement, it was also shown that the circumferential extent of the stall cell is an almost linear function of the flow rate.

Rockett considered the problem of modulation in stall cell speed. The work was conducted on a single stage rig of 0.57 hub-tip ratio in which the stator row was positioned 6 chord lengths downstream of the rotor. In this configuration, it was found that towards the extremities of the flow range covered by a particular cell configuration, the speed of rotation became unsteady. This unsteadiness was shown to be orderly and reliable data could therefore be extracted from the hot wire measurements over a wider range of flow rates. These results were then used to show that the cell speed can be a strong function of flow rate, and that the stall cell size increases steadily with a decrease in flow rate. As in the previous case, the indications are that the stall cell will not cover the entire annulus at shut-off because of the presence of reversed flow. The process of cell splitting was also studied.

Valensi observed the stalling process of a single stage compressor of 0.5 hub-tip ratio. Smoke tests were conducted in which a series of high speed photographs were obtained showing the separation of the flow from the rotor blades. In this connection, an important statement was made which can now be explained in the light of the present measurements; "as a matter of fact the air appears to be cycling in front of the rotor in the stalled region". This point will be considered further in Chapter 5. Total and static pressure measurements were also obtained using an early inductance-type transducer. Few of these results were actually presented.

2.2.2 Compressor Performance Papers

The papers included in this section cover a diversity of subjects and so will be considered separately.

a) Turner and Sparks (18). Turner and Sparks measured the performance of a single stage compressor of intermediate hub-tip ratio operating over a wide range of flow conditions. All possible flow rates were considered from high positive flow to strong flow in the negative direction, the latter being induced by an auxiliary fan. A similar variation of flow rate was also considered with the rotor operating in the reverse direction. The characteristics were presented in the conventional way, i.e. Ψ vs ϕ , and on the basis of a percentage of a chosen datum so that speed could be considered as a variable; possible Reynolds Number effects were ignored.

The negative flow characteristic demonstrates the existence of a unique relationship between pressure loss and negative flow rate. Such a characteristic was used by Gray in his performance model to express a fall in pressure from exit to inlet due to the negative flow in the stall cell. It should be noted, however, that Turner and Sparks made no attempt to monitor the details of the flow during stall, and so it is not known whether the negative flow characteristic represents steady flow operation or the average performance of a two-part flow system. Nevertheless, the measurements are useful as they are the only ones available showing the performance of a compressor under all possible flow conditions.

b) Borisov, Lokshtanov and Ol'shteyn (30). In this paper a stability argument is used to explain the discontinuity in the pressure rise characteristic of a compressor which stalls abruptly. Attempts are also made to relate the type of stall to the hub-tip ratio of the compressor.

An experiment on a high hub-tip ratio compressor is described in which the authors demonstrate a discontinuity in the characteristic and suggest that this is due to a static instability condition, i.e. the slope of the characteristic being steeper than the throttle curve. If the throttle curve is then made steeper by downstream suction, they show that the discontinuity in the characteristic can be eliminated. The break in the characteristic was thus attributed to static instability rather than the absolute impossibility of obtaining a stable cell structure in this region.

In the second part of the paper it is suggested that full-span stall gives rise to a steeper characteristic than does part-span stall and is therefore always associated with a discontinuous pressure rise. The authors then assume that, as abrupt and progressive characteristics are usually found in high and low hub-tip ratios respectively, the type of stall cell present in a particular case depends on the dimensions of the compressor annulus. A simple radial equilibrium analysis is then put forward attempting to show why part-span stall should always occur in low hub-tip ratio compressors and full-span stall in high hub-tip ratio builds.

The arguments used in the second part of this paper are tenuous and some of the physical assumptions made in the radial equilibrium analysis are very doubtful. Furthermore, part-span stall has been found in compressors of high hub-tip ratio; both by Tanaka and Murata (31) and by the present author. The experimental work reported in the first part of the paper is however useful, as it demonstrates quite clearly that the pressure rise characteristic of a particular blade row is not unique.

c) Nagano, Takata and Machida (11). Nagano et al. set out to investigate the dynamic performance of stalled blade rows using a

counter-rotating compressor in which the stall cell could be brought to rest. By measuring the distribution of velocity, pressure and flow direction upstream and downstream of the stalled blade rows, it was possible to estimate the unsteady response of the blades to changes in inlet conditions. The expression chosen to relate the steady and unsteady total pressure loss coefficient is

$$\tau_x \frac{\partial X}{\partial t} = X_{ss} - X$$

where X_{ss} and X are the steady and unsteady coefficients respectively, and τ_x is the boundary layer delay time constant. The inertia of the fluid in the blade channels was taken into account when X was estimated from the measurements, and so τ_x is only dependent on the boundary layer response time. (The boundary layer and inertial effects were actually found to be of the same order of magnitude.) The dynamic response of the outlet flow angle in terms of the inlet angle was also obtained from the measurements. These results were used by Takata and Nagano (5) in their nonlinear analysis of rotating stall.

When interpreting the measurements, the implicit assumption was made that the stalled flow passes through the blade channels with a certain constant axial component of velocity. The majority of detailed flow measurements obtained in the present work, and by other experimentors (13, 32 and 35), suggest that recirculation and tangential convection are likely to occur in a stall cell attached to a rotating blade row. The assumption of constant axial velocity between the two measuring positions upstream and downstream of the blade row, would therefore appear to be questionable.

d) Tanaka and Murata (31). This is a recently published paper concerned with the effects of hub-tip ratio and blade row spacing on the stalled performance of a single stage compressor. The stalled behaviour of three compressors of different hub-tip ratio were

observed as the stator row was moved up towards the rotor from far downstream. The results suggest that full-span and part-span stall cells are responsible for an abrupt and progressive characteristic respectively, and that part-span stall is more likely to form in compressors of low hub-tip ratio, or in compressors with large blade row spacing. Part-span stall was, however, observed in the high hub-tip ratio builds under certain conditions. The results also suggest that multi-cell configurations are usually made up of part-span cells, and that these cells always rotate at greater speed than do full-span cells in the same compressor.

This work shows that hub-tip ratio is an important parameter affecting the stalled performance of a compressor. It will be shown in Chapter 6 that another, and perhaps more important, parameter is that of design flow rate.

2.2.3 The Detailed Measurement of Stalled Flow

Some of the earliest detailed flow measurements were obtained by Costilow and Huppert in 1956 (33). Dunham (13), Bodeen (34) and Pavlenko (35) in England, America and Russia respectively, all worked in the early 1960's, but little has been published since then except for the very recent work of Tanaka and Murata in Japan (1975) (32). The experimental techniques used have improved with time and so the papers are best discussed in chronological order.

a) Costilow and Huppert investigated the stalled flow in an isolated rotor of 0.9 hub-tip ratio. Radially mounted hot wires, inductance-type pressure transducers, and high response thermocouples were all used to monitor the behaviour of the flow at a number of axial stations in the compressor. It was found that for small stall cells

the velocity fluctuations were large near the rotor, but were quick to attenuate at greater distances from the blade row. The larger stall cells, on the other hand, produced velocity fluctuations which persisted undiminished for a radius or more downstream. The static pressure measurements showed that the fluctuations upstream of the rotor were always greater than those downstream. (This observation can now be explained as a result of the present work.) It was also suggested that the unstalled flow operates at peak pressure rise on the unstalled characteristic.

No flow direction measurements were obtained and no attempt was made to interpret the results in terms of a flow model. However, some interesting temperature rise calculations were undertaken. The flow in the stall cell was assumed to rotate at blade speed and thus the temperature rise across the cell could be estimated. The result was in general agreement with the measured temperature rise. Good correlation between theory and experiment for unstalled flow was also obtained.

b) Bodeen (34) used a number of different compressor configurations to investigate the relationship between stall cell speed and the tangential velocity component of the unstalled flow. This part of the work did not seem to produce any overall conclusion, although detailed flow measurements, both in and out of the stall cells, were obtained in the process. Sophisticated, multi-wire anemometers were used to measure the velocity and flow direction at isolated points in the flow field for both full-span and part-span stall. Most measurements were obtained behind the rotor blades, but in the one case where measurements ahead of the rotor were reported, it can be seen that high tangential velocities were present in the stall cell. Behind the rotor the velocities were much lower. A flow model

as such was not contemplated, but it was observed that the classical idea of flow separation in the blade passages was not representative of the actual flow in the stall cell.

c) Dunham (13) made use of a single-hole, cylindrical pressure transducer to measure the details of the stalled flow in a single stage compressor of low hub-tip ratio. The pressure transducer was calibrated against yaw angle and so, by taking measurements at a number of probe settings, the velocity, total pressure, static pressure and flow angle could be estimated. As the calculations were done by hand from oscillograph measurements, only a limited number of results were obtained in the stalled and unstalled flow. The purpose of the work was to provide support for the parallel compressor hypothesis and the velocity measurements were therefore presented in terms of axial velocity coefficients. This method of presentation tends to obscure the fact that the flow in the stall cell ahead of the rotor has a very high tangential velocity.

The conclusions drawn from the results are summarized in the following sentences: "Air was centrifuged outwards in the stalled blade passages of the rotor and blown forward towards the I.G.V. trailing edges; the stagnation pressure of the centrifuged air was very high. Only a small flow emerged from the trailing edges of the rotor." It will be seen in Chapter 5 that this is a more than apt description of some of the results obtained in the present work, even though the hub-tip ratio of the compressor used is very different.

d) Yershov (21) reviewed some experimental work done by Pavlenko. Unfortunately the experimental technique was not mentioned and the source of the information is unavailable. From the results quoted, it is clear that in the stall cell an area of high velocity existed ahead of the rotor in which the flow moves in the tangential direction.

Behind the rotor the velocities were much lower, but in contrast to Dunham's results, reversed flow was still present downstream of the rotor. Once again these results compare favourably with specific examples from the present work.

e) Takata and Murata (32), in the most recent work in this field, used a three-hole cobra-type transducer to explore the stalled flow in an isolated rotor. The output from each probe channel was recorded and compared with calibration figures to determine the velocity, total pressure and flow direction at 10 or 12 discrete points in the stall cycle. For small stall cells this means that only 2 or 3 measurements were obtained in the stall cell itself. The flow field was examined at various measuring planes upstream and downstream of the rotor and the results presented in terms of axial and tangential velocity coefficients. The total pressure measurements were weighted by the local axial velocity coefficient. However, because the axial velocity component is almost zero in the stall cell, this means that the results obscure the fact that the total pressure is extremely high ahead of the rotor.

The measurements suggest a picture of the stalled flow which is much like that of the previous papers. Ahead of the rotor, the flow moved at high speed in the tangential direction with a small component of reversed flow. Behind the rotor, the flow was also in the reversed direction, but moving much more slowly. The reversed flow appears to be restricted to a small area near the rotor which led to the idea of recirculation in the stall cell. A picture of the flow field was given in which the stall cell is seen as a symmetrical disturbance consisting of two counter-rotating vortices, one on each side of the cell, which induce reversed flow between them. This vortex idea was suggested by the work of Krieble (36). Although the results

presented in this paper are in general agreement with the present work, the concept of symmetrical flow in the stall cell is not supported by the more detailed measurements shown in Chapter 4.

The experimental results of Dunham, Bodeen, Pavlenko, Takata and Murata and the present work, all show similar trends in the stall cell, even though the hub-tip ratios and blading configurations of the compressors used are widely different. In this thesis, the idea is put forward that a stall cell is not just a turbulent region of retarded flow, but rather a highly active disturbance with characteristic properties and a definite cell structure.

CHAPTER 3

Test Rig and Instrumentation Techniques

The experimental work can be divided into two separate categories. The first concerns the steady state measurements of compressor characteristics and torque measurements, while the second deals with the acquisition of instantaneous information about the flow in the stall cells. The equipment and techniques used in both of these areas are described in this chapter. The results are presented separately in Chapter 4.

The compressor is described first, after which the various measuring probes and supporting electronics are considered. The approach adopted towards the steady state measurements is then briefly discussed before considering the more complicated sampling techniques used for the unsteady work.

3.1 Test Compressor

As part of the initial thinking when setting up the project, it was decided that a high hub-tip ratio compressor should be used. It was hoped that this would simplify the problem by reducing radial variations in blade angles and stage performance. The 4-stage Rolls Royce compressor belonging to Derby College of Arts and Technology seemed admirably suitable, having a hub-tip ratio of 0.8 and with the added advantage of a wide range of blading. This compressor was subsequently loaned to Cambridge University for the duration of the current work.

A schematic diagram of the rig is shown in Figure 1. Air is drawn in through the bell-mouth inlet which surrounds the drive shaft, and is expelled at the rear through a diffuser and a conical throttle.

The blade tip diameter is 356 mm . A 4-stage build is illustrated here, but by removing the blade rows and replacing the gaps with blank rings, the compressor can be built up in almost any configuration, including that of an isolated rotor. The inlet guide vanes, which are externally variable, can be removed altogether, but cannot be replaced anywhere other than in the first position in the compressor. The outlet guide vanes are of fixed camber and stagger and can be positioned anywhere in the stack.

The compressor is driven via a gear-box by a 50 h.p. motor. A rotational speed of 3000 rpm was used throughout the tests, this speed giving a Reynolds Number of $.5 \times 10^{+5}$, based on a chord length of 17.8 mm . Whilst this value may be considered to be a bit low, tests with a turbulence grid demonstrated clearly that the performance was not being influenced by boundary layer effects. Furthermore, all flow angles measured in the compressor were found to be in good agreement with estimates based on Howells correlation (38), and so excessive deviations due to low Reynolds Number were not suspected.

Two sets of blading were used in the tests, one of 40° camber and the other of 20° . In all other respects the blades were identical: untwisted, of C5 aerofoil section, 10% thick, with circular camber line, 17.8 mm . in chord and 35.5 mm in span. These blades could be slotted into rotor discs and stator rings to form blade rows of various stagger angles. Settings of 20°, 35° and 50° stagger were used. A range of pitch-chord ratios was made possible by putting blades in every second or every third slot as required. In most cases 64 blades were used in each row, giving a pitch-chord ratio of 0.94 . The details of the compressor builds tested in the present work are considered in the following section.

In order that the blade rows in the compressor should be fully interchangeable, the width of each rotor disc and stator ring is the same, irrespective of the angle of the blade slots. This means that the distance between the centre lines of each blade row is fixed, but the size of the gap between the trailing edge of the one blade row and the leading edge of the next is affected by the stagger angle of the rings and discs being used. In the case of a 20^{o} stagger build (50% reaction), the axial gap is of the order of 1.0 chord lengths, but this increased to 1.5 for the highest stagger, i.e. when the blades are set at the greatest angle to the axis. These large gaps are necessary as this is an experimental compressor and space is required for instrumentation between the blade rows. An experiment is described in the next chapter where a special configuration with greatly reduced gaps was used to investigate the effects of inter-row spacing.

The various measuring positions used during the experiments are shown in Figure 1. These will be referred to by number when the results are considered. Traverse rings are fitted between the blade rows in planes 2 to 10, allowing probes mounted in the rings to be traversed circumferentially over an arc of 36^{o} .

Two static taps are fitted in each ring, 5^{o} apart, so as to record the wall static pressure in the compressor. No measuring facilities are available over the remainder of the circumference. In plane $\frac{1}{2}$, five static taps are spaced around the inlet and the average pressure from these is used in conjunction with a calibration curve to determine the compressor mass flow rate. During stall, conditions in the inlet were disturbed to such an extent that an orifice plate had to be mounted downstream of the throttle in order to obtain accurate results.

3.2 Details of Compressor Builds

The thirteen compressor configurations tested are listed in Table 1, page 174 When selecting these builds it was decided that the tests should cover as wide a range of design flow rates as possible. Three basic designs of low, intermediate and high flow rates were chosen, all of 50% reaction. As the work progressed, interest grew in the part played by design reaction and so a fourth configuration of 65% reaction was also tested. The flow rate in this case fell between the intermediate and high flow rate builds, thus providing further information for the study of the effect of design flow rate on the stalled performance. In the work described below, the 50% reaction builds are designated as Low ϕ^*, Intermediate ϕ^* and High ϕ^* builds. The 65% reaction configurations are referred to as the High Reaction builds.

3.3 Instrumentation

a) Hot Wires

Conventional, single wire, constant temperature probes were used for the greater part of the work. Temperature compensated probes were unfortunately unsuitable on account of their size, however, by operating with a high over-heat ratio, typically 1.8 to 2.0 , it was found that the results were not unduly affected by the temperature fluctuations in the flow. Measurements by other experimenters (33) show that local temperature rises occur in the stall cell, which means that velocities measured without temperature compensation are likely to be too low rather than too high. The hot wire output was filtered in all cases by a cut-off filter set at 300 times the stall cell frequency. This cut-off frequency was chosen because it gave the best results in the ensemble averaging process which will

be discussed later. The individual blade wakes were diminished by the filtering, but not entirely removed.

A conventional hot wire is directionally sensitive, but is unable to distinguish between flow directions 180^{o} apart. It is therefore at a disadvantage when reversed flow is present. Some specialised probes were developed to overcome this difficulty and examples of three of these are given in Figure 2a. These probes all work on the principle that the flow is obstructed when flowing in the reversed direction. The response of each of the probes was shown to be linear by testing in a calibration tunnel, however the two ramp probes were found to be adversely affected by any radial flow components. It should be stressed that these probes were not used for quantitative measurements, but simply for checking the flow direction in cases where doubt existed.

All of the measuring probes, including those in the following section, were mounted in a special traverse gear so that they could be traversed in both radial and circumferential directions. Once secured in the holder, the probe could be rotated about its axis in discrete increments of 10^{o} by means of a hand operated ratchet mechanism. If desired, this mechanism could be disconnected to make the angle setting infinitely variable.

b) Pressure Transducers

Two miniature pressure transducers were used, one for static pressure and the other for total pressure. Both were manufactured by Gaeltec Ltd., and had a resonant frequency of approximately 50 KHz . The transducers were used in the differential mode, i.e. referenced to atmosphere, in which condition the pressure range was limited to .15 atmospheres on each side of zero. The response was linear for both positive and negative pressures within this range, and it was

found that the difference between the two calibration constants was so small that a mean value could be assumed without introducing errors of more than $1\frac{1}{2}$ percent.

The static pressure probe consisted of a pressure sensitive diaphragm fitted across the end of a length of 3 mm hyperdermic tubing – Figure 2b. The probe was mounted in the compressor in such a way that the diaphragm was flush with the outer wall, thus allowing the static pressures to be measured directly. The transducer was statically calibrated before and after each test and the zero setting checked each time the probe was moved to a new position. Some zero shift difficulties were experienced due to temperature gradients, but by giving the rig time to warm up with the probe in position accurate measurements could be obtained.

The total pressure transducer was of the twin diaphragm type mounted in a 3 mm probe holder. A small hole in the wall of the tube served as a pressure port, as shown in Figure 2c. When properly aligned with the flow, the transducers could be used as a cylindrical total pressure probe. The two diaphragms were positioned on each side of the hole and, thus, longitudinal temperature gradients made it difficult to eliminate zero drift when the compressor was operating stalled. To overcome this a short extension was fitted so that the transducer could be mounted out of the flow field. The extension worked satisfactorily and it was shown quite clearly that, over the range of interest, the frequency response of the transducer was not affected in any way.

As before, the transducer output was filtered by a low-pass filter set at 300 times the cell frequency. This cut-off level gave the clearest overall picture of the flow field.

c) Piezo-electric Probe

This probe was invented for use as a flow direction indicator and although it proved unsuccessful in this respect, it was found to be invaluable for counting stall cells and as a position reference for the phase-lock sampling procedure.

A sketch of the probe is given in Figure 3a. It consists of a strip of piezo-electric material from a gramophone pick-up, which was bound between two copper connectors and mounted in a probe holder so that half the sensor was left protruding into the flow. Two examples of the output from the probe obtained during stall are shown in Figure 3b, the first filtered and the second unfiltered. In the filtered state, the output is suitable for use as a reference pulse, while in the unfiltered state, it provides a ready means of counting the cells and estimating the circumferential extent of the disturbance.

For fundamental work, such as cell frequency analysis, this probe has a number of advantages over a hot wire probe. As well as being simple to use and inexpensive to make, it is very robust and insensitive to the accumulation of dirt and oil. The frequency response is extremely high and can thus be used for high speed engine testing. The other obvious advantage is that it requires no supporting electronics; it can be connected directly to an oscilloscope.

d) On-line Computer Facilities

The experimental work described in this thesis was only possible with the aid of an on-line digital computer. Attempts have been made in the past to obtain the same information from oscilloscope traces, but the process was too tedious to produce results of any great detail. There have been no other reported attempts of on-line analysis of rotating stall measurements because of the irregular

behaviour of most stall cells. In the present case this difficulty has been overcome by means of a phase-lock sampling technique which will be described in a later section.

The on-line work was done on a PDP 12 computer which is specially intended for this type of work. The output from the various measuring probes was fed directly to the computer where the analogue-digital conversion was done automatically by built-in hardware. The rate at which the sampling and conversion was done could be varied at will, but for the present work it was adjusted so that 256 measurements would cover a period of about $1\frac{1}{2}$ revolutions of the stall cell. In this way, results of sufficient detail were obtained without the use of excessive computer time. (It should be noted that 256 is half of 1000 in the octal system, which was the maximum number of conversions which could be done before the digital results were transferred to core.) The final results were stored in digital form on magnetic tape.

For stalled measurements, the sampling process was initiated by a Schmidt trigger fed with a reference signal from the piezo-electric probe mounted in the compressor. This meant that sampling was always initiated when the stall cell was in exactly the same position relative to the reference probe. The data acquisition process is described in detail in the section on unsteady measurements.

3.4 Experimental Techniques

3.4.1 Time-Averaged Pressure Measurements

The performance characteristics of the various compressor builds were calculated from time-averaged measurements recorded on conventional water manometers. The outer wall static pressures were used for this purpose. The results would have been improved if the inner wall pressures were also available, however these measurements could not be

obtained because of the way in which the compressor was constructed. It should be noted that no total pressure characteristics were recorded during stall. Under these conditions, the flow direction downstream of the compressor is uncertain and insufficient settling length was available to ensure that the probes could be placed in reasonably uniform flow.

Three types of characteristics were measured:

1) Total-to-static. This characteristic represents the difference between the static pressure downstream of the last stator row and the inlet total pressure, which was assumed atmospheric in all cases.
2) Static-to-static. This term is sometimes used to refer to the difference in static pressure across the entire compressor, but in the present case it refers to the difference in static pressure measured after the IGV's and before the OGV's. The exclusion of the guide vanes is necessary if the static-to-static performance curves of compressors of different numbers of stages are to be compared directly.
3) Individual stage characteristics. These characteristics represent the increase in static pressure measured across each stage in the compressor.

When measuring the time-averaged static pressures, it was found that large circumferential variations in pressure existed in all measuring planes upstream of the rotors in compressors of high design flow rate. Downstream of the rotors the variations were much less obvious. By rotating the traverse rings and measuring the pressure at numerous circumferential intervals, it was found that this pressure variation was cyclic and of a wavelength equal to the pitch of the blades in the upstream stator row. An example of the measurements

obtained during stall is shown in Figure 4a, where it can be seen that the magnitude of the fluctuations is of the order of $.1 \times (\rho\bar{U}^2)$, where $\bar{U}$ is the mean blade speed. Fluctuations of a slightly reduced magnitude were also noted during unstalled operation.

In the case of unstalled flow, the fluctuations are thought to be explained in terms of a pitch-wise variation in flow angle which affects the pressure fields surrounding the rotor blades. During stall, on the other hand, this explanation can only be used for the unstalled part of the flow. In the stall cell itself, reversed flow is thought to impinge on the trailing edges of the stator blades at very oblique angles, thus generating local pressure fields which, on a time-averaged basis, would tend to reinforce the fluctuations in the unstalled flow. These arguments are supported by the fact that reversed flow is most severe in compressors of high design flow rate, and that downstream of the last stator, where there is no following rotor, the time-averaged static pressure is circumferentially uniform.

The non-uniformity of the wall static pressure in compressors of high flow rate can lead to erroneous measurements of inter-stage characteristics, especially for a stage positioned between two others. An example is given in Figure 4b showing the range of possible error in an inter-stage characteristic in a compressor of design flow rate $\phi^* = 1.0$. In the present experiments, large numbers of static taps were not available for the circumferential averaging of the static pressure, and so the taps which were used were carefully positioned between the wakes of the upstream stator blades so as to record, as near as possible, the true average pressure.

3.4.2 Mass Flow Rate Measurements

For unstalled operation, the flow in the compressor inlet is

steady and so the flow rate can be estimated from the inlet calibration curves. During stall, however, conditions in the inlet are seriously disturbed and the calibration curves are no longer valid. For the purpose of the present experiments, suitable ducting and an orifice plate were fitted downstream of the throttle where the flow was more or less uniform and thus accurate measurements were obtained. In view of the wide range of flow rates covered when measuring a characteristic, several pipes of different diameters with appropriate orifice plates were required.

In Figure 5a an example is given showing how the orifice plate measurements differ from those estimated from the inlet calibration. The agreement is good for unstalled flow, but when rotating stall is established, large discrepancies are immediately obvious. It should be noted that, with the throttle fully closed the inlet calibration still indicates a sizable amount of through-flow, while the orifice plate correctly indicates no flow. Figure 5b illustrates the effect of the erroneous inlet flow measurements on a typical pressure rise characteristic.

3.4.3 Unsteady Measurements

In the initial phases of the work, the unsteady measurements were conducted in the conventional manner using hot wires and a U-V oscillograph recorder. For a number of reasons this approach was found to be unsatisfactory as a means of obtaining detailed flow measurements. The U-V traces were tedious to analyse and the unsteady behaviour of the stall cells meant that consecutive traces were not identical, so that a certain amount of judgement was necessary to obtain an accurate result. It was also difficult to obtain quantitative measurements in the stall cell itself, since the flow direction was

unknown and the probe could not be correctly aligned with the flow.

To overcome these difficulties a phase-lock sampling technique was developed whereby an on-line computer was used for data acquisition and processing. This meant that the minor differences between consecutive stall cycles could be eliminated by averaging repeated measurements, and the problem of probe alignment overcome through the analysis of data acquired at numerous probe settings. The details of the technique can best be considered in three sections: data acquisition, ensemble averaging and probe alignment. These topics will be discussed below, after which a short summary of the actual experimental routine will be given.

a) Data Acquisition. The data acquisition process makes use of phase-lock sampling. This is a familiar technique in turbomachinery whereby the recording of information is phased to commence at a specific point in a cycle. In most cases the recording is initiated by a reference pulse supplied by a marker on a rotating shaft. In the case of rotating stall, however, the cell speed is not precisely linked to the shaft speed, thus the reference signal must be obtained from the cell itself. It was found that the piezo-electric probe described earlier, could be used to provide a well defined signal each time the stall cell passed. Using this signal as a reference, the computer was programmed to sample and digitize the output from measuring probes in the compressor. The rate of sampling was chosen to give sufficiently detailed information without excessive use of computer time and to demonstrate the periodicity of the measurements. For most of the work, 256 samples were taken covering a period of about $1\frac{1}{2}$ revolutions of the stall cell.

b) Ensemble Averaging. Having established a reliable method of acquiring phase-locked measurements, the use of ensemble averaging

could be considered as a way of obtaining an averaged result from repeated measurements. The approach adopted in the present case can be described as follows: repeated phase-lock samples, each consisting of 256 discrete measurements, were obtained from a particular measuring probe and stored in matrix form in the computer core. After 25 sets of measurements had been recorded, the values at corresponding points in each set were averaged to produce a single ensemble averaged result which was then stored on magnetic tape.

In symbolic terms the process can be represented as follows:

$$\text{SAMPLE 1} \quad S_1 = {}_1M_1 \;,\; {}_1M_2 \;,\; \cdots \;,\; {}_1M_{256}$$

$$\text{SAMPLE 2} \quad S_2 = {}_2M_1 \;,\; {}_2M_2 \;,\; \cdots \;,\; {}_2M_{256}$$

$$\cdots \quad \cdots \qquad \cdots \qquad \cdots \qquad \cdots \qquad \cdots$$

$$\text{SAMPLE 25} \quad S_{25} = {}_{25}M_1 \;,\; {}_{25}M_2 \;,\; \cdots \;,\; {}_{25}M_{256}$$

$$\text{ENSEMBLE AVERAGE} \quad \bar{S} = \frac{\sum_1^{25} {}_n M_1}{25} \;,\; \frac{\sum_1^{25} {}_n M_2}{25} \;,\; \cdots \;,\; \frac{\sum_1^{25} {}_n M_{256}}{25}$$

The number of samples used in this process could be varied at will, but was kept at 25 throughout the present work. This number represents a compromise between accuracy and running time.

It should be noted that if the samples used are not all perfectly in phase, the averaging process will lead to a deterioration of the basic wave form of the signal being studied. For example, the corners of a square wave signal would be rounded if the samples were occasionally out of phase. Stall cells are known to be erratic both in terms of speed and shape and so it might be thought that, as the cells themselves were used to phase the data acquisition process, the results would be distorted. To establish that this was not so, checks were carried out by comparing the ensemble averaged result with examples of the raw signal. Surprisingly, little loss of detail was

observed for single stall cells, but attempts to obtain measurements in multiple cell configurations had to be abandoned on account of the unsteadiness of the cells.

c) Probe Alignment. The flow direction in stalled flow is known to change rapidly with the passage of the stall cell. A hot wire or total pressure probe cannot, therefore, be correctly aligned with the flow at all points in the stall cycle. To overcome this difficulty, and to determine the unknown flow direction, use was made of the fact that for either probe the correct alignment (i.e. the orientation at which a true measurement is obtained) coincides with maximum probe output. Thus, by rotating a probe about its axis in finite increments and obtaining phase-locked averages at each setting, the results can be analysed to determine the orientation of the probe corresponding to maximum output at each point in the stall cycle. The true velocity or total pressure is then given by the maximum output at each point and the flow direction by the corresponding probe angle.

In the present work both probes were rotated in increments of 10 degrees. This was considered to give sufficiently good resolution in view of the turbulent nature of the flow. The number of 10 degree increments through which the probes need to be rotated depends on the type of probe. The cylindrical total pressure probe gives a correct result for flow from one direction only and therefore needs to be rotated through 360^{o} to take account of all possible flow directions. The straight-pronged hot wire, on the other hand, is symmetrical in response and needs only to be rotated through 180^{o}, but the sense of the flow is left undetermined. For this reason the directionally sensitive hot wires were developed and used to fix the sense of the flow where doubt existed. In most instances, however, total pressure measurements were also available and thus any areas of reversed flow could be picked out from these results.

In the procedure described above, it was stated that the flow direction was determined on the basis of maximum probe output. However, in the case of the hot wire, it was found to be more reliable to search for the minimum velocity, i.e. when the flow is parallel to the sensing wire, as the variations of probe output with angle change is more sharply defined in this region. The velocity itself was still obtained from the maximum output.

Typical examples of the results obtained from both hot wire and total pressure transducer are shown in Figure 6. In each case the flow directions have been plotted above the velocity or total pressure measurements, with a one-to-one correspondence between the dots in each set of results. The two examples were obtained under the same flow conditions and so the direction measurements should be in reasonable agreement. Some discrepancy can be seen at the centre of the stall cell, but in view of the turbulence of the flow in the region, the correlation is considered to be good. It should be noted that all angles are measured from the axial direction in such a way that 90^{o} represents flow in the direction of rotor movement, i.e. in the tangential direction.

Having described the sampling technique and demonstrated the results obtained, it will be useful to outline the steps involved in the actual experimental procedure.

1) The piezo-electric probe is mounted ahead of the first rotor near the blade tip and is adjusted so as to give as sharp a pulse as possible each time the stall cell passes. The probe is then fixed rigidly in this position and the output fed to the Schmidt trigger in the computer.
2) The hot wire or total pressure transducer is then mounted in a special probe holder and positioned at the desired measuring

station. The initial orientation of the probe, relative to the compressor axis, being carefully noted.

3) When triggered by the reference pulse, the computer starts sampling the output from the measuring probe, taking 256 discrete measurements over approximately $1\frac{1}{2}$ revolutions of the stall cell. This sampling is repeated 25 times, after which the computer produces an ensemble averaged result which is stored on magnetic tape.

4) The ensemble averaged results on the tape can now be analysed. The computer determined the flow direction by searching each point in the stall cycle for the probe setting at which the velocity is a minimum or the pressure a maximum, as the case may be. The magnitude of the velocity or pressure is then found from the maximum probe output at each point, and the results finally plotted out in the form shown in Figure 6.

The process described here is a lengthy one and it has been suggested that a crossed hot wire could have been used to resolve the velocity and flow direction with less difficulty. The flow angles can change by as much as 120^{o} in any one stall cycle and thus the working range of a crossed hot wire, which is approximately 45^{o}, would clearly be exceeded. Moreover, with the technique used here, the hot wire and total pressure measurements are treated in the same way and the direction results can be compared directly.

Wall static pressures were also recorded and ensemble averaged by the same method, but in this case there was no need to rotate the probe. By using the same triggering probe for all measurements, the total pressure, velocity and static pressure traces were all in phase, thus providing a fairly complete picture of the flow field. Under these circumstances, the velocities and total pressures measured near

the outer wall could be used to calculate a static pressure, which could then be compared with that recorded by the static pressure transducer. An example comparing the trace deduced in this way with that measured directly, is shown in Figure 7. The correlation is good, even though the velocity and the total pressure were measured 5 mm in from the outer wall. This provides fairly convincing evidence that the measurements are accurate and that the piezo-electric probe is allowing consistent ensemble averaging.

CHAPTER 4

Experimental Results

The information obtained from the present experimental work will be presented in this chapter. Apart from explanatory notes, the interpretation and discussion of the results will be left to the following chapters.

The time-averaged measurements are considered in Section 4.1. These measurements include the pressure rise characteristics of the various compressor builds and demonstrate the change in performance associated with the systematic variation of design parameters. Observations of the stall cell type are included here and some examples of torque measurements are given. Section 4.2 is devoted to the general properties of rotating stall, such as: rotational speed, number of cells and variation of cell size with mass flow rate. In Section 4.3 the phase-lock sampling results for full-span stall are considered. Particular attention is paid to the results from the 3-stage compressor builds. The single stage measurements are compared with the multi-stage results in Section 4.4 to ascertain the effect of the number of stages on the cell details. Finally, the results obtained during part-span stall are considered in Section 4.5.

4.1 Time-Averaged Measurements

For each compressor configuration, the total-to-static and static-to-static characteristics were measured, along with the individual stage characteristics. Of these three, the total-to-static characteristic is the most important and will be presented in detail for each compressor build. The static-to-static and individual stage characteristics are of lesser importance and only selected examples

will be considered at the end of the section.

4.1.1 Total-to-Static Characteristics

The single stage and 3-stage characteristics of the Low ϕ^* compressor builds are shown in Figure 8. The design flow coefficient for this blading is 0.35 , which is low by comparison with current engine designs. Stall inception occurs at $\phi \simeq 0.33$ in both builds, thus indicating that the number of stages has little effect on the stalling flow rate. The characteristics can be described as being of the progressive type as no abrupt change in the pressure rise occurs at stall inception. In both cases, multi-cell part-span stall is found at high flow coefficients, and single-cell stall at lower values. At very low flow rates rotating stall gives way to axisymmetric stall. No hysteresis loop appears in the performance curve, as the same changes in stall behaviour which occur on closing the throttle, occur again in reverse order at the same flow coefficient when opening the throttle.

The characteristics for the four Intermediate ϕ^* builds are shown in Figure 9. By comparison with the Low ϕ^* results in Figure 8, it is clear that the increase in design flow rate from 0.35 to 0.55 is accompanied by an increase in pressure rise. The flow coefficient at which stall occurs is again found to be the same for each build. The pressure rise falls abruptly at stall, but in the 1, 2 and 3-stage builds, stabilises in part-span stall before changing to full-span stall. In the 4-stage build, no part-span stall occurs on reducing the mass flow rate. On increasing the flow rate, full-span stall gives way to part-span stall, with a minimal amount of hysteresis, in all four builds. The 4-stage build is thus unique in that the flow regime differs depending on the direction of approach. All builds exhibited axisymmetric stall near shut-off.

The three configurations tested with the 65% reaction blading ($\phi^* = 0.71$) are shown in Figure 10. The single stage characteristic shows an area of part-span not present in the other builds. On increasing the mass flow rate in all the builds, the flow regime changes directly from full-span stall to steady operation, leading to a noticeable hysteresis loop. The size of the loop increases with the number of stages. A small area of axisymmetric stall is again detected near shut-off.

The single stage and 3-stage characteristics of the High ϕ^* builds are given in Figure 11. (The 2 and 4-stage characteristics of this design are unfortunately incomplete.) Here the design flow coefficient is 1.0 . As in the High Reaction case, only the single stage build exhibits part-span stall. The hysteresis loops are very large in this configuration, especially for the 3-stage build, and unlike the previous configurations, full-span stall persists right up to zero flow.

In reviewing the compressor characteristics of the four different categories of blading, it can be seen that as the design flow rate increases so does the peak pressure rise. This is illustrated more clearly in Figure 12 where the characteristics of all the 3-stage builds have been replotted on a single set of axes. The peak pressure rise can be seen to increase almost linearly with increasing design flow rate and, at the same time, the slope of the unstalled part of the characteristic becomes less steep. Both of these trends may be predicted from elementary theory on unstalled blade performance. It should be noted that the pressure rise at zero flow would appear to be more or less independent of the blading used.

In the previous chapter it was mentioned that a 3-stage build of Low ϕ^* blading was tested with greatly reduced axial spacing.

The three configurations tested with the 65% reaction blading ($\phi^* = 0.71$) are shown in Figure 10. The single stage characteristic shows an area of part-span not present in the other builds. On increasing the mass flow rate in all the builds, the flow regime changes directly from full-span stall to steady operation, leading to a noticeable hysteresis loop. The size of the loop increases with the number of stages. A small area of axisymmetric stall is again detected near shut-off.

The single stage and 3-stage characteristics of the High ϕ^* builds are given in Figure 11. (The 2 and 4-stage characteristics of this design are unfortunately incomplete.) Here the design flow coefficient is 1.0 . As in the High Reaction case, only the single stage build exhibits part-span stall. The hysteresis loops are very large in this configuration, especially for the 3-stage build, and unlike the previous configurations, full-span stall persists right up to zero flow.

In reviewing the compressor characteristics of the four different categories of blading, it can be seen that as the design flow rate increases so does the peak pressure rise. This is illustrated more clearly in Figure 12 where the characteristics of all the 3-stage builds have been replotted on a single set of axes. The peak pressure rise can be seen to increase almost linearly with increasing design flow rate and, at the same time, the slope of the unstalled part of the characteristic becomes less steep. Both of these trends may be predicted from elementary theory on unstalled blade performance. It should be noted that the pressure rise at zero flow would appear to be more or less independent of the blading used.

In the previous chapter it was mentioned that a 3-stage build of Low ϕ^* blading was tested with greatly reduced axial spacing.

The purpose of this test was to prove that the picture of the stall cell obtained from the unsteady measurements would still be representative under conditions of small axial clearance. It was only possible to conduct such a test in the case of the Low ϕ^* blading where, by removing some of the spacing rings and adjusting the position of the rotor discs on the compressor shaft, the axial gaps could be reduced from 1.5 chord lengths to 0.35 . The detailed flow measurements showed little change in cell structure, as will be demonstrated in Section 4.3. The total-to-static characteristic is shown in Figure 13, where the results with the original spacing are shown as a broken line for comparative purposes. The sequence of stall regimes is little affected by the reduction in spacing, but the flow coefficient at which each change occurs is altered from that given in Figure 8. The most obvious change is, however, the increase in pressure rise during stall. No satisfactory explanation for this has yet been found.

4.1.2 Static-to-Static Characteristics

Having presented the total-to-static characteristics in detail, the static-to-static characteristics are really only of interest in terms of the relationship they bear to the total-to-static characteristics. It was mentioned in Chapter 3 that, where comparisons are to be made between compressors of different numbers of stages, the static-to-static characteristics should be measured after the IGV's and before the OGV's. The characteristics considered here have been measured in this way. (Measurements taken across the whole compressor produce curves of a different form and will be discussed later.)

The static-to-static characteristics measured between planes 2 and 8 for each of the 3-stage compressor builds are shown in Figure 14.

The corresponding total-to-static curves are shown as dotted lines for comparative purposes. During unstalled operation the two characteristics are similar in form, but in stall they are markedly different and even cross each other near the centre of the stalled region. The relationship between the characteristics is of some interest and will be considered in Chapter 5.

4.1.3 Individual Stage Characteristics

The individual stage characteristics give the static pressure rise across each stage in the compressor. Two representative examples will be considered here. Figure 15 shows the results from the single stage and 3-stage builds of the Low ϕ^* compressors, while Figure 16 shows the corresponding measurements for the High ϕ^* builds. It should be noted that the scales used in these two figures are different.

In both cases it can be seen that all stages perform similarly in unstalled flow; it is only in stalled operation that differences are noticeable. The first two stages in the 3-stage build give similar performances, but the last stage, like that of the single stage, seems to perform poorly. The other compressor builds show these observations to be general. As a rule, therefore, the last stage in a multi-stage build always appears to perform poorly in stall by comparison with preceding stages, and the performance of a single stage build is much like that of the last stage in a multi-stage configuration. A study of the stall cell structure provides an explanation of this phenomenon, as will be shown in Chapter 5.

4.1.4 Torque Measurements

Torque measurements for small, low speed, compressors are often difficult to make and are frequently unreliable. The forces involved

are small and easily distorted by friction in the measuring system. Some torque measurements were obtained in the present experiments and, although their accuracy is slightly questionable, the results are useful in demonstrating the trends to be expected. For unstalled flow, torque measurements are often interpreted in terms of temperature rise characteristics from which estimates of compressor efficiency can be obtained. In stall, however, the flow rate can approach zero, in which case the temperature rise characteristic will go to infinity. For this reason it is better, where the entire flow range is being considered, to nondimensionalize the torque by some reference value. The value chosen here is $(\frac{1}{2}\rho\bar{U}^2 AR_m)$, which is the mean blade speed dynamic pressure acting over the annulus area, A, at the mean radius, R_m.

Figure 17 shows the measurements for the 3-stage builds of the Low ϕ^* and High ϕ^* compressors. The High ϕ^* build has the greater blade loading and so it is to be expected that this build will require more torque in the unstalled region. In deep stall, however, the two compressors produce almost the same pressure rise, thus the reason for the difference in torque levels is less obvious. An explanation can only be given by examining the details of the stalled flow in the two compressors. This will be done in the following chapter.

4.2 Overall Stall Cell Properties

Introduction

The stall cell features to be considered in this section include the number of cells, the speed of rotation, the radial and circumferential extent of the cells, and the variation of each of these quantities with the change in compressor flow rate. All of

these can be measured fairly easily with conventional instrumentation, but before presenting the results there are two experimental points which should be noted.

The first point concerns the detection of very small cells. It sometimes happens that near the peak of the unstalled characteristic, rotating stall is suspected, but no cells can be found. This may be due to the fact that the cells are so small that, unless every measuring plane is carefully traversed, the cells remain undetected. In the single stage build of the Low ϕ^* compressor, cells were found extending only 3 or 4 mm from the hub on the stator blades. Disturbances were first detected downstream of the stator row, but nothing could be seen ahead of the row. It was only with the aid of a "kinked" hot wire probe that the upstream disturbances could be found. Small cells such as these do not have a marked effect on the compressor performance, however, they may be responsible for the turning over of the characteristic at peak pressure rise prior to more severe stalling.

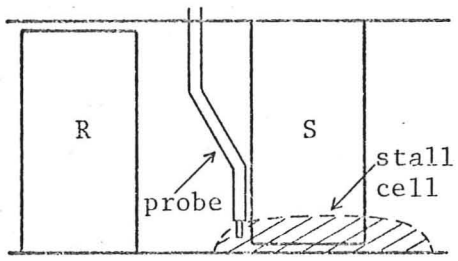

The second point concerns the radial extent of the stall cells. The distinction between full-span and part-span stall is usually based on whether velocity fluctuations are recorded over the full height of the annulus, or only over a part of it. This distinction is not always valid as velocity fluctuations need not imply that the blade is stalled. A more precise method of establishing the type of stall is therefore required. The change in absolute velocity across the rotor can be used for this purpose, since, if the absolute velocity decreases across the rotor instead of increasing, the flow must be

considered stalled. In cases of doubt, two velocity measurements, one on each side of the rotor, are therefore necessary to decide between full-span and part-span stall.

4.2.1 Cell Property Measurements

A table is given on page 175 setting out the number of cells, the type, and the speed of rotation of all of the stall cell regimes encountered when measuring the pressure rise characteristics described in Section 4.1. From the table, and the corresponding characteristics, a number of general observations about the behaviour of the stall cells can be made. These are listed below:

1) The multi-cell stall configurations in this high hub-tip ratio compressor are restricted to the Low ϕ^* builds.
2) All the multi-cell configurations are made up of part-span cells.
3) Full-span stall is always associated with a single stall cell.
4) Part-span cells, where present, always occur at higher flow rates than full-span cells.
5) Part-span cells always rotate at greater speed than full-span cells in the same compressor build.
6) Part-span stall always gives a greater pressure rise than full-span stall in the same compressor build.

These observations are of a general nature. The more specific aspects of the measurements can now be considered.

The cell velocities given in Table 2 (page 175) were, of necessity, average values because the cell speed can be shown to depend on the compressor flow rate. Considering only full-span stall, as this mode of operation covers the greater part of the flow range, the

results of cell speed measurements in the 3-stage, 50% reaction, builds are shown in Figure 18. In each case the cell speed has been plotted as a function of mass flow rate. In the Low ϕ^* and Intermediate ϕ^* builds, a marked variation of speed with flow rate can be seen, whereas in the High ϕ^* build, the cell speed is comparatively constant. No explanation for this behaviour has been found.

A more interesting aspect of the measurement of cell speed is the change which takes place when the compressor build is changed. A comparison of the cell speeds for the various builds can be made from the bar chart shown in Figure 19. This chart was compiled from measurements taken at the point where the stall cell covers 50% of the compressor annulus. It can clearly be seen that for a particular compressor design the cell speed increases with the number of stages. This observation has not been seen in any of the literature, although it must be of particular interest to any theoretician attempting to predict the cell speed.

The circumferential extent of the stall cells depends on the compressor mass flow rate. This is demonstrated in Figure 20, where examples of the measurements obtained during full-span stall have been plotted for the 3-stage builds of the Low ϕ^* and High ϕ^* compressors. The estimates of cell size were taken from hot wire recordings and, although a certain amount of judgement was required in their interpretation, a reasonably consistent line was obtained in both cases. The size of the cells can be seen to increase almost linearly with a decrease in mass flow rate.

An important difference exists between the two examples given in Figure 20. In the Low ϕ^* build, the measurements show that the circumferential extent of the cell will reach 100% at a positive flow

coefficient of 0.08 . This flow coefficient corresponds to the point at which axisymmetric stall begins, as shown in Figure 8. The implication of this observation is that the stall cell does not represent a complete blockage of the flow, but allows the passage of a certain amount of through-flow. In contrast, the measurements for the High ϕ^* build show that the stall cell covers only 90% of the annulus at shut-off, and therefore suggests reversed flow in the stall cell. Confirmation of these ideas was obtained when the details of the flow in the stall cells were measured.

4.3 Unsteady Flow Measurements

Introduction

When the phase-lock sampling procedure was first developed attention was focused on full-span stall. This mode of operation accounts for the greater part of the stalled characteristic and the large well-defined cells made it easier to obtain reliable results. Towards the end of the project when the technique was more advanced, it became possible to measure the flow in the smaller part-span cells. These measurements were less extensive, however, and are regarded as a secondary part of the work. The full-span results will therefore be considered first, the part-span results being left to the end of the chapter.

In view of the time required to measure and process the unsteady results, it was not possible to test all 13 compressor builds and, therefore, a smaller number were selected for detailed study. In making this selection, two considerations were employed. Firstly, the design flow rate clearly influences the details of the flow in the stall cell, thus as wide a range of design flow rates as possible should be tested. Secondly, since most unsteady work in the past has

been done on single stage compressors, information on multi-stage builds would be particularly useful. It was therefore decided to focus attention on the 3-stage builds of the 50% reaction designs. These results will be discussed first and in the greatest detail. Measurements were later obtained for the single stage builds of the same three designs. By doing so, it was hoped to establish the differences which exist between the stalled performance of single stage and multi-stage compressors. The results from the single stage builds and the comparison with the multi-stage results, will be considered in Section 4.4. Limited full-span stall measurements were taken in nearly all of the other builds, but these will only be referred to where necessary.

Having selected the builds to be tested, it was necessary to decide where in the compressor the measurements should be taken. In a multi-stage compressor, detailed traverses in every measuring plane were impossible on account of the computer time required; however, once it was established that each stage in the compressor performs similarly in stall, it was only necessary to study one stage in detail. The first stage was selected for this purpose, as direct comparison would then be possible with the results obtained from a single stage build. The principal measuring positions used in the 3-stage builds are indicated in the following diagram.

MEASURING PLANES:

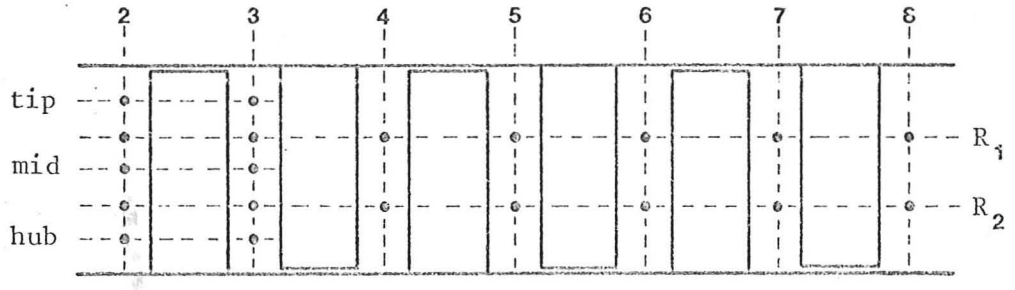

Measurements in planes 2 and 3 provide information about the radial structure of the stall cell, while those in planes R_1 and R_2 can be used to monitor the axial behaviour of the cell. It should be noted that even after restricting the detailed study to one stage, with limited measurements in the other stages, more information was obtained than can be presented here. Only selected examples will be provided, the remainder of the results, although not shown, have nevertheless been used to support statements made and to substantiate the conclusions reached.

4.3.1 Full-Span Results in Three Stage Builds

Examples of the results obtained in each of the measuring planes throughout the full length of the compressor will be considered first. These provide information about the axial profile of the stall cell and show that each stage in the compressor performs similarly. The additional information required to complete the study of the flow in the stall cell will be left to the following section, where the detailed measurements obtained before and after the first rotor will be considered.

1) Axial Study of Stalled Flow

Measurements were taken at all axial positions in each compressor build at two radial positions: R_1 and R_2. Most of the important information can be obtained by studying just one of these, and so the measurements from R_1 only will be considered. The results from the three compressor builds are presented simultaneously so as to emphasise any dependence on design flow rate.

a) Velocity Measurements. The absolute velocities measured in planes 2 to 8, at radius R_1, are shown in Figure 21. Parallel lines

have been drawn through each set of results to indicate the areas of stalled and unstalled flow. The flow coefficient at which each set of measurements was obtained is given in the figure. In choosing these values, attempts were made to balance the size of the stalled and unstalled areas without taking measurements at any point on the characteristics which could not be reached from either direction of approach.

Consider first the measurements in the unstalled section of the annulus. In each build it can be seen that the absolute flow is accelerated through the rotors, and decelerated through the stators; as expected from consideration of simple velocity triangles. The unstalled part of the annulus thus behaves, at least qualitatively, as it would do with no stall in the compressor at all. Comparison of the three sets of measurements shows that the absolute velocity of the unstalled flow increases as the design flow rate of the compressor is increased.

In the stall cell itself, it can be seen that ahead of the rotors the velocities are very high, being comparable with, or even greater than, blade speed. Behind the rotors, i.e. in planes 3, 5 and 7 , the velocities in the cell are generally very low. This pattern of high velocity ahead of the rotor and low velocity behind, is true for each rotor in each of the builds. This observation is important, because it indicates two features of stalled flow not previously recognised. It shows that each stage in a multi-stage build operates under the same flow conditions, instead of the latter stages working in the wake of a stall cell attached to the first stage. It also shows that the same basic cell structure is present in compressors of widely different designs.

All of the measurements in any one build were synchronised by the same reference probe, and so the velocity plots of Figure 21 give an instantaneous picture of the flow field. The parallel lines drawn to mark the stalled and unstalled areas can therefore be used to show that the stall cell extends axially through the compressor. This observation, which is surprising in view of conventional ideas about cell structure, is supported by numerous other measurements and will play an important part in the development of a flow model in Chapter 5.

b) Flow Direction Measurements. Having presented the velocity measurements at length and shown that the individual stages perform similarly in stall, the flow direction measurements may be presented more succinctly; it being sufficient to show representative examples of the measurements upstream and downstream of the first rotor and downstream of the last stator. These are presented in Figure 22, where the measurements downstream of the last stator are intended to complete the overall picture of the compressor. The parallel lines used in the previous figure have been transposed onto these plots so that direct comparisons can be made. It should be noted that flow angles in excess of 90^{o} correspond to reversed flow, that is to say, a negative value of C_x. The angles shown were measured with a total pressure probe which allowed the unequivocal resolution of reversed flow.

In each of the compressor builds, the flow angle in the unstalled part of the annulus increases as the flow passes through the rotor and then decreases again through the stator. The unstalled flow is thus again shown to behave qualitatively as it would under uniform flow conditions. Also, in keeping with the reduction in stagger angle (or mean flow angle) associated with an increase in compressor design flow rate, the magnitude of the unstalled flow angles

can be seen to decrease from build to build.

In the stall cell itself, the flow direction alters radically. Ahead of the rotor, where the velocity is high, the flow can be seen to be predominantly in the tangential direction, i.e. approximately 90°, as though it were being whirled around by the rotor blades. From the measurements behind the rotor, it is clear that the stall cells do not operate in precisely the same way in each build. In the Low ϕ^{*} build, the flow is still moving in the through-flow direction (i.e. $<90^{\circ}$), albeit with a large tangential component. In the other two builds, reversed flow is clearly indicated over part, if not most, of the stalled area. It should be recalled that the velocities downstream of the rotor are very low and the net mass transfer in the reversed direction is therefore small.

In the exit plane the flow direction is not circumferentially uniform, but is different in the stalled and unstalled regions. This is in contrast with the usual assumption that the exit angle of flow leaving a stalled blade row is constant.

c) Total Pressure Measurement. As with the direction measurements, only representative results before and after the first rotor and downstream of the last stator are given – Figure 23. The parallel lines marking the stalled and unstalled areas are again imposed on the measurements. The pressures have been nondimensionalized by the dynamic head based on the blade velocity at mid-height.

The total pressures in the unstalled parts of the annulus are all approximately atmospheric ahead of the first rotor; the discrepancies which exist are thought to be due to reversed flow and unsteady effects in the compressor inlet. As the unstalled flow passes through the rotor, the pressure rises sharply. Similarly, rises

occur through the second and third rotors until, in the exit plane, the total pressure in the unstalled flow can be seen to be well above atmospheric pressure.

In the stall cell the situation is obviously different. The measurements ahead of the rotor show exceedingly high pressures, suggesting that the fast moving tangential flow in this region has received energy from the rotor. Behind the rotor where the velocities are much lower, the total pressure is also low, in spite of the fact that in the Intermediate and High ϕ^* builds some of this flow has come forward from an area of high total pressure ahead of the second rotor. The results thus show localised regions of high total pressure ahead of each rotor in the stall cell.

In the exit plane the total pressure in the stall cell is much lower than that in the through-flow region, especially in the High ϕ^* build. The angle measurements in this area (Figure 22) show the flow direction to be highly disturbed, thus underlining the point that a fixed pitot probe in the exit plane cannot be used to record the average total pressure during stall.

d) Static Pressure Measurements. The outer wall static pressure measurements are presented in full for all three compressor builds, but it has been necessary to spread the results over two pages. The measurements in planes 2 and 3 are given in Figure 24a, while the remainder, planes 4 to 8 , are given in Figure 24b. The pressures are again referenced to atmosphere and have been nondimensionalized by the mean blade speed dynamic head.

In the unstalled flow ahead of the first rotor, the total pressure was shown to be approximately atmospheric and so the static pressure in this region will be less than atmospheric; by an amount equal to the dynamic head of the unstalled flow. This is confirmed

by the measurements in plane 2 , Figure 24a, where it can be seen that the level of the static pressure in the unstalled flow decreases with the increase in compressor design flow rate. Through the remainder of the compressor, the unstalled static pressure rises in each blade row as if under steady conditions, until in the exit plane the pressure is above atmospheric.

In the stall cell ahead of the first rotor, the pressure is positive and approximately of the same magnitude in all three builds. Tracing the pressure rise in the stall cell back through the compressor it can be seen that, by comparison with the unstalled flow, the pressure increases little from inlet to exit.

The static pressure distribution in the exit plane requires special attention. The wave form of the pressure fluctuation in the compressor changes from an approximate square wave in plane 2 to a triangular wave in plane 8 ; the waves being roughly 90^{o} out of phase. The circumferentially averaged pressure in the stalled part of the exit plane is therefore approximately equal to the averaged pressure of the unstalled part. Thus, although the pressure itself is not circumferentially uniform, as is sometimes assumed it will be, the averaged pressure in the stalled and unstalled regions are equal. It will be shown in the next chapter that this will always be the case when a rotating velocity distortion is imposed on a row of compressor blades.

2) Radial Study of Stalled Flow

When considering the axial structure of the stall cell, measurements at one radius only were presented. There are, however, radial gradients within the stall cell, in spite of the high hub-tip ratio of the compressor. Measurements were therefore obtained at 5 radial positions before and after the first rotor in each compressor

for the purpose of studying these effects. As before, the results from the three different builds will be presented simultaneously.

To illustrate the radial gradients in the cell, the measurements of velocity and total pressure obtained ahead of the first rotor in each of the three builds are shown in Figures 25a,b,c. The results from only three of the five radial positions have been included here in order to preserve the clarity of the diagrams. The stalled and unstalled areas of the flow are again separated by parallel lines. In all three builds, the radial variation in velocity and total pressure is comparatively small in the unstalled flow. In the stall cell the radial gradients, which are very large in the Low ϕ^* build, become smaller as the design flow rates of the builds increases. The precise details of the flow in the cells in the three builds are thus very different, even though the general features of the flow are broadly similar.

It is impossible to present all the results obtained at 5 radial positions before and after the rotor, in all three builds, in the same detail as in Figure 25. A method of condensing the results is therefore required. The radial gradients in the unstalled flow have been shown to be relatively small, and so, only the flow variations in the stalled areas are of interest. The measurements obtained at the circumferential centre of the stall cell have therefore been plotted as a function of the blade height in Figures 26 to 29.

a) Velocity Measurements. The absolute velocities measured at the circumferential centre of the stall cell are plotted in Figure 26 for all three compressor builds. Each graph shows the measurements before and after the first rotor, along with the corresponding velocity components resolved in the tangential direction. These tangential components have been designated as C_θ or $C_{-\theta}$ depending on whether

the sense of the flow is in the direction of blade rotation or in the opposite direction.

In each build the velocity upstream of the rotor is higher than that downstream, at all radii. This, according to the previously stated definition of stall, indicates that the flow is stalled from hub to tip in each case, i.e. full-span stall. (From the velocity measurements for the Low ϕ^* build shown in Figure 25a, it may be thought that the flow at the hub in this build is unstalled, but, because the velocity is shown to decrease across the rotor, full-span stall must be assumed.) Considering the builds in turn shows that the level of the velocity in the stall cell increases from build to build, but that the radial gradients decrease with increase in design flow rate. It should be noted that in the High ϕ^* build the tangential component of the velocity is greater than the blade speed at all radii.

b) Flow Direction Measurements. The flow direction measurements at the circumferential centre of the stall cell are shown in Figure 27. When studying these results, it should be recalled that the velocities are high ahead of the rotor, and comparatively low behind.

For the Low ϕ^* build, the flow direction in the stall cell ahead of the rotor changes from 50° near the hub to 100° at the tip, implying that the flow is entering the rotor at the hub, becoming tangential (90°) near mid-height and flowing in the reverse direction at the tip. Behind the rotor the angles indicate a change from through-flow at the hub ($<90^\circ$) to tangential flow at the tip ($=90^\circ$). In the Intermediate ϕ^* build, the flow ahead of the rotor is tangential at the hub and slightly reversed at the tip (100°). Apart from a small amount of through-flow at the tip, the flow behind the rotor is reversed with a strong component in the tangential direction opposite to that of rotation ($\sim 250^\circ$). The High ϕ^* compressor

exhibits circumferential flow before the rotor (90^{o} to 100^{o}) and reversed, counter-rotational, flow behind the rotor (240^{o} to 250^{o}).

In terms of reversed and through-flow, a visual interpretation of the flow directions is suggested in the sketches below. The blades are assumed to be moving out of the paper, as are the solid arrows; the dotted arrows indicate flow in the opposite direction, i.e. against rotation.

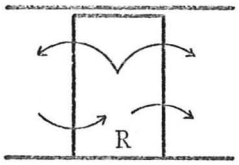

LOW ϕ^*

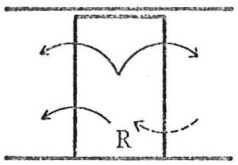

INTERMEDIATE ϕ^*

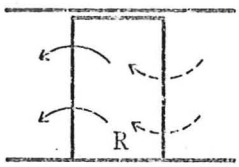

HIGH ϕ^*

It should be emphasized that the velocities in the meridional plane shown here are very small compared with the velocities in the tangential plane, and therefore the flow should be visualised on a three-dimensional basis.

c) Pressure Measurements. The total pressure measurements are presented in Figure 28. Once again the values are higher ahead of the rotor than behind the rotor; except near the hub in the case of the Low ϕ^* build. The pressure also rises from hub to tip in each case and increases in level from build to build.

From the absolute velocities and the total pressures at the various radial positions, it is possible to calculate the radial distribution of static pressure. The results are presented in Figure 29, where, for the sake of clarity, the pressures before and after the rotor have been plotted on separate axes. Also shown in Figure 29, are the instantaneously measured outer wall static pressures, with which the calculated pressures can be compared. The square of the velocity is used in calculating the static pressure and this is therefore very sensitive to errors in the velocity measurements. The

effect of the local temperature variations on the hot wire calibration is a possible source of error here; nevertheless, the calculated and measured pressures are generally found to be in good agreement. (A 3% error in velocity would be sufficient to explain the discrepancy between the measured and calculated values in the High ϕ^* build.)

In the Low ϕ^* build, the static pressure was also measured on the inner wall just ahead of the rotor. No static tap was possible here and a wafer thin static probe had to be stuck to the inner wall of the rig. Satisfactory results were obtained, agreeing well with the calculated pressures, but in view of the difficulties involved in getting the probe past the IGV's, the experiment was not repeated for the other builds.

Figure 29 shows that the difference in pressure level before and after the rotor is comparatively small, but that the gradients from hub to tip are steeper ahead of the rotor, and increase from build to build. It will be shown in the next chapter that these gradients can be related to centrifugal effects in the swirling flow ahead of the rotors.

4.3.2 Additional Three Stage Results

1) Measurements in the High Reaction Builds

The 65% reaction builds were introduced into the test program to investigate the effects of the design reaction on the details of the flow in the stall cell. Similar sets of measurements to those taken in the 50% reaction build were obtained. These were then compared with the above results for any unusual features which could be attributed to a change in design reaction.

The unstalled flow was again found to behave qualitatively as steady flow, and in the stall cell the velocities, flow angles, total

pressures and radial gradients were all commensurate with a design flow rate mid-way between the Intermediate and High ϕ^* builds — which is in fact the case for the high reaction builds, i.e. $\phi = 0.71$. The stall cell speeds were not unusual by comparison with the 50% reaction builds, nor were the pressure rise characteristics. Nothing could therefore be found to suggest that the design reaction affected the stalling behaviour in any way. On the other hand, the design flow rate appears to be a far more important factor in determining the details of the flow in the stall cell.

An example of the velocity and total pressure measurements obtained at three radial positions ahead of the first rotor in the 3-stage build, is given in Figure 30. This can be compared with the results for the 50% reaction builds shown in Figures 25a,b,c.

2) Reduced Axial Spacing Results

It will be recalled that in Section 4.1 a characteristic was presented showing the performance of a 3-stage build of Low ϕ^* design in which the blade row spacing had been greatly reduced. The purpose of the test was to establish whether a reduction in blade row spacing to a value more typical of normal compressors, would affect the structure of the stall cell.

The velocity and flow direction measurements at 3 radial positions ahead of the first rotor for the reduced spacing build are shown in Figure 31. The results were obtained by using a sub-miniature hot wire, as there was insufficient space for the usual 3 mm probes. The measurements show the familiar pattern of high tangential velocities ahead of the rotor in the stall cell. The only notable difference to be found between these measurements and those obtained previously with the larger spacing, is that the stall cell seems to be larger in

circumferential extent at the tip than at the hub. Apart from this point, the basic features of the cell are unaltered.

3) The Effect of Operating Flow Rate on Cell Structure

The preceding studies of the radial and axial structure of the stall cells in the different compressor builds were conducted using measurements obtained at a particular flow rate in each case. It remains to be shown that the basic structure of the stall cells will not be radically different at some other flow rate.

The circumferential extent of the stall cell has been shown to depend on the overall flow rate of the compressor (Figure 20), but more detailed measurements are required to demonstrate that the change in cell width does not affect the general pattern of the flow. Measurements were therefore taken at a number of different flow rates in various compressor builds to investigate this point. An example of the results obtained in the 3-stage Low ϕ^* build is given in Figure 32. The conclusions drawn from measurements in other builds are generally the same and so only one example is given here; this particular example being chosen because the measurements cover the widest range of cell widths.

Figure 32 shows the velocity and static pressure fluctuations measured ahead of the first rotor at 4 different flow coefficients. It can be seen that as the flow rate decreases, the region of high velocity in the stall cell remains unchanged except in circumferential extent. Likewise, the area of high static pressure in the cell increases in width without much change in amplitude. The flow direction measurements, which are not shown here, also show similar changes in proportion rather than in detail, and thus it may be concluded that the basic structure of the stall cell is independent of the compressor flow rate.

It should be noted, however, that the above conclusions are not always true at the extremities of the operating range. In most builds it has been found that when the width of a full-span cell shrinks to around 30% of the annulus, the cell structure begins to break down and an alternative flow regime is established; either part-span stall or a complete change to steady flow. Alternatively, at the other end of the operating range where the cell becomes very large (>90%), the region of unstalled flow becomes unstable, and in the present example (Low ϕ^* blading) gives way to axisymmetric flow. These considerations receive further attention in the following chapter.

4) Inlet Flow Measurements

The measurements presented so far have all been obtained within the compressor itself, however, the flow in the compressor inlet is also of interest. Rotating stall imposes velocity distortions on the incoming flow, the form of which depend on the size of the cell and severity of the stall. Unsteady effects are also present in the inlet where the flow is not directly disturbed by reverse flow.

If measurements are obtained at some distance from the inlet guide vanes, potential flow conditions are found to exist. An example of velocity and total pressure measurements obtained under these conditions, as measured in plane $\frac{1}{2}$, are given in Figure 33. The results show approximately sinusoidal distortions with a 90° phase lag between the two measurements. The unsteady analysis presented in the following chapter shows that this phase shift, and the fluctuation in the total pressure, are to be expected in a potential field subject to a rotating disturbance.

Nearer the inlet guide vanes, reversed flow is often detected and potential flow can no longer be assumed. In this region the flow

tends to separate about the stall cell, dividing itself into clearly defined areas of through-flow and retarded flow. The velocity and static pressure measurements obtained in plane 1 ($1\frac{1}{2}$ chord lengths ahead of the IGV's) are shown in Figure 34. It can be seen that the area of low static pressure is associated with the area of through-flow, while in the stalled region where the velocity is low, the pressure is almost atmospheric. These observations are of interest when attempting to predict the time-averaged static pressure to be expected during stall, and will be referred to again in Chapter 5.

4.4 Single Stage Builds

4.4.1 Results and Comparison with Three Stage Measurements

Single stage builds of the same three compressor designs used above were also studied, so as to compare the cell structure in a single stage build with that in a 3-stage build. The results show the same basic features in the stall cell, however, some differences were noted, leading to the conclusion that a single stage build cannot be used as a substitute for a multi-stage rig when studying the stall cell details.

It will not be necessary to consider the single stage measurements in the same detail as before, but representative examples of the results from all three builds will be given. Figures 35 and 36 show the velocity and flow direction measurements obtained at three radial positions before and after the rotor in the Low and Intermediate ϕ^* builds. Similar measurements for the High ϕ^* build are shown in Figure 37, but in this case the velocity measurements downstream of the stator row have also been included (on a separate page) to illustrate a particular point not observed in the other two builds.

When comparing the measurements of Figures 35, 36 and 37 with those presented previously for the multi-stage builds, four distinct differences can be noted:

1) In the single stage builds, the size of the stall cell increases in circumferential extent from hub to tip, i.e. the sides of the cells are not radial as they were in all of the three stage builds; except in the reduced spacing case. (Note specifically Figs.36 & 37.)

2) In Figure 35 for the Low ϕ^* design, it can be seen that although the stall cell is clearly present at the blade tip, the disturbance does not extend all the way to the hub. The single stage build thus exhibits part-span stall, whereas full-span stall was found in the 3-stage build.

3) It was noted in the multi-stage builds that the circumferential extent of the reduced velocity area behind the rotor was comparable with that of the stall cell. Figures 36 and 37 show that while the width of the cell is the same upstream and downstream of the rotor, the area of reduced velocity behind the rotor is not always as wide as the cell itself, especially near the blade tips. In the Low ϕ^* build (Figure 35) there is hardly any indication of a reduction in velocity downstream of the rotor, in spite of the large velocity fluctuations upstream.

4) Whilst the three points above have been concerned with the flow in the stall cell, differences can also be found in the unstalled flow. Consider the measurements for the Low ϕ^* build; Figure 35. Ahead of the rotor the areas of stalled and unstalled flow are clearly distinguishable. Behind the rotor no velocity fluctuations are evident and the angle measurements suggest the flow is swirling uniformly in a predominantly tangential direction, ~80° . The areas of through-flow and stalled flow are thus not clearly

separable as they were in the 3-stage builds. A second example of this is given in Figure 37 where downstream of the stator, plane 4 , the through-flow velocity near the blade tip is clearly too low to be considered unstalled in a build of high design flow rate. In cases such as these, where the stalled and unstalled flow areas are not well defined, the application of the parallel compressor model would not be justified.

Differences in performance between the single stage and the 3-stage builds have been established, and these are considered important enough to preclude the extrapolation of the flow details from a single stage to a multi-stage build.

4.4.2 Rotor Alone Test

Tests were performed in which an isolated rotor of High ϕ^* design was the only blade row in the compressor. With this configuration it was not found possible to obtain unstalled flow, and a set of outlet guide vanes were subsequently installed 14 chord lengths downstream of the rotor, in order to straighten the flow before it entered the diffuser. Unstalled flow was then possible and the performance of the rotor was examined. This work was carried out before the development of the phase-lock sampling technique and conventional instrumentation was used. Although precise details of the flow were not obtained, the hot wire measurements indicated high velocities ahead of the rotor in the stall cell and low velocities behind. This implies that the structure of a full-span cell in an isolated rotor is basically similar to that in a rotor which is part of a complete stage. It would therefore appear that the passage of the rotor blades through the region of retarded flow, plays a large part in determining the structure of the stall cell. This idea will

be considered further in the next chapter.

4.5 Part-Span Stall

The phase-lock sampling technique developed for full-span stall was used successfully to examine part-span stall, but only in those cases where a stable, single, stall cell existed. The multi-cell configuration in the two Low ϕ^* builds could not be tested because the cells were so unsteady as to make phase-lock sampling impossible. Nevertheless, part-span results were obtained in the five compressor builds which are listed below:

Group I	1 stage	Intermediate ϕ^*
	2 stage	Intermediate ϕ^*
	3 stage	Intermediate ϕ^*
Group II	1 stage	High Reaction
	1 stage	High ϕ^*

The compressors are divided into two groups on the basis of the results obtained. An example of the measurements from each group will be given.

In the case of the first group, the results suggest that the structure of the part-span cells is little different from that of full-span stall. An example is given in Figures 38a,b. Here the velocity, flow direction and total pressure measurements in the 3-stage Intermediate ϕ^* build are shown at three radial positions before and after the first rotor. The outer wall static pressure measurements have also been included in the figure. Although the cell is localised at the blade tip and covers only 25% of the compressor circumference, the familiar features of high tangential velocities ahead of the rotor and low velocities behind, are immediately obvious. The outer wall static pressure is again above atmospheric pressure in the stall cell,

and, as in the 3-stage build of this compressor, the cell was found to extend axially through the blade rows. It can therefore be seen that the general behaviour of the part-span cells in this group of compressors is very similar to the behaviour of the full-span cells examined previously.

A different stall behaviour was found during part-span stall in the two builds of Group II. This is illustrated in Figures 39a,b,c, which show the measurements for the single stage High ϕ^* build. (Measurements downstream of the stator row have been specially included in this case; Figure 39c.) It was found that instead of an increase in velocity and total pressure ahead of the rotor, there was a marked decrease in both these quantities. The outer wall static pressure was still higher in the stall cell than in the unstalled flow, but did not exceed atmospheric pressure as in all preceding cases. The reason for the change in cell behaviour is unknown, and without further information it is not possible to say whether these changes are common to all single stage builds of relatively high design flow rate, or just a peculiarity of the particular builds tested.

The measurements downstream of the stator, Figure 39c , show an annular region of stalled flow near the blade tip. The velocities in this region are exceedingly low and the angle measurements show the flow to be predominantly in the tangential direction. This suggests axisymmetric stall near the outer wall, which is surprising in view of the rotating stall elsewhere. A similar observation was made when the compressor build was tested during full-span stall; Figure 37c. Part-span stall thus resembles full-span stall from this point of view, but in all other respects, the part-span behaviour of the cells in this group of compressors is very different from the behaviour in either full-span or part-span stall in any of the other builds.

It is interesting to note that as the velocity and total pressure falls in the stall cell ahead of the rotor in Figure 39a, these part-span measurements are the only ones to support the classical idea of stall in which the cell is viewed as an inactive region of dead fluid.

Summary

Section 4.1

The total-to-static pressure rise characteristics of four groups of compressors of various numbers of stages have been presented with emphasis on the stalled part of the characteristics. The compressor designs covered a wide range of flow rates and included one group of 65% reaction; the other groups were all of 50% reaction. It was shown that the peak pressure rise in each case is proportional to the design flow rate and that, at shut-off, the pressure rise appears to be almost independent of the compressor design. The static-to-static characteristics of the four 3-stage compressors were presented for comparison with the total-to-static characteristics, and examples of the individual stage characteristics were given. In the latter case, it is found that the last stage in a multi-stage compressor appears to perform less efficiently than the preceding stages, and when only one stage is present, this stage performs like the last stage in a multi-stage build.

Section 4.2

The overall behaviour of the stall cells in the various compressor builds were considered in this section. It was found that full-span stall was always associated with a single stall cell and that part-span stall always gave a higher pressure rise, and rotated

at greater speed than part-span stall. The speed of rotation of the full-span cells was found to be weakly influenced by the operating flow rate of the compressor, but to be markedly dependent on the number of stages in the build. The circumferential extent of the cell was shown to be directly related to the operating flow rate.

Section 4.3

The phase-lock sampling measurements of full-span stall in the 3-stage, 50% reaction, compressors were presented and analysed from the point of view of cell structure. In all cases, it was found that the stall cells extend axially through the blade rows, and that the behaviour of the stalled flow in each stage of the compressor was similar. A study of the details of the flow showed the unstalled part of the annulus to operate qualitatively as if there were no stall cells in the compressor. In the cell itself, the flow was shown to be strongly three-dimensional, especially in the lower flow rate builds, and was characterised by high tangential velocities ahead of the rotor and low velocities behind. Marked areas of reversed flow were found in the higher flow rate builds. The overall pattern of the flow in the cell was shown to be generally unchanged by a change in blade-row spacing or design reaction, but the precise details of the flow were found to be strongly influenced by the design flow rate of the compressor.

Section 4.4

Flow measurements were presented for the single stage builds of the three 50% reaction compressors. These were compared with the results of the 3-stage builds, and it was shown that the stall cell in a single stage build is, in some ways, different from that in a multi-stage build. The differences concerned the radial shape of the

stall cell, a change from full-span to part-span stall in the case of the Low ϕ^* compressor, and the blurring of the distinction between stalled and unstalled flow. It was concluded that the flow details of a single stage build should not be expected to apply to a multi-stage compressor.

Section 4.5

Examples of part-span results were presented to show that in most cases, part-span stall is very similar in structure to full-span stall. Some exceptions were noted however, but these were only observed in two single stage builds of high design flow rate.

CHAPTER 5

Discussion of Experimental Results

In this chapter, the unsteady measurements are analysed from the point of view of obtaining an overall model of the flow, which can then be used to describe the stalled behaviour of an axial flow compressor. Although greatest use will be made of the three stage results, the basic conclusions are applicable to all the other compressor builds tested and are intended to be of interest during both full-span and part-span stall.

The discussion has been divided into four parts. The first, Section 5.1, is concerned with the kinematics of the flow in the compressor, i.e. with the patterns of the fluid motion in and around the stall cell. The questions considered here are those of cell structure, axial movement of the fluid in the stalled region, the effect of stall on the torque and temperature characteristics, and the details of the unstalled flow surrounding the cell. These topics all rely on a study of the velocity and flow direction measurements. In Section 5.2, the emphasis is shifted to the unsteady pressure measurements, where the radial and circumferential gradients in the static pressure are considered. Some attention is given to the question of absolute pressure levels in the stall cells, and an analysis is undertaken of the influence of a rotating disturbance on the flow fields upstream and downstream of the compressor. In Section 5.3, the velocity and pressure fields considered in the previous sections are brought together to produce an overall model of the flow. This model is then used to study the effect of rotating stall on the compressor performance and to explain the relationships between the various types of pressure rise characteristics.

Finally, in Section 5.4, a comparison will be made between the ideas proposed here and those to be found in the literature.

5.1 Kinematics of Stalled Flow in Axial Compressors

The first part of this section is devoted to the description of a fundamental cell structure, which is applicable in all cases, and can be used to explain the similarities in the measurements obtained from the various compressor builds. Once the existence of such a generalised structure has been established, the details of the flow in the different configurations can be examined more precisely and related to the external features which characterise the performance of a compressor operating in stall.

5.1.1 Stall Cell Structure

a) Evidence from unsteady measurements

From the velocity and flow direction measurements presented in the previous chapter, a number of general observations can be made about the flow in a stalled compressor. It is clear that in most cases the flow can be divided into distinct areas of stalled and unstalled flow. In the unstalled area, the flow appears to behave as it would under steady conditions, i.e. as if there were no stall cell in the compressor at all. In the stalled area, on the other hand, the results suggest a basic structure to the flow which is responsible for the measurements from each compressor build being generally similar. In this respect, it was found that ahead of the rotors the velocities in the stall cell were consistently near blade speed, and always in the direction of rotation. Behind the rotors, the velocities were much lower by comparison and less predictable in direction. This pattern of high velocities ahead of the rotors and

low velocities behind, was observed in all the compressor builds and in the multi-stage configurations gave rise to a cell profile which was invariably found to be axial.

The fact that the stall cell extends axially through the multi-stage compressors has been verified by numerous measurements, apart from those presented in the previous chapter. This observation is surprising in view of the conventional idea of stall cell structure. In the past, it has been assumed (27) that the stall cell may be viewed as an inactive region of dead fluid, which extends through the blade rows like the wake of a bluff body. Under these conditions, the edges of the cell would coincide with streamlines in the unstalled flow surrounding the cell. The present measurements show, however, that the speed of the cell in all the multi-stage builds is such that, for the edges of the cell to form streamlines in the unstalled flow, the cell would need to assume an obvious helical twist. The consistent recording of high tangential velocities in the stalled region, and the fact that the cell does not exhibit a helical twist, suggests that the cell structure cannot be like that of a dead wake and, therefore, some alternative structure must be considered.

It should be emphasised at this point that the cell structure referred to here is concerned only with the details of the flow within the blade rows of the compressor itself. The behaviour of the velocity distortion in the swirling flow downstream of the last stator row is not of interest.

To investigate the question of cell structure in greater detail, consider the sketch given below in which the compressor annulus has been unwrapped at the mean radius. An axial stall cell is superimposed on the blade rows and is shown moving to the left in

low velocities behind, was observed in all the compressor builds and in the multi-stage configurations gave rise to a cell profile which was invariably found to be axial.

The fact that the stall cell extends axially through the multi-stage compressors has been verified by numerous measurements, apart from those presented in the previous chapter. This observation is surprising in view of the conventional idea of stall cell structure. In the past, it has been assumed (27) that the stall cell may be viewed as an inactive region of dead fluid, which extends through the blade rows like the wake of a bluff body. Under these conditions, the edges of the cell would coincide with streamlines in the unstalled flow surrounding the cell. The present measurements show, however, that the speed of the cell in all the multi-stage builds is such that, for the edges of the cell to form streamlines in the unstalled flow, the cell would need to assume an obvious helical twist. The consistent recording of high tangential velocities in the stalled region, and the fact that the cell does not exhibit a helical twist, suggests that the cell structure cannot be like that of a dead wake and, therefore, some alternative structure must be considered.

It should be emphasised at this point that the cell structure referred to here is concerned only with the details of the flow within the blade rows of the compressor itself. The behaviour of the velocity distortion in the swirling flow downstream of the last stator row is not of interest.

To investigate the question of cell structure in greater detail, consider the sketch given below in which the compressor annulus has been unwrapped at the mean radius. An axial stall cell is superimposed on the blade rows and is shown moving to the left in

low velocities behind, was observed in all the compressor builds and in the multi-stage configurations gave rise to a cell profile which was invariably found to be axial.

The fact that the stall cell extends axially through the multi-stage compressors has been verified by numerous measurements, apart from those presented in the previous chapter. This observation is surprising in view of the conventional idea of stall cell structure. In the past, it has been assumed (27) that the stall cell may be viewed as an inactive region of dead fluid, which extends through the blade rows like the wake of a bluff body. Under these conditions, the edges of the cell would coincide with streamlines in the unstalled flow surrounding the cell. The present measurements show, however, that the speed of the cell in all the multi-stage builds is such that, for the edges of the cell to form streamlines in the unstalled flow, the cell would need to assume an obvious helical twist. The consistent recording of high tangential velocities in the stalled region, and the fact that the cell does not exhibit a helical twist, suggests that the cell structure cannot be like that of a dead wake and, therefore, some alternative structure must be considered.

It should be emphasised at this point that the cell structure referred to here is concerned only with the details of the flow within the blade rows of the compressor itself. The behaviour of the velocity distortion in the swirling flow downstream of the last stator row is not of interest.

To investigate the question of cell structure in greater detail, consider the sketch given below in which the compressor annulus has been unwrapped at the mean radius. An axial stall cell is superimposed on the blade rows and is shown moving to the left in

the absolute reference frame.

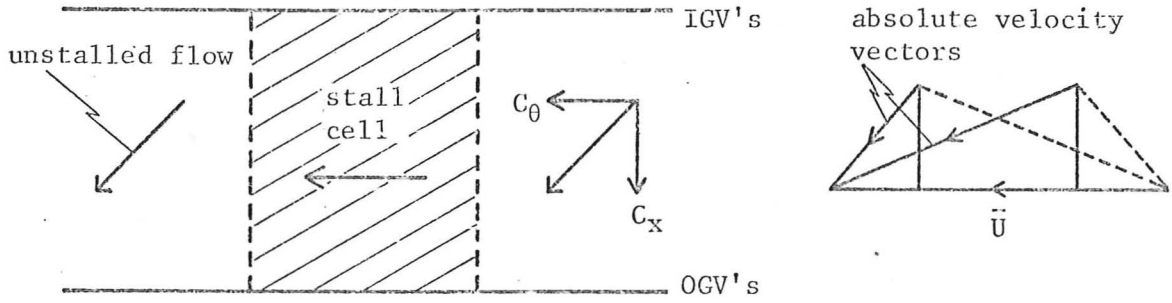

The edges of the cell have been drawn parallel. This was usually found to be the case; except in the Low ϕ^* build where the left-hand edge of the cell sloped inwards, thereby reducing the width of the cell at the rear of the compressor. This decrease in width was, in any case, only of the order of 10% of the width at inlet, and therefore may be neglected here.

The unstalled flow surrounding the cell has a mean flow direction as indicated by the arrows in the sketch. This flow has a component of whirl in the tangential direction which, for a 50% reaction compressor, is always equal to half the mean blade speed, i.e. $.5\ \bar{U}$. (This can be seen by taking the mean tangential component of the two absolute velocity vectors in the triangles on the right-hand side of the sketch.) In the absolute frame of reference, the unstalled flow thus has a component of movement in the same direction as that of the stall cell. It follows, therefore, that if the speed of the cell is equal to 50% of the rotor speed, there will be no interaction between the stalled and unstalled parts of the flow. If, on the other hand, the stall cell is moving at a lower speed, say 30% (which is roughly the case in all the 3-stage builds), the unstalled flow will be going faster than the stall cell, and fluid will have to cross from one side of the stalled region to the other in order to preserve continuity in the tangential direction.

This simple argument, based on the axial profile of the cell

and the relative speeds of the stalled and unstalled parts of the flow, gives rise to a picture of the flow in the compressor which can be illustrated by the sketch in Figure 40. The sketch is drawn in the absolute reference frame and shows a slow moving cell ($V_{cell} < .5 \bar{U}$), in which unstalled flow crosses the cell from one side to the other. It should be noted that this figure is only intended to illustrate tangential movement in the stalled region, and does not take into account any flow which might be drifting through the cell in the axial direction. The question of axial movement in the stalled region will be considered separately in the following section, i.e. 5.1.2.

The picture of the cell in Figure 40 is supported by the repeated observations of high tangential velocities in the stall cell. However, before examining the unsteady measurements for further support of this type of flow structure, the question of mass transfer across the stalled region should be considered in greater detail. It was suggested by Rannie (27) that mass transfer was an "unlikely result", and so it is important not only to establish the feasibility of such flow, but also to determine what behavioural characteristics might be expected of a cell with this type of structure. In the following sub-section it is therefore proposed to examine the idea of an axial cell structure within the context of an ideal compressor.

b) Study of cell structure in an ideal compressor

Consider an idealised compressor of 50% reaction in which the stall cell extends axially through the blade rows. The rotor and stator blade chord lengths are assumed equal, and the gaps between the blade rows are provisionally taken to be infinitely small. A sketch is given below, drawn in the absolute reference frame, showing the stall cell on the unwrapped annulus of a 3-stage compressor. Only

that part of the flow between the trailing edges of the IGV's and the exit plane of the last stator row is considered here.

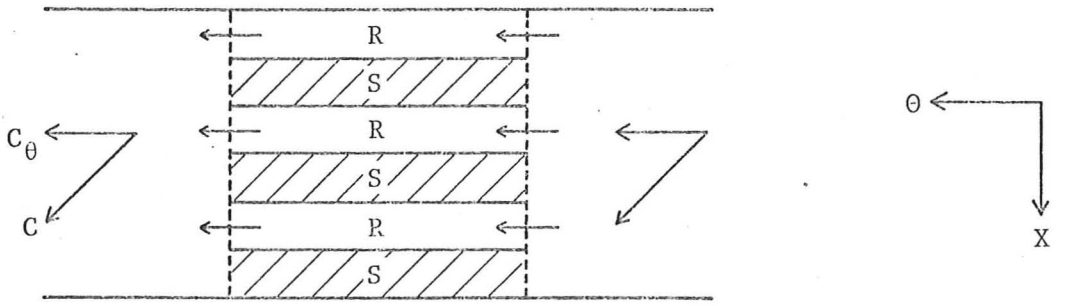

If it is assumed that there is no axial movement of the fluid in the stall cell, then, under ideal conditions, the flow trapped in the stator blade passages will be stationary, while the flow in the rotor blades will be transported in the tangential direction at blade speed, i.e. $\bar{U}$. As the axial projection of the rotor blades occupies half the cross-sectional flow area in the meridional plane, A_θ , the net mass of the fluid being transported to the left in the stall cell at any instant is given by: $\frac{1}{2}\rho A_\theta \bar{U}$. In the unstalled flow, on the other hand, the mean tangential velocity in a 50% reaction compressor is $.5\ \bar{U}$ over the entire flow area, and so the mass being transported to the left in this region is also $\frac{1}{2}\rho A_\theta \bar{U}$. In terms of tangential continuity, therefore, the stalled and unstalled flow regimes are entirely compatible, and the concept of an axial cell structure is physically plausible under the assumed conditions.

It should be noted that, as the two flow regimes are compatible at every instant in time, the speed of rotation of the cell will have no effect on the details of the flow in the stalled region; the fluid in the stators will always be instantaneously stationary and that in the rotors, always instantaneously moving at blade speed. This study of the cell structure is, therefore, not expected to provide any useful information towards solving the problem of predicting the speed of rotation of the stall cell.

In the preceding argument it was assumed that the gaps between the blade rows were vanishingly small. If the compressor is now expanded in the axial direction to create gaps of finite size, the area in the stall cell available for tangential mass transfer will be increased. At the same time, the length of the cell boundaries will be increased proportionately, thus allowing more fluid to enter the cell. It follows, therefore, that if the stalled and unstalled parts of the flow are to remain compatible and the cell to retain its axial orientation, then the area-averaged tangential velocity of the fluid in the gaps between the blade rows in the cell must be equal to $.5\,\bar{U}$ for a 50% reaction compressor. The unsteady measurements can be used to ascertain whether this is true for the flow in a real compressor, a point which will be considered in the following section.

If the camber angle and chord length of the rotor and stator blades are held equal, but the stagger of one of the blade rows is altered to change the reaction of the compressor, as was done in the present tests, the axial structure of the cell will not necessarily be affected. This can be seen by considering the blades and velocity triangles shown below for an ideal compressor of high reaction.

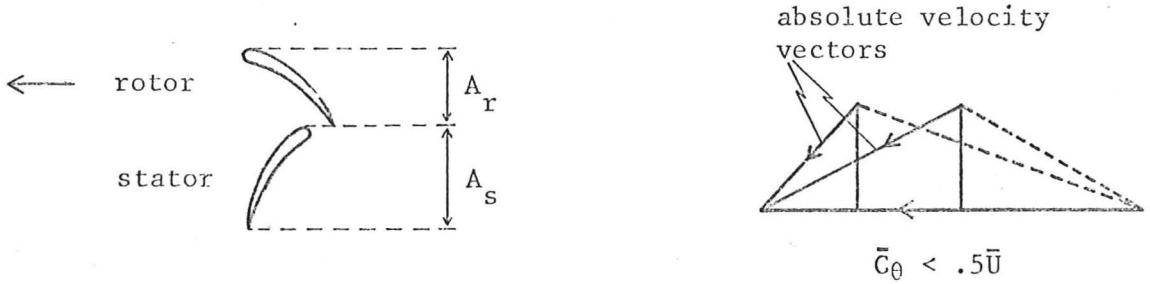

The axial projections of the blade chord lengths show that the cross-sectional area available for tangential movement of the fluid in the stall cell, will be reduced by an increase in design

reaction. But, from the velocity triangles it can be seen that, at the same time, the mean tangential component of the two absolute velocity vectors has been reduced below .5 $\bar{U}$. The changes which occur in the stalled and unstalled areas are therefore complementary, and so a change in design reaction (over a limited range) is not likely to produce any noticeable change in overall cell structure.

Consider now the case in which the rotor and stator blades are of markedly different chord lengths. Under these conditions, the only way in which the capacity of the stalled blades to transport fluid across the cell can be matched with that of the unstalled flow to supply fluid to the cell, would be for the cell to assume a helical twist. The sense of this twist would naturally depend on whether the rotor blades are larger than the stators, or vice versa. This shows that the preceding cases in which an axial cell was necessary to satisfy the continuity requirements were, in fact, special cases of an infinite range of possible cell configurations. Only in those instances where the mass transfer capabilities of the two flow regimes are equal, will the stall cell actually maintain an axial profile. It is unfortunate that no example of a cell exhibiting a helical twist was obtained in the present work to confirm these ideas, as all the blade rows used were of equal chord and thus correspond to the special case in which the cell is axial.

Having examined the feasibility of a cell structure in which mass transfer is acceptable, it will be useful to make a comparison between this type of structure and that of a cell considered as a dead wake. The fundamental differences between the two types of cells are illustrated in the figures below; both of which are drawn in the cell reference frame.

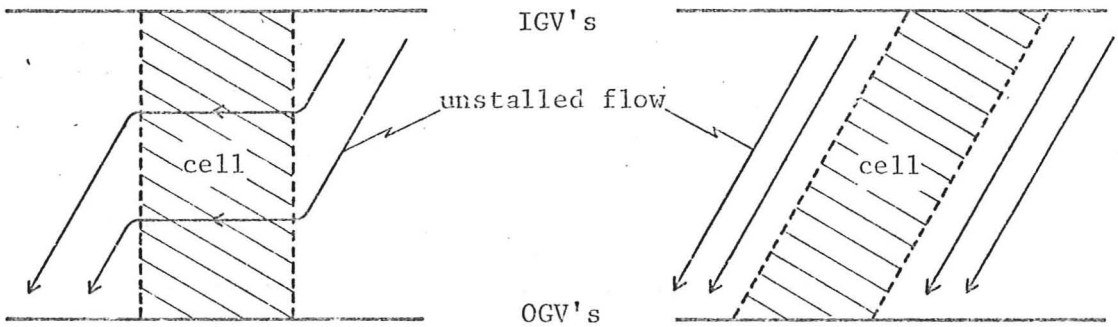

ACTIVE CELL STRUCTURE PASSIVE CELL STRUCTURE

In the case of the active structure, so called to distinguish it from that of a dead wake, the profile of the cell is independent of the cell speed, and continuity between the stalled and unstalled parts of the flow is maintained by the transfer of fluid from one side of the cell to the other. Alternatively, in the passive case, interaction between the two flow regimes is precluded by assuming the edges of the cell to be streamlines in the unstalled flow. The helical angle of the cell is, therefore, dependent on the speed of rotation of the cell.

The concept of a dead wake type of cell structure makes no provision for the influence of the physical movement of the blade rows through the stalled region. In this sense, the active cell structure would appear to be more practical and is, in fact, the mode of operation supported by the experimental results; as will be demonstrated below.

c) Experimental support for active cell structure

By considering the flow in an idealised compressor, it has been shown that the model of the stalled flow given in Figure 40, is physically plausible. It remains to be shown that the experimental results support the consequences of this type of structure, and to see how well conditions in the real compressor reflect those deduced from the idealised assumptions.

It has been shown that the fundamental feature which characterises an active, axial, cell is that the rate of mass transfer in the tangential direction is the same in the stalled and unstalled parts of the annulus. In the 3-stage 50% reaction compressors, the mean tangential velocity in the unstalled flow is equal to $.5\ \bar{U}$. From the detailed velocity measurements it should therefore be possible to show that this is also true of the flow in the stall cell. In this respect, it should be noted that the experimental results can only provide information about the flow in the gaps between the blade rows, but, if there is little axial movement in the stall cell, the preceding analysis suggests that this requirement will automatically be true for the flow within the blade rows themselves.

The results in Figure 26 give the tangential components of velocity at the circumferential centre of the stall cell measured at five radial positions before and after the first rotor in the 3-stage compressor builds. (As the flow patterns in a multi-stage compressor have been shown to repeat stage-by-stage, it will suffice to examine the flow in the first stage only.) Furthermore, explorations with the kinked hot-wire probe, illustrated on page 58, suggest that the axial variation in velocity across the gaps is small, and therefore the velocities in Figure 26 can be taken to represent the mean velocity of the flow between the blade rows. By graphical integration of the measurements before and after the rotor, the following area averaged velocities were obtained for the tangential flow in the three compressor builds:

Low ϕ^*	$\bar{C}_\theta = .51\ \bar{U}$
Intermediate ϕ^*	$\bar{C}_\theta = .54\ \bar{U}$
High ϕ^*	$\bar{C}_\theta = .49\ \bar{U}$

In each case the mean velocity is near $.5\ \bar{U}$. Since the velocity of the stall cell itself is only $.3\ \bar{U}$, these measurements firmly establish the existence of tangential flow through the cell, and provide convincing support for the concept of an active cell structure.

It is of interest to note that, while the fluid crossing the stall cell might well do so in both the gaps before and after the rotor, the experimental results show quite clearly that the greater part of the fluid is concentrated in the gap ahead of the rotor. The fluid in the gap behind the rotor is inactive by comparison. It appears that any high velocity fluid drifting out of the stalled rotor blades always does so on the upstream side, irrespective of the sense of the local pressure gradient across the blade row. Similar observations have been made by Dunham (13), Pavlenko (35) and Tanaka and Murata (32) in compressors of widely different designs. Centrifugal effects in the blade passages may be partly responsible for this, but, until a suitable explanation for the apparent upstream bias is found, it will not be possible to make any real progress towards predicting the compressor performance from first principles.

A corollary of the concept of an active cell structure is that the inclination of the cell profile, which is axial in the present case, is independent of the speed of rotation of the cell. It is not possible to check this point directly as the speed of rotation cannot be independently varied. However, the cell speed does change with the number of stages in the build (Figure 19) and in the two, three and four stage compressors, where it was possible to monitor the shape of the cell, no deviation from an axial profile was observed. If, on the other hand, the structure of the cell was more like that of a dead wake, the cell would have assumed an

obvious helical twist at the speeds shown in Figure 19, and the angle of this twist would have altered from build to build.

It was also suggested in the previous section that the structure of the cell should be unaffected by a change in design reaction, or by a change in blade row spacing. Both of these points were verified over a limited range by results obtained during the current experimental program. With regard to the first point, it will be recalled that the testing of a 65% reaction build led to the conclusion that an increase in reaction had little effect on the details of the flow in the stalled region or on the axial nature of the cell. The influence of blade row spacing was investigated when a special build of the 3-stage Low ϕ* compressor was tested with greatly reduced spacing. The results of this experiment were quoted in the previous chapter and show that, apart from a small change in the radial shape, the basic structure of the cell was unaffected by the change in gap/chord ratio.

The concept of an active cell structure is thus supported in most respects by the experimental results, and the sketch given in Figure 40 can therefore be regarded as a reasonable model of the flow in the compressor. It should be emphasised that although multi-stage data has been used to study the cell structure, the concept of an active cell, in which the stalled blades behave as crude paddle wheels, is not restricted to multi-stage blading. The orientation of the cell, as such, is obviously not an important factor in short compressors such as single stage or isolated rotor builds, nevertheless, the fundamental idea of mass transfer across the cell, due to the physical influence of the rotor blades moving through the retarded flow, is applicable in all cases.

5.1.2 Axial Movement of Fluid in the Stall Cell

The description of the cell structure given in the previous section was predominantly concerned with flow in the tangential direction; in fact, all flow in the axial direction was assumed negligible. It can be seen from the experimental results, however, that, although small by comparison with the tangential flow, a certain amount of fluid does move axially through the blade rows. This axial movement may manifest itself as either a net flow towards the front or back of the compressor, or else as a recirculation within the blade rows themselves.

The first of the two sub-sections which follow, is concerned with the question of net axial drift in the stall cell and the possible influence of this flow on the behaviour of the compressor as a whole. In the second sub-section, attention is given to the finer details of the flow within the blade rows, and an attempt made to show how the tangential and axial components of the velocity are combined in the different compressor builds to produce the observed three-dimensional flow patterns.

a) Axial drift and continuity equation

The axial movement of fluid through a compressor is most easily studied by considering the flow direction measurements in the plane behind the rotor. The flow is usually less tangential in this region and, therefore, the angles provide a clearer indication of the sense of the flow. The appropriate measurements for the 3-stage builds are given in Figure 22, where it can be seen that the details of the flow in each build are different. To assist with the interpretation of these measurements, a pictorial sketch is provided in Figure 41 showing the flow patterns in the Intermediate ψ^* build.

Although this sketch is only a two-dimensional view of a highly complex three-dimensional situation, it can be seen that the stall cell may be divided into two parts: one in which the flow has an axial component of velocity towards the front of the compressor, i.e. reversed flow, and the other in which the axial component of the flow is towards the rear of the compressor, i.e. through-flow.

In the Intermediate ϕ^* build, the areas of reversed and through-flow appear to be of roughly equal proportions, but the measurements of Figure 22 indicate that this is not true for the other two builds. The Low ϕ^* compressor shows a complete absence of reversed flow, while in the High ϕ^* build, the measurements suggest that almost the entire cell is occupied by this type of flow. In terms of through-flow and reversed flow, the situation in the three compressor builds can be summarised by the sketches given below.

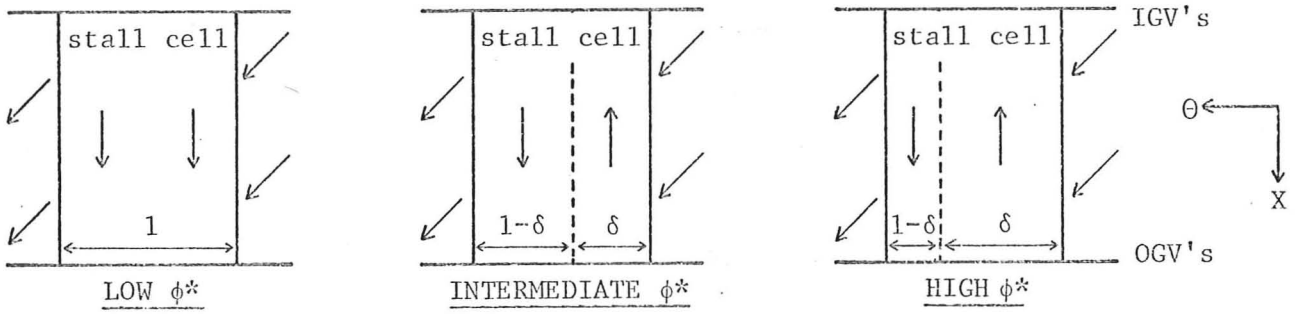

It should be noted that these sketches are only representative of conditions in the three stage builds. In the sense considered here, the details of the flow are influenced by the number of stages in the compressor - as was demonstrated when the single stage results were compared with the 3-stage measurements in the previous chapter and were found to be somewhat different.

If a mean axial velocity component is assumed for each of the various parts of the flow field, then a simple continuity equation can be written to express the net flow through the annulus in any of the compressor builds. If δ is the fraction of the cell

occupied by reversed flow and $1-\delta$ the through-flow fraction, and if λ represents the total fraction of the annulus covered by the stall cell, then the following equation can be used to represent the flow in the compressor:

overall flow rate = unstalled flow + through flow − reversed flow

i.e. $$\rho A_x \bar{C}_x = \left((1-\lambda) C_{x_{us}} + (1-\delta)\lambda C_{x_{+s}} - \delta\lambda C_{x_{-s}} \right) \rho A_x$$

where $\bar{C}_x$ is the velocity of the net flow averaged over the whole annulus area, and $C_{x_{us}}$ is the axial component of the unstalled flow surrounding the cell. The symbols $C_{x_{+s}}$ and $C_{x_{-s}}$ respectively, represent the positive and negative components of velocity in the stall cell. Since the annulus area, A_x, appears on both sides of the equation and changes in density can be ignored, the equation can be expressed more simply in terms of axial velocity coefficients:

$$\bar{\phi} = (1-\lambda)\phi_{us} + (1-\delta)\lambda\phi_{+s} - \delta\lambda\phi_{-s}$$

By using this equation to relate the circumferential extent of the stall cell, λ, to the overall flow rate, $\bar{\phi}$, it is possible to show how the axial movement of relatively small amounts of fluid through the stall cell can influence the behaviour of the compressor as a whole. To illustrate this point, two examples of the relationship between λ and $\bar{\phi}$ will be considered below; one for the Low ϕ^* build and the other for the High ϕ^* build.

Consider first the Low ϕ^* compressor. In this case there is no reversed flow in the stall cell and so $\delta = 0$. Taking $\phi_{us} = .35$ and $\phi_{+s} = .1$, which are approximate values estimated from the velocity measurements, the above equation reduces to:

$$\bar{\phi} = (1-\lambda)\ .35 + .1\ \lambda + 0$$

i.e. $$\lambda = (.35 - \bar{\phi})/.25$$

Thus, $\lambda = 1$ when $\bar{\phi} = .1$, signifying that the stall cell will cover the entire annulus area when the compressor flow rate is still positive. This conclusion is supported by the relationship between λ and $\bar{\phi}$ obtained by direct measurement; as shown in Figure 20.

Similarly, for the High ϕ^* build, taking $\delta = .85$, $\phi_{us} = 1.15$ and $\phi_{+s} \sim \phi_{-s} \sim .2$, as suggested by the unsteady measurements, the continuity equation becomes

$$\bar{\phi} = (1-\lambda)\ 1.15 + .2\ (1 - .85)\ \lambda - .2\ (.85)\ \lambda$$

giving

$$\lambda = (1.15 - \bar{\phi}) \ / \ 1.29$$

Here, $\lambda = 1$ when $\bar{\phi} = -.14$, thus indicating that the stall cell will not cover the entire annulus at shut-off, i.e. at $\bar{\phi} = 0$. As before, this is in agreement with the measurements in Figure 20, where it can be seen that in this build the stall cell occupies only 89% of the compressor annulus at $\bar{\phi} = 0$.

The two examples considered here provide some idea of the possible order of magnitude of the axial drift through the stall cell and show how the sense of the net drift, either positive or negative, can influence the overall behaviour of the compressor. In the Low ϕ^* build, where the stall cell reaches maximum size at a positive flow rate, rotating stall is replaced by axisymmetric stall with an accompanying discontinuity in delivery pressure rise, as can be seen from the three stage characteristic in Figure 8. Alternatively, in the High ϕ^* build, rotating stall is still present at $\bar{\phi} = 0$ and so the characteristic shows no obvious change in behaviour as the flow rate approaches zero; Figure 11.

With regard to the general question of axial drift in the stalled region, it will be recalled that Dunham (14), McKenzie (16) and Gray (17) assumed positive flow, zero flow and negative flow in

the stall cell, respectively. From the above discussion, it is clear that these assumptions are based on an over-simplified concept of the cell as, in reality, both positive and negative flow can exist simultaneously in the stalled region. The continuity equation used here makes provision for a slightly more realistic model of the flow; but is not of any great use without prior knowledge of the details of the flow in the stall cell.

The division of the cell into areas of positive and negative drift is not always possible. It has been done here on a one-dimensional basis for the three stage compressor builds in order to demonstrate the existence, and effects, of axial drift. It could not have been done in the single stage builds, for example, where the distinction between stalled and unstalled flow is less clearly defined. The finer details of the cell structure in each compressor build are different, but, by studying specific examples in this way, some understanding is gained of how axial flow in the stall cell can influence the overall performance of the compressor.

b) Three-dimensional flow details

In this section, the flow in the two compressors used as examples above will be considered in greater detail to show how the actual flow patterns in the stall cells give rise to the observed movement of fluid in the tangential and axial directions. As before, the Intermediate ϕ^* compressor will not be specifically examined, as the behaviour of this build may be regarded as a compromise between that of the other two builds.

Sketches were provided in the previous chapter (page 71) to assist with the visual interpretation of the flow patterns obtained from the velocity and direction measurements. For the purpose of

the present discussions, similar sketches for the Low and High ϕ^* builds are repeated below:

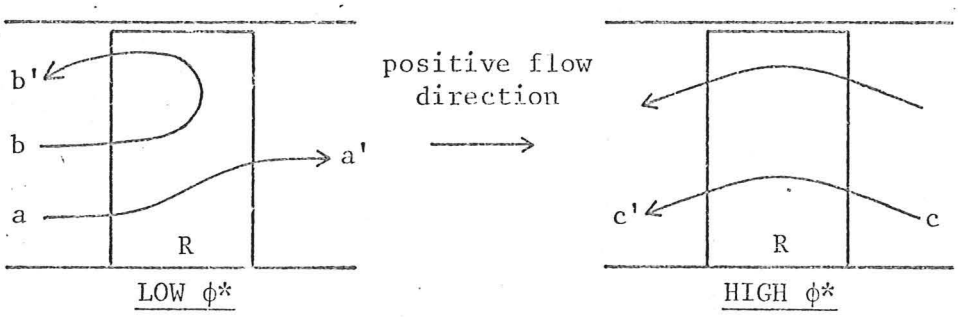

LOW ϕ^* HIGH ϕ^*

In the Low ϕ^* build, the flow pattern is strongly three-dimensional, and shows movement of fluid in both the positive and negative x directions. Part of the flow entering the rotor at the hub moves through the blade row and emerges from the trailing edge plane with a comparatively low velocity and in a direction which is predominantly tangential, i.e. at 70^o or 80^o to axial. The remainder of the flow entering the rotor is centrifuged outwards and at the same time acquires a very high velocity in the whirl direction. This centrifuged fluid leaves the blade row on the upstream side with a small component of velocity in the negative direction (100^o to downstream axial) and, after interacting with any blade row ahead of the rotor (either stator or IGV), may re-enter the rotor in a recirculatory fashion. It should be stressed, however, that the velocities in the tangential direction are much greater than those in the meridional plane shown here, and therefore a particular fluid particle may only complete a fraction of this cyclic process in the time it takes for the particle to move from one side of the cell to the other.

In the High ϕ^* build, the flow is more two-dimensional in nature and moves consistently in the reversed flow direction, i.e. negative x . The fluid entering the rotor does so at a very oblique angle, as in the absolute reference frame it is moving in a counter-

rotational direction ($\sim 250^{\circ}$ to downstream axial) with a velocity which is sometimes as high as $.5\ \bar{U}$. Considerable losses must occur during the actual entry process, but once the fluid emerges from the upstream side of the blade row it has acquired a velocity which is well in excess of that of the blades themselves; sometimes as high as $1.5\ \bar{U}$. It is only through the presence of a net flow in the reversed direction that these exceedingly high velocities ahead of the rotor can be explained.

The two examples given here show how, in spite of the marked differences in detail, both flow patterns lead to high tangential velocities ahead of the blade row and, thus, provide the tangential mass transfer necessary to sustain an active cell structure. The examples also show that the overall axial drift observed in the two compressors, i.e. negative flow in the High ϕ^* build and positive flow in the Low ϕ^* build, can be related to the precise details of the flow within the blade rows. A further point about these two flow patterns is that, although they both give rise to the same delivery pressure during stall, the differences in momentum changes which occur lead to noticeable differences in the torque and temperature rise characteristics of the two compressors. This aspect is discussed in the following section.

5.1.3 Torque Measurement and Energy Dissipation

The torque characteristics for the 3-stage builds of the Low and High ϕ^* compressors are shown in Figure 17. During unstalled operation it is to be expected that the torque levels in these two machines will be different due to the difference in design blade loading. Near the shut-off point, however, where the overall pressure rise produced by the two builds is roughly equal, the sustained high

level of the torque in the High ϕ^* build, can only be explained in terms of greater energy dissipation in the stall cell. In the discussion which follows, an attempt will be made to relate the momentum changes taking place in the stall cell to the measured torque characteristics, and to examine the questions of energy dissipation and temperature rise.

The picture of the cell structure given in Figure 40 suggests that the fraction of the total torque attributable to the stalled part of the flow could be calculated solely from the momentum changes which occur at the edges of the cell, since, under ideal conditions, the flow in the centre of the cell would require very little work to keep it moving in the tangential direction. In reality, however, there is always some axial movement of the fluid in the cell, either due to meridional recirculation or net axial drift, leading to interaction between the rotor and stator rows and so to the dissipation of large amounts of energy. The actual amount of energy dissipated will depend on the precise details of the flow in the stall cell. To explain why the torque measurements indicate greater losses in the case of the High ϕ^* build than in the Low ϕ^* build, the details of the flow in these two compressor builds should be examined more carefully.

In the case of the Low ϕ^* compressor, some of the fluid entering the rotor at the hub drifts axially through the rotor (line a a', page 101), while the remainder experiences recirculation in the meridional plane (line b b'). The mass flow rate of the fluid which passes through the rotor is comparatively small and, as the velocity and flow direction are found to change little in crossing the blade row (Figure 26), the energy absorbed by this fluid is thought to be insignificant. In the case of the recirculating fluid, on the other hand, the velocity changes which occur are considerably

larger. The measurements in Figure 26 show fluid entering the rotor near the hub with a tangential component of velocity of about .5 $\bar{U}$, and leaving the rotor at the tip with a tangential velocity approaching that of blade speed, i.e. 1.0 $\bar{U}$. The net change in tangential velocity undergone by the recirculating fluid is therefore given by:

$$\Delta C_\theta = 1.0\,\bar{U} - .5\,\bar{U}$$
$$= .5\,\bar{U}$$

It is not possible to estimate the mass flow rate of the fluid involved in this recirculatory process, and therefore no momentum change calculations can be made. Nevertheless, when the corresponding velocity change in the High ϕ^* build is calculated, it will become clear why the torque levels in these two compressors should be so different during stall.

The High ϕ^* compressor build provides a more interesting opportunity to study the energy interchange between rotor and stalled fluid, as the cell is roughly two-dimensional and some numerical calculations are possible. It will be recalled that the flow in this build is fairly uniform radially, and that the greater part of the cell, about 85% , is occupied by reversed flow (line c c', page 101). From the velocity and direction measurements of Figures 26 and 27, the following sketch can be drawn to represent the flow passing through the rotor.

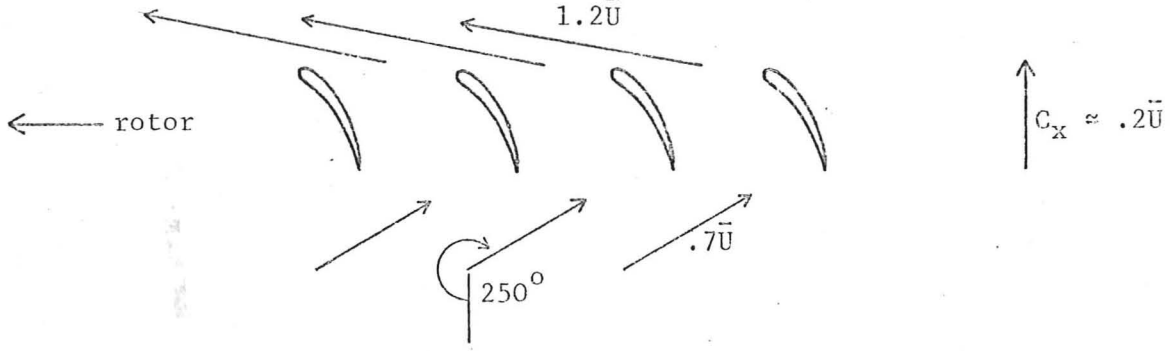

It is surprising to find the fluid entering the blade row at such oblique angles, especially when it is noted that the angles shown here are the absolute ones, not those relative to the moving rotor. Nevertheless, the flow does pass through the rotor, as it is only in terms of reversed flow leaving the blades with a finite relative velocity that the very high absolute velocities ahead of the rotor can be explained.

If the flow direction ahead of the rotor is taken to be more or less tangential, the change in the tangential component of velocity which occurs as the flow passes through the rotor is given by:

$$\Delta C_\theta \simeq 1.2\ \bar{U} - (.7\ \bar{U} \sin 250^\circ)$$
$$\simeq 1.85\ \bar{U}$$

It can be seen that ΔC_θ in this build is almost four times as great as that in the Low ϕ* build. In the present case it is possible, by making certain simplifying assumptions, to estimate the mass flow rate of the fluid undergoing this change in tangential velocity, and thus to calculate the torque absorbed by the stalled flow. Although such a calculation could not be expected to produce any definitive results, it will serve to illustrate how a relatively small rate of axial drift can lead to the dissipation of large amounts of mechanical energy.

For the sake of simplicity, the torque will be calculated at the point where the stall cell covers the entire annulus, i.e. where $\lambda = 1$. By doing so the fraction of the total torque due to the unstalled part of the flow becomes zero, and the momentum changes occurring at the edges of the cell need not be considered. It will also be assumed that the entire annulus area is occupied by reversed flow. It has been shown that this will only be true over 85% of the stalled region in this build, but as the calculation is being undertaken for qualitative rather than quantitative reasons, this

assumption is not considered unreasonable.

The mass flow rate of the fluid drifting through the annulus can be calculated from the mean axial velocity coefficient, which the velocity measurements suggest to be of the order of $0.2\ \bar{U}$. The mass flow rate is therefore equal to $\rho A_x(.2\ \bar{U})$, where A_x is the cross-sectional area of the compressor annulus. This fluid undergoes a change in tangential velocity of $1.85\ \bar{U}$, as shown above, and so for a 3-stage compressor the net torque is given by:

$$\tau = 3(\dot{M}\ \Delta C_\theta\ R_m)$$
$$= 3(\rho A_x .2\ \bar{U} \times 1.85\ \bar{U} \times R_m)$$

where R_m is the mean radius of the compressor. This torque can be nondimensionalized by a reference value, $\frac{1}{2}\rho\bar{U}^2 A_x R_m$, which is the torque associated with the mean blade speed dynamic head acting over the annulus area, A_x, at a radius R_m. The nondimensionalized torque for the fully stalled compressor is thus:

$$\frac{\tau}{\frac{1}{2}\rho\bar{U}^2 A_x R_m} = 2.2$$

By comparing this calculated value with the measured value at shut-off in the High ϕ^* build in Figure 17, it can be seen that the calculated torque is a reasonably good estimate. In making this comparison, it should be recalled that in the real compressor the stall cell does not cover the entire annulus at $\bar{\phi} = 0$.

The above discussion of the tangential velocity changes in the Low and High ϕ^* compressor builds has been intended to demonstrate how the details of the flow in the stall cell can influence the external behaviour of the compressor. It has been shown that even though the rate of axial drift through the cell is small by comparison with the unstalled flow, the changes in momentum which occur in the

stall cell can lead to the dissipation of large amounts of mechanical energy. The precise amount of energy depends on the details of the flow in the stall cell. In so far as an increase in total pressure can be regarded as an indication of energy input, the preceding calculations also show why areas of high total pressure should exist ahead of the rotor blades in the stall cell (Figure 25a,b,c), and why the level of the total pressure in the High ϕ^* build should be greater than that in the Low ϕ^* build.

Having considered the part played by the rotor blades in putting energy into the stalled flow, the role of the stator blades in dissipating this energy should now be considered. The sketches on page 101, used to illustrate the flow patterns in the stall cell, show that in both compressor builds the high velocity fluid leaving the rotor blades has a small negative component of velocity, and will, therefore, impinge at a very oblique angle on the trailing edges of the blades in the upstream stator row. In view of these oblique angles, it is thought that most of the energy in the flow will be dissipated through turbulence and separation and will therefore lead to a temperature rise in the compressor.

The idea that the energy in the fast moving fluid ahead of the rotor is lost, rather than converted to useful pressure, is supported by two observations. Firstly, the regions of high total pressure in the cell are strictly limited to the areas ahead of the rotor rows. This pressure is not convected into the spaces ahead of the stators or into the unstalled flow surrounding the cell, as can be seen from the measurements in Figure 23. Secondly, because the rate of axial drift through the compressor is small, the greater part of the fluid discharging through the exit throttle will have experienced its pressure rise by passing through the compressor in the unstalled state.

It has been shown, however, that a finite amount of energy is also supplied to the fluid in the stall cell, and, as this energy does not leave the compressor in the form of pressure, it must be irreversibly converted to heat and so manifest itself as an increase in temperature.

Although no temperature measurements were taken in the present tests, it was obvious when working on the test rig that the temperature rise in the High ϕ^* build was far greater than that in the Low ϕ^* build. This is to be expected in view of the difference in the flow patterns in these two machines, and provides another example where the details of the flow in the stall cell can be seen to influence the overall behaviour of the compressor.

5.1.4 Details of Unstalled Flow

The discussion so far has centred on the details of the flow in the stall cell. In this, the final section on the kinematics of the flow, brief consideration will be given to certain aspects of the flow in the unstalled part of the annulus.

From Chapter 2 it will be recalled that the parallel compressor models of Dunham, McKenzie, Gray and Fabri all make the suggestion that the unstalled part of the annulus behaves as it would under steady conditions, and that the flow coefficient in this region will be such as to ensure that the unstalled delivery pressure in the exit plane is the same as that in the stall cell. The unsteady flow measurements can be used to determine whether this is, in fact, a correct description of the flow.

To investigate this point, consider the specific example of the 3-stage Intermediate ϕ^* build. The total-to-static characteristic for this build is shown in Figure 42, along with the axial velocity recorded at mid-blade height behind the first rotor. The velocity

trace was taken at a mean flow coefficient of $\bar{\phi} = .33$ and, therefore, a horizontal line has been drawn through the point, B, on the stalled branch of the characteristic corresponding to this flow coefficient. The line can be seen to intersect the steady-state curve at A ; which, according to the parallel compressor model, will be the operating point of the unstalled part of the annulus. The flow coefficient at A is 0.56 , which compares favourably with the value of 0.57 measured in the unstalled part of the flow. Although only one example is given here, the measurements in the other compressor builds all show that the parallel compressor model does indeed provide a realistic method of predicting the flow coefficient in the unstalled part of the annulus.

At this juncture it is convenient to use the information in Figure 42 to check the method of estimating the size of the stall cell from the measured compressor characteristic. It will be recalled from Chapter 2 that the fraction of the annulus occupied by the stall cell is given by

$$\lambda = \frac{\phi_{us} - \bar{\phi}}{\phi_{us} - \phi_s}$$

where ϕ_{us} is the flow coefficient of the unstalled flow (0.56 in this Intermediate ϕ^* case) and $\bar{\phi}$ is the operating flow coefficient (i.e. 0.33). The symbol ϕ_s represents the average axial flow in the stall cell, which, in this compressor build, can be taken to be zero. The fraction of the annulus stalled is therefore given by

$$\lambda = \frac{.56 - .33}{.56 - 0} \times 100 = 41\%$$

which is in reasonable agreement with the value of 39% estimated from the velocity recordings shown in Figure 42. The assumption of zero flow in the stall cell could not have been made for the Low or High ϕ^* builds without introducing errors into the results.

Nevertheless, the present example illustrates how, by assuming zero flow in the stall cell, useful estimates of the size of the stall cell can be obtained from the compressor characteristic.

The parallel compressor model, as applied here, makes the implicit assumption that the velocity in the unstalled part of the annulus is constant and independent of the size of the stall cell. While this is true over the greater part of the operating range, the unsteady measurements show that as the area of unstalled flow becomes very small, the velocity in this region decreases. This effect can be seen in Figure 43, where the unstalled velocity is plotted as a function of cell size for two different compressor builds. The velocity is hardly affected by cell size in the Low ϕ^* build, but in the High ϕ^* case, it falls away quite markedly as the unstalled flow area is decreased. These results are of interest as they question the reason for the linear relationship between cell size and flow rate as suggested in Figure 20, and again demonstrate the complexity of the laws governing rotating stall.

5.2 Pressure Fluctuations During Stall

The picture of the flow in the stalled compressor will now be extended by taking into account the pressure fluctuations which accompany the velocity disturbances considered in the previous section. Attention will be given to the radial and circumferential variations in static pressure within the blade rows and to unsteady effects in the inlet and exit planes.

5.2.1 Static Pressure Gradients in R-θ Plane

Strong radial gradients of static and stagnation pressure are found within the stall cell itself, while circumferential differences

in static pressure exist between the stalled and unstalled parts of the flow. These pressure gradients will be considered below.

a) Radial pressure gradients in the stall cell

The presence of very high tangential velocities ahead of the rotors in the stall cell has been noted many times in the preceding work. These tangential velocities give rise to centrifugal accelerations which must be balanced by radial gradients in static pressure. The resulting difference in pressure between the inner and outer walls can be estimated from the simple radial equilibrium equation:

$$P_{tip} - P_{hub} = \int_{hub}^{tip} \rho \frac{C_\theta^2}{R} dR$$

where R is the radius at any point between the inner and outer wall, and C_θ is the corresponding tangential component of velocity in the stall cell. The variation in C_θ from hub to tip at the circumferential centre of the stall cell in the 3-stage compressor builds, can be obtained from the velocity measurements shown in Figure 26. By substituting the measured values of C_θ into the radial equilibrium equation, estimates of $(P_{tip} - P_{hub})$ can be obtained and compared with the pressure differences shown in Figure 29.

It should be noted at this point that the static pressures shown in Figure 29 were not measured directly, but were calculated from local velocity and total pressure recordings. Outer wall static pressure measurements were taken to check the accuracy of these calculated pressures and in most cases good agreement was observed. The errors which do exist are attributed to the influence of local temperature fluctuations on the hot wire calibration, but as the discrepancies are relatively small, the calculated static pressures are considered accurate enough to give realistic estimates of $(P_{tip} - P_{hub})$.

In the table below, the static pressure differences estimated from the radial equilibrium equation are compared with those obtained from Figure 29. In each case the comparisons are made for the flow ahead of the first rotor.

Compressor build	$(P_{tip}-P_{hub})/\frac{1}{2}\rho\bar{U}^2$ from R.E. equation	$(P_{tip}-P_{hub})/\frac{1}{2}\rho\bar{U}^2$ from Figure 29
Low ϕ^*	.17	.34
Intermediate ϕ^*	.25	.48
High ϕ^*	.43	.47

(Note: In the unstalled flow surrounding the cell, the radial variation in static pressure is of the order of 0.06 $(\frac{1}{2}\rho\bar{U}^2)$ for all three builds.)

In keeping with the fact that the tangential velocities increase with compressor design flow rate (Figure 26), the static pressure differences in both columns can be seen to increase with ϕ^*. The values of ΔP based on the radial equilibrium equation are, however, lower in all three cases than the values suggested by the static pressure in Figure 29. The discrepancies between the two columns suggest that centrifugal effects in the tangential plane are not the only factors causing the radial pressure gradients in the stall cell. Curvature of the streamlines in the meridional plane, or even radial flow itself, may also be contributory factors. In this respect, it is interesting to note that the difference between the values of ΔP in the two columns is largest in the case of the Low ϕ^* build, where the flow is strongly three-dimensional, and smallest in the case of the High ϕ^* build, where the flow is more or less uniform in the radial direction.

In spite of the differences between the two columns, it is

clear that centrifugal effects in the swirling flow ahead of the rotor account for the greater part of the radial pressure gradient in the stall cell. This observation is important in view of the fact that none of the existing rotating stall theories, except that of Fabri, take any account of the centrifugal effects in the stall cell. It is also important because it shows that the rotor and stator rows will perform differently in stalled flow; the former is moving in the absolute reference frame and the latter is not. Thus, even for a high hub-tip ratio compressor, the character of the stalled flow is dominated by radial effects.

b) Mean pressure level in stalled flow ahead of first rotor

It was suggested in the previous chapter that the level of the static pressure in the unstalled part of the flow ahead of the first rotor would be approximately equal to $P_o - \frac{1}{2}\rho C^2$, where P_o is atmospheric pressure and C is the local velocity of the unstalled flow. This suggestion is supported by the measurements in Figure 24a, plane 2, where it can be seen that the static pressure in the unstalled flow decreases markedly with the increase in compressor design flow rate. The level of the pressure in the stall cell, on the other hand, is above atmospheric and roughly the same in each case. A possible explanation for this observation can be found by examining the flow in the stalled part of the annulus ahead of the first rotor.

In Figure 29 it is shown that for the Low ϕ^* compressor build, the radial pressure gradient ahead of the first rotor is centred about atmospheric pressure. This point is more clearly illustrated in Figure 44, where the inner and outer wall static pressures for this build are traced through the compressor inlet as far as the plane ahead of the first rotor. It can be seen that, in contrast with the unstalled flow, the mean pressure in the stall cell remains

approximately equal to atmospheric pressure right up to the rotor inlet. This is attributed to the fact that in a large stall cell, covering a third of the annulus or more, the flow in the area ahead of the cell is almost stagnant, and so the static pressure in this region will be atmospheric. (Unsteady effects in the inlet flow are small by comparison with the pressures being considered and, therefore, need not be taken into account. In any event, it will be shown in Section 5.2.2 that measurements such as these, taken at the circumferential centre of the cell, will not be influenced by any pressure fluctuations due to unsteady effects in the flow.)

In cases where strong reversed flow is absent, it is therefore suggested that the level of the static pressure in the stall cell ahead of the first rotor, should be such that the integral of the pressure over the height of the cell will be equal to atmospheric pressure. When reversed flow is present, atmospheric pressure cannot be assumed in the compressor inlet, and allowance must then be made for the resulting increase in static pressure. Indeed, for the Intermediate and High ϕ^* builds, it can be seen from Figure 29 that the mean pressure level in the stall cell in these two builds is above atmospheric.

It follows from these ideas that if the mean static pressure in the stall cell is approximately atmospheric, then the static pressure recorded on the outer wall in the stalled region will be above atmospheric pressure by an amount roughly equal to half the difference in pressure between hub and tip, i.e. by $\frac{1}{2}(P_{tip}-P_{hub})$. This is confirmed by the measurements in Figure 24a, plane 2, where it can be seen that the outer wall static pressure in the stall cell increases slightly from build to build as the mean pressure level in the cell rises and the size of $(P_{tip}-P_{hub})$ increases.

c) Circumferential pressure gradients

From the outer wall static measurements in Figure 24a,b it can be seen that strong circumferential pressure gradients exist between the stalled and unstalled parts of the flow, especially in the High ϕ^* build. It might be thought that these pressure gradients would play a part in the circumferential movement of fluid in the stall cell, but there is little evidence to suggest that this is true. Ahead of the rotor, the flow is always moving in the whirl direction – even at the very edges of the cell where the pressure gradients indicate that the flow might be induced to move in the opposite direction. More important, however, the circumferential static pressure gradients diminish towards the rear of the compressor and, yet, the velocity and flow direction measurements show that the general behaviour of the flow in the last stage of the compressor is the same as that in the first. From this it would appear that the pressure gradients are more a consequence of the kinematic details of the flow, rather than the actual cause of the flow itself.

5.2.2 Unsteady Effects in Compressor Inlet

The velocity distortions in the compressor caused by rotating stall are responsible for unsteady effects in the compressor inlet. The influence of these unsteady effects is demonstrated for the High ϕ^* build in Figure 33, where it can be seen that the total pressure of the incoming flow is not circumferentially uniform, and that the velocity and total pressure fluctuations are approximately 90° out of phase with each other. In order to explain these observations, and to allow the unsteady effects to be examined in greater detail, an analytic description of the flow suggested by Grietzer will be given below.

As a first approximation, it will be assumed that the flow in the inlet region is irrotational. The measuring plane under consideration is taken to be sufficiently far upstream of the IGV's for the incoming flow to be unaffected by any reversed flow in the stall cell. Experimental evidence suggests that, for this to be true, the plane need not be more than a radius or so upstream of the IGV's and can, in most cases, be far less. Since the compressor is of high hub-tip ratio, the analysis can be done on a two-dimensional basis using a co-ordinate system as shown below.

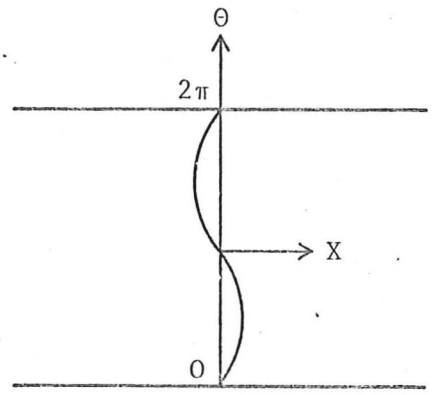

It is assumed that the flow can be represented by a mean velocity component and a superimposed perturbation; which need not necessarily be small. Because the flow is irrotational and incompressible, a velocity potential can therefore be defined for the perturbation, which obeys the equation

$$\nabla^2 \phi = 0$$

A solution to this equation, which has the correct behaviour at upstream infinity, is of the form

$$\phi = \sum_{n=1}^{\infty} A e^{nx/R_m + i\, n(\theta - \sigma t)} \qquad (1)$$

where R_m is the mean compressor radius and σ is the stall cell frequency.

As the axial velocity at any point can be written as:

$$C_x = \bar{C}_x + C'_x$$

it follows from the definition of the velocity potential that:

$$C'_x(x,\theta,t) = \frac{\partial \phi}{\partial x}(x,\theta,t).$$

Consider the velocity perturbations at $x = 0$ to be of the form

$$C'_x(x,\theta,t) = \varepsilon e^{i\,n(\theta-\sigma t)}$$

This means that the constant A in equation (1) will be given by

$$A = \varepsilon R_m/n$$

where ε is the amplitude of the velocity perturbation.

For the sake of simplicity, assume a single stall cell of sinusoidal profile. Only one Fourier component need therefore be considered, and the velocity potential can be written as:

$$\phi = \varepsilon R_m e^{x/R_m + i(\theta-\sigma t)} \tag{2}$$

The first integral of the momentum equation for incompressible flow is

$$P'_o = -\rho \frac{\partial \phi}{\partial t} \tag{3}$$

where P'_o is the total pressure perturbation. From equations (2) and (3),

$$P'_o = -\rho(-i\sigma)\varepsilon R_m e^{x/R_m + i(\theta-\sigma t)}$$

which, at $x = 0$, gives:

$$P'_o = \rho i\sigma\varepsilon R_m e^{i(\theta-\sigma t)}$$

and as $\varepsilon e^{i(\theta-\sigma t)}$ is equal to velocity perturbation C'_x, it follows that

$$P'_o = \rho\sigma R i(C'_x)$$

This expression shows that the total pressure in the inlet will not be circumferentially uniform, and that the pressure perturbation will be proportional to the stall cell frequency and the amplitude of the velocity fluctuation. It also shows that in

terms of phase relationship, the pressure and velocity fluctuations will be 90^{o} out of phase with each other. These observations are well supported by the experimental results shown in Figure 33. From this figure, it can be seen that because of the quadrature between the velocity and pressure fluctuations, the total pressure at the circumferential centres of the stalled and unstalled parts of the flow will be equal to the mean pressure level, i.e. atmospheric in this case. This is an important point because it implies that measurements taken at the centres of the stalled or unstalled areas will be unaffected by any unsteady effects in the compressor inlet. The neglect of unsteady effects in the discussion of the static pressure gradients in the previous section was therefore justified.

5.2.3 Fluctuations in Exit Plane Static Pressure

In the past, it has often been assumed that the static pressure in the exit plane of the compressor is circumferentially uniform during stall. This assumption was made by Fabri (22), Stenning and Krieble (8), McKenzie (16), Gray (17) and others, and is also one of the basic axioms of the parallel compressor model. Because the experimental measurements show that this assumption is strictly incorrect, it is important that the pressure fluctuations in the exit plane should receive specific attention.

Two sets of static pressure measurements are shown in Figure 45. These results were obtained downstream of the OGV's in the three stage builds of the Low and High ϕ^{*} compressors. The areas of stalled and unstalled flow have been demarcated on the figure by means of parallel lines. It can immediately be seen that the static pressure is not circumferentially uniform. In addition, the pressure wave is in quadrature with the velocity distribution, i.e. the

minimum and maximum pressures occur at the boundaries between the stalled and unstalled flow, rather than at the centres of these two regions. This shift in the static pressure wave relative to the velocity distribution means that the averaged pressure in the stall cell is very nearly the same as that in the unstalled area, as is demonstrated in the figure. Thus, although the pressure itself is non-uniform in the exit plane, the average pressures in the stalled and unstalled parts of the flow are equal.

It should be noted here that as the form of the static pressure wave has been found to change very little across the outlet guide vane row, the above conclusion is applicable to measurements obtained both before and after the OGV's.

The static pressure distribution in the exit plane was considered analytically by Dunham in his two-dimensional theory in Reference (4). An expression for the static pressure perturbation in terms of the velocity perturbation was obtained from a linearized analysis in which the exit flow angle was assumed circumferentially uniform. If the exit angle is zero, the expression takes the form:

$$P' = \rho\bar{U}\Sigma i\varepsilon\sigma e^{i\,n\theta-\sigma t)} = i\rho\bar{U}\sigma(C_x')$$

where σ is the stall cell frequency. The form of this equation gives the phase relation between the pressure and velocity perturbations. To illustrate this point, Dunham gave the following sketch of a square wave velocity distortion with the associated static pressure wave.

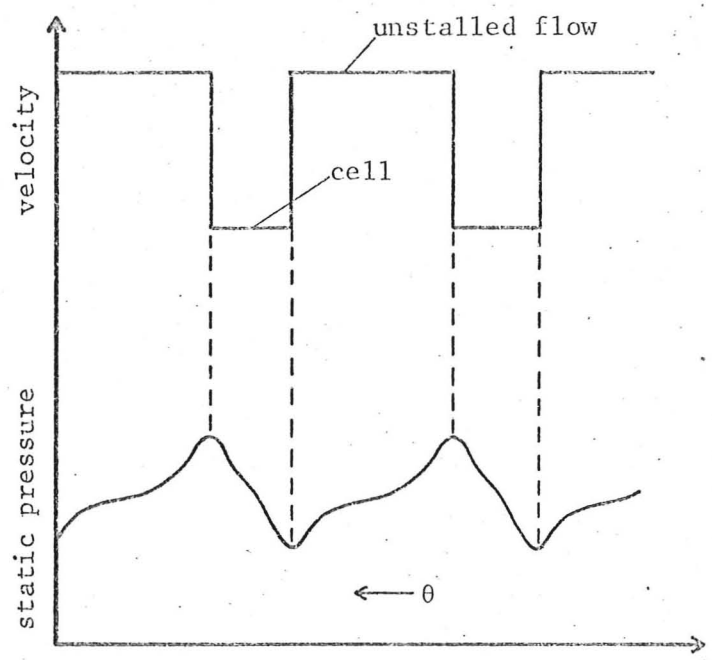

It is interesting to note that the shape of the calculated pressure wave is very similar to the measured waves shown in Figure 45. As a result of the analysis, Dunham was able to conclude that "the circumferential average static pressure within the stall cell is the same as that outside the stall cell".

Thus, both theory and experiment show that, while the exit plane pressure is not circumferentially uniform, the average pressures in the stalled and unstalled parts of the annulus will be equal. It follows, therefore, that the use of the assumption of constant exit plane pressure in elementary stall models has some basis in fact, and will not lead to erroneous estimates of overall pressure rise.

5.3 Overall Flow Model and Effect of Rotating Stall on Time-Averaged Performance

The velocity and pressure fields considered in the previous two sections can now be brought together to provide an overall model of the flow in the compressor. This model will be used to examine the influence of rotating stall on the time-averaged performance of the compressor, and to relate the details of the flow to the measured

pressure rise characteristics.

5.3.1 Overall Flow Model

In the interest of providing a clear description of the flow, it is convenient to give a brief summary of the pertinent observations made in the preceding work.

1) The flow in the compressor can be divided into areas of stalled and unstalled flow which behave as compressors in parallel, discharging into the same exit ducting. The unstalled flow behaves as it would under steady conditions, while the stalled flow moves predominantly in the tangential direction, giving rise to centrifugal pressure gradients and adding little to the overall flow rate through the compressor.

2) In the inlet plane immediately ahead of the IGV's, the flow is already separated into areas of through-flow and retarded flow. The absence of flow in the retarded area means that the average pressure in this region will be approximately atmospheric, while in the through-flow part of the annulus, the static pressure will be below atmospheric by an amount equal to the local dynamic head of the flow. The unsteady analysis of the flow in this region shows that measurements taken at the circumferential centres of the two flow areas will be unaffected by any unsteady effects in the compressor inlet.

3) The static pressure in the exit plane of the compressor, either before or after the OGV's, is not circumferentially uniform, but the average pressures in the stalled and unstalled parts of the flow are equal.

4) The fraction of the annulus occupied by the stall cell at any time appears to be linearly related to the net flow rate through the

compressor. Over a wide range, a change in flow rate simply alters the proportions of the stalled and unstalled parts of the annulus without causing any fundamental change in the behaviour of the flow in either region.

5) During stall the delivery pressure remains constant and is independent of the operating flow rate. From the 3-stage characteristics in Figure 12 it can be seen that this is not altogether true, but for the purpose of building up a simple overall picture of the flow, the use of such an assumption will not lead to any significant errors.

The combination of the above observations into an overall model of the flow in the compressor can best be illustrated by means of a composite diagram, like that shown in Figure 46. In keeping with the general line of the discussion, a three stage compressor is used here, but the basic ideas are applicable to a compressor of any number of whole stages.

In Figure 46, the unstalled flow shown entering the compressor is accelerated to a velocity of $C_{x_{us}}$ in the inlet, so that in plane 1 the static pressure in the unstalled region will be equal to $P_o - \frac{1}{2}\rho C_{x_{us}}^2$. From plane 1, this flow passes through the IGV's to plane 2, where the pressure will now be $P_o - \frac{1}{2}\rho C_{x_{us}}^2 \sec^2\alpha_1$, where α_1 is the exit angle of the IGV row. Through the remainder of the compressor the unstalled flow behaves as it would under steady conditions. The static pressure will, therefore, rise continuously through each blade row until, in the exit plane, it is normally above atmospheric pressure.

In the stalled region, on the other hand, there is little or no net flow in the compressor inlet and the static pressure here

remains almost atmospheric. Immediately downstream of the IGV's, the outer wall pressure rises sharply; mainly due to centrifugal effects in the swirling flow ahead of the first rotor. Similar step rises in static pressure are also shown ahead of the rotors in planes 4 and 6. It should be reiterated that the mechanism whereby a net pressure rise is achieved in each stage, is not understood. It is true that the unstalled flow entering the cell from the side will have sustained an increase in total pressure in its unstalled passage through the preceding stages (Figure 40), however, conditions at the edges of the cell are so disturbed that this explanation cannot be advanced with any real seriousness. Without understanding the reason for the stage by stage pressure rise in the stall cell, no condition can be set on the actual pressure level at the exit plane. At present, the empirical observation of McKenzie (16), i.e. that the pressure rise during stall is usually between $\Psi_{T-S} = .1$ and $\Psi_{T-S} = .15$ per stage, is the only way of estimating the final pressure level in a multi-stage compressor.

The picture of the compressor behaviour given here is, of necessity, an idealised one. In reality the boundaries between the stalled and unstalled flow are blurred, and the pressure rises do not occur in the precisely ordered fashion shown in Figure 46. Nevertheless, the basic model of the flow is thought to be correct, and is supported by the instantaneous static pressure measurements taken at the circumferential centres of the stalled and unstalled parts of the annulus. These measurements, for the three principal compressor builds, are shown in Figures 47a,b,c. It can be seen that in most cases the pressure in the stalled flow does rise abruptly ahead of each rotor, and that the unstalled flow enters the compressor at a level which falls further and further below atmospheric as the local velocity of

the flow increases from one build to the next. The unstalled pressure can also be seen to rise more or less steadily through the blade rows, as suggested by the model. Thus, although the model in Figure 46 is idealised to a degree, it is, nonetheless, a realistic model of the flow and can be used to discuss the implications of rotating stall on the time-average performance of the compressor.

5.3.2 Time-Averaged Compressor Performance

The instantaneous picture of the flow which has been obtained makes it possible to consider the relationship between the structure of the flow and the time-averaged performance of the compressor.

a) Overall characteristics

Considering the compressor shown in Figure 46, the overall total-to-static performance could be represented by the expression

$$\Psi_{T-S} = (\bar{P}_8 - P_o)/\rho\bar{U}^2$$

where $\bar{P}$ signifies the time-average static pressure, and the accompanying subscript, the number of the plane in which it is measured. The pressure in plane 9 (after the OGV's) could have been used in place of that in plane 8 (before the OGV's) in the above expression, however, as the static pressures in these two planes are not very different, for either stalled or unstalled operation, $\bar{P}_8$ will be used throughout the following discussion. An alternative method of expressing the overall performance of the compressor would be to use a static-to-static characteristic:

$$\Psi_{S-S} = (\bar{P}_8 - \bar{P}_1)/\rho\bar{U}^2$$

where plane 1 is the measuring plane just upstream of the IGV's.

During unstalled operation, a simple relationship between these two characteristic can be established by noting that:

$$\bar{P}_1 = P_o - \tfrac{1}{2}\rho C_x^2$$

and therefore

$$\bar{P}_8 - \bar{P}_1 = \bar{P}_8 - P_o + \tfrac{1}{2}\rho C_x^2$$

Dividing through by $\rho\bar{U}^2$ to nondimensionalize the pressure differences gives:

$$\frac{(\bar{P}_8 - \bar{P}_1)}{\rho\bar{U}^2} = \frac{(\bar{P}_8 - P_o)}{\rho\bar{U}^2} + \tfrac{1}{2}\frac{\rho C_x^2}{\rho\bar{U}^2}$$

which is:

$$8\text{-}1\,\Psi_{S\text{-}S} = 8\text{-}0\,\Psi_{T\text{-}S} + \tfrac{1}{2}\phi^2$$

This shows that for unstalled flow only one of the characteristics needs to be measured, the other can be deduced from the first by using the simple relationship shown here.

During stalled operation, on the other hand, the same relationship between the total-to-static and static-to-static characteristics cannot be used, because of the division of the flow into stalled and unstalled areas in the compressor inlet. In the unstalled part of the annulus in plane 1, the static pressure is equal to $P_o - \tfrac{1}{2}\rho C_{x_{us}}^2$ where $C_{x_{us}}$ is the local velocity of the unstalled flow and is assumed constant over the width of the unstalled area. In the stall cell itself, the static pressure is approximately atmospheric, due to the absence of flow in this region. Now, if λ is taken to represent the fraction of the annulus occupied by the stall cell, and $1-\lambda$ the fraction of the annulus unstalled, then, due to the rotation of the cell, the time-average static pressure in plane 1 will be given by:

$$\bar{P}_1 = \lambda(P_o) + (1-\lambda)(P_o - \tfrac{1}{2}\rho C_{x_{us}}^2)$$

i.e.
$$\bar{P}_1 = P_o + (1-\lambda)(\tfrac{1}{2}\rho C_{x_{us}}^2)$$

From this expression, the following relationship between the static-to-static and total-to-static characteristics for stalled operation can be obtained:

$$8\text{-}1\,\psi_{S\text{-}S} = 8\text{-}0\,\psi_{T\text{-}S} + (1-\lambda)\tfrac{1}{2}\phi_{us}^2 \qquad (4)$$

This expression, although based on an idealised picture of the flow, shows that during stall the total-to-static and static-to-static characteristics cannot be related to each other without precise information about λ and ϕ_{us}. Rough estimates of these quantities can be obtained from the characteristics themselves as was demonstrated in Section 5.1.4, but, if accurate results are required, it is imperative that both characteristics should be recorded separately. It is because of the difficulties involved in deducing one type of characteristic from another during stall, that some of the experimental data reported in the literature has not been included in the performance correlation given in Chapter 6.

The static-to-static characteristics considered above were measured between planes 8 and 1; however, if it is necessary to eliminate the effect of the IGV's for the purpose of comparing the stalled performance of compressors of different number of stages, then the characteristic between planes 8 and 2 may be required. In this case, the static pressure in the unstalled part of the annulus ahead of the first rotor (plane 2) will be given by $P_o - \tfrac{1}{2}\rho C_{x_{us}}^2 \sec^2\alpha_1$, where α_1 is the angle of flow leaving the IGV's. In the stalled area, on the other hand, the pressure in plane 2 will be above atmospheric pressure due to the influence of centrifugal effects in the swirling

flow ahead of the rotor, as indicated in Figure 46. If H_s is assumed to represent the step increase in static pressure which occurs in the stalled flow ahead of each rotor, then the time-averaged pressure in plane 2 will be given by

$$\bar{P}_2 = \lambda(P_o+H_s) + (1-\lambda)(P_o-\tfrac{1}{2}\rho C_{x_{us}}^2 \sec^2\alpha_1)$$

Subtracting from $\bar{P}_8$ and dividing through by $\rho\bar{U}^2$, leads to the following relationship between the static-to-static and total-to-static characteristics:

$$8\text{-}2\Psi_{S-S} = 8\text{-}0\Psi_{T-S} - \lambda H_s + (1-\lambda)(\tfrac{1}{2}\phi_{us}^2 \sec^2\alpha_1) \qquad (5)$$

Once again it can be seen that detailed information is necessary if one characteristic is to be derived from the other. The expression also shows that as the stall cell grows in size, i.e. as λ increases, the λH_s term will become larger and the $(1-\lambda)$ term smaller, until eventually Ψ_{S-S} will become smaller than Ψ_{T-S}. In other words, the two characteristics will cross in the deep stall region - as is well illustrated by the four sets of characteristics shown in Figure 14. It should be noted that prior to the detailed study of the flow in the stall cell, no explanation for the crossing of the two characteristics could be found.

One further point should be made about the overall perfromance characteristics. The above expressions for $8\text{-}1\Psi_{S-S}$ and $8\text{-}2\Psi_{S-S}$ (equations 4 and 5) show that if the total-to-static pressure rise is more or less constant during stall, then the static-to-static characteristic will be a line of positive slope, and thereby indicates a reduction in overall pressure rise as the flow rate is reduced. From the preceding discussion, it can be seen that as $\bar{P}_8$ is approximately constant during stall, this reduction in pressure rise is due to the changing proportions of stalled and unstalled areas

in the compressor inlet, rather than to actual changes in pressure rise across the two segments of the compressor. It follows, therefore, that when studying rotating stall from the point of view of a two-part flow system, the total-to-static characteristic should be used in preference to the static-to-static characteristic, since the former is uninfluenced by the relative proportion of the stalled and unstalled flow.

b) Individual stage characteristics

When the individual stage characteristics were presented in Chapter 4, it was noted that the last stage of the compressor always appeared to perform poorly by comparison with the preceding stages. When the number of stages was reduced to one, the performance of this stage was much like the last stage in a multi-stage build. (The characteristics used to illustrate this point are shown in Figures 15 and 16.) It was subsequently noted, however, that the detailed velocity and direction measurements revealed no unusual behaviour of the flow in the last stage of the compressor. The reason for this apparent anomaly can be found by considering the flow model given in Figure 46.

If H_s represents the step pressure rise ahead of each rotor in the stall cell, and H_{us} the static pressure rise across each stage in the unstalled flow, then for the three stage compressor in Figure 46

$$\frac{H_s}{\rho \bar{U}^2} \sim \frac{1}{3} \Psi_{T-S} \qquad \text{and} \qquad \frac{H_{us}}{\rho \bar{U}^2} \sim \frac{1}{3} \Psi_{S-S\ (unstalled)}$$

and therefore

$$H_{us} > H_s$$

where Ψ_{T-S} and $\Psi_{S-S(unstalled)}$ are assumed constant during stall.

Using H_s and H_{us}, expressions can be written for the time-averaged pressure at each of the inter-stage measuring planes in the compressor. Recalling that λ represents the stalled fraction of the annulus:

$$\bar{P}_2 = (\lambda)(P_o+H_s) + (1-\lambda)(P_o-\tfrac{1}{2}\rho C_{x_{us}}^2 \sec^2\alpha_1)$$

$$\bar{P}_4 = (\lambda)(P_o+2H_s) + (1-\lambda)(P_o-\tfrac{1}{2}\rho C_{x_{us}}^2 \sec^2\alpha_1 + H_{us})$$

$$\bar{P}_6 = (\lambda)(P_o+3H_s) + (1-\lambda)(P_o-\tfrac{1}{2}\rho C_{x_{us}}^2 \sec^2\alpha_1 + 2H_{us})$$

$$\bar{P}_8 = (\lambda)(P_o+3H_s) + (1-\lambda)(P_o-\tfrac{1}{2}\rho C_{x_{us}}^2 \sec^2\alpha_1 + 3H_{us})$$

It should be noted that the pressures in the stalled region (i.e. the terms multiplied by λ) are the same in planes 6 and 8. This is because the pressure rise occurs ahead of the rotors in each stage, and there is no rotor following plane 8.

By subtraction of the appropriate expressions above, the following pressure differences are obtained:

$$\bar{P}_4 - \bar{P}_2 = \lambda H_s + (1-\lambda)H_{us}$$

$$\bar{P}_6 - \bar{P}_4 = \lambda H_s + (1-\lambda)H_{us}$$

$$\bar{P}_8 - \bar{P}_6 = 0 + (1-\lambda)H_{us}$$

As $(1-\lambda)$ is proportional to the operating flow coefficient, $\bar{\phi}$, and $H_{us} > H_s$, the static-to-static characteristics of the individual stages may be expected to look as follows:

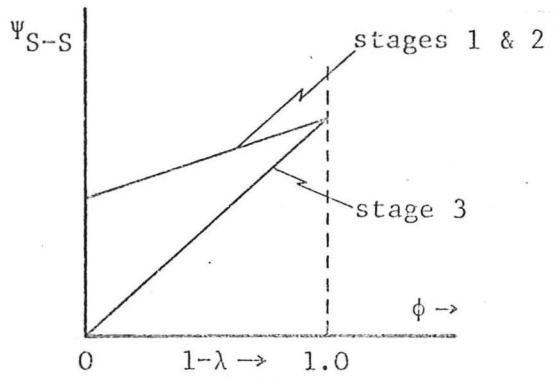

Although an idealised model has been used in this analysis, it is clear that the actual compressor characteristics shown in Figures 15 and 16 support predictions made.

It can thus be seen that if the individual stage characteristics are measured in the conventional way, the last stage in the compressor will always appear to give a smaller pressure rise during stall than the preceding stages. The apparent ineffectiveness of the last stage is only brought about by the way in which the pressure rise is generated ahead of the rotor in the stall cells, and does not imply that the detailed behaviour of the flow in the last stage is any different from that in the other stages. Once again, it was only by studying the details of the flow in the stall cell that an explanation has been found for the observed behaviour of the compressor.

5.4 Discussion of Flow Models in the Literature in Relation to the Present Work

The experimental results have been used to formulate a picture of the velocity and pressure fields in the stall cell, and to provide a model of the overall behaviour of the compressor. By way of a conclusion to this chapter, the ideas and assumptions about rotating stall which appear in the literature will be discussed in the light of the work presented in the preceding sections.

Consideration will first be given to the flow models embodied in the rotating stall analyses. Although most of the current work has been done on full-span stall in multi-stage compressors, the experimental results obtained during part-span stall in the single stage and isolated rotor builds show that the basic flow patterns are the same in either type of stall, and in all compressor configurations. It is, therefore, considered justifiable to use the concepts of stalled

behaviour developed in this chapter to assess the practicability of the flow models used in the theoretical analyses.

It will be recalled from Chapter 2 that all the perturbation theories make use of a potential flow field which is assumed to extend from upstream infinity to the blade row inlet plane. It has been found by experiment, however, that even in the case of a small, part-span stall cell, fast moving tangential flow exists ahead of the blade row in the stall cell and, therefore, indicates that the flow in this region is not irrotational. This means that the instantaneous inlet conditions to any blade passage cannot be specified by a perturbation potential and indicates a serious defect in the analytical approach. The turbulence in the upstream flow field becomes more intense as the stall cell grows in size and can be shown to extend well upstream of the IGV's in many cases. From this point of view, the nonlinear model of Takata and Nagano (5), which considers cells of finite size, is therefore even less realistic than the small perturbation theories in assuming an upstream potential flow field.

The perturbation theories also rely on unsteady blade row characteristics to provide a unique relationship between the inlet and outlet conditions of a particular blade passage. The definition of such a relationship usually rests on the assumption of a reduction, rather than a cessation or reversal, of the flow through the blade passage. In almost every case tested, however, it has been found that the total pressure is greater ahead of a rotor than behind it, thus indicating that recirculation or reversed flow is more likely than direct flow through the blade row. A further objection to the idea of a stalled blade passage as simply being one in which the flow rate is reduced below normal, is that this picture of the flow is totally incapable of explaining the very high torque and temperature levels

recorded during stalled operation. Thus, the perturbation analyses quite obviously take an over-simplified view of the flow within the stall cell.

It may be said that the objections put forward here would not apply in the case of a stationary blade row. Whilst this is true, most perturbation theories are expected to apply equally well to both moving and fixed blade rows. The present work has shown that centrifugal effects play a crucial part in determining the details of the flow within the stall cell. It may be, therefore, that the omission of centrifugal effects from the theoretical models means that the existing perturbation theories should be limited to stationary rows.

The vortex theory put forward by Stenning and Krieble (8) does not depend on the assumption of an upstream potential field and is capable of accepting reversed flow in the stall cell. This theory may therefore appear to be more realistic than the perturbation models, however, the experimental results suggest that the physical movement of the rotor blades through the retarded flow, and the accompanying centrifugal effects, are likely to play a larger part in determining the structure of the cell than are the velocities induced by a train of detached vortices in the downstream flow. Again the theory may be more applicable to a stationary blade row.

Certain aspects of the stalled performance models proposed by Dunham (14), McKenzie (16) and Gray (17) can also be evaluated in the light of the experimental results discussed in this chapter. It will be recalled that as far as the flow in the stall cell is concerned, Gray assumed a net negative flow, Dunham a net positive flow and McKenzie zero flow. It was shown, however, that the flow in the cell can usually be divided into two parts, one admitting reversed flow and

and the other through flow. It follows that a stall cell with only negative flow, or only positive flow, may thus be regarded as a special case of what is generally a more complex situation. The McKenzie assumption of zero flow in the cell is a compromise between positive and negative flow in the cell, and in view of the inability to predict the details of the flow in advance, this model is considered to be the most practical of the three.

The performance models are all based on the parallel compressor hypothesis and, therefore, rely on the assumption of circumferentially uniform static pressure in the exit plane. It was shown in Section 5.2.3 that this assumption is not strictly true, but the equality of the average pressure in the stalled and unstalled parts of the flow means that the models are not invalidated on this account.

With regard to the pressure rise generated during stall, it will be recalled from Chapter 2 that Dunham suggested this would be determined by the requirement of equal slopes on the fully stalled and unstalled branches of the performance curves. Apart from showing that positive flow in the stall cell does not occur in all compressor builds, little has been found to confirm or reject this idea. McKenzie, on the other hand, fixed the operating pressure level in the exit plane by invoking the empirical observation that the total-to-static pressure rise increases by a fixed amount for each stage in the compressor. Although no explanation can be given of how the pressure rise is generated in the stalled flow, it can be seen from Figure 46 that the observations made by McKenzie are in agreement with what might be expected from the detailed flow model shown in this figure.

The McKenzie model thus appears to give a good overall description of the behaviour of the compressor, both from a point of view of the flow in the cell, and the prediction of the overall pressure

rise during stall. In the following chapter, the basic ideas put forward by McKenzie will be combined with the detailed measurements from the present work, to produce a new and more comprehensive model for predicting the performance of a stalled compressor.

CHAPTER 6

Stalled Performance Correlation

In spite of the new experimental data and the improved understanding of the phenomena of stall itself, there are certain aspects of the flow which remain unexplained, making it impossible to estimate the stalled performance of a compressor from first principles. It has been found, however, that through the use of what can now be shown to be a physically plausible model of the flow, the available experimental information can be correlated in such a way as to allow quantitative predictions of the stalling behaviour of single stage or multi-stage compressors. The correlation is based on the parallel compressor hypothesis and makes use of the concept of the blockage associated with the stall cells.

The results of the correlation make it possible to obtain some idea of the pressure rise during stall, to predict whether a given compressor will exhibit part-span or full-span stall and to estimate the size of the stall/unstall hysteresis loop. The trends in stall behaviour to be expected when the design parameters of the compressors are varied are also predictable. Although the correlation is based mainly on data from the present experimental work, the information available in the literature is found to be in support of the approach adopted.

A general introduction to the correlation is given in section 6.1, where consideration is given to previous work on stalled performance prediction. In section 6.2 a basic model of the flow is developed and the various assumptions on which the correlation rests are presented. Experimental support for these assumptions is provided in section 6.3, while the correlation itself is given in section 6.4.

In section 6.5, an idealised analysis is undertaken to examine the trends in stalled behaviour to be expected when either the number of stages or the design flow rate of the compressor is altered. These trends are then illustrated with examples from the present experimental work. Finally, in section 6.6 the influence of the throttle and other downstream components on the stalled performance of the compressor is investigated.

6.1 Introduction

In Chapter 2 it was pointed out that the greater part of the theoretical work on rotating stall has been concerned with the question of stall inception and the prediction of the number and speed of rotation of small perturbations in the compressor. This type of approach is inherently unsuitable for predicting the performance of the compressor during deep stall, where the flow disturbances will always be large. Some nonlinear analyses have been developed in which finite disturbances are admissible. These are, however, restricted to isolated rotors or single stages and are more useful for "qualitative clarification of certain aspects of rotating stall", rather than for the prediction of stalled performance over a wide range of flow rates. Furthermore, both small perturbations and nonlinear analyses assume a throttle of infinite impedance, which means that the annulus averaged flow rate is maintained at a constant value when the flow regime changes from unstalled to stalled flow. In reality, any drop in pressure rise at stall inception would be accompanied by a change in mass flow rate, as determined by the throttle characteristic , and therefore the analyses are not able to provide information about the stall/unstall hysteresis which is observed in practice.

A large amount of experimental work has been done on rotating

stall, but the emphasis has usually been on specific aspects of the flow, rather than on the performance of the compressor as a whole. The diversity of the results obtained appears to have prevented the emergence of any sort of clear understanding of the physical parameters which control rotating stall, or of the influence of design variables such as $Cx/\bar{U}$, reaction, number of stages, etc., on the overall performance of the compressor.

Experimental observations have given rise to some theoretical models of stalled performance, namely those of Dunham, McKenzie and Gray, but these models are of a qualitative rather than quantitative nature and are somewhat limited in scope. They do not, for example, differentiate between operation in full-span or part-span stall, and are unable to give any idea of the size of the hysteresis loop to be expected in a particular case. As a result of these limitations, the models are also unable to provide a basis for unifying the experimental data obtained from various sources.

In view of the lack of a quantitative description of stalled performance, the present work is aimed at producing a framework upon which to build a systematic understanding of the influence of certain physical parameters on the overall behaviour of a stalled compressor. Since this cannot be done on a theoretical basis at the present time, a correlative approach to the problem has been adopted. The results from the current series of experiments are well suited to this purpose, as a wide range of design parameters were included in the tests. Where possible, relevant data from the literature has also been used, but it was often found that potentially useful data was rendered unusable by lack of vital information about the test conditions. From the experimental results, a correlation has been developed by means of which the basic features of the stalled performance characteristic of single

stage or multi-stage compressors can be predicted.

Before going on to consider the ideas on which the correlation is based, it should be stressed that the work is restricted to compressors of moderate or high hub-tip ratio. The lowest value of the hub-tip ratio which will be used is 0.6 . Furthermore, all the data has been taken from low speed compressors in which compressibility effects are not significant. The smallest compressor unit that is considered is the stage, i.e. IGV's, rotor and stator. Isolated blade rows have been found to exhibit quite different behaviour from that of single or multi-stage compressors and are therefore not included in the correlation.

6.2 Fundamental Concepts Embodied in Performance Correlation

6.2.1 Influence of Flow Regimes on Performance Characteristics

From an introductory point of view, it will be useful to describe the various flow regimes observed during stall and to relate these to the basic features of the stalled performance characteristics. As a general rule, compressor characteristics can be classified as either "abrupt" or "progressive", according to whether the pressure rise falls abruptly or progressively at stall inception. Hypothetical examples of these two types of characteristics are shown in Figures 48a and b. These characteristics, like all others considered in this work, are total-to-static characteristics and reflect the increase in exit plane static pressure above the inlet total pressure. As explained in the previous chapter, this type of characteristic is used in preference to any other, as the total pressure in the inlet plane, and the static pressure in the exit plane, are circumferentially quasi-uniform and, therefore, the time-averaged records of these pressures are unaffected by the relative proportions of the stalled and unstalled parts of the flow.

Consider first the example of a progressive characteristic shown in Figure 48a. Here the performance curve is either continuous at the stall point, i.e. point A, or has a small discontinuity in pressure rise, as illustrated in the present example. This type of behaviour, where there is only a gradual drop in delivery pressure at stall inception, is found to be associated with part-span stall; as is suggested by the multi-cell flow regime indicated in the figure. If the flow rate through the compressor is now reduced from the point of initial stalling, the performance curve will eventually exhibit a discontinuity, where the pressure rise and mass flow rate jump to significantly reduced values; as indicated by the drop from B to C. This jump is associated with a change from part-span to full-span stall and results in a single stall cell covering a sizable fraction of the compressor annulus. Additional throttling causes the cell to increase in size with the delivery pressure remaining relatively constant; as from point C to D. When the flow rate approaches zero, the stall cell may grow to fill the entire annulus so that, at E, the flow will again be basically axisymmetric. If the throttle is then opened from this point, the compressor would leave the full-span regime at a flow rate which was greater than that at which it first entered it, i.e. at point F as opposed to point G, and thus a hysteresis loop is established. Hysteresis of this nature is seldom observed for the onset and cessation of part-span stall.

The example of a typical abrupt characteristic given in Figure 48b shows a somewhat different sequence of stalling behaviour. In this case, the compressor goes straight into single-cell full-span stall with a large accompanying drop in pressure rise; as indicated from H to I. Further throttling causes the stall cell to grow in size while the delivery pressure remains almost constant, i.e. from I to J. At shut-off the stall cell may still be present, covering nearly

all of the compressor annulus. Opening the throttle from the shut-off positions will again lead to a hysteresis loop, due to the cessation of full-span stall occurring at a flow rate greater than that at which it was first established.

The two examples of compressor characteristics given in Figures 48a and b, show that the sustained level of pressure rise at the stall limit in progressive stall is associated with part-span stall, whereas the sudden drop in output which occurs in both characteristics is linked to the formation of full-span cells. These observations are supported by the measurements in Chapter 4, which show that part-span cells always operate at a greater pressure rise than full-span cells. Thus, in order to predict the compressor performance subsequent to the onset of stall, it is important to be able to predict which type of stall cell, either full-span or part-span, will form at the stall limit.

6.2.2 Basic Model of Compressor Behaviour During Stall

In this section a basic model of the flow in the compressor will be described, after which consideration will be given to the additional hypotheses necessary to allow the model to be used for quantitative predictions.

a) Parallel compressor view of rotating stall

In order to provide a simple, physically plausible concept of the flow on which to base the performance correlation, use will be made of the parallel compressor model. As was shown in the previous chapter, this model assumes the stalled and unstalled parts of the flow to operate independently of each other, but to discharge to the same average static pressure in the exit plane. The unstalled flow is seen as a region of undisturbed "through-flow", in which the axial velocity component is slightly greater than the compressor design

value, while in the stalled region, the axial velocity is taken to be zero. This last assumption has been shown to be strictly incorrect, but for the sake of simplicity, and in view of other less rigorous assumptions which will be made, it is considered to be sufficiently realistic for the present purpose.

With regard to the behaviour of this flow model in terms of compressor performance, it is further assumed that the pressure rise during stall will be constant, i.e. the stalled performance on a total-to-static characteristic can be represented by a horizontal line. This assumption, although not always precisely true, is supported to a large extent by the experimental results and has been used in all preceding stall performance models. The operating points of the stalled and unstalled parts of the flow on a typical total-to-static diagram are illustrated in Figure 49. Under these conditions the annulus averaged flow rate is determined by the throttle area, and is related to the flow in the unstalled region by the expression

$$\bar{\phi} = \phi_{us}(1-\lambda)$$

where λ is the fraction of the annulus blocked by the stall cell, i.e. that fraction through which there is no flow. The concept of blockage as defined here will play an important part in the understanding of the shape of the performance curves. It should be noted that as the throttle area is reduced, the mean flow will decrease and λ will therefore approach unity as the flow rate approaches zero.

b) Operating pressure levels and concept of critical blockage

The model of the flow assumed thus far provides only a qualitative description of the behaviour of the flow in the compressor. Without further empirical hypotheses it is not possible to conclude

anything quantitative about the stalled performance characteristics. The additional assumptions required to make quantitative predictions possible are considered below.

In order to fix the pressure levels at which the compressor will operate during stall, use is made of the experimental observation (first noted by McKenzie) that the nondimensionalized inlet total to exit static pressure rise per stage is a constant for all compressors; irrespective of the blading used. This is assumed to be true for both part-span and full-span stall. Thus, for N stages, the pressure rise during stall will be N times that for one stage.

It should be noted that, as the pressure rise being considered is the inlet total to exit static, the hypothesis assumed here implies a behaviour in stall which is fundamentally different from that in unstalled operation. This can be seen if the pressure rise for N identical stages is examined out of stall. Under these conditions it is reasonable to assume that the total-to-total (or static-to-static) pressure rise for N stages, is N times that for one stage, i.e.

$$N\Delta P_{T-T}(1) = \Delta P_{T-T}(N)$$

It follows that the relation between the total-to-static pressure rise for N stages is <u>not</u> simply N times that for one stage, since the total-to-static pressure rise is given by (for axial exit):

$$\Delta P_{T-S} = \Delta P_{T-T} - \frac{1}{2}\rho C_x^2$$

Thus $$\Delta P_{T-S}(N) = N\Delta P_{T-T}(1) - \frac{1}{2}\rho C_x^2$$

But $$N\Delta P_{T-S}(1) = N\Delta P_{T-T}(1) - \frac{N}{2}\rho C_x^2$$

and therefore $N\Delta P_{T-S}(1) \neq \Delta P_{T-S}(N)$ for unstalled flow. Thus, the hypothesis for the stalled behaviour, which effectively implies that $N\Delta P_{T-S}(1) = \Delta P_{T-S}(N)$ in stall, is not merely an obvious consequence of adding stages, but must be regarded as having been derived from

careful examination of the experimental data; as will be shown below. It should be emphasised that the pressure rise per stage is not the same for part-span as for full-span stall, since the experimental results indicate that it has a higher value during operation in the former mode.

One further assumption is necessary to complete the stall model. This is that there is a critical value of blockage λ_{crit}, which determines whether the compressor will operate in full-span or part-span stall. If the blockage is larger than λ_{crit}, a full-span regime will be established, whereas if the blockage is less, part-span stall will be found.

6.2.3 Application of the Basic Model to Stall Performance Prediction

The assumptions about the stalled pressure levels and the concept of a critical blockage can, if substantially correct, be used along with the parallel compressor model of the flow to make predictions about the stalled performance curve. In particular, it is possible to ascertain whether a given compressor will operate in full-span or part-span stall, and to make quantitative predictions about the extent of the stall/unstall hysteresis loop. In order to make these predictions a knowledge of the unstalled performance curve of the compressor is all that is required.

To illustrate the application of the concepts involved, reference is made to Figure 50. This figure shows the unstalled characteristic of a particular compressor with two superimposed throttle lines. The first of these, line I, corresponds to the throttle setting at which the compressor flow becomes unstable and intersects the unstalled characteristic at the stall limit; point A. The other, line II, represents a somewhat larger throttle opening and corresponds

to the throttle setting for the cessation of rotating stall. Initially, it is assumed that only the unstalled part of the characteristic from A' to A is known; the point G is unknown.

In a conventional compressor rig in which the compressor discharges to atmosphere through an exit throttle, the throttle curves will all be parabolae passing through the origin. Thus, if the stall limit, A, is known, then the stall throttle line, I, can also be assumed known.

In Figure 50, the two lines LL' and MM' represent the operating levels for part-span and full-span stall respectively. The stalling throttle line intersects these two lines at points B and C, where, according to the assumed model of the flow, the compressor could operate in either part-span or full-span stall. In order to determine which flow regime will be selected in a particular case, the compressor operating point is assumed to be moving transiently down the stalling throttle line with the blockage continually increasing. If the blockage at point B is less than the critical value, the compressor will operate at this level in part-span stall. If, on the other hand, the blockage is greater, part-span stall will not be possible and the operating point will drop to point C and stabilise there in full-span stall. Thus, to determine which flow regime will be selected, it is only necessary to estimate the blockage at point B, i.e. the ratio of the distances BD to LD, and to ascertain whether this is greater or smaller than the critical value.

The concept of a critical blockage can also be used to determine the extent of the hysteresis between stall onset and stall cessation for full-span stall. Assume the compressor in Figure 50 is operating in full-span stall at point M, i.e. at shut-off. To return to unstalled operation from this point, the flow rate must be

increased by opening the throttle. In doing so, the operating point is moved to the right along line MM' and the cell blockage is decreased. When the blockage has been decreased past the critical value for operation in full-span stall, this mode is no longer possible and the compressor will undergo a rapid transient to unstalled operation. This will occur at point F. At this point the blockage is equal to the critical value, λ_{crit}, so that

$$\lambda_{crit} = \frac{FE}{ME},$$

which defines point F. Since the throttle lines are parabolae, a knowledge of the location of point F means that the size of the hysteresis loop is fully determined. It can thus be seen that the hypotheses about stalled pressure rise and cell blockage, if experimentally verified, make it possible to obtain quantitative information about certain features of the stalled performance curve.

It should be noted that the size of the hysteresis region, and the selection of either part-span or full-span stall, depends on the shape of the compressor and throttle characteristics. Thus, the mode of rotating stall is not only determined by the details of the compressor blading, but also by the properties of the compression system as a whole. This is in contrast with the rotating stall analyses given in the literature, where a constant annulus averaged mass flow rate is assumed during the development of the cell. This assumption is equivalent to the imposition of a vertical throttle line and is clearly not in agreement with the conditions under which compressor testing is usually carried out. If, as is suggested here, the throttle line does influence the type of stall cell which forms at the stall limit, then reservation must be expressed about the cell behaviour determined by the analytic models.

Having set out the fundamental framework on which the performance correlation is to be based, attention will now be focussed on the experimental verification of the assumptions which have been made.

6.3 Experimental Results

The first hypothesis to be checked experimentally is that the pressure rise developed per stage during stall will be independent of the design parameters of the particular compressor, for both part-span and full-span stall. A striking illustration of support for the idea is provided by the results of numerous single stage tests, in which the design parameters of the blading were widely varied. This work was reported by Yershov in Reference 21 and the results have been reproduced in Figure 51. It can be seen that, while the peak unstalled pressure rise differs by a factor of almost two, the pressure rise in stall shows comparatively little variation. In addition, there appears to be no systematic dependence of stalled pressure rise on the design parameters of the blading.

The results of the present series of experiments confirm this conclusion and can be used to provide numerical values for the operating pressure levels in both full-span and part-span stall. For full-span stall, Figure 52 shows the shut-off pressure rise per stage (inlet total to exit static) for all the compressor builds tested. It can be seen that the measurements are reasonably clustered about $\Psi_{T-S} = .11$, with the largest departures from the mean generally being the single stage rather than the multi-stage builds. It will be recalled from Chapter 2 that McKenzie found the shut-off pressure rise per stage to fall between the limits of 0.1 and 0.15, so that the current results are in agreement with his observations. For part-span operation the data is more limited, but suggests a nondimensionalized total-to-static

pressure rise of approximately 0.17 per stage. This value will therefore be used in the correlation below.

It should be emphasised here that the precision with which the individual assumptions of the model are verified, is held to be subsidiary to the general success of the correlation; as will be demonstrated in the following section. In any event, the vagaries of stalled flow are such that a certain amount of generalisation is necessary to obtain any information about stalled behaviour at all.

The idea of a critical blockage can also be examined experimentally. Figure 53 shows a plot of the blockage for the different compressor builds in both part-span and full-span stall. The open points represent the minimum measured blockage for operation in full-span stall, while the solid points represent the maximum blockage measured in part-span stall. It can be seen that the two groups are divided by a band which lies between twenty-five and thirty percent. A more precise division than this would be unrealistic because of the limited amount of data, and because of the idealised assumption of zero flow in the stall cell which was used when estimating these blockages from compressor characteristics. Furthermore, it appears that the design flow rate of the compressor may have some influence on the division between the two modes of operation; but this point cannot be resolved without substantially more data. In view of these limitations, it is thought justifiable to assume that the upper limit for part-span stall, and the lower limit for full-span stall, are the same, and that the division between the two types of cells should occur at a blockage of about 30% , i.e. λ_{crit} is taken as 0.3 . Thus, in the predictions made below, the mode of stall, either part-span or full-span, is decided by whether the blockage is greater or lesser than this critical value.

It should be noted that, as part-span and full-span stall operate at different pressure levels, there is no reason why the maximum blockage associated with part-span stall and the minimum blockage associated with full-span stall should be the same. It would probably be more realistic to define two separate critical limits, one for part-span and one for full-span stall, but because of the limited data available and the simplicity which it affords, a common critical value of 30% has been chosen.

6.4 Stall Performance Prediction

The hypothetical model of the flow built up in the previous sections will be used here as a basis for correlating the available stall performance data. The specific aspects which will be examined are: a) the question of whether a given compressor will exhibit part-span or full-span stall at the stall limit, and b) the extent of the hysteresis region. These two aspects will be considered separately below.

To determine whether the compressor will go into part-span or full-span stall at the instability point, it is necessary to examine the blockage on the inception throttle line at a pressure level of 0.17 N . If the blockage at this level is less than 30% , part-span stall will be possible, and if not, full-span stall will occur at 0.11 N . (Compressors which do not have an unstalled pressure rise as high as 0.17 N, are assumed to operate in part-span stall at their peak where the blockage will be zero. This is because the value of 0.17 N represents a maximum operating level for part-span stall, rather than a necessary level.) The estimates of cell blockage at 0.17 N , calculated from the unstalled characteristics of all the compressors listed in Table 1, are shown in Figure 54. From this

figure it can be seen that the idea of a critical blockage does successfully divide those compressors which go into part-span stall from those which go into full-span stall. Furthermore, it is noteworthy that the stalling behaviour of both the Greitzer and Iura and Rannie compressors (N and O in Figure 54) is correctly predicted, even though these compressors were not considered when formulating the rules for the correlation.

The extent of the stall/unstall hysteresis in the performance curve is also readily determined. According to the assumed model, the cessation of full-span stall will occur when the cell blockage (measured at a level of 0.11 N) decreases to the critical value of 30% . From the definition of blockage, this criterion can be expressed in terms of the annulus averaged flow rate, $\bar{\phi}$, and the flow coefficient of the unstalled flow, ϕ_{us} , in the following way:

$$\bar{\phi}_{cessation} = 0.7\ \phi_{us \text{ at } .11N}$$

or

$$\bar{\phi}_{cessation}/\phi_{us \text{ at } .11N} = 0.7$$

The actual value of this ratio measured from the characteristics of all the compressors in Table 1,is compared with the predicted value of 0.7 in Figure 55. It can be seen that the correlation is quite good for all the compressor builds, including those of Iura and Rannie and Greitzer.

It should be stressed again that the preciseness with which the details of the flow in any particular compressor agree with the assumed numerical constants in the model,is of secondary importance to the success of the correlation as a whole. For example, the operating level of part-span stall in the Iura and Rannie compressor (19) is really 0.24 N, rather than 0.17 N, and yet the occurrence of part-span or full-span stall was correctly predicted. In other words, the

actual numerical values assumed for the pressure levels and the critical blockage should not be regarded as precise statements in themselves, but rather as prerequisites for the development of useful performance prediction criteria.

6.5 Overall Compressor Performance Trends

The concepts which have been developed can be used to provide an understanding of the trends in stalled performance which occur when the compressor design parameters are changed. From this point of view, the influence of design C_x/U (written here as ϕ^*) and the number of stages in the compressor, are of primary interest. The effect of these parameters can best be illustrated by carrying out a simple analysis of the unstalled performance of a compressor consisting of IGV's and N identical stages. To avoid unwarranted complexity, it will be assumed that the compressor is of 50% reaction and that the blade leaving angles are constant. In addition, all losses over the unstalled flow range will be assumed to be negligible. These idealisations will not affect the qualitative nature of the analysis and will greatly simplify the calculations.

A family of compressors of various numbers of stages is to be considered in which each build has the same design point loading; expressed here by having the same value of $\Delta P/q$. Here ΔP is the change in static pressure across any blade row and q is the local dynamic head of the flow entering the row. The value of this quotient will be taken to be 0.4 at design; which is a value representative of conventional compressors in gas turbine engines. It will also be assumed that the stalling point can be fixed by choosing a critical value of $\Delta P/q$ which is a given percentage greater than the design point value. Specifically, it is assumed that $(\Delta P/q)_{stall} = .55$. The

definition of the stalling point in this way, is roughly equivalent to imposing a diffusion limit on the performance of the blade rows and, although it is not as precise as some of the newer stall point correlations which have been developed, it is nevertheless sufficiently realistic for the present purpose.

Under the assumed ideal conditions the total-to-total (or static-to-static) pressure rise per stage can be written as:

$$P_{T_3} - P_{T_1} = 1 - \frac{C_x}{\bar{U}} (\tan \alpha_3 + \tan \beta_2)$$

$$= 1 - 2\phi \tan \alpha_3$$

The subscript 1 refers to the rotor leading edge, 2 to the rotor trailing edge and 3 to the stator trailing edge, and $\beta_2 = \alpha_3$ for a 50% reaction stage. Including the IGV's, which have a discharge angle of α_1 (where $\alpha_1 = \alpha_3$), the overall total-to-static characteristic for an unstalled compressor of N stages is given by:

$$\Psi_{T-S} = \frac{(P_{S_{exit}} - P_{T_{inlet}})}{\rho \bar{U}^2} = N[1 - 2\phi \tan \alpha_3] - \tfrac{1}{2}\phi^2 \sec^2 \alpha_3 \qquad (1)$$

In order to study the influence of the number of stages, and ϕ^*, on the performance of the hypothetical family of compressors, it is necessary to establish a relationship between ϕ^* and the leaving angle, α_3. This can be done by combining the design loading criteria:

$$C_p^* = (\Delta P/q)_{design} = 0.4$$

and the velocity triangle relationships to give the following expression for ϕ^* in terms of C_p^* and α_3:

$$1/\phi^* = \frac{[C_p^* + (1-C_p^*)\sin^2 \alpha_3]^{1/2}}{\sqrt{1-C_p^*} \cos \alpha_3} + \tan \alpha_3$$

Once a value of ϕ^* is chosen, α_3 can be found and equation (1) then used to generate the unstalled performance curves of a family of

compressors of that design. These curves will, of course, be defined up to the value of ϕ for which $\Delta P/q = .55$, i.e. up to the stall point.

To show the general trends implied by a change in design parameters, Figure 56 presents four unstalled total-to-static characteristics. These are for one and three stage builds of two specific values of ϕ^*. The important features to be observed from this figure are: 1) the peak pressure rise for a machine of given ϕ^* increases faster than proportional to N; 2) for a given number of stages the peak pressure rise increases with ϕ^*; and 3) the slope of the characteristic decreases as ϕ^* increases. Although only isolated examples have been used here to demonstrate these trends, the analytic expressions above show that they are generally true.

These behavioural trends lead to the idea that the blockage, evaluated at a level of Ψ_{T-S} equal to N times a given constant, will increase with both ϕ^* and the number of stages. This can be seen more clearly in Figure 57, where the blockage on the throttle line through the inception point has been calculated at a level of $\Psi_{T-S} = 0.11\ N$ for a range of design flow rates and for various numbers of stages. Although $0.11\ N$ has been used here, similar trends would occur at other physically plausible values. An increase in blockage, which implies a tendency towards full-span stall, can be seen to occur with an increase in either the design flow rate of the compressor or the number of stages. In addition, the greater the blockage at stall inception, the greater the increase in annulus averaged flow rate necessary to reduce the blockage to the critical value for the cessation of full-span stall. Thus, the factors which increase the blockage, i.e. greater N or ϕ^*, will also increase the size of the hysteresis loop.

Having used this simple analysis to make quantitative predictions about the influence of different design variables on the stalled performance of the compressor, the experimental results from the current tests can now be examined to ascertain whether the predicted trends are observed in practice. In addition, an attempt will be made to use the blockage concept to understand the transition from part-span to full-span stall which occurs in compressors with progressive performance characteristics.

The effect of the number of stages will be considered first. It has been noted, both in the present work and by Yershov (21), that identical compressor stages will sometimes exhibit part-span stall when tested individually, but will go into full-span stall when tested in a multi-stage configuration. The reason for this can be seen from the analysis. The peak total-to-static pressure rise has been shown to increase faster than proportional to N (Figure 56 or equation 1) and thus the inception blockage, which is measured at a pressure level proportional to N, will increase as the number of stages increases. Therefore, the larger the number of stages, the larger the blockage and the greater the likelihood of the compressor going into full-span stall.

This prediction is well illustrated in Figure 58 which shows the measured compressor characteristics for configurations of one, two and three stage builds of the same blading. (These characteristics are actually those of the High Reaction compressor builds, but as a change in reaction does not affect the conclusions from the analysis, these curves can legitimately be used as an example in the present discussion.) The stalling throttle lines have been superimposed on the characteristics as broken lines joining the stalled and unstalled parts of the curves. It can be seen that, as the peak pressure rise

increases more rapidly than N , the blockage will increase from build to build. In the three configurations shown, the actual blockage at a pressure rise of 0.17 N, is 9%, 33% and 45% for one, two and three stages respectively. Since $\lambda_{crit} = 0.3$, the single stage build would be expected to exhibit part-span stall, and the two and three stage builds, full-span stall. This prediction is clearly supported by the results.

It should be noted that both these types of stall have been encountered in compressor builds which have the same stagger, camber, gap/chord ratio and, most important, hub-tip ratio. The last point is noteworthy, as it has sometimes been suggested in the literature that the division of compressors into those exhibiting part-span or full-span stall can be done on the basis of hub-tip ratio. Although it is true that compressors of low hub-tip ratio generally tend to favour part-span stall (possibly because of the range of design conditions over the blade height), the behaviour of high hub-tip ratio compressors can be either part-span or full-span depending on the blockage conditions.

Another aspect of the compressor behaviour which can be seen in Figure 58, is the size of the hysteresis loop. The analysis suggests that this should increase with the number of stages, because, once full-span stall has been established, the value of ϕ required to reduce the blockage to the critical value necessary to unstall the compressor, increases with the number of stages. This is well supported by the results in Figure 58, where it can be seen that the point at which full-span stall ceases (points A, B and C for the one, two and three stage compressors), moves to larger and larger values of ϕ as N increases. The results of the High ϕ^* compressor builds (Figure 11) also provide support for the general observations made here.

The number of stages has thus been shown to have a definite effect on the nature of the stalled performance of the compressor. The other design variable which is also important from this point of view is ϕ^*, as this influences the relative position, and slope, of the unstalled part of the characteristic. The analytical results show that as ϕ^* is increased, the ratio of peak pressure level to stalled pressure level increases for compressors of a given number of stages. This is well confirmed in Figure 59 which shows the unstalled characteristics for the 3-stage compressor builds tested in the present work. The throttle lines at stall inception have been superimposed on the characteristics along with a constant pressure line at $\Psi_{T-S} = 0.33$ (i.e. 0.11 N for each of the three stages). It can be seen that although the builds all have roughly the same shut-off pressure rise, the peak unstalled pressure rise is very different in each case. Since the blockage is proportional to the horizontal distance between the inception throttle line and the unstalled part of the characteristic, it is clear that the higher the value of ϕ^*, the greater will be the blockage; whatever the precise level at which it is measured. From this it may be concluded that there will be a tendency for high ϕ^* compressors to exhibit full-span stall and for low ϕ^* compressors to exhibit part-span stall. This is supported by the results as the only one of the four compressors shown here that went into part-span stall, was the Low ϕ^* build, i.e. compressor I .

The influence of the axial velocity parameter on the hysteresis loop should also be considered. In Figure 59 it can be seen that the inception throttle lines are relatively close together, but that the unstalled part of the characteristics for the four machines are quite different. Since the blockage is proportional to the horizontal

distance between the two curves, it is clear that the throttle will have to be opened considerably further in the case of the High ϕ^* compressor in order to decrease the blockage to the critical thirty percent necessary for the cessation of full-span stall. This tendency towards larger hysteresis with increasing design flow rate was implied by the simple performance analysis when it was shown in Figure 57 that, the blockage on the inception throttle line at a level of .11 N increases as ϕ^* increases. The hysteresis loops for the four compressor builds are shown separately in Figure 60, thus providing clear support for the trends suggested.

The general concepts which have been used in the stall model can also be applied to the question of part-span/full-span transition for compressors with progressive characteristics, like that shown in Figure 48a. It has been concluded that part-span stall will not exist if the total blockage is larger than thirty percent. This condition can be used as a rough criterion for the transition from part-span to full-span stall. Consider a compressor which goes into part-span stall when it first encounters stall. Closing the throttle will cause the blockage to increase until the critical value of 30% is reached, whereupon the flow regime will change to full-span stall. Although this prediction is seldom quantitatively precise, the available data does tend to support this kind of behaviour. The model is, therefore, able to provide some understanding of the overall trends in compressors with progressive characteristics.

6.6 The Effect of Throttle Line Slope and other Downstream Components

As a further example of the usefulness of the concepts which have been developed, consideration will be given to the influence of the slope of the throttle line on the stalled performance curves. The

basic ideas required are sketched in Figure 61, where an unstalled compressor characteristic is shown with two different throttle lines passing through the stall point. Line I corresponds to the usual case where the throttle curve is a parabola through the origin. Line II, on the other hand, corresponds to the case where an exhauster or auxiliary compressor is used downstream of the throttle so that the throttle is dumping to a pressure lower than atmospheric. In this case the curve will still be a parabola, but will cross the vertical axis somewhere below the point of zero pressure rise.

The important point to note in Figure 61 is the difference in blockage which exists along any line of constant pressure rise; for example, line LL'. It can be seen that the steeper the slope of the throttle line, the smaller will be the blockage. Thus, if two tests were carried out, one with the throttle dumping to atmosphere and the other using a downstream exhauster, the resulting difference in blockage might be sufficient to change the mode of operation from full-span stall in the first case (with the larger blockage) to part-span stall in the second case.

An experiment to check these ideas could not be carried out with the present apparatus; however, such a test was actually performed by Borisov et al. (30), using a number of single stage compressors of different hub-tip ratios. The results of a test with a hub-tip ratio of 0.875 are reproduced in Figure 62. With the usual throttle exhausting to atmosphere, a discontinuity in the characteristic at stall was observed leading to operation with a single stall cell; a behaviour usually associated with the onset of full-span stall. The use of downstream suction, on the other hand, produced an almost continuous characteristic. Although no details of the cell structure were provided in this case, it can only be assumed that the gradual

fall in efficiency and pressure rise is associated with operation in part-span stall rather than in full-span stall. These experiments, therefore, provide support for the argument that the mode of stall encountered at the inception point is dependent on the throttle conditions. Therefore, for a stall model to give quantitative agreement with the actual behaviour of a real compressor, it is necessary that the effect of the throttle line slope be taken into consideration.

There is a further aspect of practical compressor operation which is also of interest. This is the influence of any downstream components on the stalled performance curve. In order to explore this aspect, an experiment was conducted in which a throttling gauze was placed just downstream of the three stage build of the High ϕ^* compressor. The effect of the gauze was to provide a measure of independent throttling of the stalled and unstalled parts of the flow. Because of the greater pressure drop across the gauze in the unstalled flow, the average exit plane pressure in the two flow regimes was no longer equal, but differed quite markedly, as shown in Figure 63a. Under these circumstances, the inequality of the two pressure levels needs to be included in the basic stall model to make it representative of the true situation in the compressor. The modifications necessary are illustrated schematically in Figure 63b.

The application of the model with non-uniform exit plane pressure suggests that the compressor performance curve would be sloping rather than flat, since the overall delivery pressure can be regarded as the time-averaged value of the pressure in the stalled and unstalled parts of the flow. This conclusion is supported by Figure 64, which shows the performance curves for the compressor with, and without, the gauze. Besides altering the slope of the

characteristic, the gauze also reduces the flow coefficient of the unstalled flow, and therefore reduces the cell blockage. Thus, the flow model is able to explain why the gauze is responsible for the presence of a small region of part-span stall in a compressor which would otherwise only exhibit full-span stall.

Summary and Conclusion

1) A model has been developed for the stalled flow in an axial flow compressor. The approach adopted has been to view the compressor as two separate compressors; one operating at zero flow, and the other at a flow rate which is generally higher than the design value.

2) The blockage associated with the stalled region appears to be an important parameter when correlating stalled performance.

3) Besides the assumption of constant pressure rise during stall, three hypotheses have been made about the behaviour of stalled flow: a) that there is a critical value of stall cell blockage of 30% above which part-span stall does not exist, and below which full-span stall does not occur; b) that the onset of part-span or full-span stall is determined by the blockage at a non-dimensional pressure rise of 0.17 per stage; and c) that the cessation of full-span stall is determined by the blockage at a non-dimensional pressure rise per stage of 0.11 .

4) These hypotheses make it possible to correlate all the available data from single and multi-stage compressors of moderate or high hub-tip ratio, and to formulate general guidelines for predicting the influence of certain design parameters on the stalled performance curves.

The results of the correlation show that:

1) For a given design flow rate, the addition of further identical

stages to a compressor will increase both the chance of encountering full-span stall at the stall point, and the size of the stall/unstall hysteresis loop.

2) For a given number of stages, an increase in the design flow rate of the compressor will increase the probability of full-span stall at the stall point, and will lead to the formation of larger hysteresis loops.

3) Contrary to what has been assumed in the past, the compression system as a whole has a significant effect on the compressor performance because of the part played by the throttle line in determining the cell blockage.

CHAPTER 7

Conclusions

The conclusions which have been drawn during the course of the current work are listed below. Short introductions will be used to divide the ideas into a number of topical groups. The chapter will be concluded with recommendations for further work.

From the point of view of experimental technique, the following conclusions have been drawn:

1) Phase-lock sampling, triggered by the stall cell itself, has been shown to be a viable technique during full-span and single cell part-span stall. In its current form (Chapter 3), it is not suitable for use under multi-cell conditions, where modulation in cell speed has been found to produce unsynchronized recordings. Being able to obtain phase locked signals, opens the way to ensemble averaging, to the computer analysis of rotating data and to the automatic phasing measurements obtained from various locations in the compressor. The technique therefore represents a significant improvement in the general experimental approach to rotating stall.

2) Although local temperature fluctuations are known to affect the hot wire response, the errors were found to be small and the use of temperature compensated probes is therefore not considered essential in low speed machinery.

3) As a result of its insensitivity to dirt, and the general ease with which it can be used, the piezo-electric probe developed during the course of this work is a useful instrument for monitoring the behaviour of rotating stall.

4) When measuring compressor performance for the purpose of studying rotating stall, the total-to-static pressure rise should be recorded

in preference to any other. This is because the circumferentially averaged total pressures in the stalled and unstalled parts of the flow are approximately equal in the inlet plane. The same is true of the averaged static pressures in the exit plane and, therefore, a performance characteristic based on the time-averaged measurement of these pressures will be unaffected by the relative proportions of the stalled and unstalled parts of the flow.

5) It has been observed that the time-averaged wall static pressure at inter-stage measuring positions is not circumferentially uniform in a high flow rate compressor, i.e. $\phi^* \geq 0.7$. For this reason, great care should be taken when measuring the individual stage characteristics in such compressors, as significant errors are possible.

The analysis of the velocity and flow direction measurements obtained by the phase lock sampling technique leads to the following conclusions:

6) In terms of cell structure, it was established that the edges of the cell within the blade rows of the compressor do not follow streamlines in the unstalled flow, and therefore the customary idea of the cell as a dead wake cannot be correct. Instead, it has been shown that unstalled flow crosses tangentially from one side of the cell to the other, thus giving rise to the concept of an active rather than a passive type of structure (Figure 40).

7) The reason for the tangential movement of the fluid in the cell is ascribed to the influence of the rotor blades, which, when stalled, behave as paddle wheels, dragging the flow circumferentially around the annulus. This physical influence of the rotor blades on the stalled flow explains the general similarity of the flow patterns observed in compressors of all design configurations, from isolated rotors to multi-stage builds. It also permits an explanation of why the flow

patterns in a multi-stage rig are repeated stage by stage through the compressor, instead of the latter stages operating in the wake of a disturbance attached to the first stage.

8) In spite of the general similarity between the stalled flow patterns in all compressor builds, it was found that the finer details of the flow are affected by the stagger angle of the blades (or alternatively the design flow rate) and the number of stages in the compressor. In the latter respect, it was concluded that although the flow in a single stage build shows similarities with that in a multi-stage configuration of the same blading, the finer details of the flow are sufficiently different to preclude the extrapolation of single stage data to multi-stage configurations.

9) In all compressor builds, it was found that the flow in the stall cell is characterised by high velocities ahead of the rotor and low velocities behind. Fluid trapped in the stalled rotor blade passages always appears to drift from the blade row on the upstream side, thus giving rise to the observed high velocities in the area ahead of the rotor. (No explanation for this can be given.) This fast moving fluid is brought to rest by the stator blades, during which process most of its kinetic energy is dissipated in the form of losses. This is responsible for the marked temperature rise observed during stall, and indicates why it is possible for a stalled compressor to absorb almost as much torque as an unstalled compressor.

10) Although the compressor used in the tests was of high hub-tip ratio, it was found that the flow in the stall cell is dominated by three-dimensional effects, especially during full-span stall. The observed gradients in velocity, total pressure and static pressure provide clear evidence of the three-dimensional nature of the flow.

11) It has been observed that the flow in a part-span stall cell is much like that in a full-span cell. (Two unexplained exceptions to

this rule were noted, however. These occurred in single stage builds of high flow rate and showed a combination of rotating stall associated with the rotor and axisymmetric wall-stall associated with the stator.) It was also noted that part-span stall always gives a greater pressure rise, and rotates at greater speed, than does full-span stall. No explanation for these observations was obtained.

12) It was concluded that centrifugal effects distinguish the rotor rows from the stator rows, thereby dispelling the traditional notion that the stall cell should rotate at 50% of the rotor speed in order to preserve symmetry between rotor and stator performance during stall. No further observations were made on the subject of cell speed, except that the number of stages in the compressor has a very definite influence on the speed of rotation of full-span stall cells.

The conclusions drawn from the study of the pressure fluctuations which accompany the velocity distortions in the compressor are listed below. Included in this section are points concerning the overall performance of the compressor.

13) Although the velocity perturbations during stall give rise to unsteady effects in the compressor inlet, the phase relationship between the velocity and total pressure fluctuations are such that measurements taken at the circumferential centre of the stalled or unstalled regions of the annulus will not be influenced by the unsteadiness of the flow.

14) The static pressure in the exit plane is not circumferentially uniform, as has often been assumed in the past. However, the phase relationship between the pressure and velocity fluctuations is such that the circumferentially averaged pressures in the stalled and unstalled parts of the flow will always be equal. This means that elementary stall models based on the parallel compressor hypothesis

are not invalidated by assuming constant static pressure in the exit plane.

15) Although the circumferential static pressure gradients between the stalled and unstalled parts of the flow can be very large, it was concluded that these gradients do not have any direct influence on the details of the flow in the stall cell. The flow in the last stage of a multi-stage compressor behaves much like that in the first stage, even though the pressure gradients are greatly reduced towards the rear of the compressor.

16) Centrifugal effects in the stalled flow ahead of the rotor blades are responsible for strong radial gradients in static pressure, and are also thought to contribute to the step increase in static pressure which occurs ahead of each stage in the stalled parts of the compressor (Figure 46).

17) By attributing the overall pressure rise in the stall cell to the influence of centrifugal effects in the swirling flow ahead of the rotor, a possible explanation is provided for the observation that the total-to-static pressure rise per stage appears to be the same for all compressors, i.e. independent of the details of blading used. This observation was first made by McKenzie, and is supported by the model of compressor behaviour developed in Chapter 5 (Figure 46).

18) The observation that the pressure rise in the stall cell occurs in the swirling flow ahead of the rotor can be used to explain why the total-to-static (Ψ_{T-S}) and the static-to-static (Ψ_{S-S}) characteristics are found to cross in the deep stall region. It also explains why the last stage of a multi-stage compressor always appears to give a smaller pressure rise than the preceding stages, even though the details of the flow in this stage are no different from those in any of the other stages.

19) It was also concluded that the rule usually used to relate the overall total-to-static and static-to-static characteristics during

unstalled operation, cannot be used during stall. If accurate stalled results are required, both characteristics must be measured independently, rather than the one deduced from the other.

Consideration of the unsteady measurements obtained during this work lead to the following conclusions concerning the validity of the flow models commonly used in the perturbation analyses of rotating stall:

20) It was observed that the assumption of irrotational flow immediately ahead of the rotor is not viable on account of circumferential swirl which accompanies the intense disturbance within the stall cell. This means that a simple potential equation cannot be used to specify the precise inlet condition of all the blade passages around the annulus.

21) The analytic assumption that the velocity of the flow in the stalled blade passages is merely reduced below normal by boundary layer separation, is a gross over-simplification of the real situation. Recirculation under the influence of centrifugal effects, or even net reversed flow, is more probable than a simple reduction in the local flow rate. An additional factor pointing to the lack of realism in the assumed model of the flow, is that it is totally incapable of explaining how sufficient energy can be put into the stalled flow to generate the large temperature rises observed during unsteady operation.

22) In view of the significance of centrifugal effects in the rotor blade passages, it was suggested that the perturbation analyses, which take no account of centrifugal effects, might be more applicable to stationary rather than moving blade rows.

23) All the analytic models make the assumption of constant annulus averaged flow rate during the stalling process. This assumption does not accurately reflect the conditions under which compressor testing

is usually carried out. Besides which, it has been shown that the slope of the throttle line plays an important part in determining the mode of stall which is established at stall inception. The use of an infinitely steep throttle line in the analyses is therefore also seen as a limitation.

By postulating a number of simple hypotheses based on empirical observations, it has been shown that all the available stalled performance data from moderate and high hub/tip ratio compressors, can be correlated to decide whether full-span or part-span stall will occur at stall inception, and to determine the size of the stall/unstall hysteresis loop. This correlation model marks a big improvement on any of the existing performance models and makes possible the quantitative prediction of the entire compressor characteristic. From this work, the following conclusions were drawn:

24) It has been shown that the concept of stall cell blockage is a crucial factor in correlating the stalled performance of an axial flow compressor. The blockage is influenced by the shape of the throttle line and the unstalled characteristic, and can be used to predict whether a given compressor will go into full-span or part-span stall at stall inception. This is in direct contrast with the traditional assumption that the type of stall cell is predetermined by the hub-tip ratio of the compressor.

25) The addition of further stages to a compressor of a given design flow rate will increase the probability of full-span stall at stall onset, and will lead to the formation of a larger hysteresis loop.

26) For a fixed number of stages, an increase in the design flow rate of the compressor will lead to an increase in the probability of full-span stall at stall inception, and to an increase in the size of the hysteresis loop.

27) Contrary to what has always been assumed in the past, the behaviour of the compressor during stall is not purely a function of the blading details, but also depends on the compression system as a whole. The slope of the throttle line affects the stall cell blockage, as does an inequality in exit plane pressure imposed by downstream components in the system, and so may influence the stalling behaviour of the compressor.

Recommendations for Further Work

Opportunities for further work arise in three main areas: experimental, analytical and performance modelling. Although an adequate analytic description of rotating stall would do away with the necessity for performance models, the complexity of the phenomenon suggests that such an adequate description will not be easily achieved, especially for multi-stage compressors.

From an experimental point of view, the practicality of phase-lock sampling opens up a whole new field in the study of rotating stall. With adequate computer facilities, the opportunities for monitoring the behaviour of the flow in the compressor become limitless. Specifically, however, the principal areas requiring further investigation appear to be:

a) The flow within the blade passages of a stalled rotor or stator row.
b) The measurement of radial velocities in the stall cell.
c) A study of the temperature distribution within the compressor.
d) A closer investigation of the details of part-span stall to ascertain why this mode of stall always gives a greater pressure rise, and rotates at greater speed, than full-span stall.

Still on the experimental side, but directed more towards a fundamental understanding of rotating stall, work is also necessary on the behaviour of stalled blade rows. This should not be done from the

27) Contrary to what has always been assumed in the past, the behaviour of the compressor during stall is not purely a function of the blading details, but also depends on the compression system as a whole. The slope of the throttle line affects the stall cell blockage, as does an inequality in exit plane pressure imposed by downstream components in the system, and so may influence the stalling behaviour of the compressor.

Recommendations for Further Work

Opportunities for further work arise in three main areas: experimental, analytical and performance modelling. Although an adequate analytic description of rotating stall would do away with the necessity for performance models, the complexity of the phenomenon suggests that such an adequate description will not be easily achieved, especially for multi-stage compressors.

From an experimental point of view, the practicality of phase-lock sampling opens up a whole new field in the study of rotating stall. With adequate computer facilities, the opportunities for monitoring the behaviour of the flow in the compressor become limitless. Specifically, however, the principal areas requiring further investigation appear to be:

a) The flow within the blade passages of a stalled rotor or stator row.
b) The measurement of radial velocities in the stall cell.
c) A study of the temperature distribution within the compressor.
d) A closer investigation of the details of part-span stall to ascertain why this mode of stall always gives a greater pressure rise, and rotates at greater speed, than full-span stall.

Still on the experimental side, but directed more towards a fundamental understanding of rotating stall, work is also necessary on the behaviour of stalled blade rows. This should not be done from the

point of view of studying the dynamic performance of the blades, as has been the line of approach in the past, but from the point of view of the blades behaving as rough paddle wheels. This could be done with a rotor of unstaggered blades in an open tank, considering first the vortex systems set up when the blade row is encased, and then examining the influence of stagger and pressure gradients on the details of the flow surrounding the rotor. In this way, it may be possible to find out why highly staggered blades appear to favour centrifugal recirculation, whereas lower staggers produce a two-dimensional flow system with fluid moving primarily in the reversed direction.

The present work has shown up a number of deficiencies in the existing rotating stall analyses. The most important among these has been the unrealistic modelling of the flow within the stall cell, the neglect of centrifugal effects, and the assumption of a constant annulus averaged flow rate during the stall inception process. Some progress has been made towards a more accurate description of the flow in the stall cell, but as yet the factors which actually control the flow have not been isolated. It may be, therefore, that before further analytic work is attempted, attention should be focussed on more fundamental research in the experimental field.

Although the performance correlation presented in Chapter 6 is an advance on any of the existing performance models, it is rather limited in terms of the design variables which have been included. Only the design flow coefficient and the number of stages has been considered thus far, but it is possible that other less obvious parameters, such as solidity and aspect ratio, should also be taken into account. In addition there is, of course, the all important question of the influence of hub-tip ratio which has not been considered in the present work.

Interest in rotating stall has gained impetus over the past 5 years, and it is hoped that the efforts made here will go some way towards drawing together the results obtained over the last 30 years, and towards providing some sort of basis for the work which will undoubtedly be done in the future.

REFERENCES

1) Greitzer, E.M., "Surge and rotating stall in axial flow compressors. Part I, Theoretical compression system model" A.S.M.E. Paper No.75-GT-9, 1975.

2) Greitzer, E.M., "Surge and rotating stall in axial flow compressors. Part II, Experimental results and comparison with theory" A.S.M.E. Paper No.75-GT-10, 1975.

3) Emmons, H.W., Kronauer, R.E. and Rockett, J.A., "A survey of stall propagation - experiment and theory" Trans.A.S.M.E., 1959, 81 (Series D, No.3), 409.

4) Dunham, J., "Non-axisymmetric flows in axial compressors" Cambridge University Ph.D. thesis, 1962.

5) Takata, H. and Nagano, S., "Nonlinear analysis of rotating stall" A.S.M.E. Paper No.72-GT-3, 1972.

6) Horlock, J.H., "Axial flow Compressors" Published by the Robert E. Krieger Publishing Company, Huntingdon, New York.

7) Emmons, H.W., Pearson, C.E. and Grant, H.P., "Compressor surge and stall propagation" (A.S.M.E. 53A 65) Trans.A.S.M.E., 1955, 77, 4, 455.

8) Stenning, A.H. and Kriebel, A.R., "Stall propagation in a cascade of aerofoils" Trans.A.S.M.E., 1958, 80, 777.

9) Fabri, J. and Siestrunck, R., "Rotating stall in axial flow compressors" J. of Aero.Sci., 1957, 24 (No.11), 805.

10) Marble, F.E., "Propagation of stall in a compressor blade row" J. of Aero.Sci., 1955, 22, pp.541-554.

11) Nagano, S., Takata, H. and Machida, Y., "Dynamic performance of stalled blade rows" Preprint of Tokyo Joint International Gas Turbine Conference and Product Show, Paper No. J.S.M.E. 11, Oct. 1971.

12) Ludwig, G.R., Nenni, J.P. and Arendt, R.H., "Investigation of rotating stall in axial flow compressors and the development of a prototype rotating stall control system" U.S.A.F. Aero Propulsion Laboratory, Wright-Patterson Air Force Base, Ohio Technical Report AFAPL-TR-73-45, May 1973.

13) Dunham, J., "Observation of stall cells in a single stage compressor" A.R.C. C.P. 589, 1961.

14) Dunham, J., "Non-axisymmetric flows in axial compressors" I.Mech.E., Monograph No.3, Oct. 1965.

15) Smith, A.G. and Fletcher, P.J., "Observations on the surging of various low-speed fans and compressors" N.G.T.E. Memorandum No. M.219, July 1954.

16) McKenzie, A.B. Private communication, Oct. 1973.

17) Gray, S. Private communication, Oct. 1973.

18) Turner, R.C. and Sparks, P.W., "Complete characteristics for a single-stage axial-flow fan" Paper No.29, Thermodynamics and Fluid Mechanics Convention, Cambridge, 9-10th April 1964 (I.Mech.E.).

19) Iura, T. and Rannie, W.D., "Experimental investigations of propagating stall in axial-flow compressors" Trans.A.S.M.E., 1954, 78, 3.

20) Cornell, W., "The stall performance of cascades" Proceedings of the Second U.S. National Congress of Applied Mechanics, 1954, 705. Published by the A.S.M.E., New York.

21) Yershov, V.N., "Unstable conditions of turbodynamics. Rotating stall" Translated by the Foreign Technology Division of the U.S.A., reference FTD-MT-24-04-71. Source: "Neustoychivyye reshimy turbomachin" Urashchayushchiysya Sryv, Moscow, Izd-vo Mashinostroyeniye, 1966.

22) Fabri, J., "Rotating stall in axial flow compressors" Symposium on Turbomachinery, Cambridge, 1957. Published by I.Mech.E. under the title of "Internal Aerodynamics (Turbomachinery)" London, 1970.

23) Le Bot, Y., "Conditions of rotating stall suppression in axial compressors" Private translation of "Conditions de suppression du decollement toumant dans les compresseurs axiaux" O.N.E.R.A. Report T.P. No.1240, 1973.

24) Huppert, M.C. and Benser, W.A., "Some stall and surge phenomena in axial flow compressors" J. of Aero.Sci., 1953, 20 (No.12), 835.

25) Benser, W.A., "Analysis of part-speed operation for high-pressure-ratio multistage axial-flow compressors" NACA, Research Memorandum, E53I15.

26) Doyle, M.D.C. and Dixon, S.L., "The stacking of compressor stage characteristics to give an overall compressor performance map" Aero. Quarterly, Vol.XIII, 349, Nov. 1962.

27) Rannie, W.D., Page 256, "The axial compressor stage" Section F, Volume X of the Princeton Series 'Aerodynamics of Turbines and Compressors' Edited by W.R. Hawthorne and published by Oxford University Press, 1964.

28) Rockett, J.A., "Modulation phenomena in stall propagation" Journal of Basic Engineering, No.417, Sept. 1959.

29) Valensi, J., "Experimental investigation of the rotating stall in a single-stage axial compressor" J. of Aero.Sci., 1958, Vol.25, pp.1-10, 72.

30) Borishov, G.A., Lokshtanov Ye.A. and Ol'shteyn, L.Ye., "Causes of break of characteristics of axial compressor stage with large relative hub diameter" Source unknown.

31) Tanaka, S. and Murata, S., "On the partial flow rate performance of axial flow compressor and rotating stall. First Report; Influence of hub-tip ratio and stators" Bulletin of the J.S.M.E., Vol.18, No.117, March 1975.

32) Tanaka, S. and Murata, S., "On the partial flow rate performance of axial flow compressor and rotating stall. Second Report; Influences of impeller load and a study of the mechanism of unstable performances" Bulletin of the J.S.M.E., Vol.18, No.117, March 1975.

33) Costilow, E.L. and Huppert, M.C., "Rotating-stall characteristics of a rotor with high hub-tip radius ratio" NACA T.N. 3518, 1955.

34) Bodeen, C.A., "Vector velocity fluctuations of propagating stall in axial flow compressors" Thesis, California Institute of Technology, 1961.

35) Pavlenko, G.V. Work reviewed by Yershov, Reference 21 above. Source unknown.

36) Krieble, A.R., Seidel, B.S. and Schwind, R.G., "Stall propagation in a cascade of aerofoils" NACA T.N. 4134, 1958.

37) Morritz, R.R., "Axial compressor stall" Lecture to the Von Karman Institute, Rhode-Saint-Genese, Belgium, 1970.

38) Howell, A.R., "Fluid dynamics of axial compressors" Proc.I.Mech.E. 153, London, 1945.

TABLE I

COMPRESSOR DESIGN PARAMETERS

COMPRESSOR	NO. OF STAGES	DESIGN ϕ^*	DESIGN REACTION	STAGGER ANGLE ROTOR/STATOR	CAMBER ANGLE ROTOR/STATOR	HUB/TIP RATIO	Nº OF BLADES
A (Low ϕ^*)	1	.35	50%	$50^\circ/50^\circ$	$20^\circ/20^\circ$	.8	60
B "	3	.35	50%	"	"	.8	"
C(Intermediateϕ^*)	1	.55	50%	$35^\circ/35^\circ$	$20^\circ/20^\circ$	.8	72
D "	2	.55	50%	"	"	.8	"
E "	3	.55	50%	"	"	.8	"
F "	4	.55	50%	"	"	.8	"
G (High reaction)	1	.71	65%	$35^\circ/20^\circ$	$20^\circ/40^\circ$	.8	72/60
H "	2	.71	65%	"	"	.8	"
I "	3	.71	65%	"	"	.8	"
J (High ϕ^*)	1	1.0	50%	$20^\circ/20^\circ$	$40^\circ/40^\circ$	.8	64
K "	2	1.0	50%	"	"	.8	"
L "	3	1.0	50%	"	"	.8	"
M "	4	1.0	50%	"	"	.8	"
OTHER BUILDS REFERED TO IN CHAPTER 6							
N (Greitzer)	3	.65	45%	$26.3^\circ/30.4^\circ$	$38.8^\circ/10.1^\circ$	.7	
O (Iura and Rannie)	3	.57	50%	$43.9^\circ/28.9^\circ$	$20.2^\circ/30^\circ$	.6	

TABLE 2

STALL CELL DETAILS

COMPRESSOR	NO. OF STAGES	NO. OF CELLS	TYPE OF CELLS	SPEED OF ROTATION
Low ϕ*:	1	6	Part-Span	31% Rotor Speed
"		12	Part-Span	66%
"		1	~~Part~~ Full-Span	19%
"	3	4	Part-Span	40%
"		12	Part-Span	60%
"		1	Full-Span	32%
"	3	1	Part-Span	29%
"	(reduced	5	Part-Span	54%
"	spacing)	1	Full-Span	27%
Intermediate ϕ*:	1	1	Part-Span	23%
"		1	Full-Span	15%
"	2	1	Part-Span	33%
"		1	Full-Span	22%
"	3	1	Part-Span	41%
"		1	Full-Span	26%
"	4	1	Part-Span	43%
"		1	Full-Span	31%
High Reaction :	1	1	Part-Span	25%
"		1	Full-Span	14%
"	2	1	Full-Span	24%
"	3	1	Full-Span	30%
High ϕ* :	1	1	Part-Span	24%
"		1	Full-Span	11%
"	2	1	Full-Span	20%
"	3	1	Full-Span	24%
"	4	1	Full-Span	28%

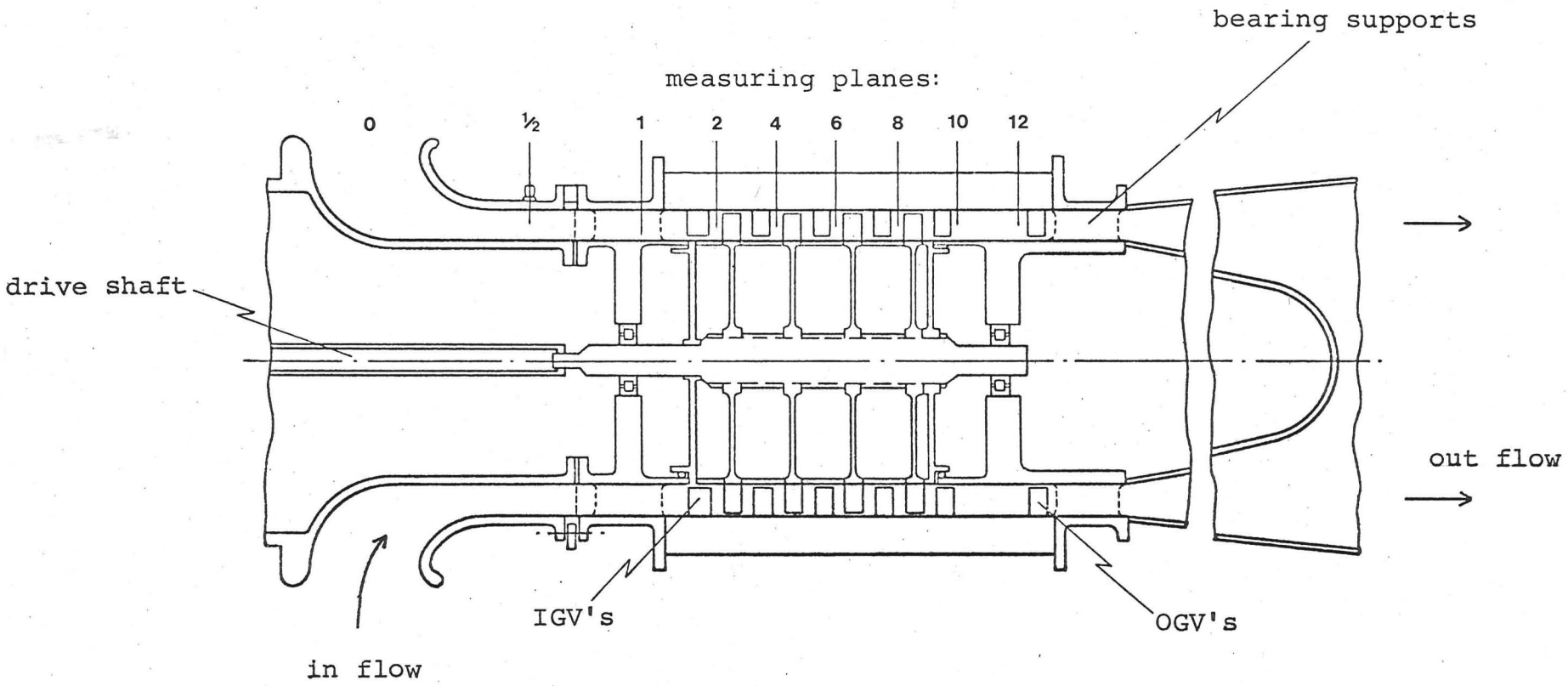

Overall view of compressor showing measuring planes.

FIGURE 1

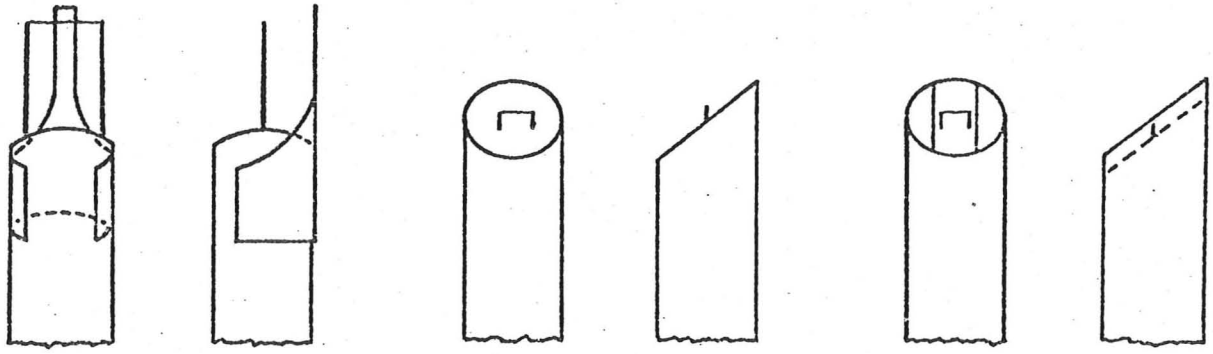

Examples of directionally sensitive hot wires.

FIGURE 2a

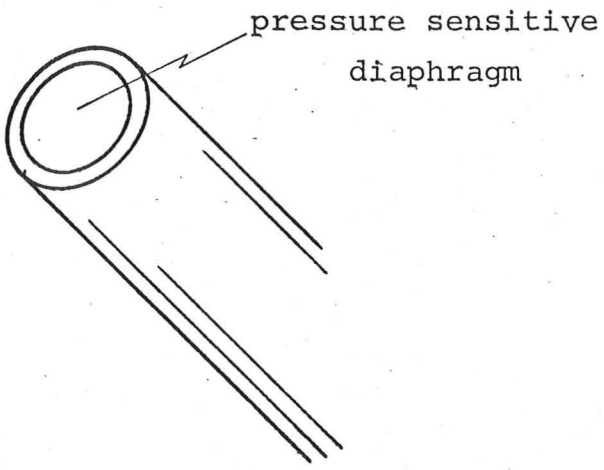

Static pressure transducer

FIGURE 2b

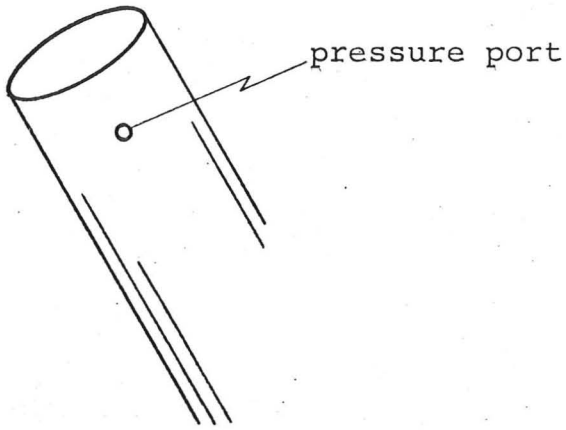

Total pressure transducer

FIGURE 2c

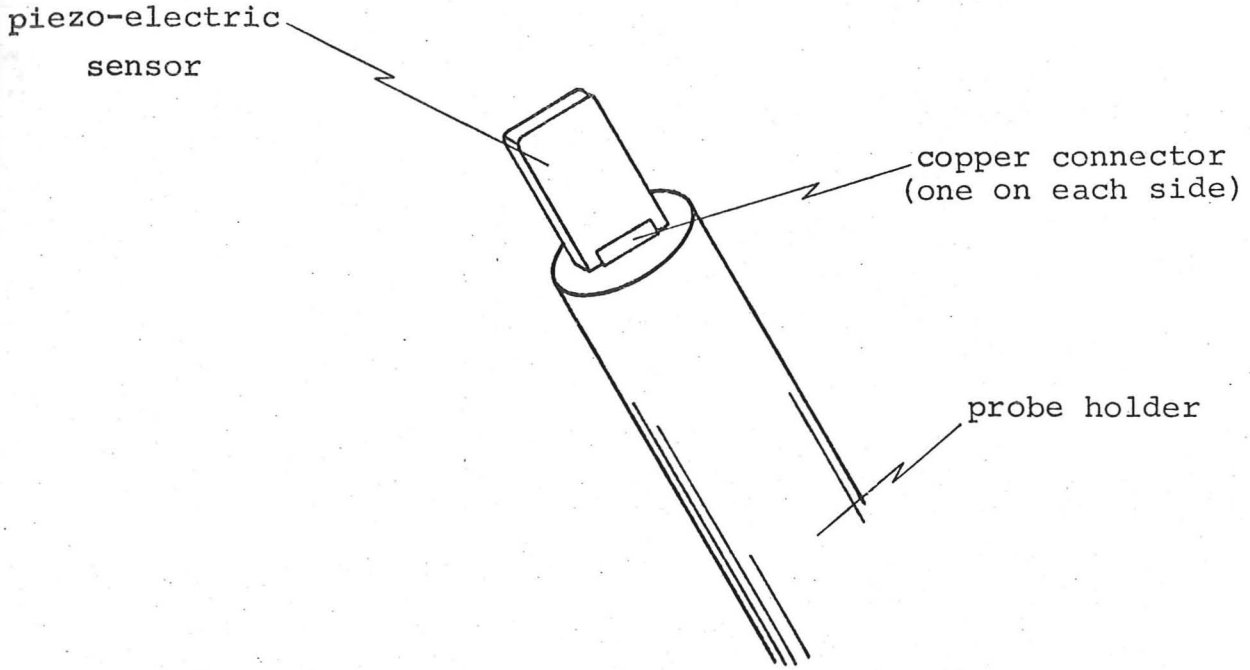

Piezo-electric probe.

FIGURE 3a

example of filtered output, suitable for use as
a reference pulse.

example of unfiltered output, suitable for measuring
the circumferential extent of a stall cell.

Examples of piezo-electric probe output.

FIGURE 3b

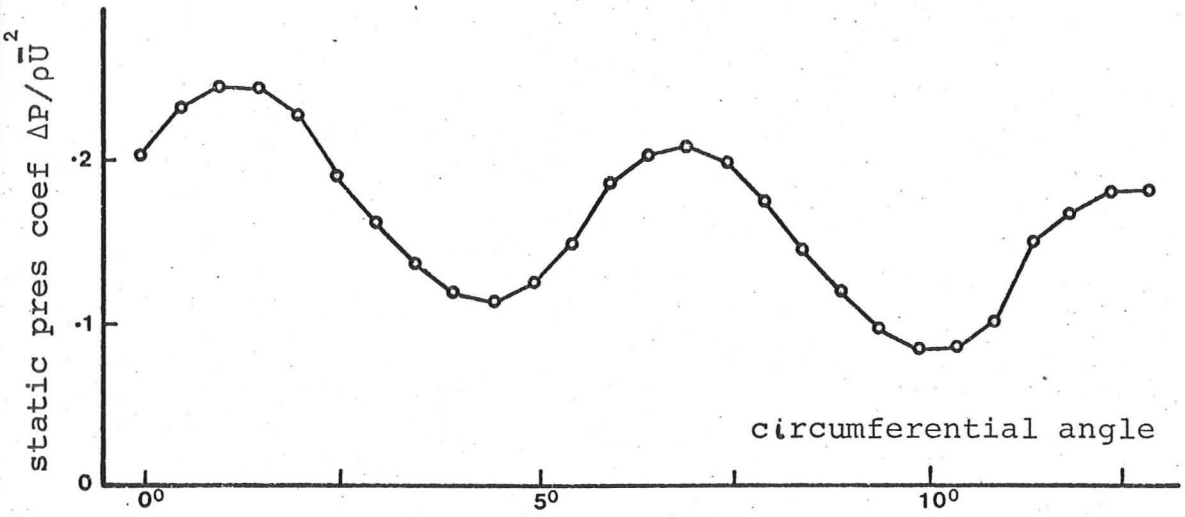

Example of circumferential variation of time-averaged outer wall static pressure obtained ahead of second rotor in the three stage build of High ϕ * compressor. (Test flow coefficient of 0.17).

FIGURE 4a

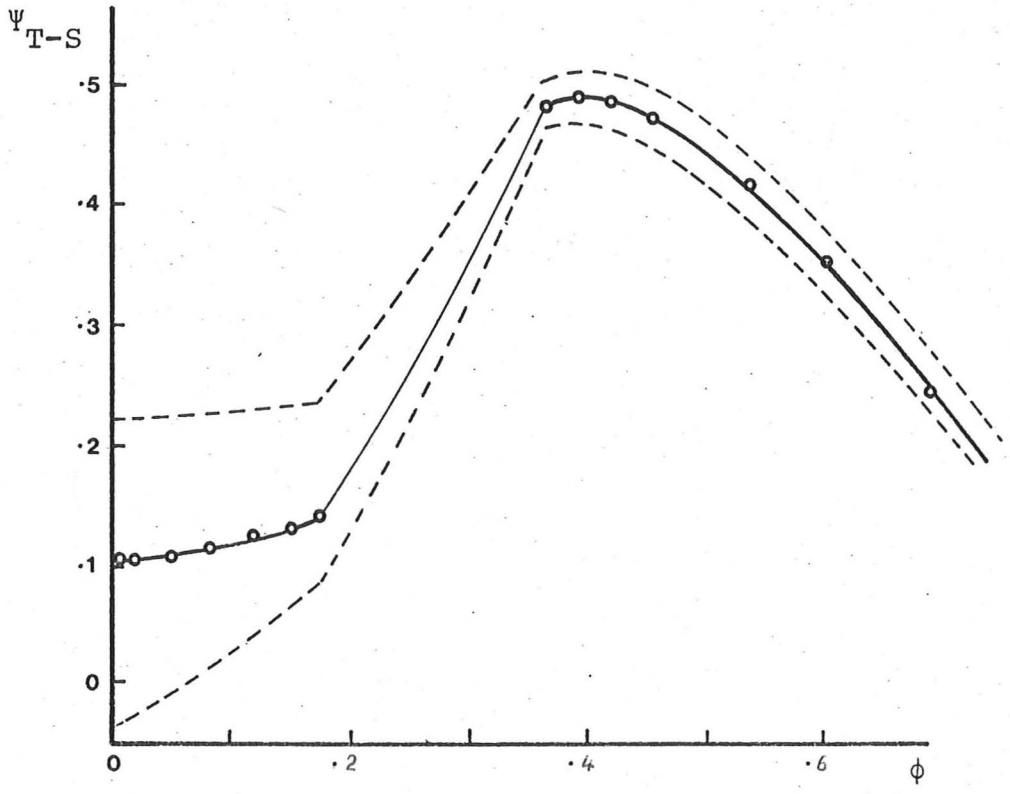

Characteristic showing possible effect of above circumferential variation in static pressure on the second stage characteristic of a three stage build. Note that static pressure fluctuations exist in both the measuring planes before and after the stage.

FIGURE 4b

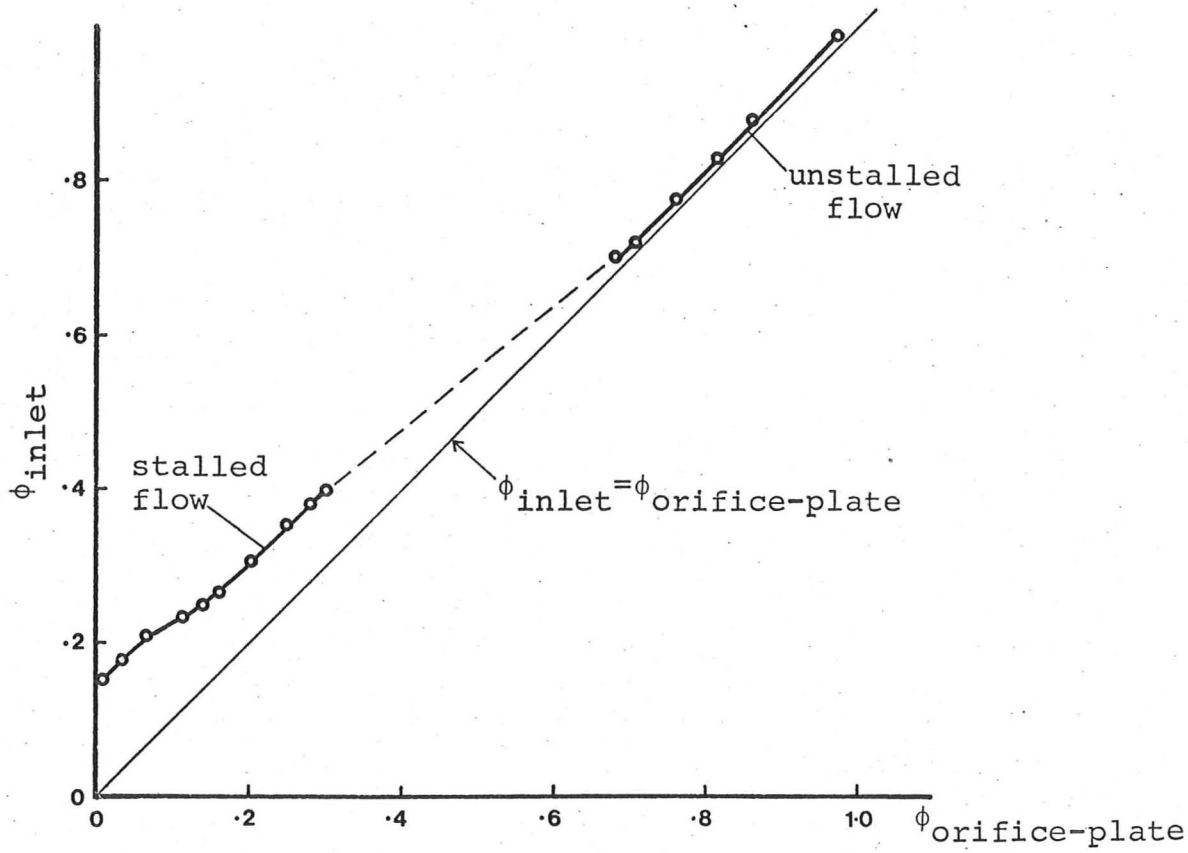

Comparison of flow rate measurements obtained from inlet calibration and from downstream orifice-plate.

FIGURE 5a

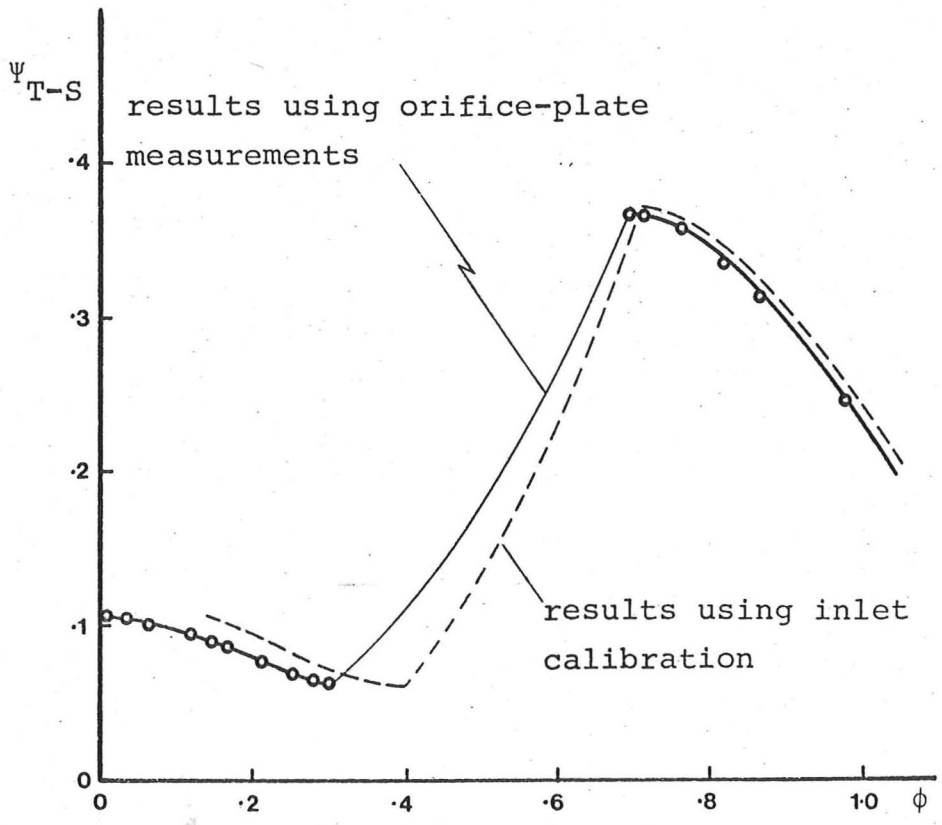

Example showing the influence of eroneous inlet flow rate measurements on a typical compressor characteristic.

FIGURE 5b

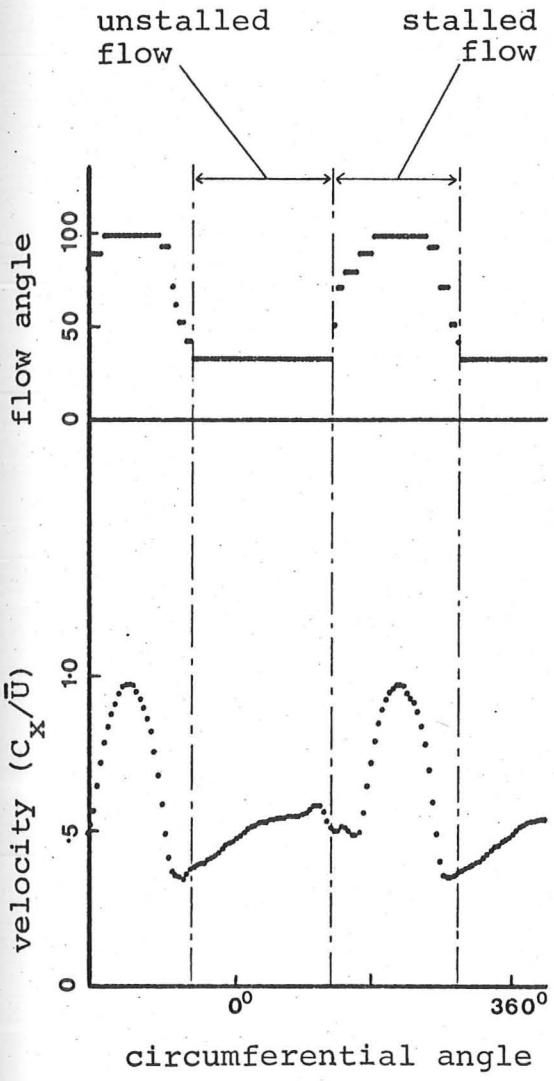

HOT WIRE RESULTS

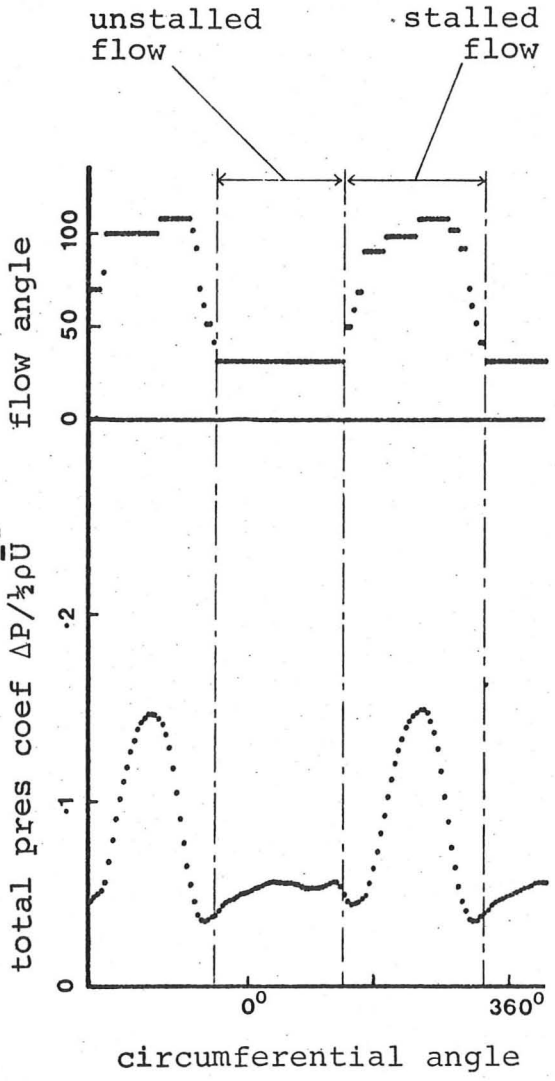

TOTAL PRESSURE TRANSDUCER RESULTS

Typical examples of results obtained from hot wire and total pressure transducers.

FIGURE 6

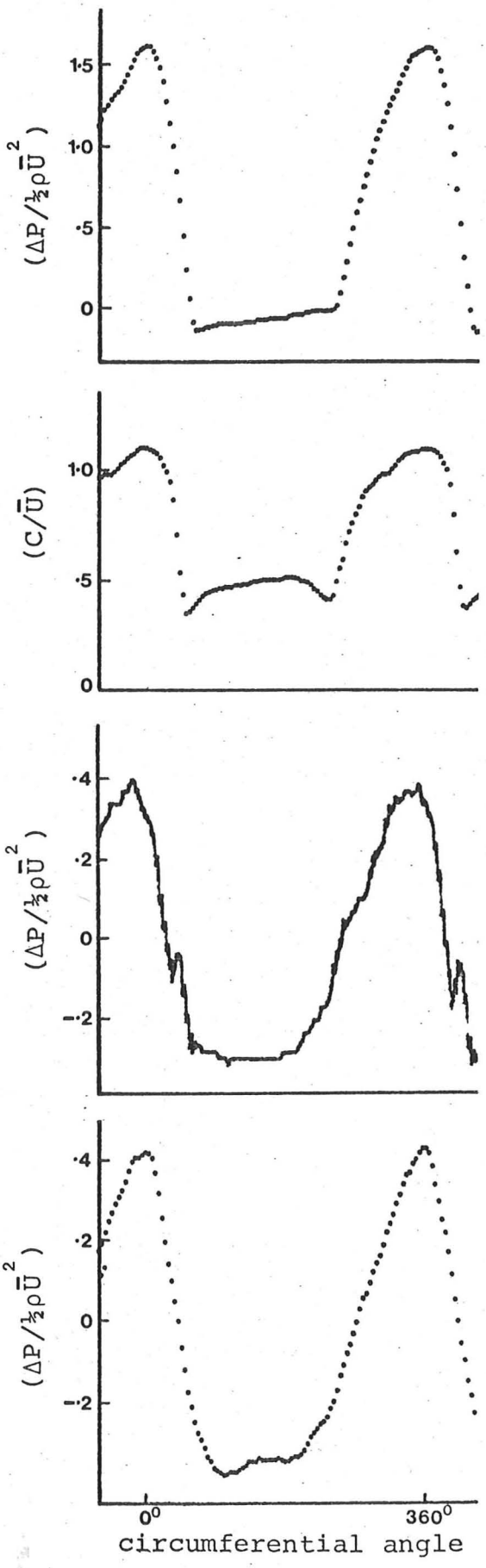

Comparison of calculated and measured static pressures.

FIGURE 7

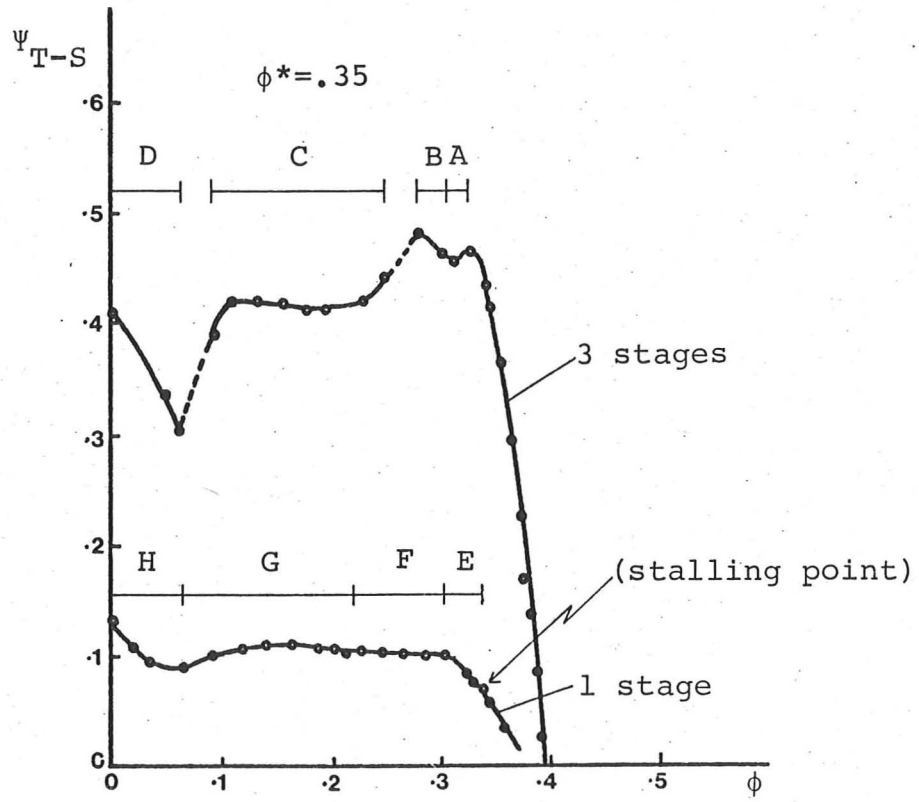

A part-span stall, 4 cells
B part-span stall, 12 cells
C full-span stall, 1 cell
D axisymmetric swirling flow
E part-span stall, 6 cells
F part-span stall, 12 cells
G part-span stall, 1 cell
H axisymmetric swirling flow

Total-to-static characteristics for Low Φ^* builds.

FIGURE 8

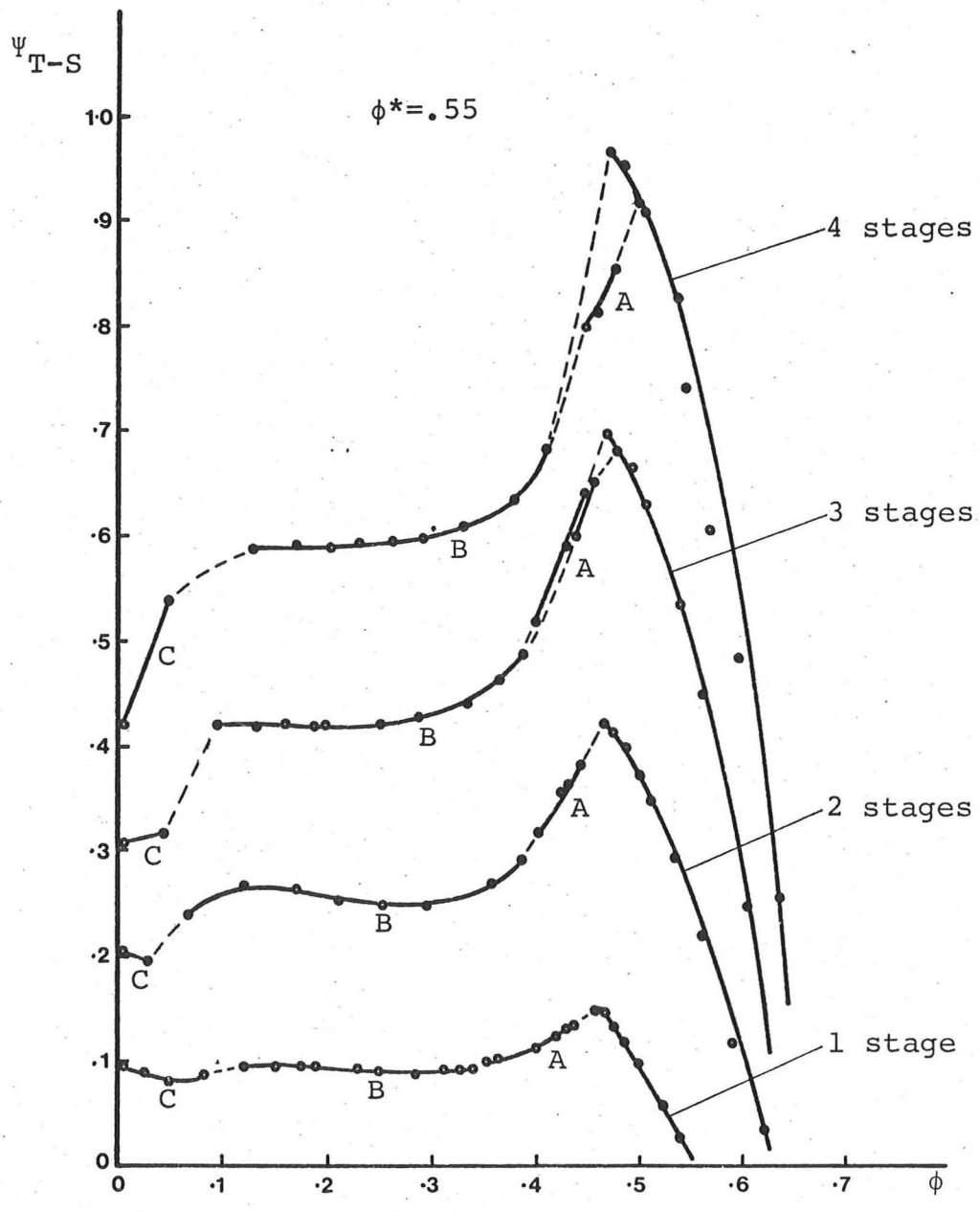

A part-span stall, 1 cell
B full-span stall, 1 cell
C axisymmetric flow

Total-to-static characteristics for the Intermediate Φ^* builds.

FIGURE 9

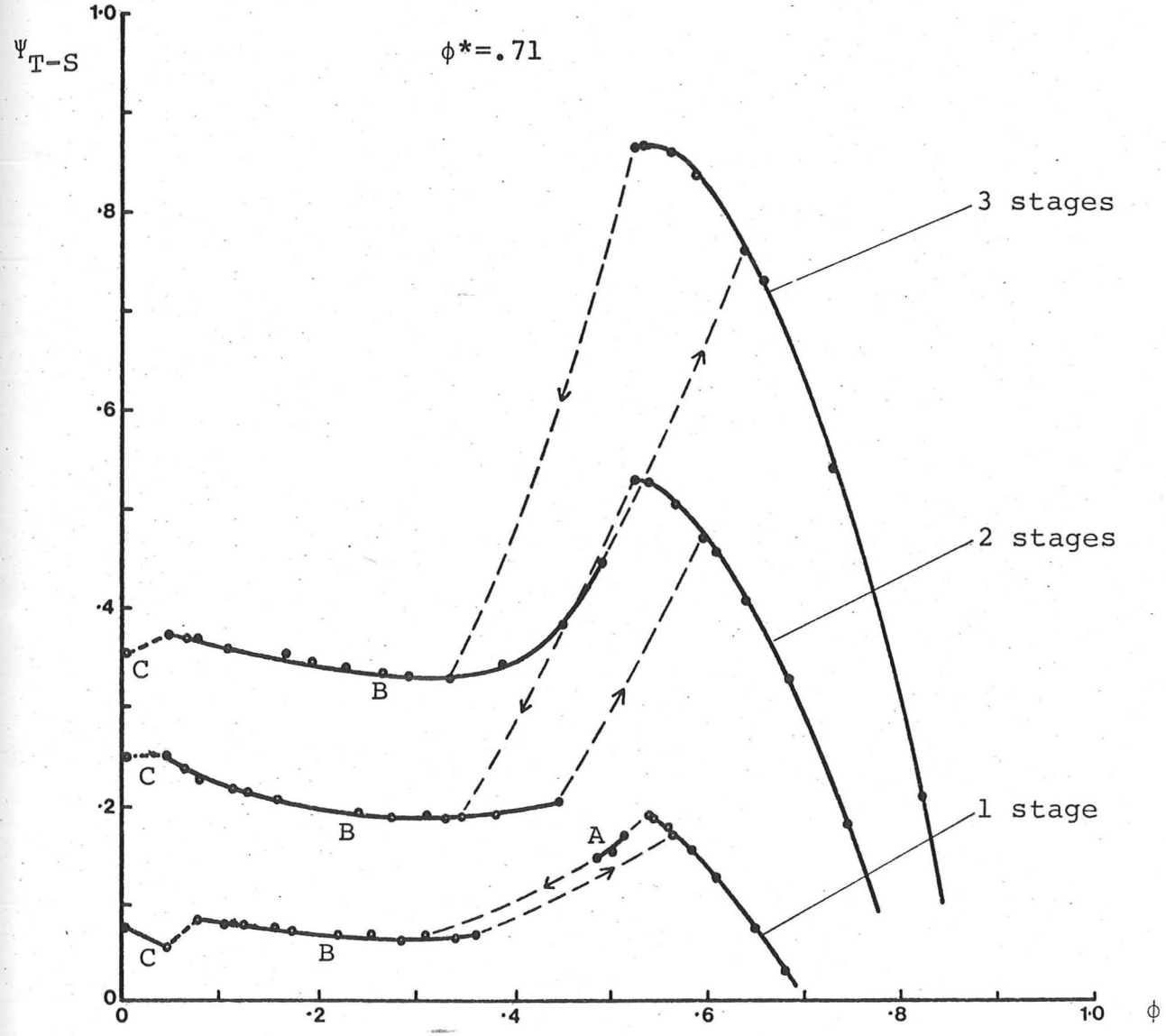

A part-span stall, 1 cell
B full-span stall, 1 cell
c axisymmetric flow

Total-to-static characteristics for High Reaction builds.

FIGURE 10

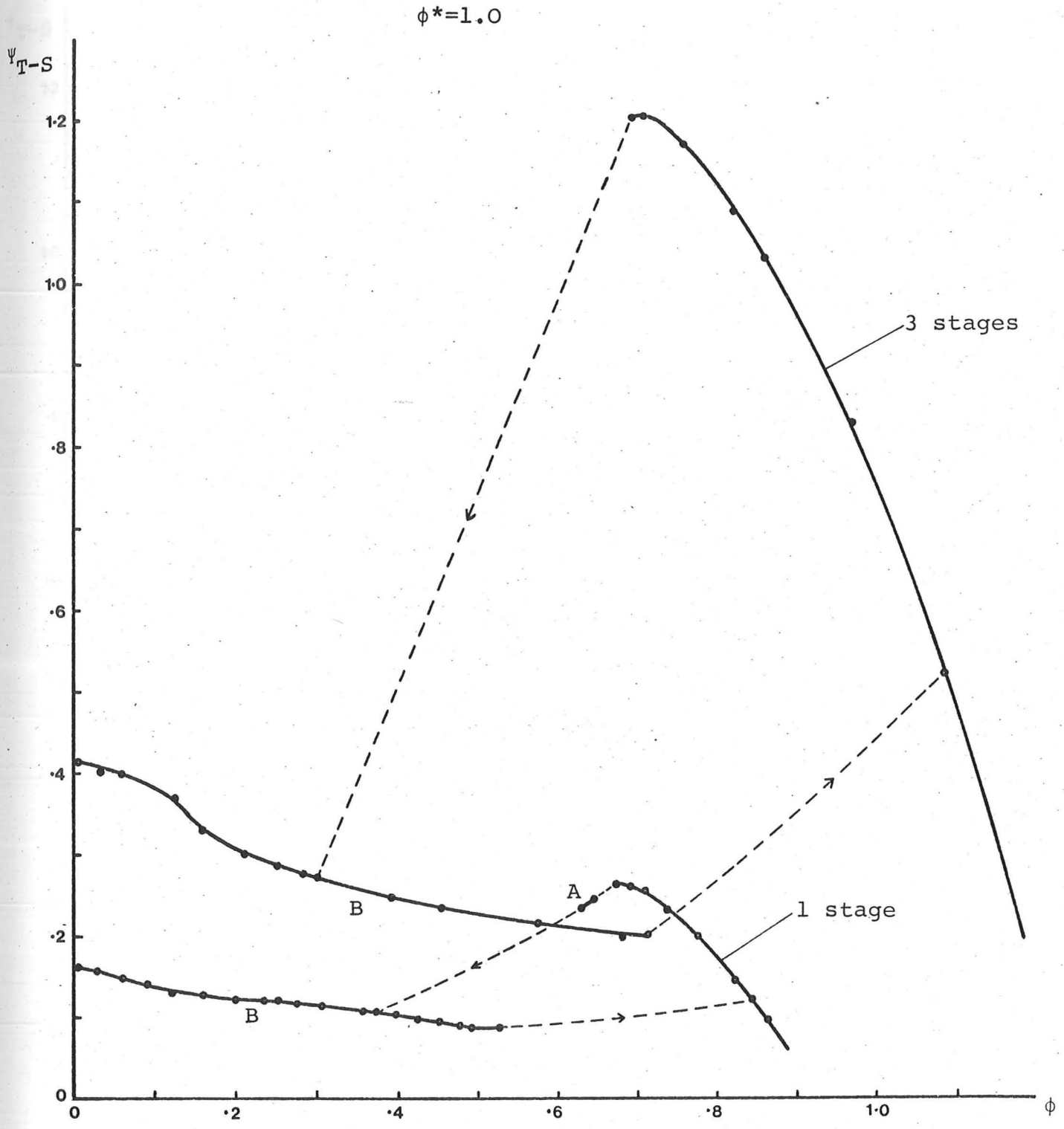

A part-span stall, 1 cell
B full-span stall, 1 cell

Total-to-static characteristics for High Φ^* builds.

FIGURE 11

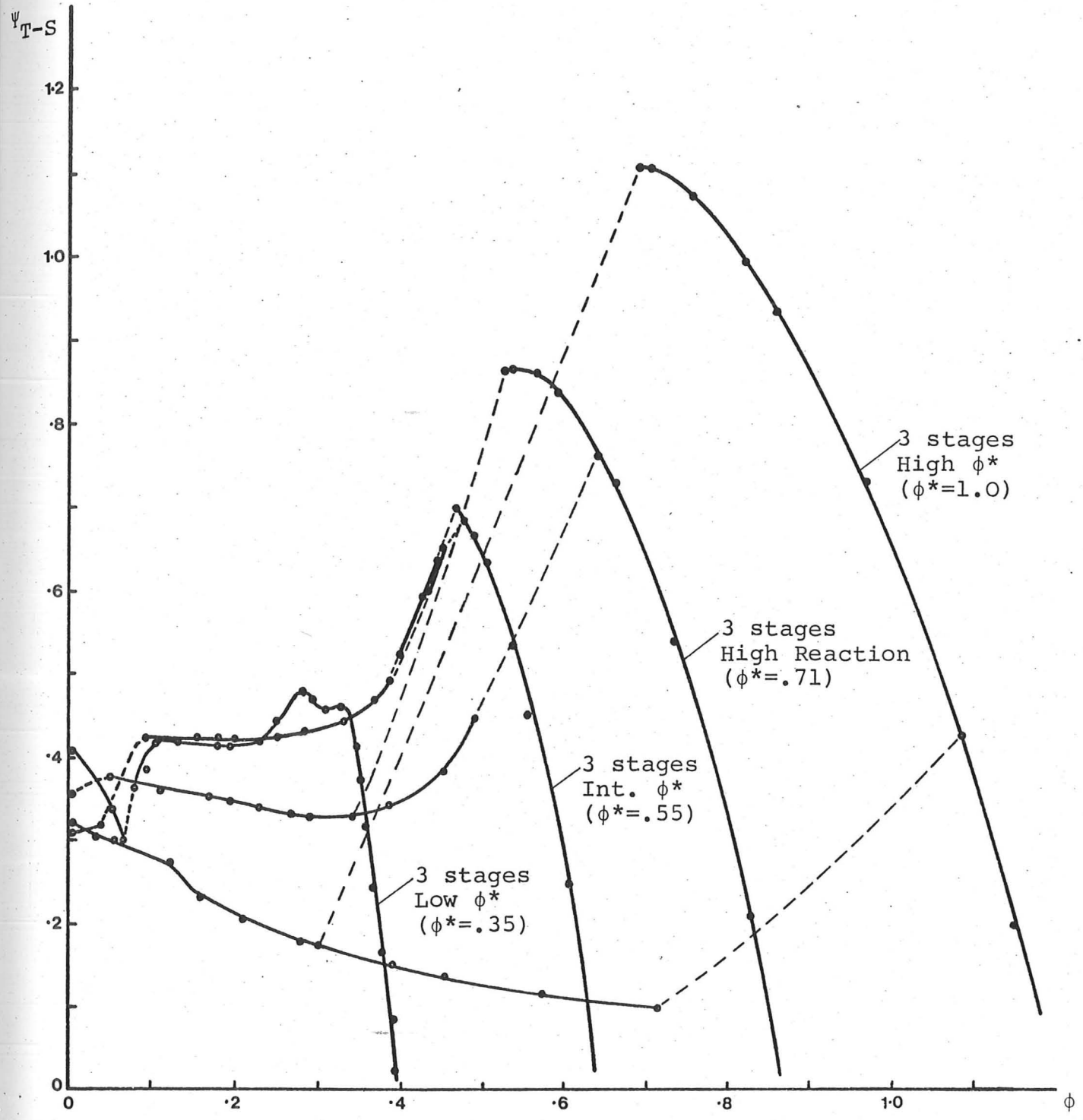

Total-to-static characteristics of four 3-stage builds of different designs.

FIGURE 12

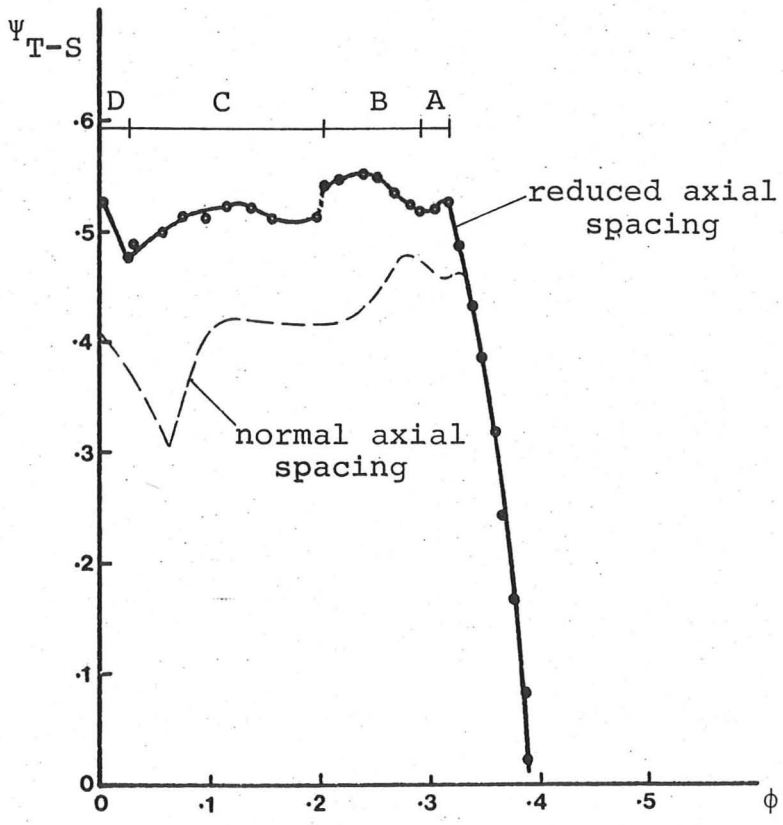

A part-span stall, 1 cell
B part-span stall, 4 cells
C full-span stall, 1 cell
D axisymmetric swirling flow

Total-to-static characteristics of 3-stage Low Φ* builds showing the effect of reduced axial spacing.

FIGURE 13

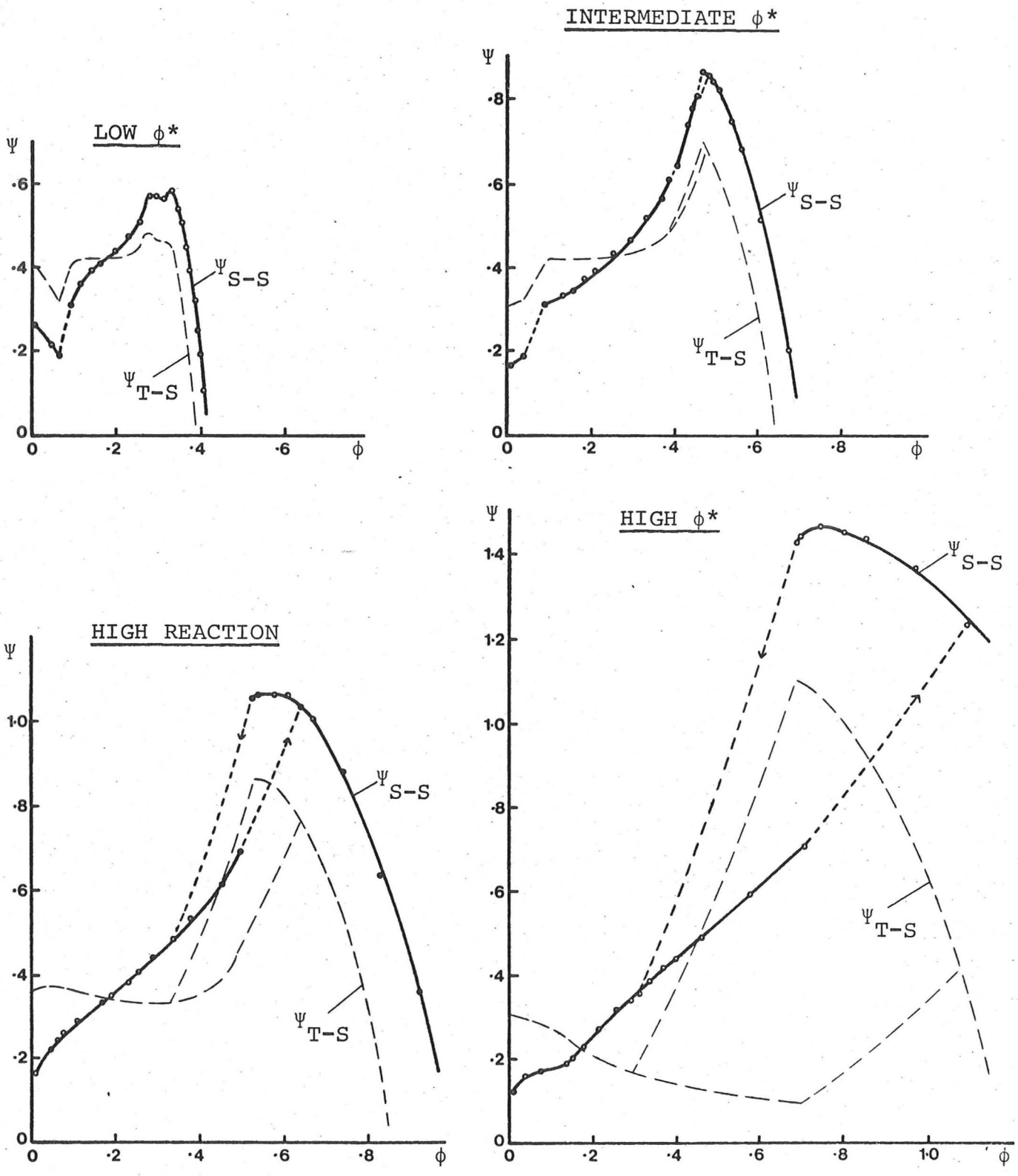

Comparison of static-to-static characteristics with total-to-static characteristics (shown dotted) for four 3-stage compressor builds.

FIGURE 14

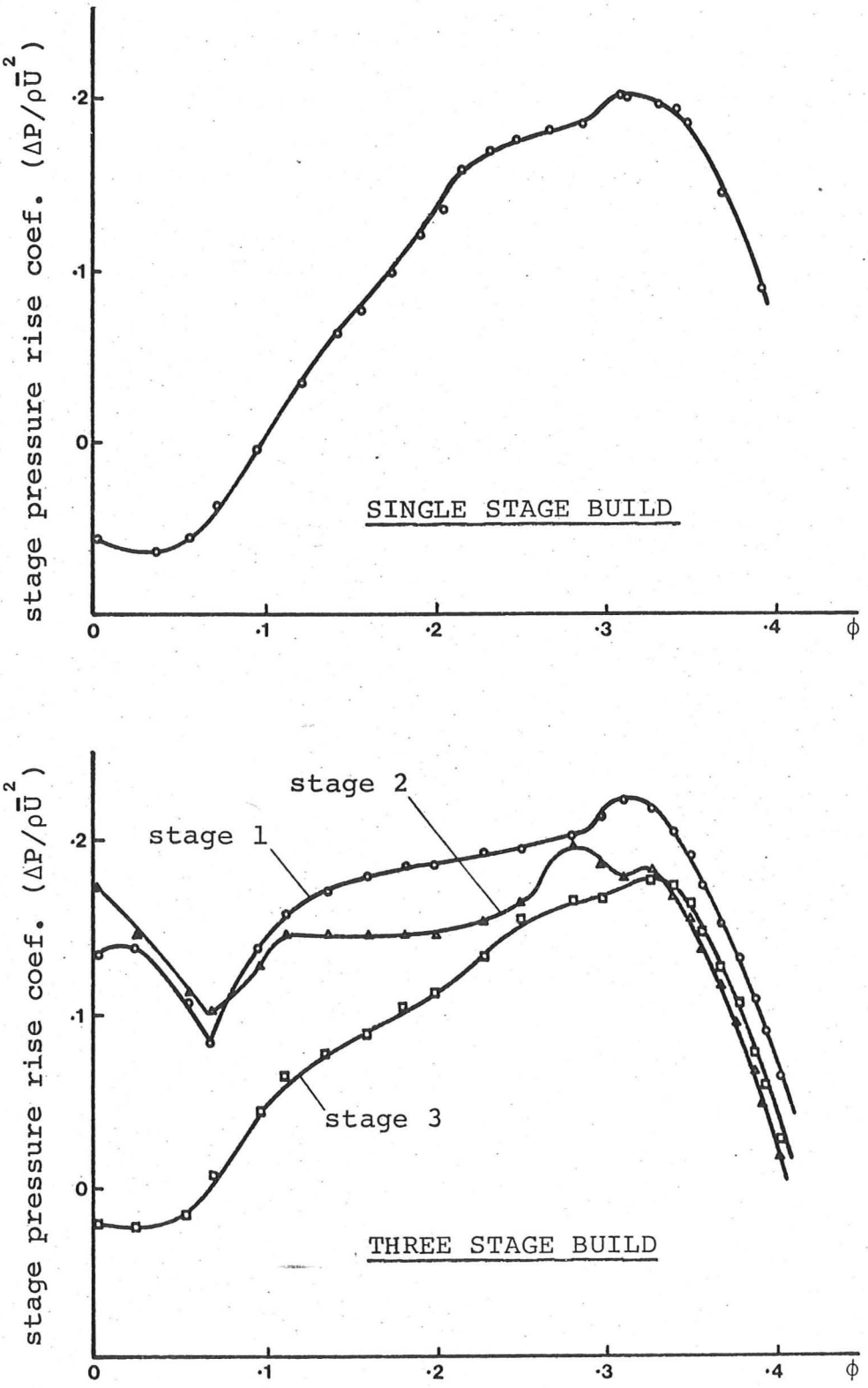

Individual stage characteristics from a 1-stage and a 3-stage build of Low Φ^* design.

FIGURE 15

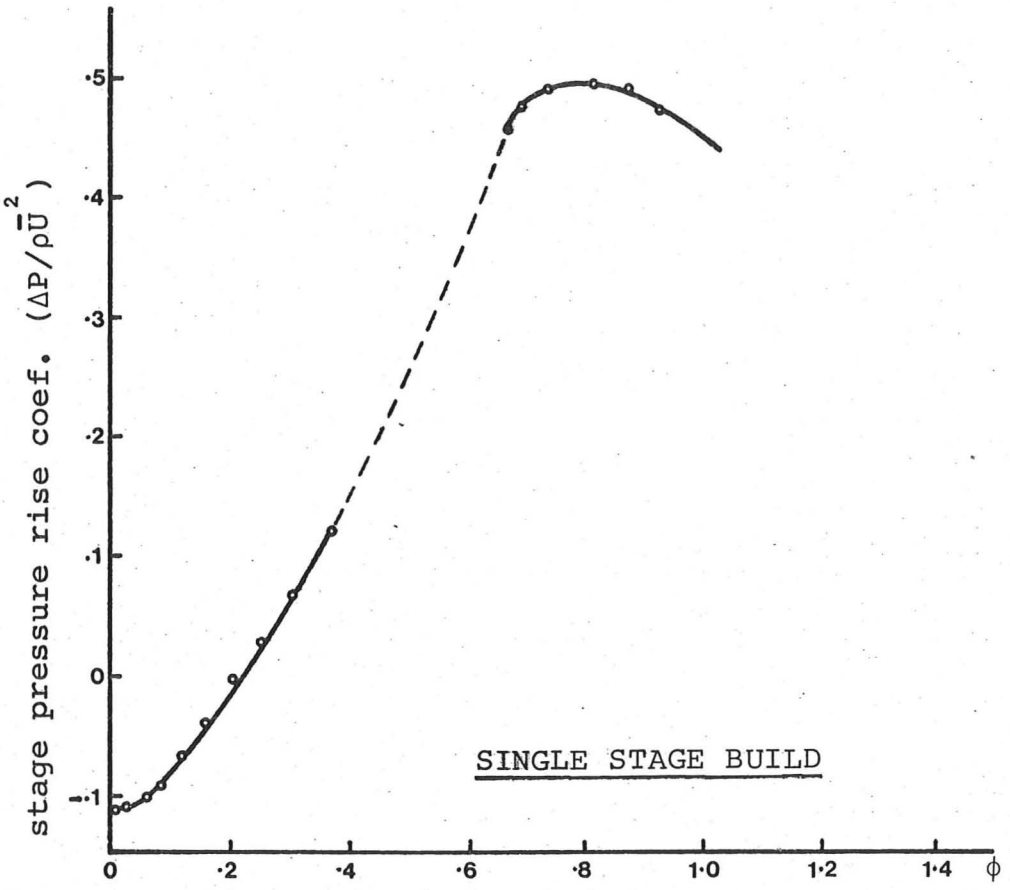

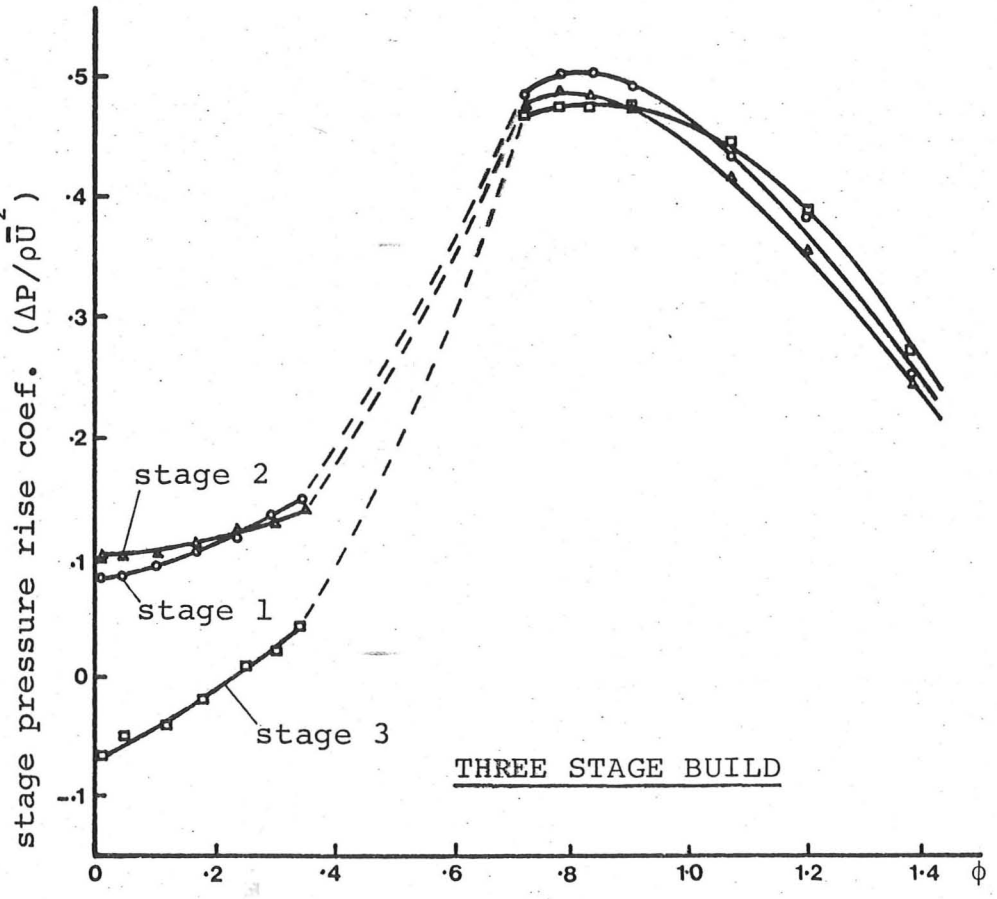

Individual stage characteristics from a 1-stage and a 3-stage build of High ϕ^* design.

FIGURE 16

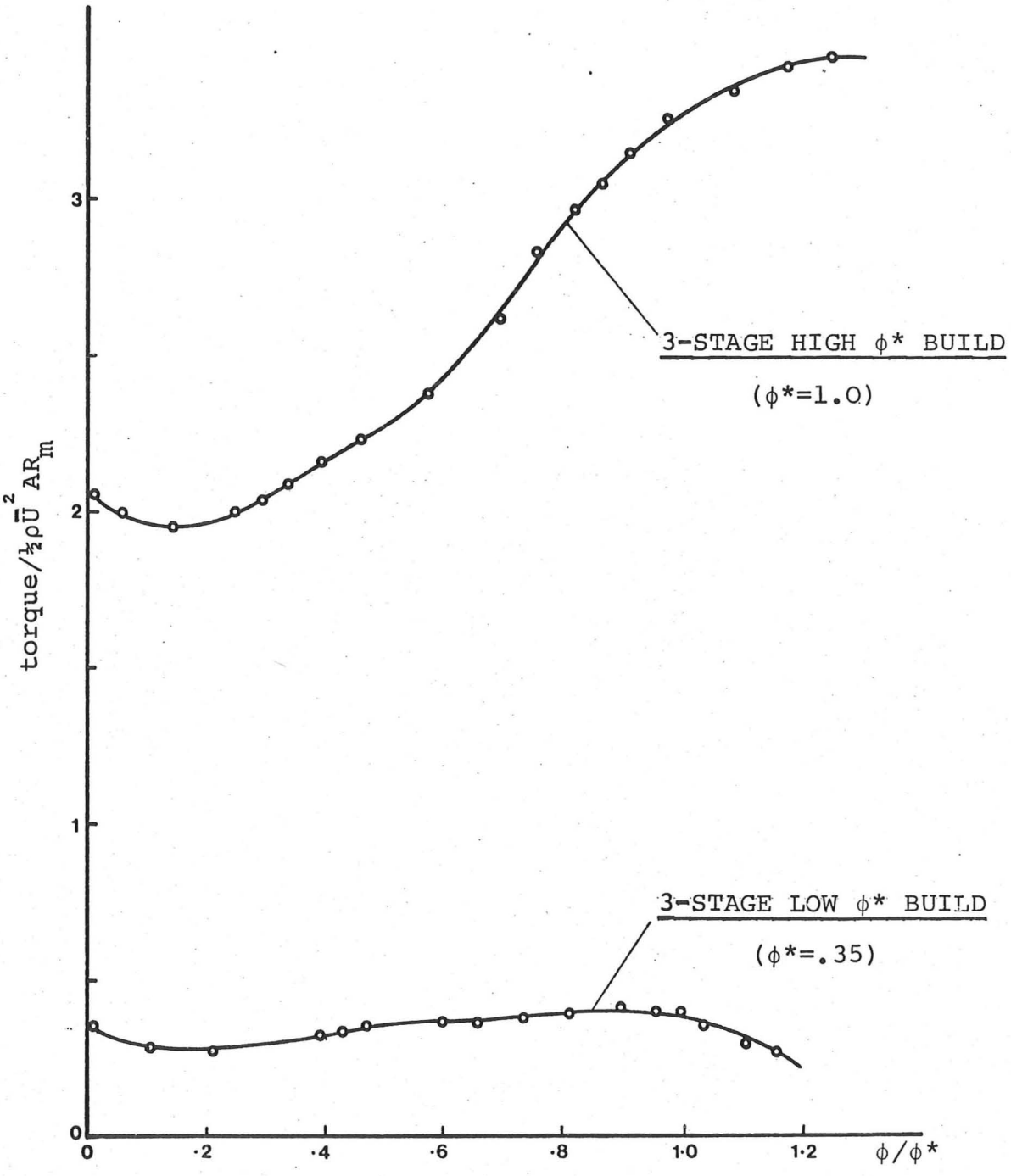

Comparison of torque measurements in two compressors of different design.

FIGURE 17

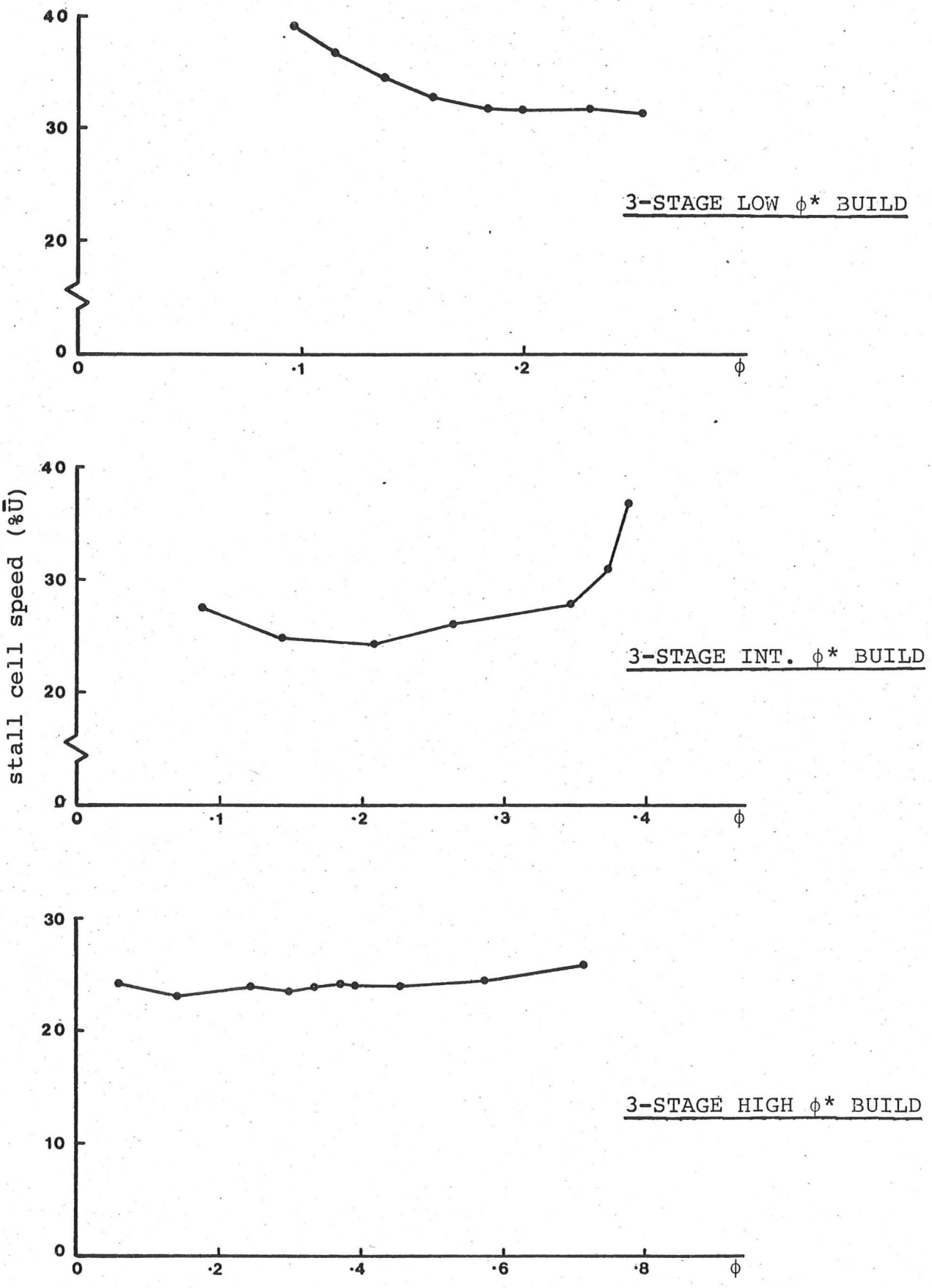

Stall cell speed as a function of flow coefficient for three compressor builds.

FIGURE 18

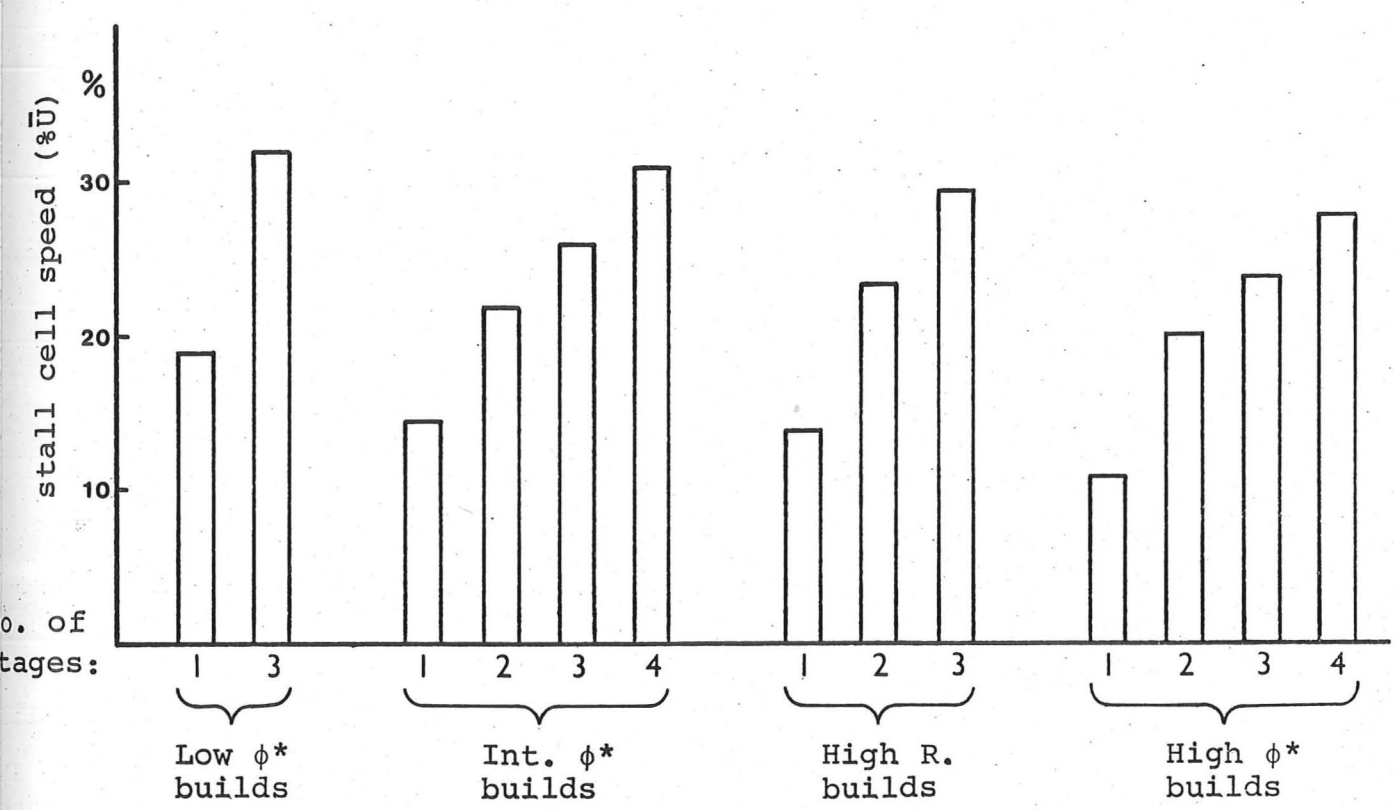

Comparison of cell speeds for cells covering 50% of annulus in the various compressor builds.

FIGURE 19

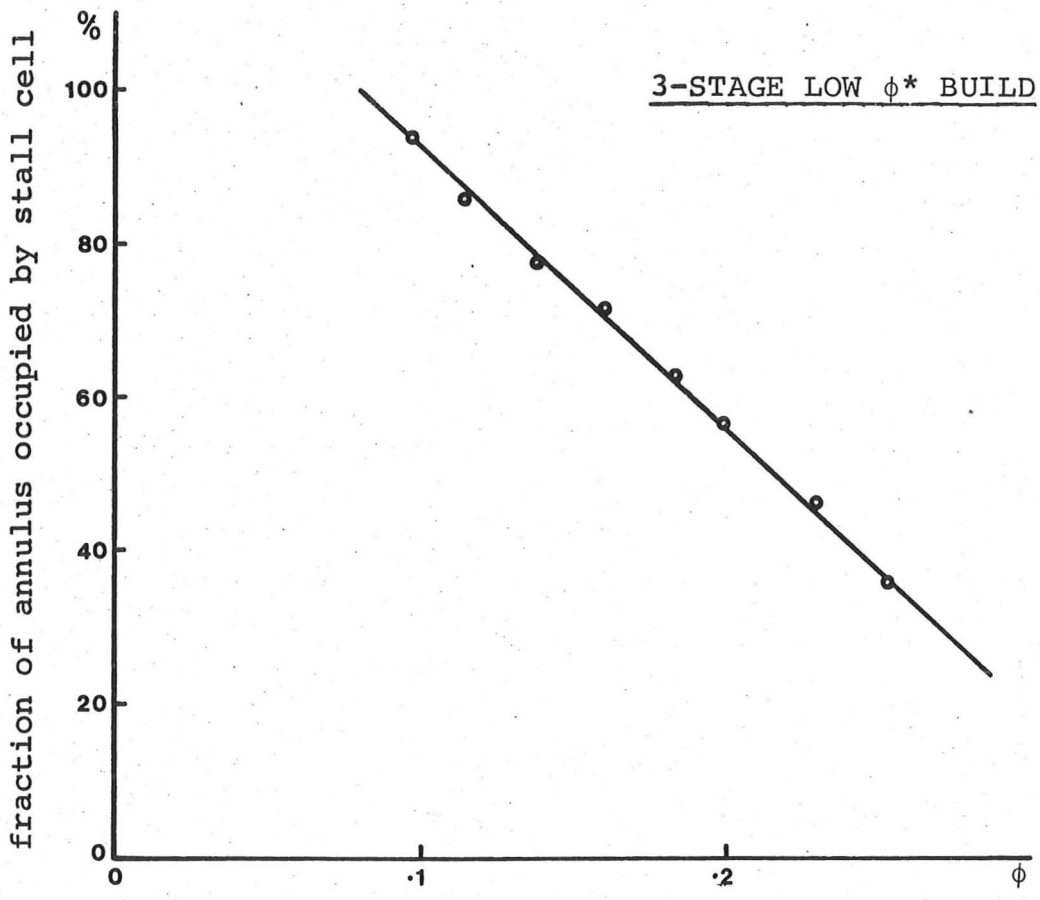

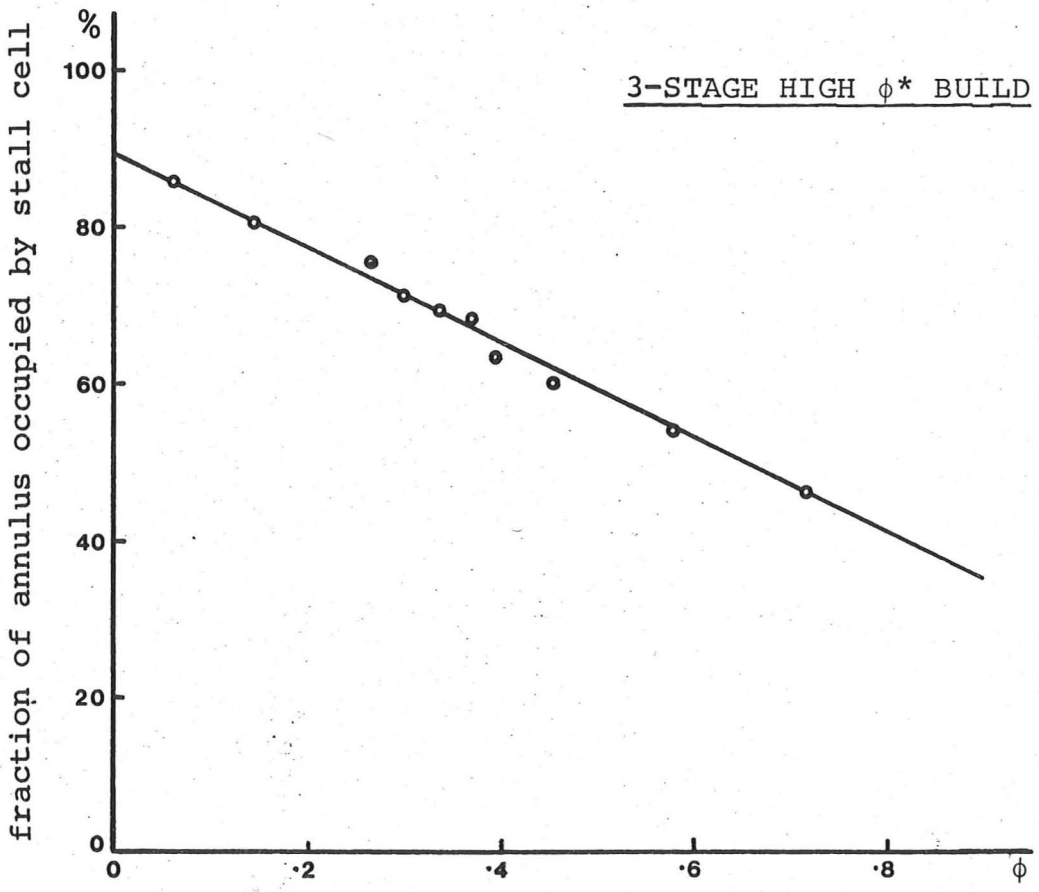

Percentage of annulus covered by stall cell as a function of compressor flow rate.

FIGURE 20

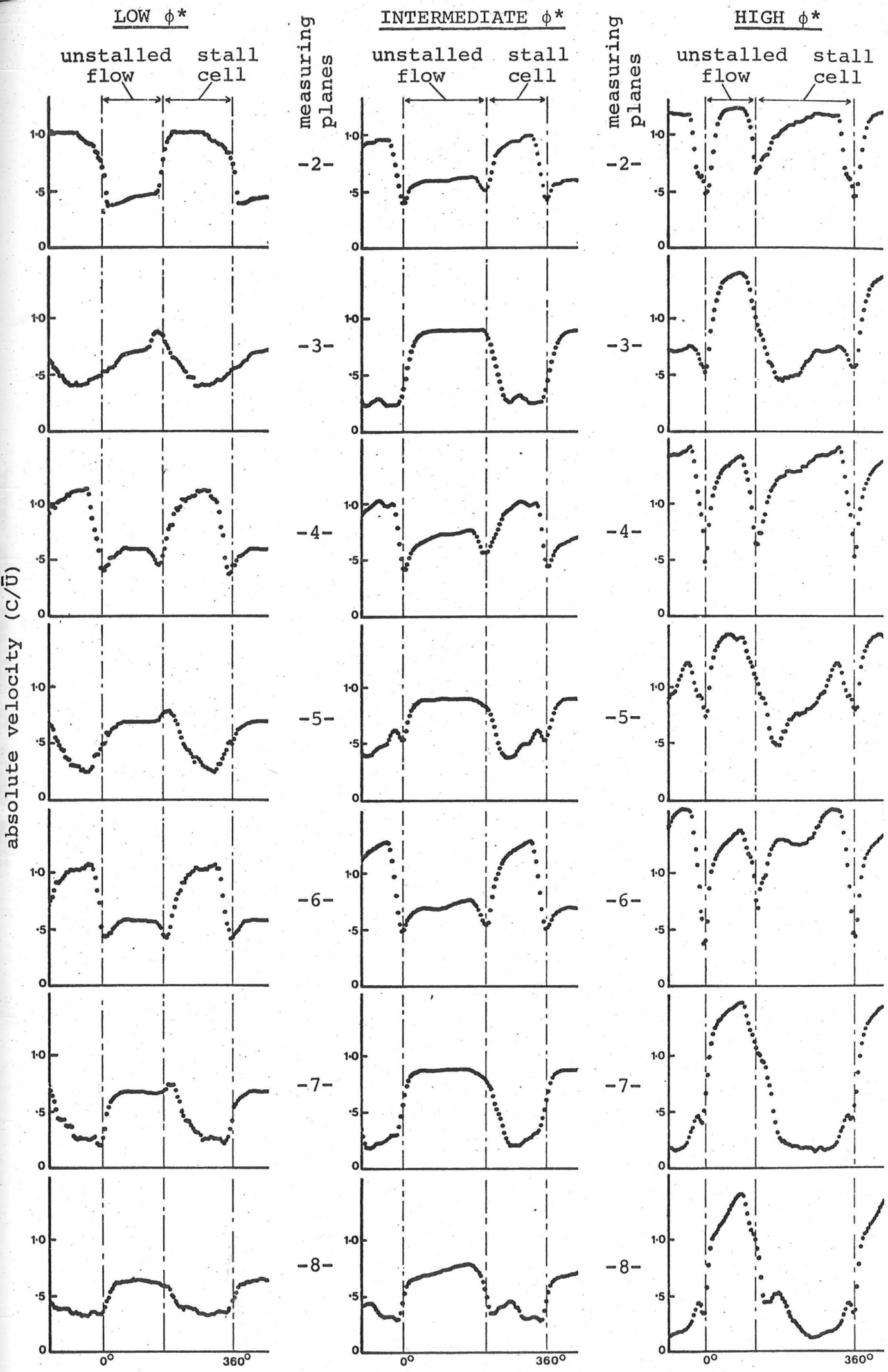

Absolute velocity in three 3-stage compressor builds.
(Plane R_1, page 62. ϕ_{test}=.20, .33, .30 respectively)

FIGURE 21

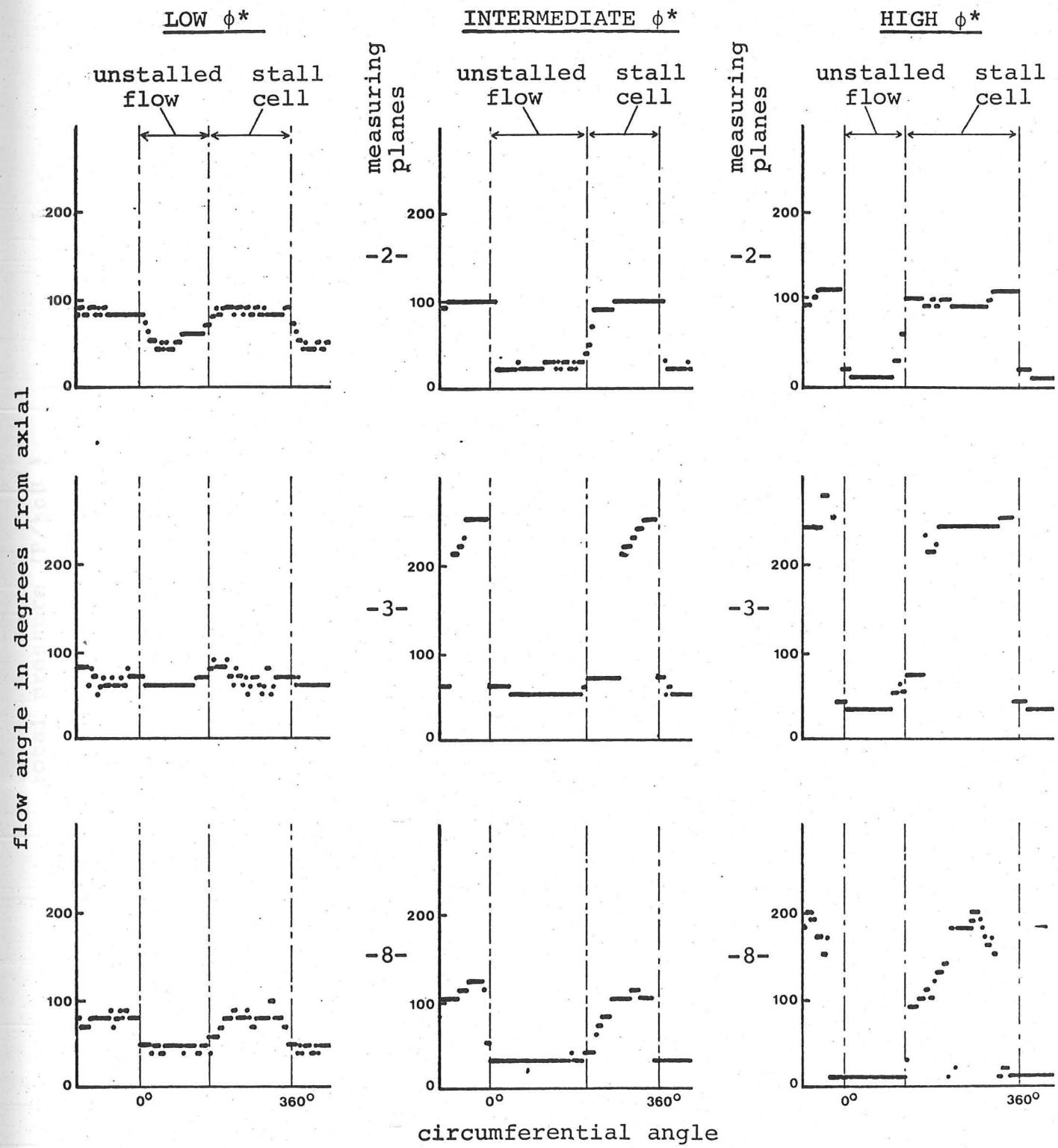

Flow direction measurements in three compressor builds.

FIGURE 22

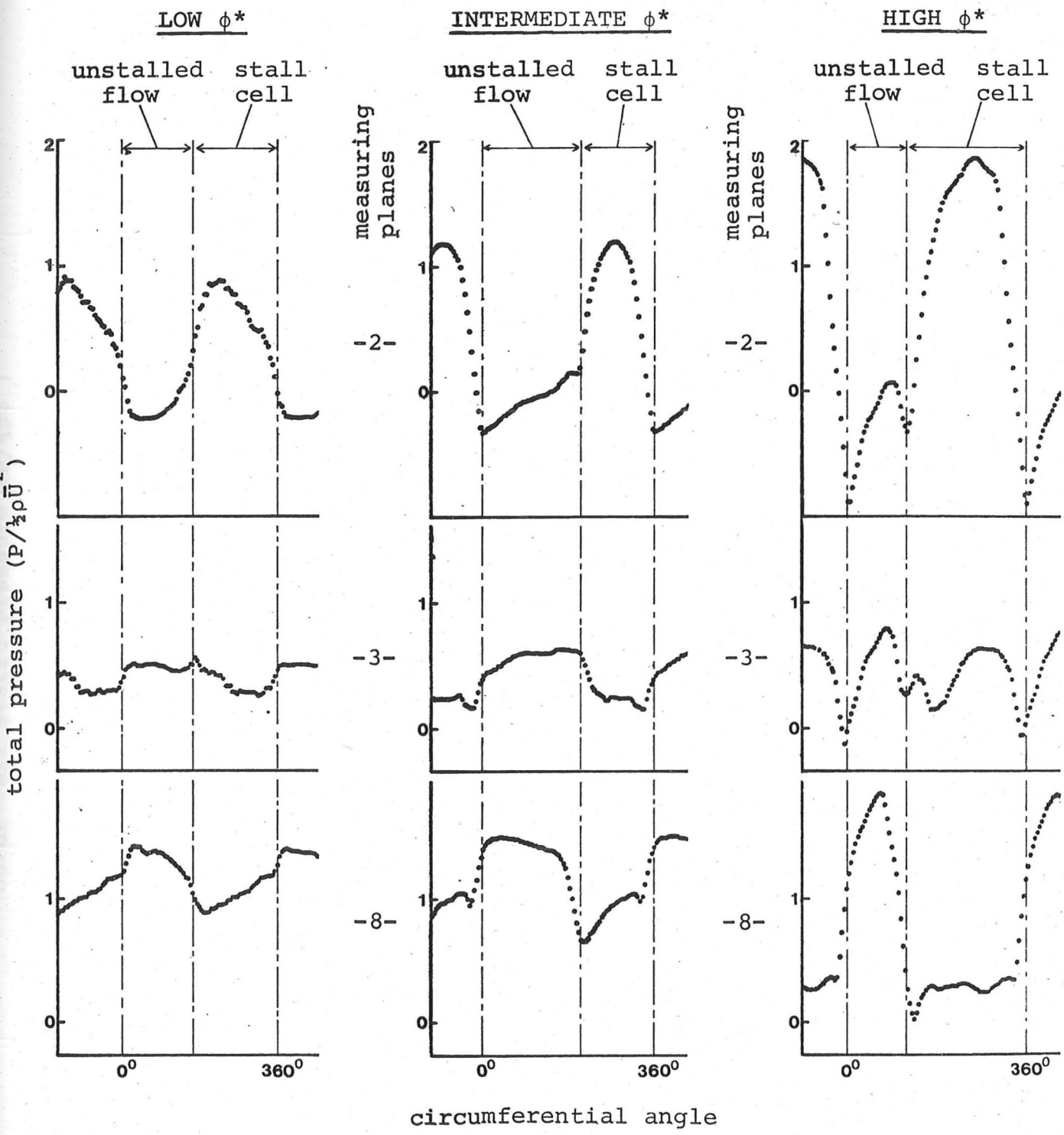

Total pressure measurements in three compressor builds.

FIGURE 23

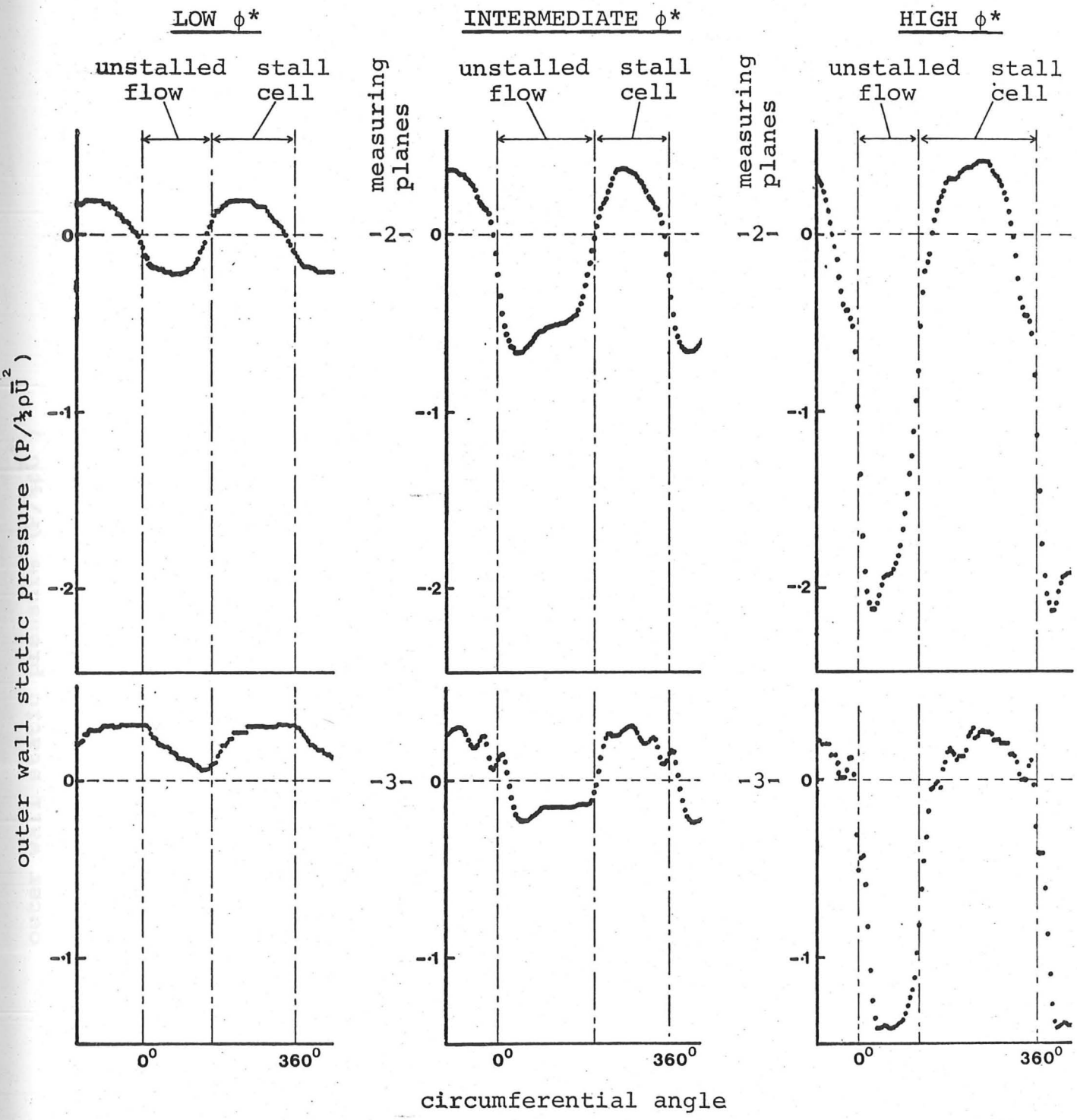

Outer wall static pressures before and after the first rotor in three compressor builds.

FIGURE 24a

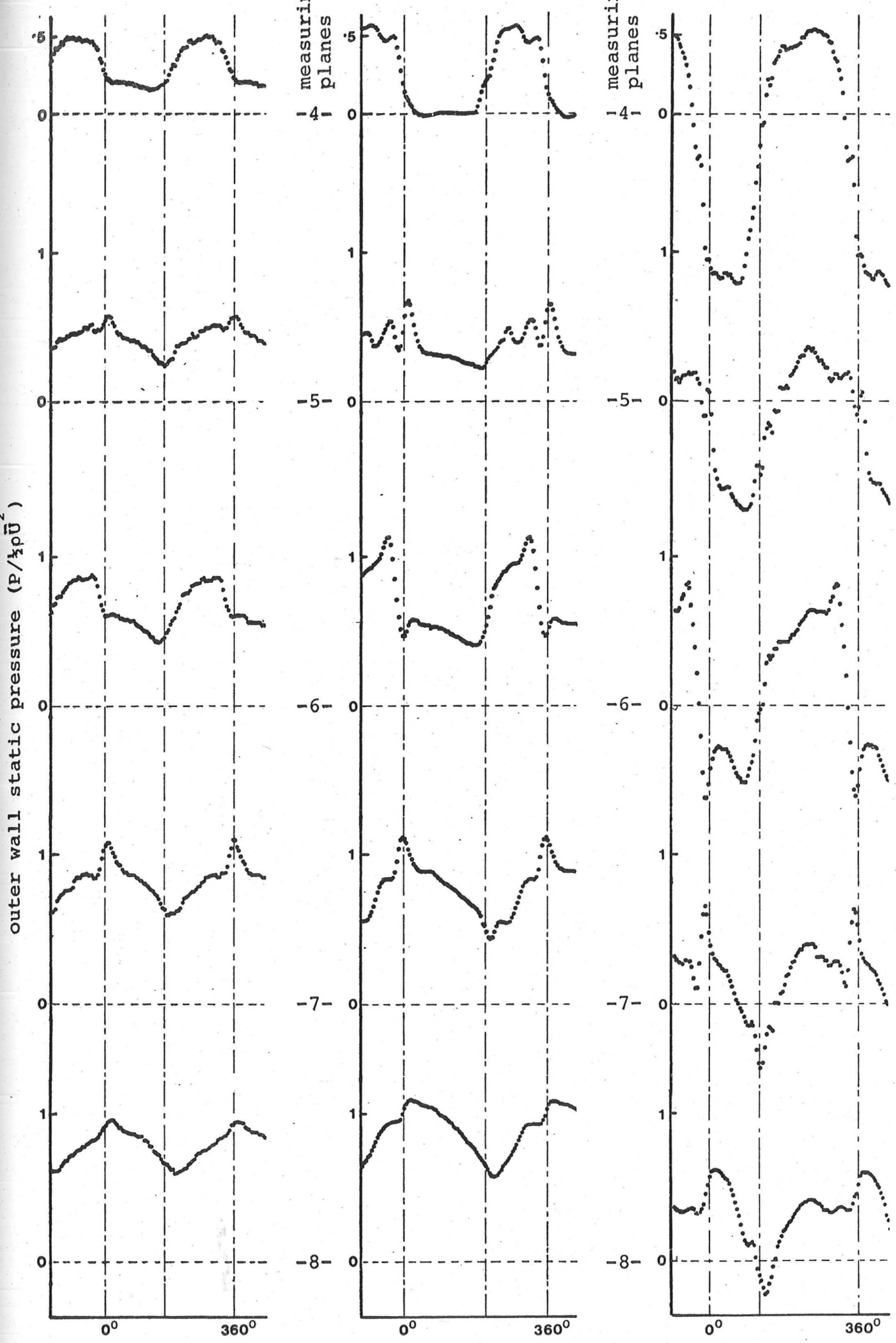

Outer wall static pressure measurements continued. FIGURE 24b

VELOCITY

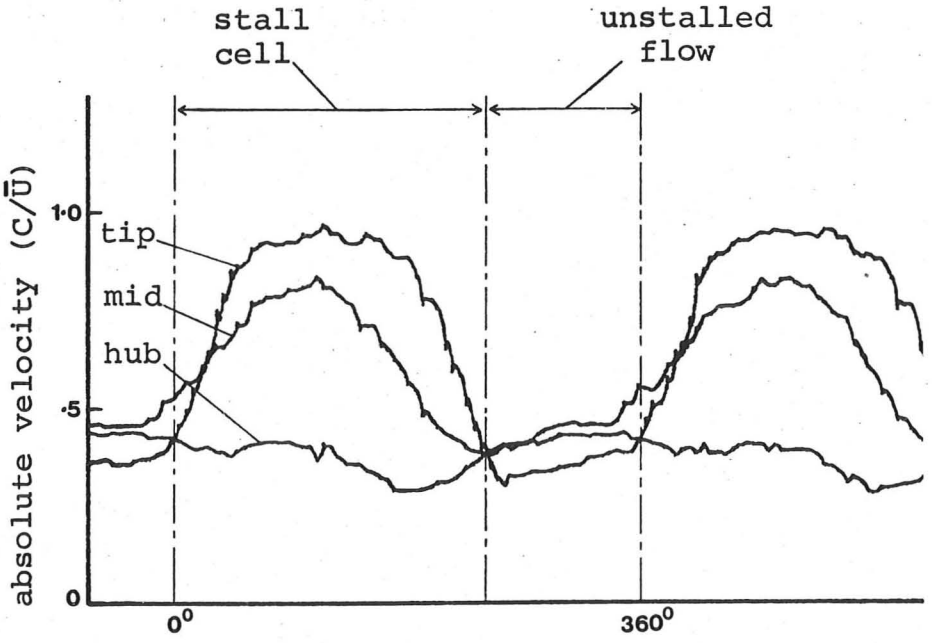

TOTAL PRESSURE

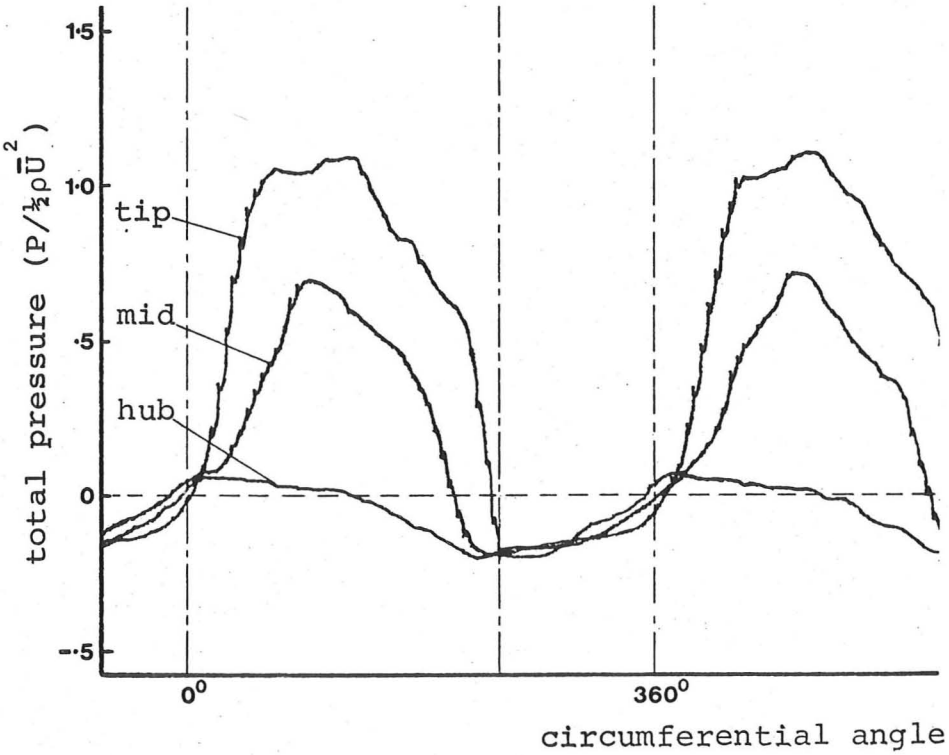

Measurements showing radial differences in stall cell ahead of first rotor in 3-stage Low ϕ^* compressor. (ϕ^* = .20)

FIGURE 25a

VELOCITY

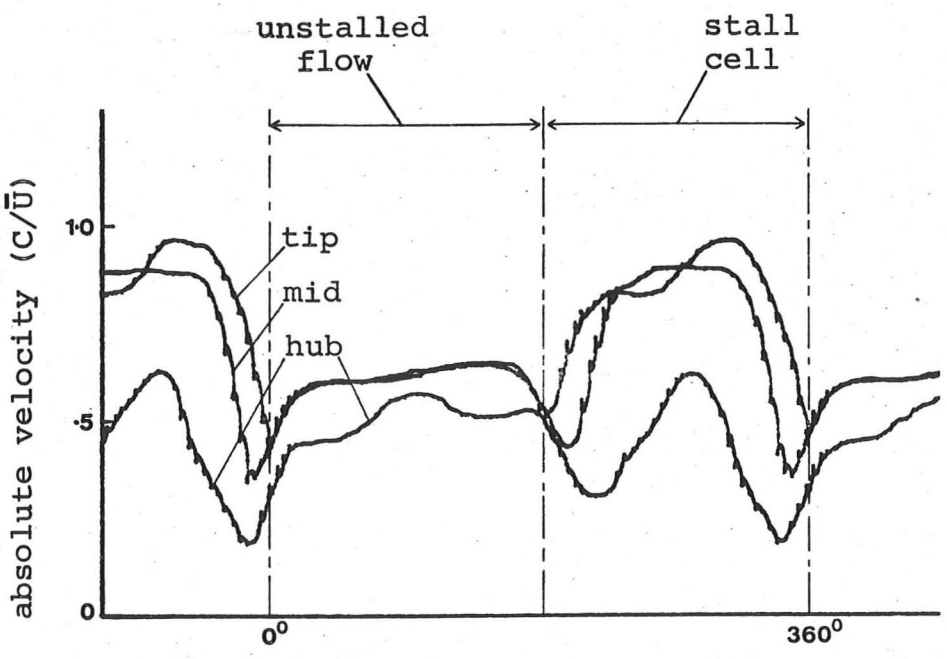

TOTAL PRESSURE

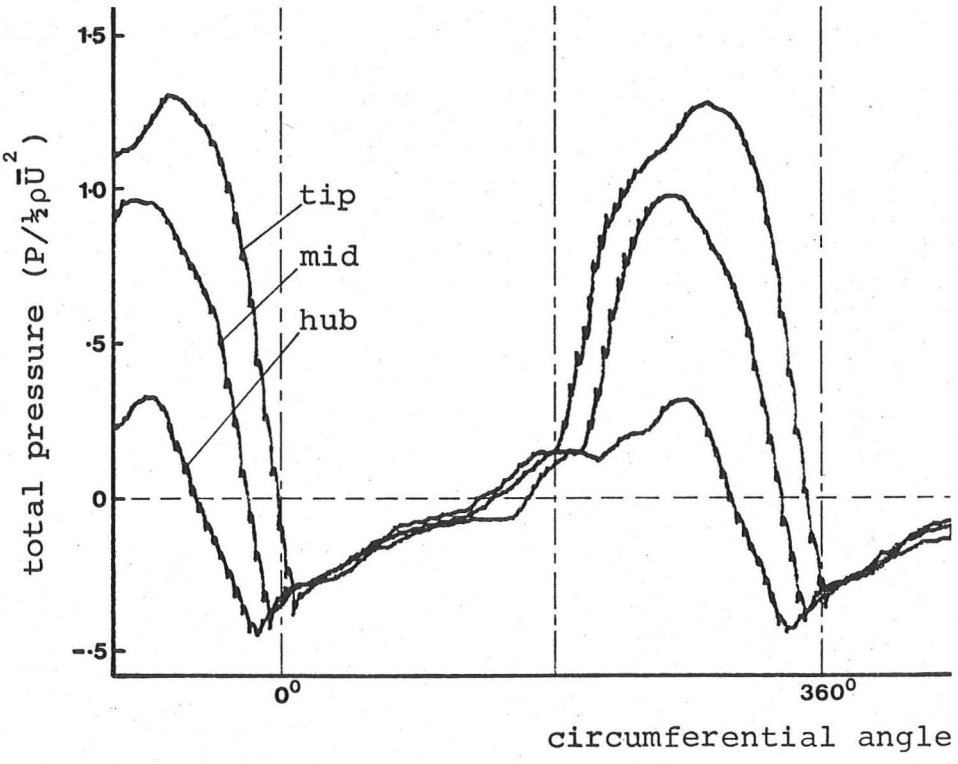

Measurements showing radial differences in stall cell ahead of first rotor in 3-stage Int. ϕ^* compressor. (ϕ^* = .33)

FIGURE 25b

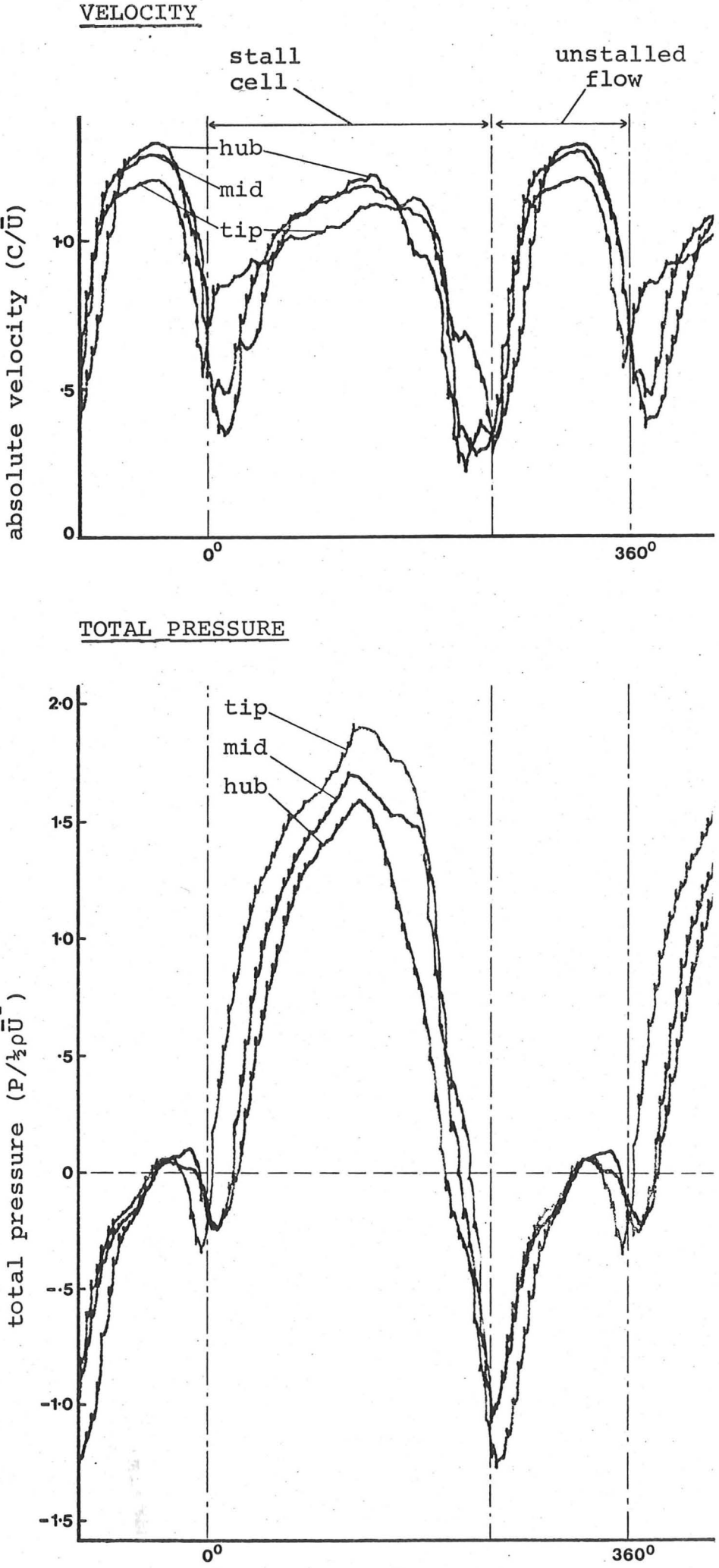

Measurements showing radial differences in stall cell ahead of first rotor in 3-stage High ϕ^* compressor. (ϕ^* = . 30)

FIGURE 25c

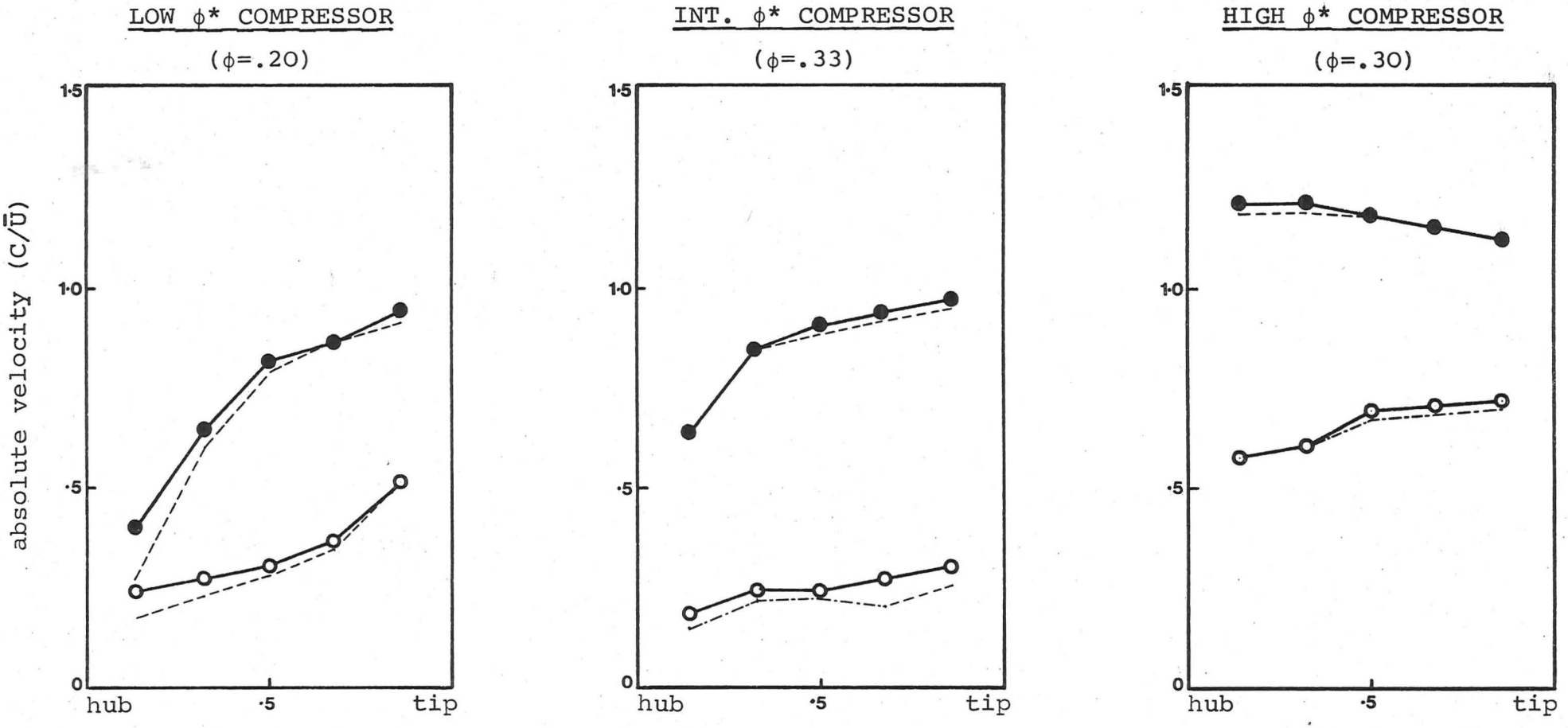

Absolute velocity at circumferential centre of stall cell in 3-stage compressor builds. FIGURE 26

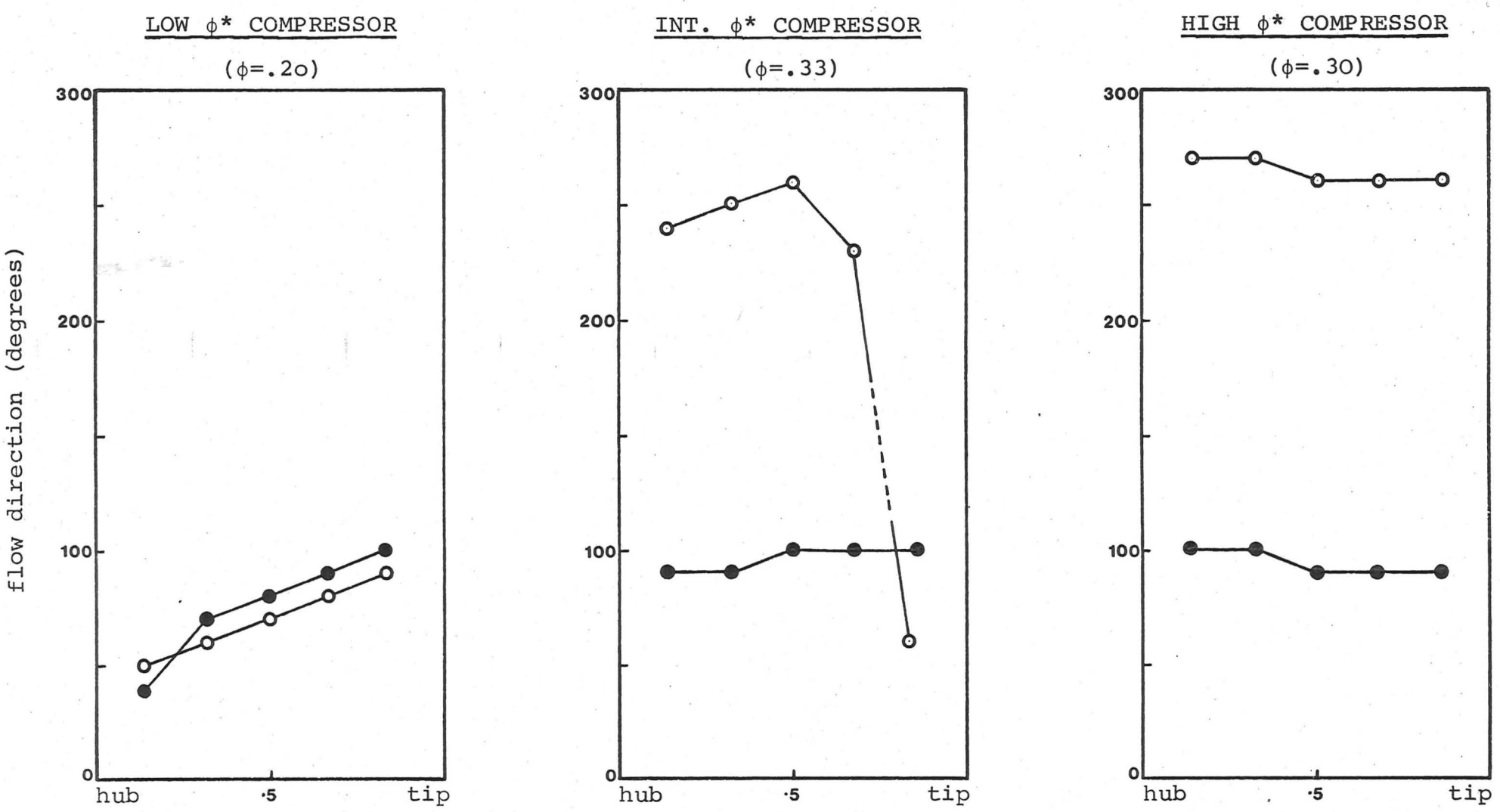

Flow direction at circumferential centre of stall cell in 3-stage compressor builds. FIGURE 27

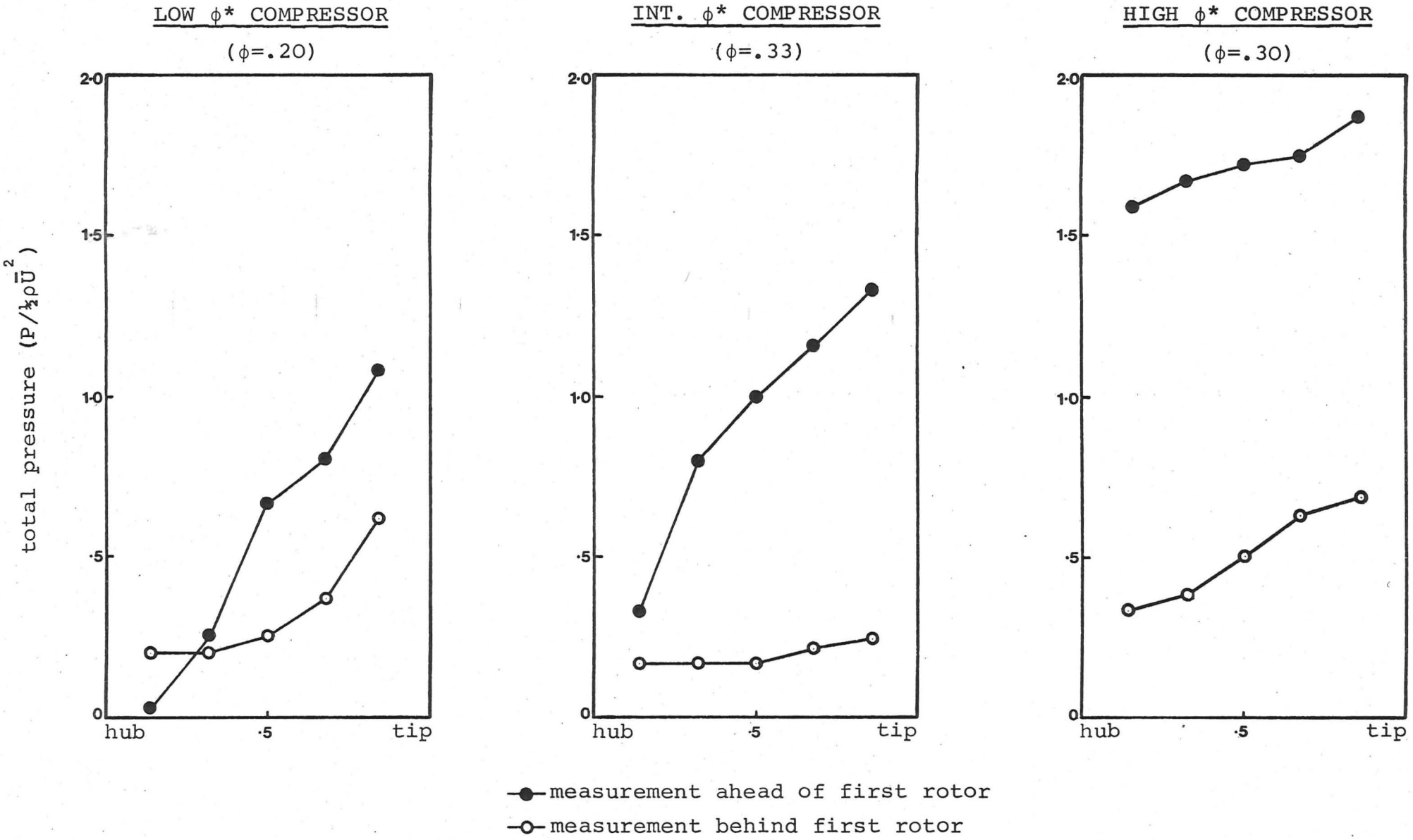

Total pressure at circumferential centre of stall cell in 3-stage compressor builds. FIGURE 28

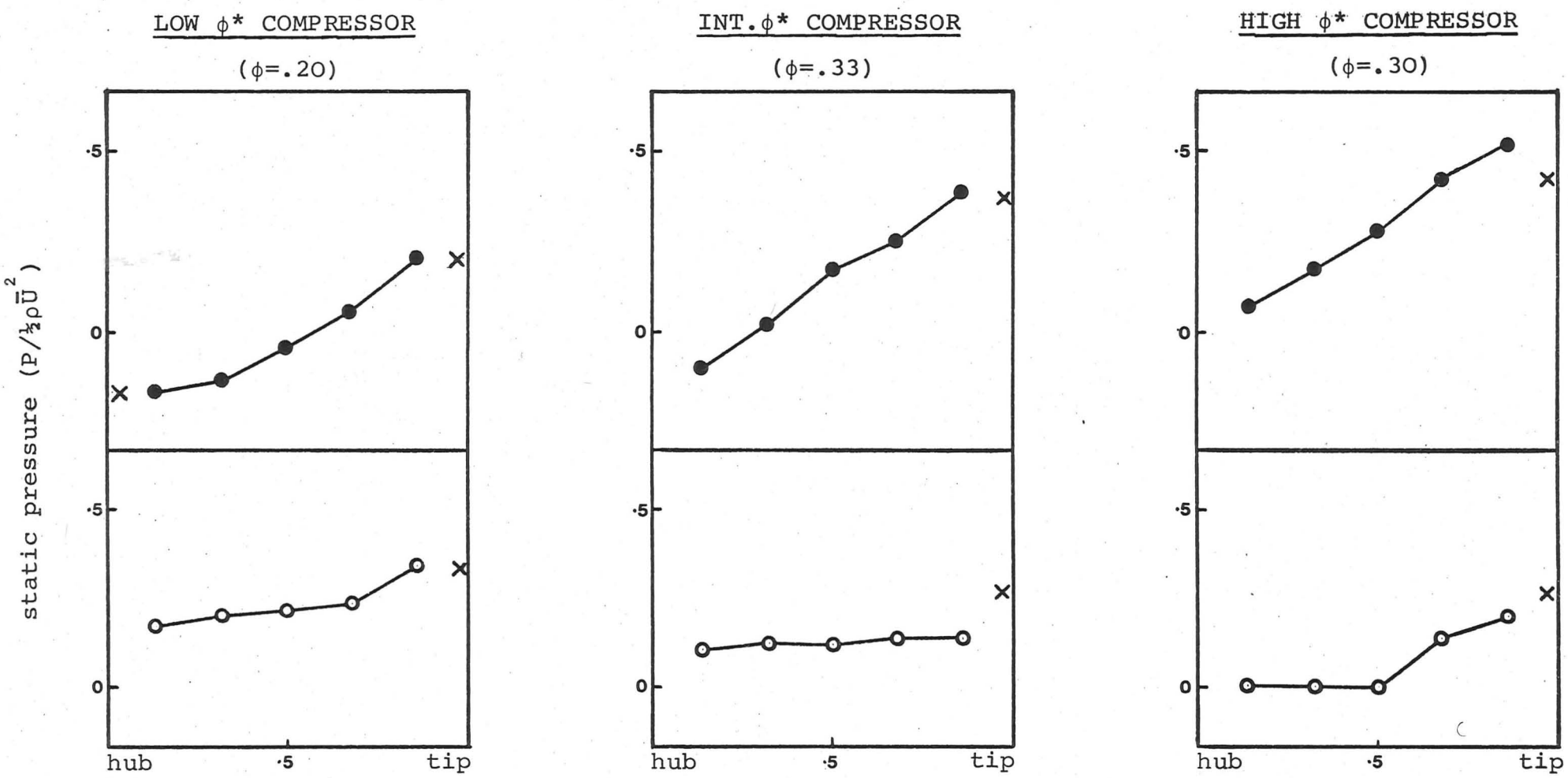

Static pressure in stall cell calculated from velocity and total pressure measurements in 3-stage compressor builds.

FIGURE 29

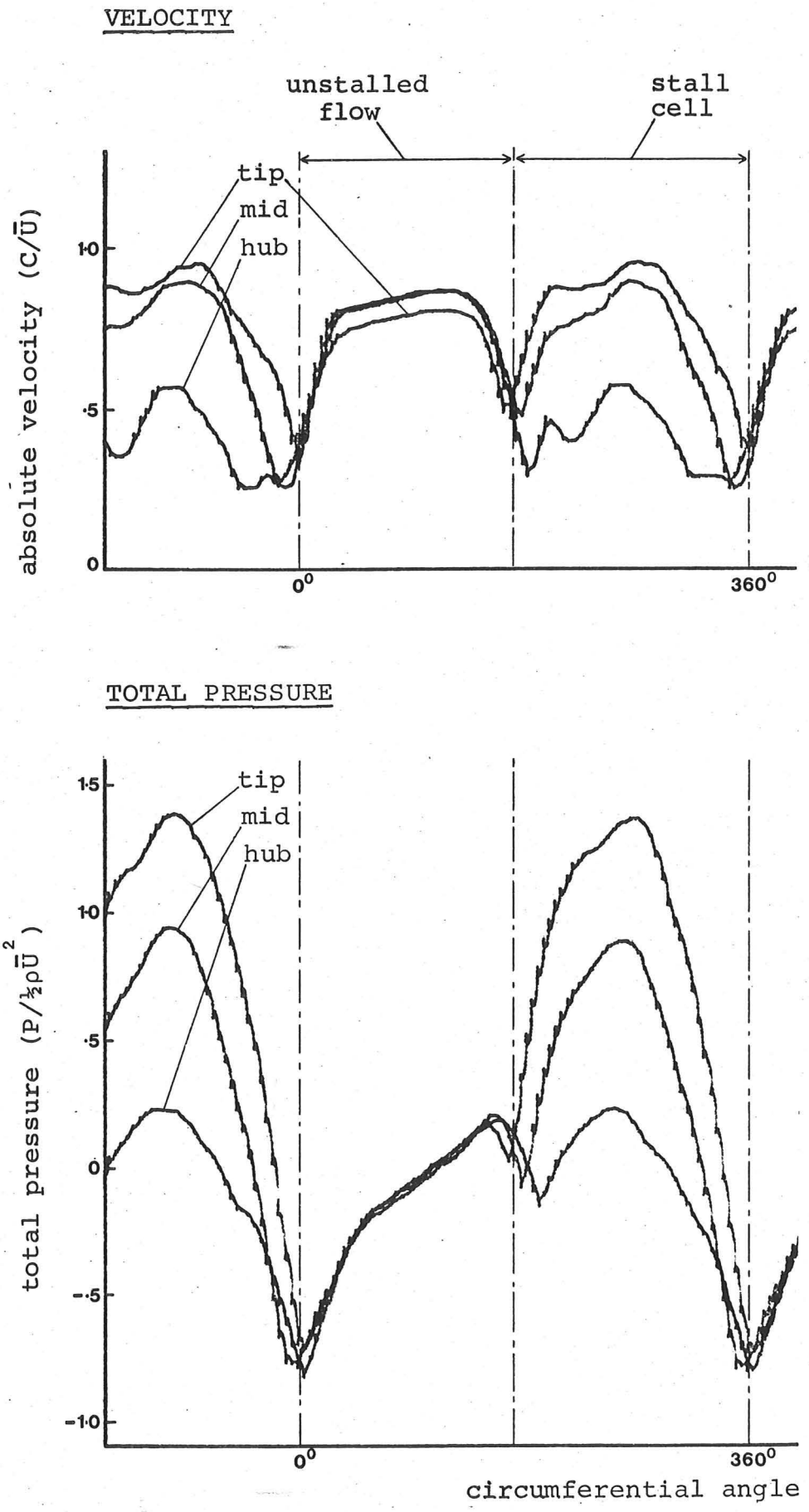

Measurements showing radial differences in stall cell ahead of first rotor in 3-stage High Reaction compressor.

FIGURE 30

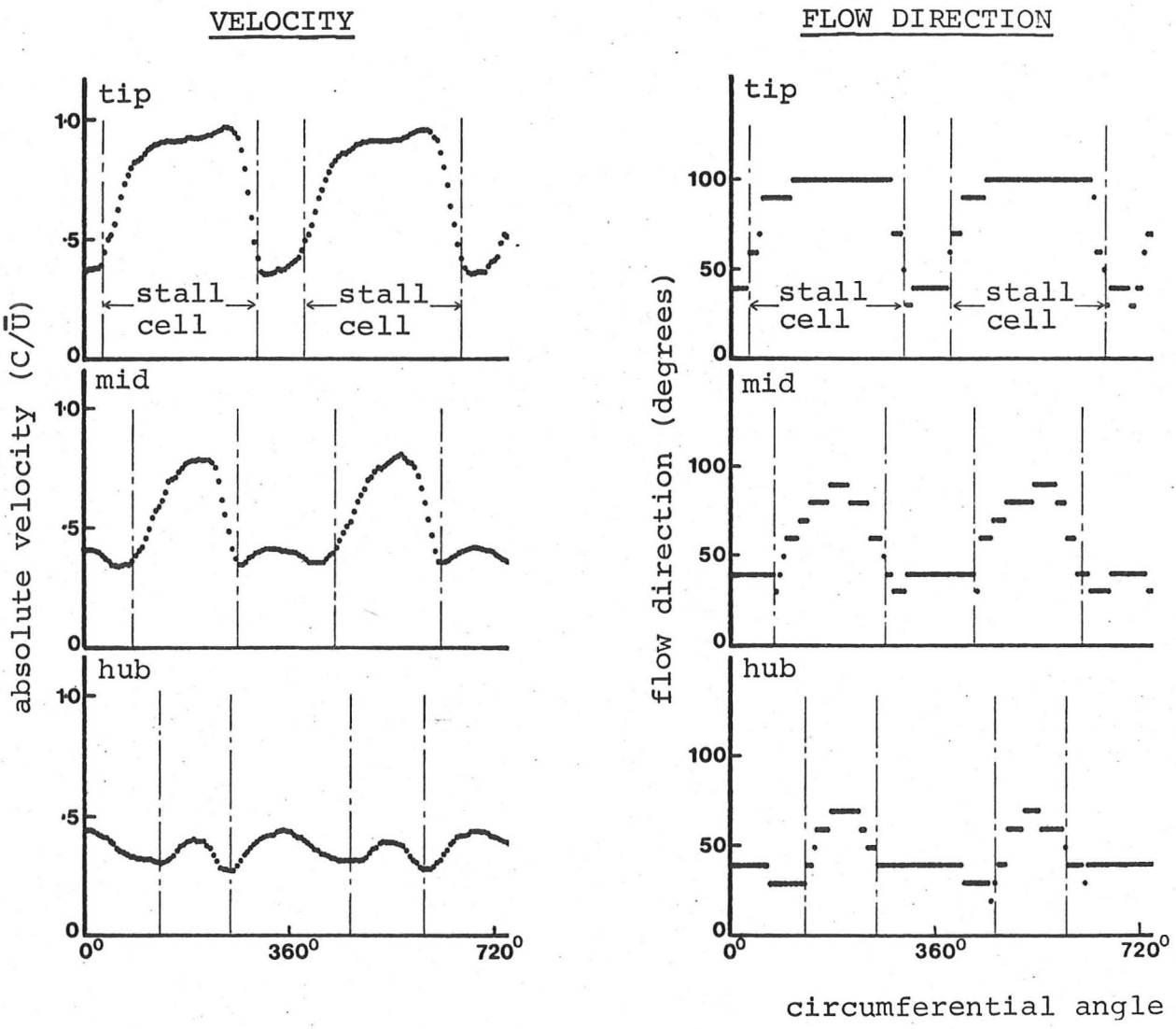

Velocity and flow direction measured at three radial positions ahead of first rotor in Low Φ* compressor build with rediced axial spacing.

(ϕ=.20)

FIGURE 31

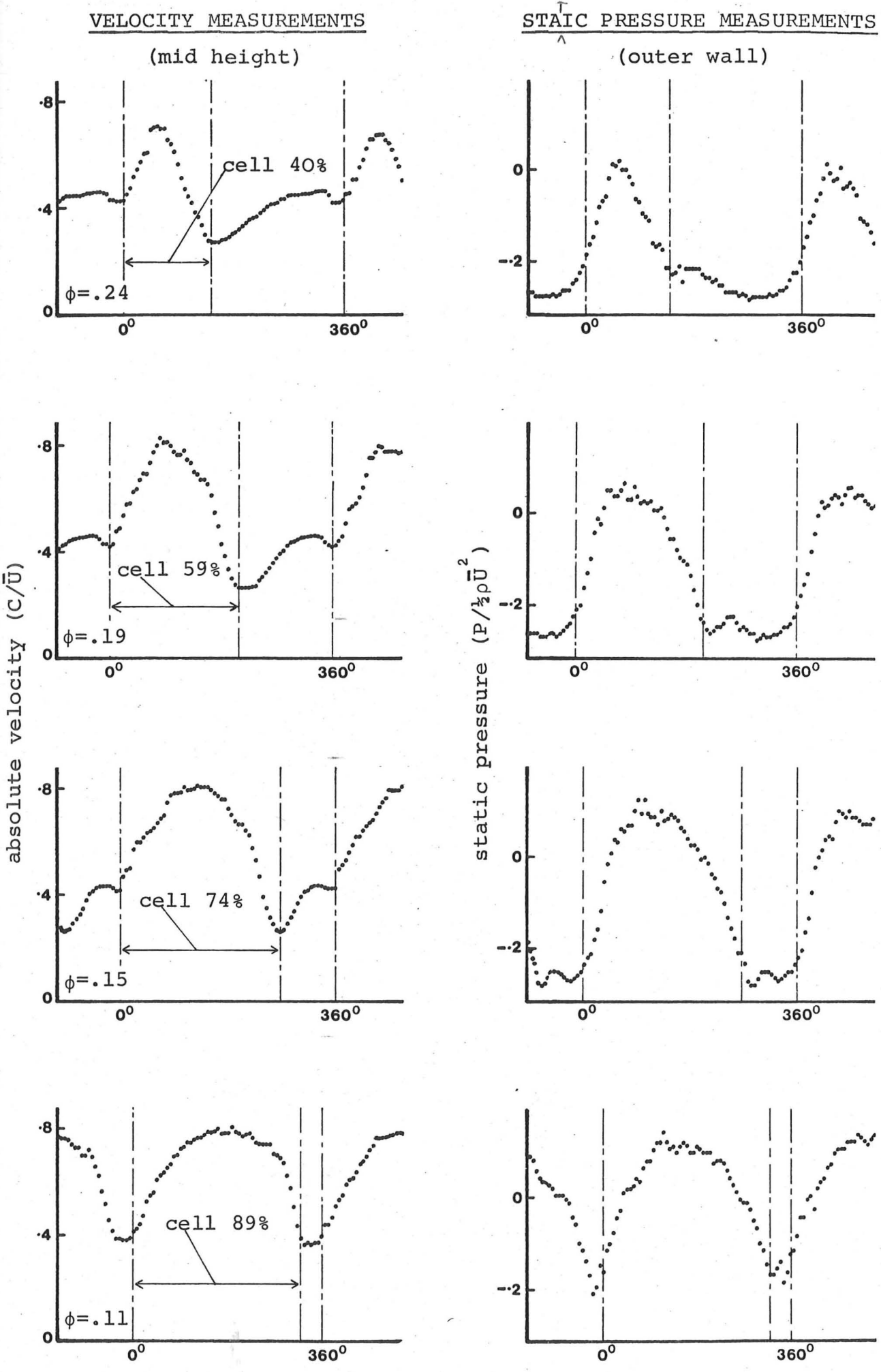

Velocity and static pressure measurements showing changes in cell size with decrease in compressor flow rate. (Measured ahead of first rotor in 3-stage Low ϕ^* compressor)

FIGURE 32

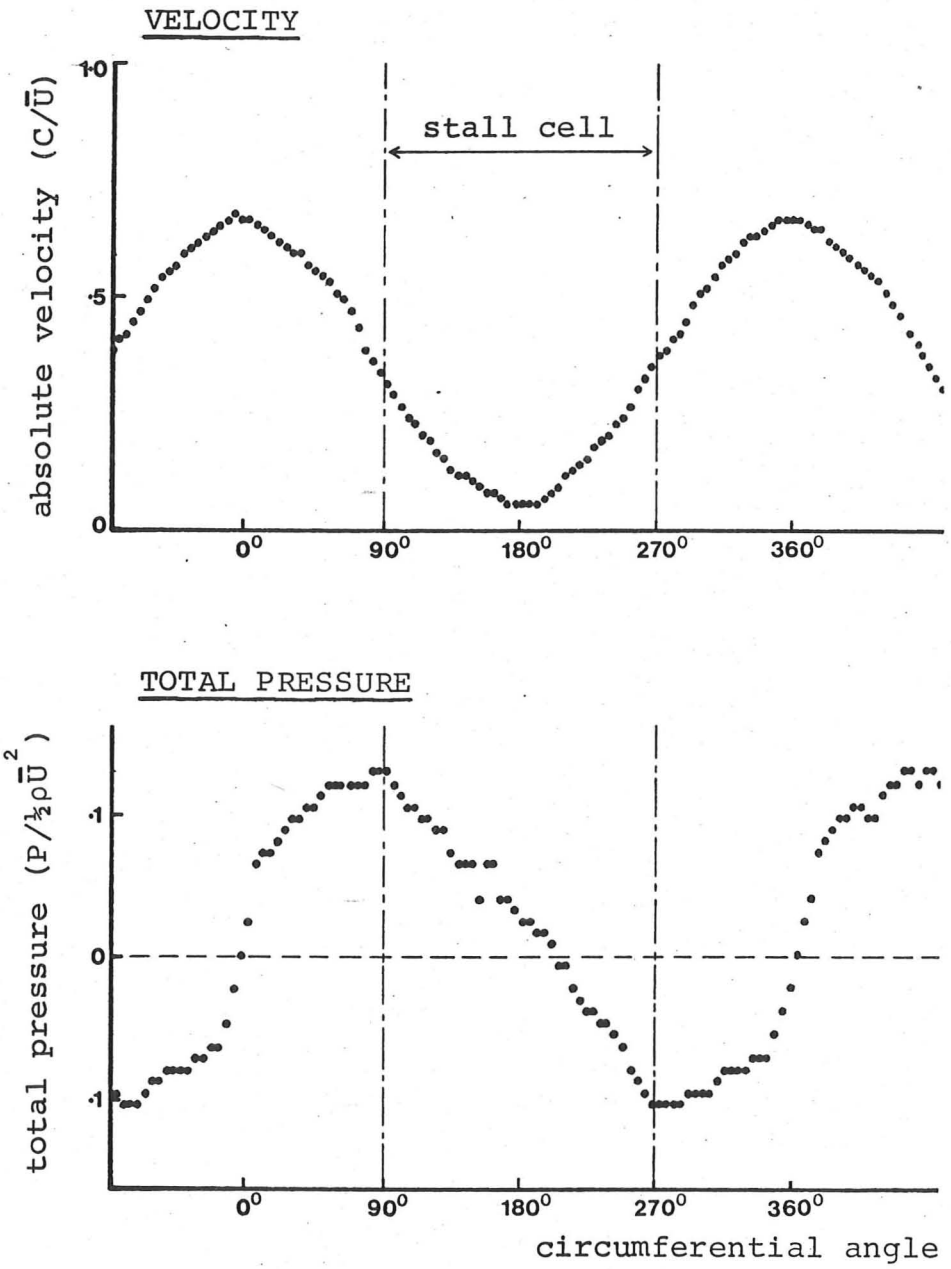

Velocity and total pressure measurements upstream of IGV's (plane ½, Figure 1), showing phase shift of 90°.
(High ϕ^* compressor.)

FIGURE 33

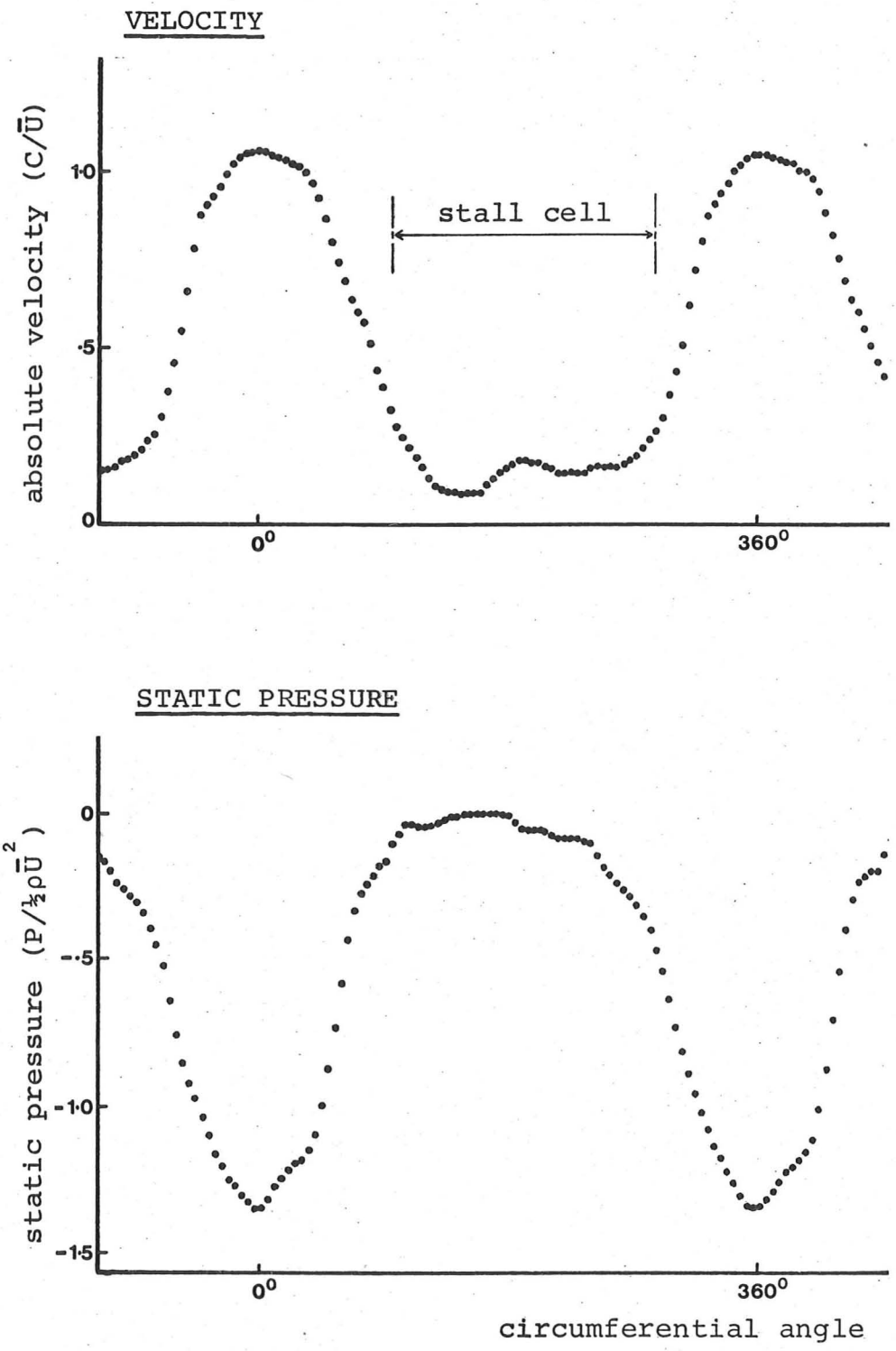

Velocity and static pressure just upstream of IGV's.
(Plane 1, Figure 1. High ϕ^* build.)

FIGURE 34

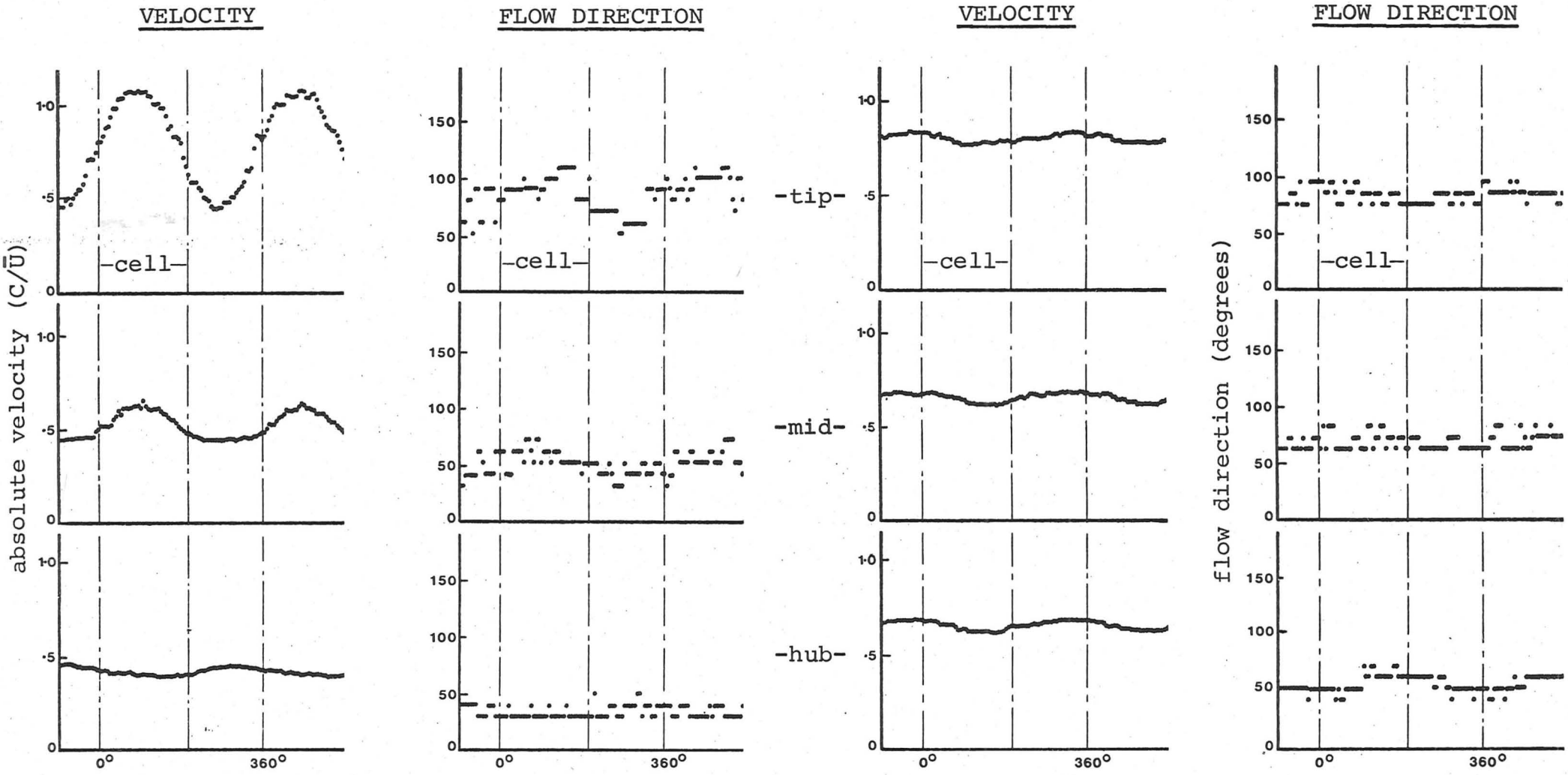

AHEAD OF ROTOR (Plane 2)

BEHIND ROTOR (Plane 3)

Velocity and flow direction measurements at three radial positions before and after rotor in 1-stage Low Φ* compressor.

FIGURE 35

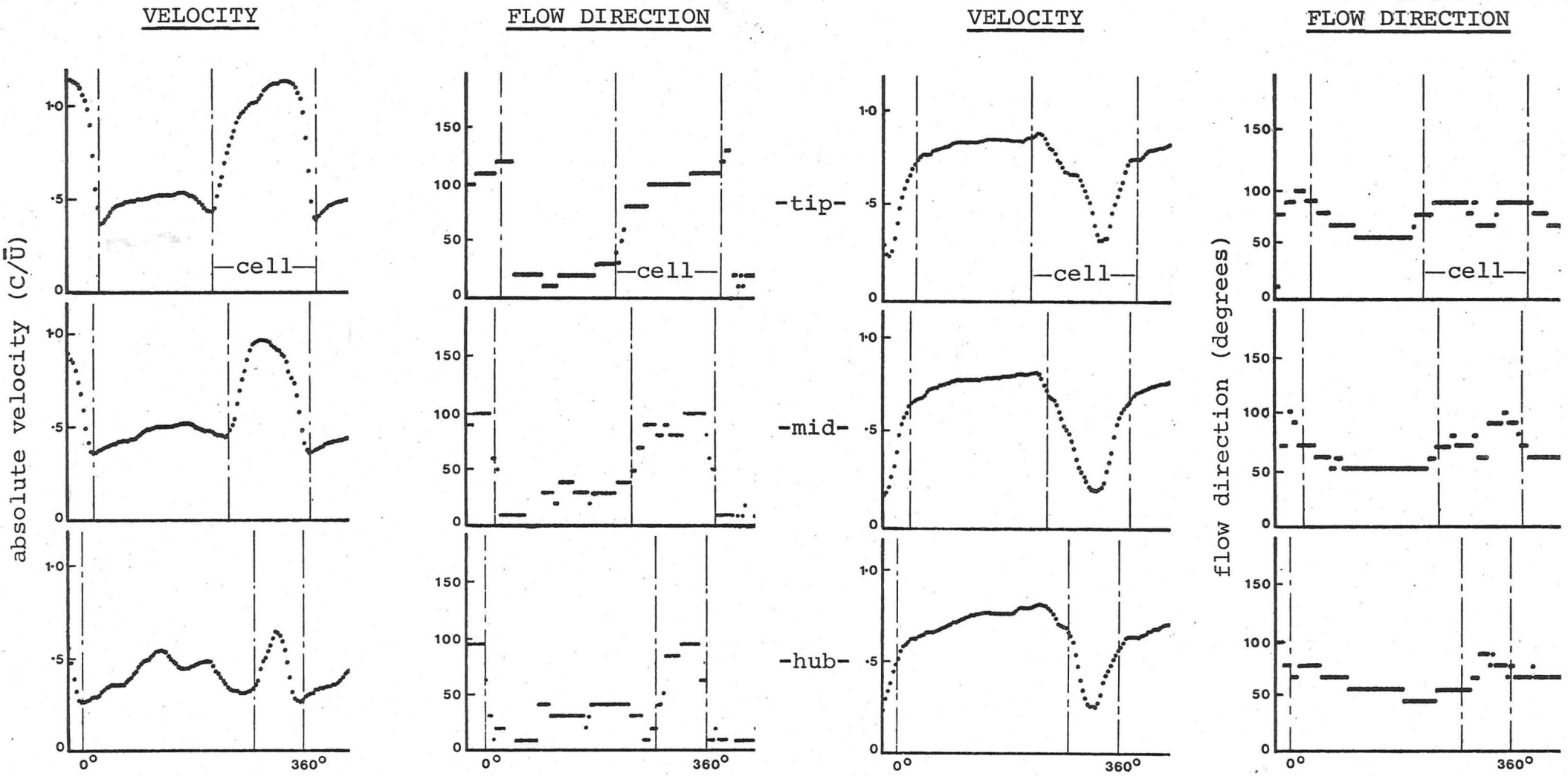

Velocity and flow direction measurements at three radial positions before and after rotor in 1-stage Intermediate Φ* compressor.

FIGURE 36

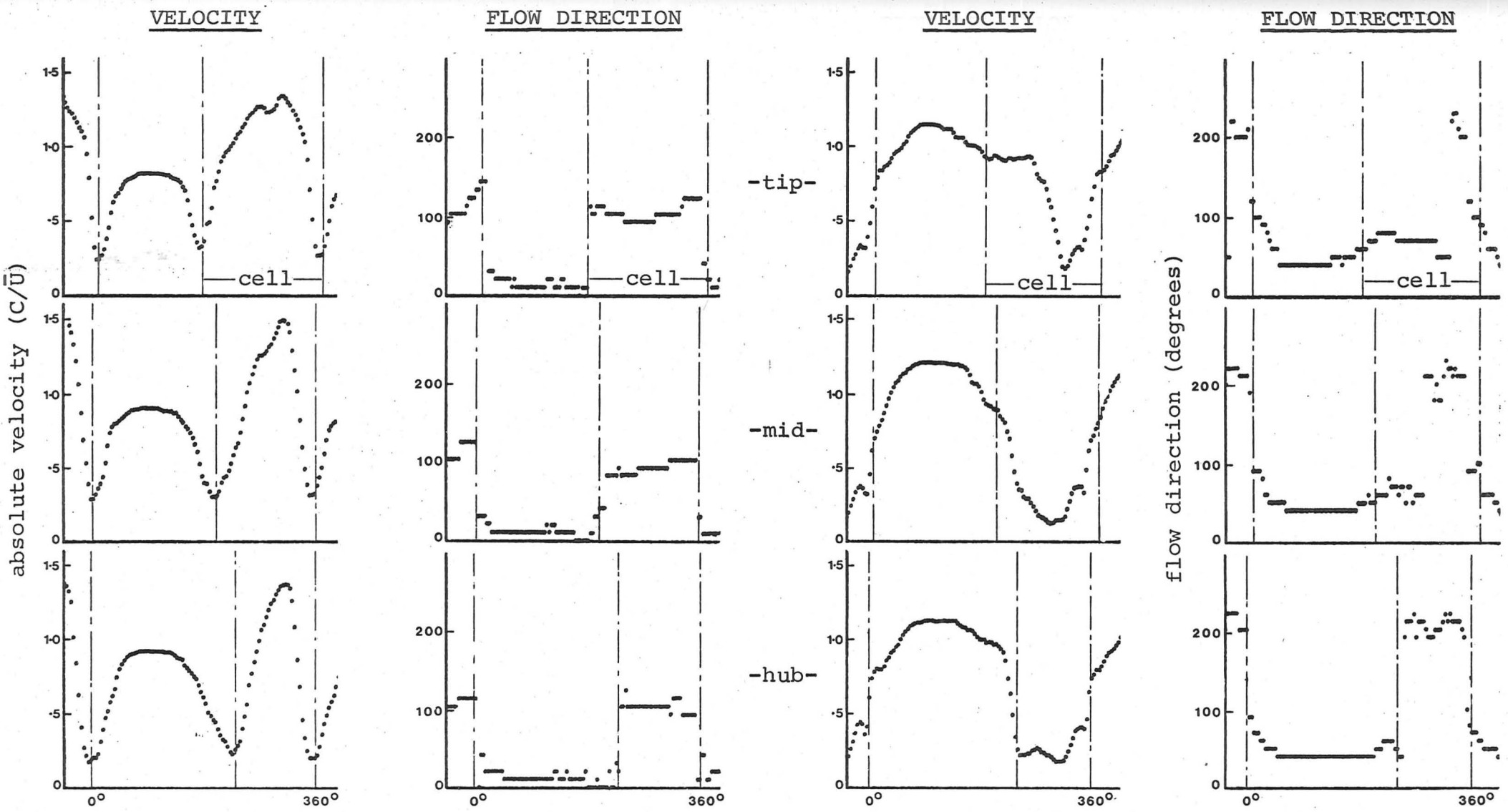

Velocity and flow direction measurements at three radial positions before and after rotor in 1-stage High Φ* compressor.

FIGURE 37

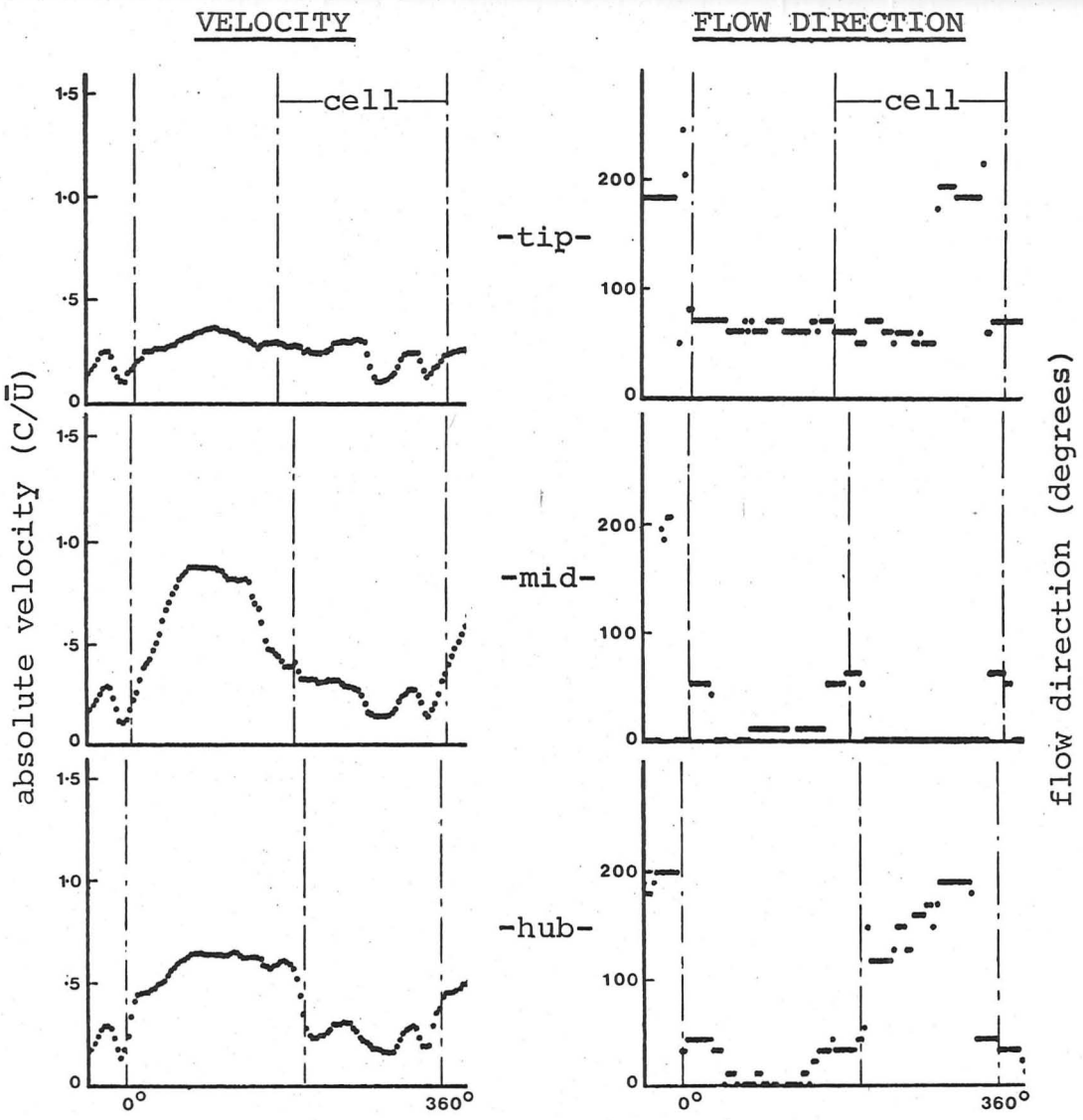

Velocity and flow direction measurements at three radial positions after stator in 1-stage High Φ^* compressor.

FIGURE 37 continued

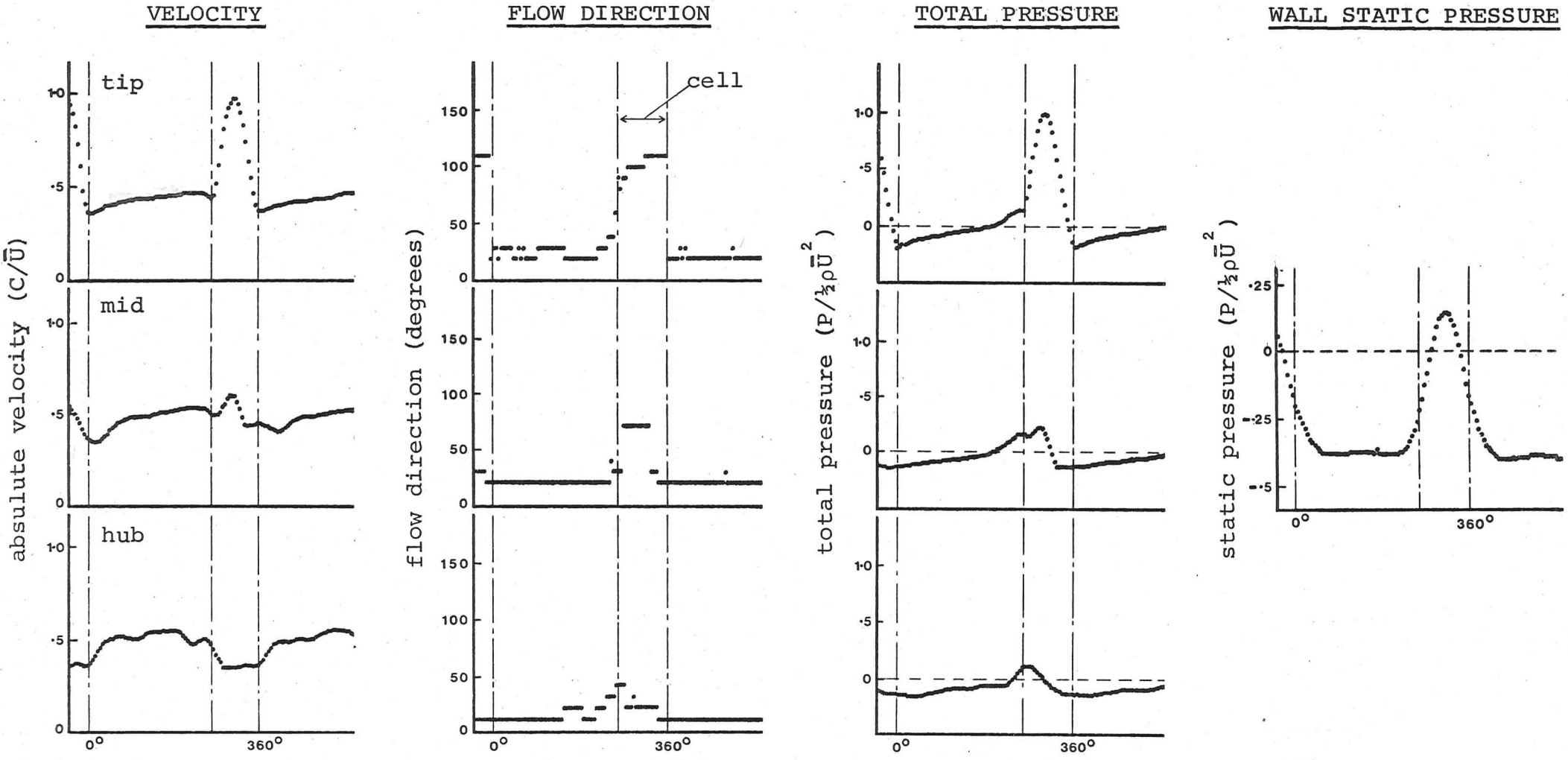

Part-span stall measurements at three radial positions ahead of first rotor in 2-stage Intermediate Φ* compressor.

FIGURE 38a

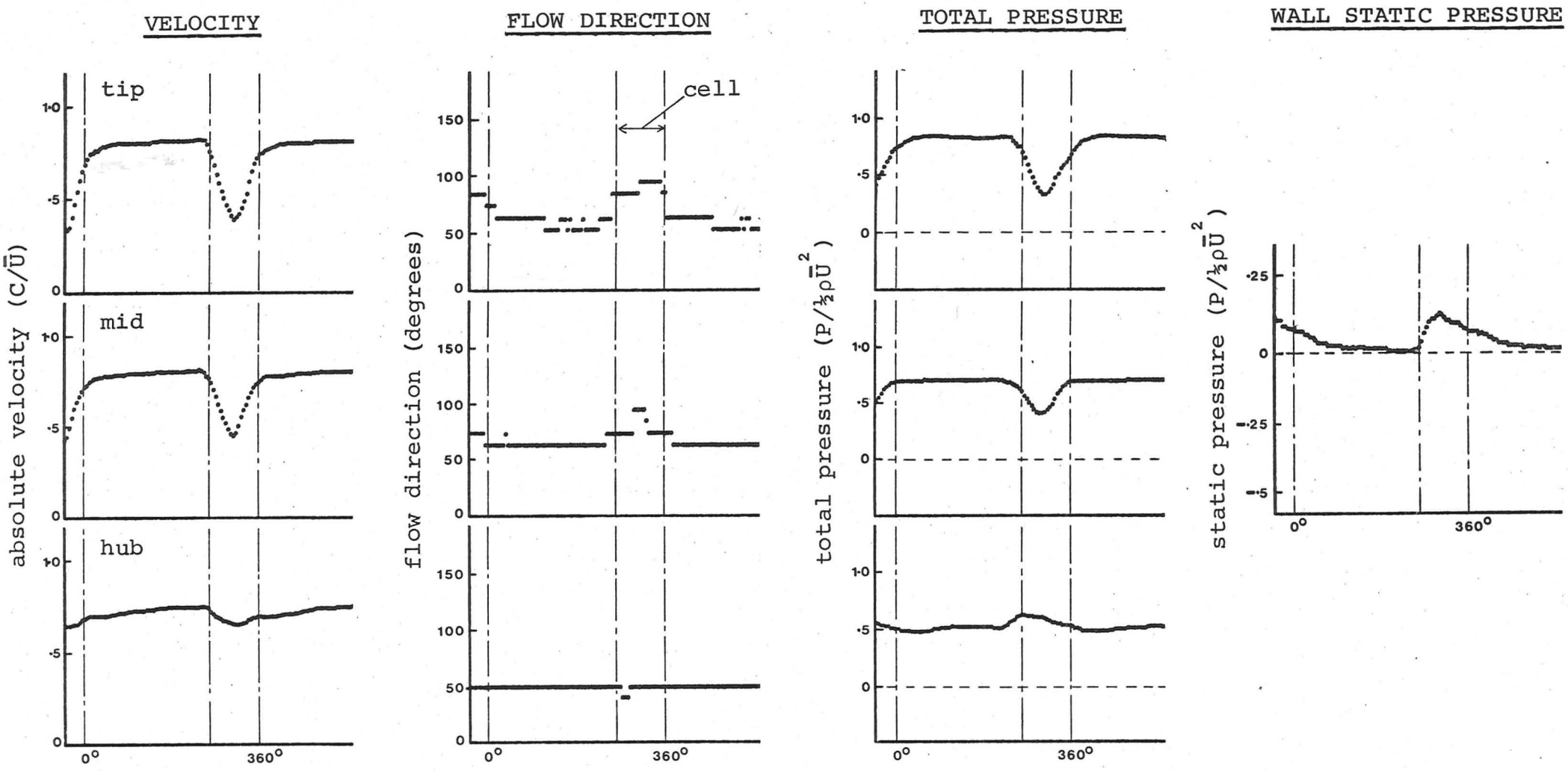

Part-span stall measurements at three radial positions behind first rotor in 2-stage Intermediate Φ* compressor.

FIGURE 38b

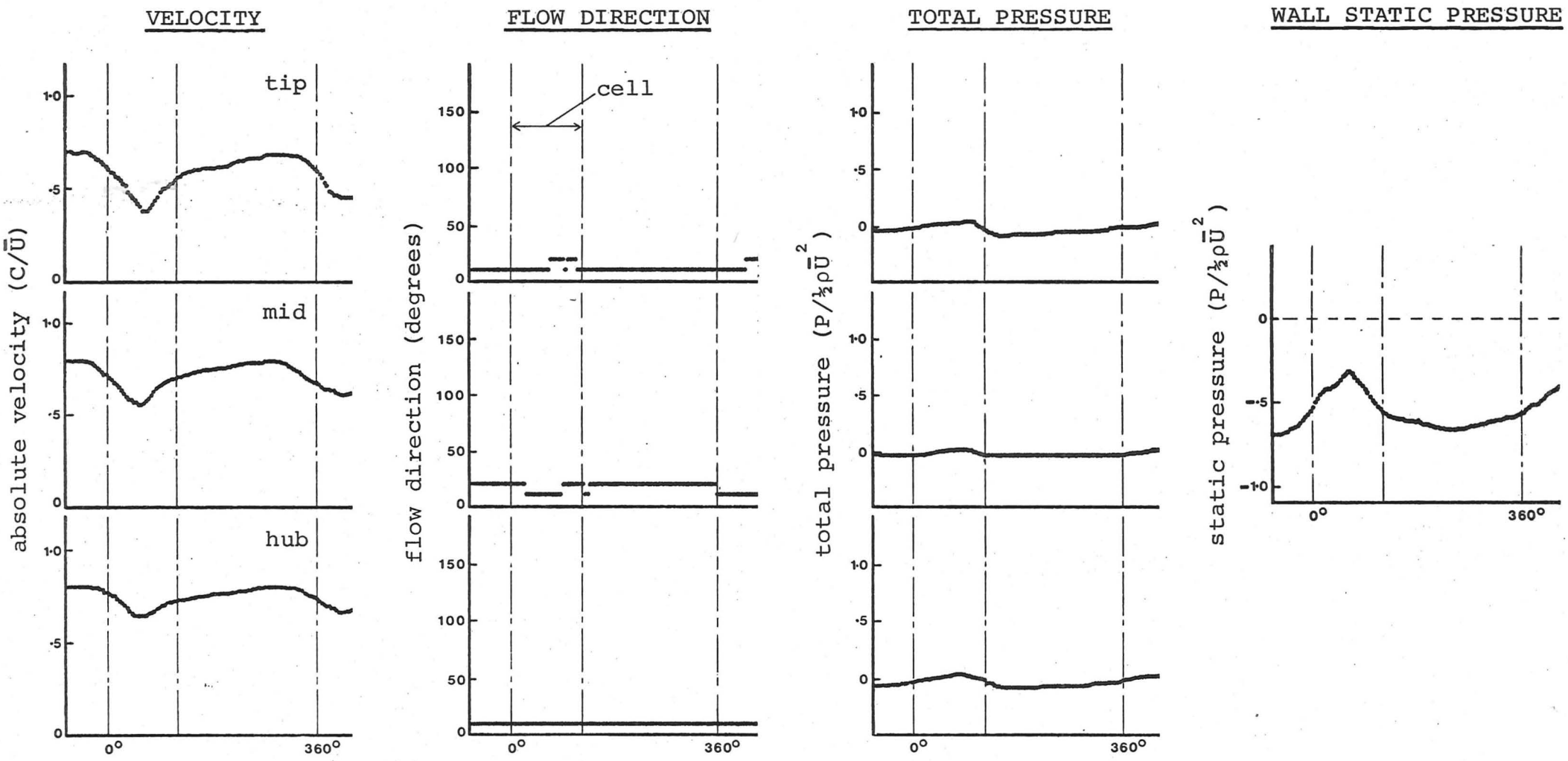

Part-span stall measurements at three radial positions ahead of rotor in 1-stage High Φ* compressor.

FIGURE 39a

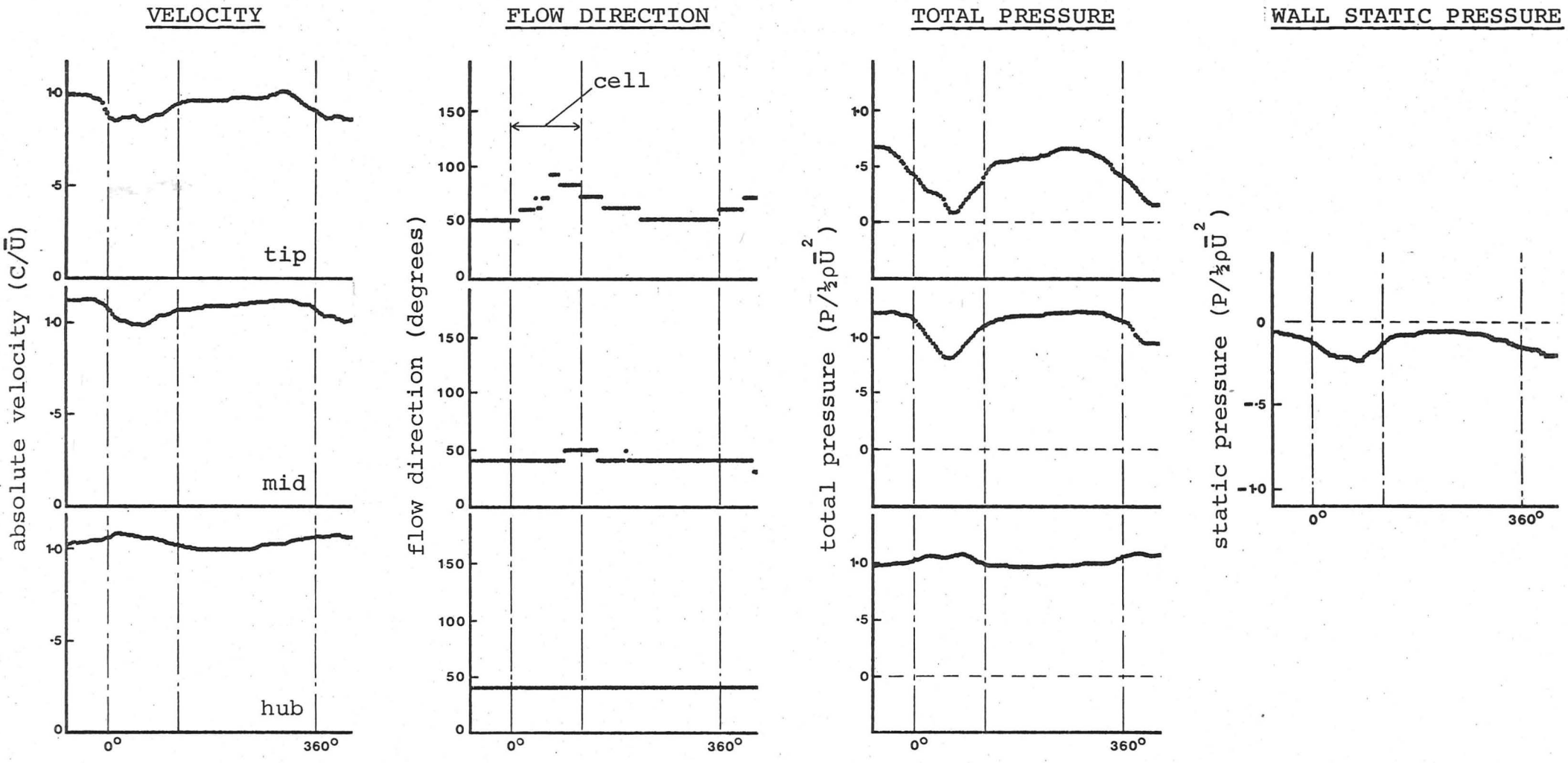

Part-span measurements at three radial positions behind rotor in 1-stage High Φ* compressor.

FIGURE 39b

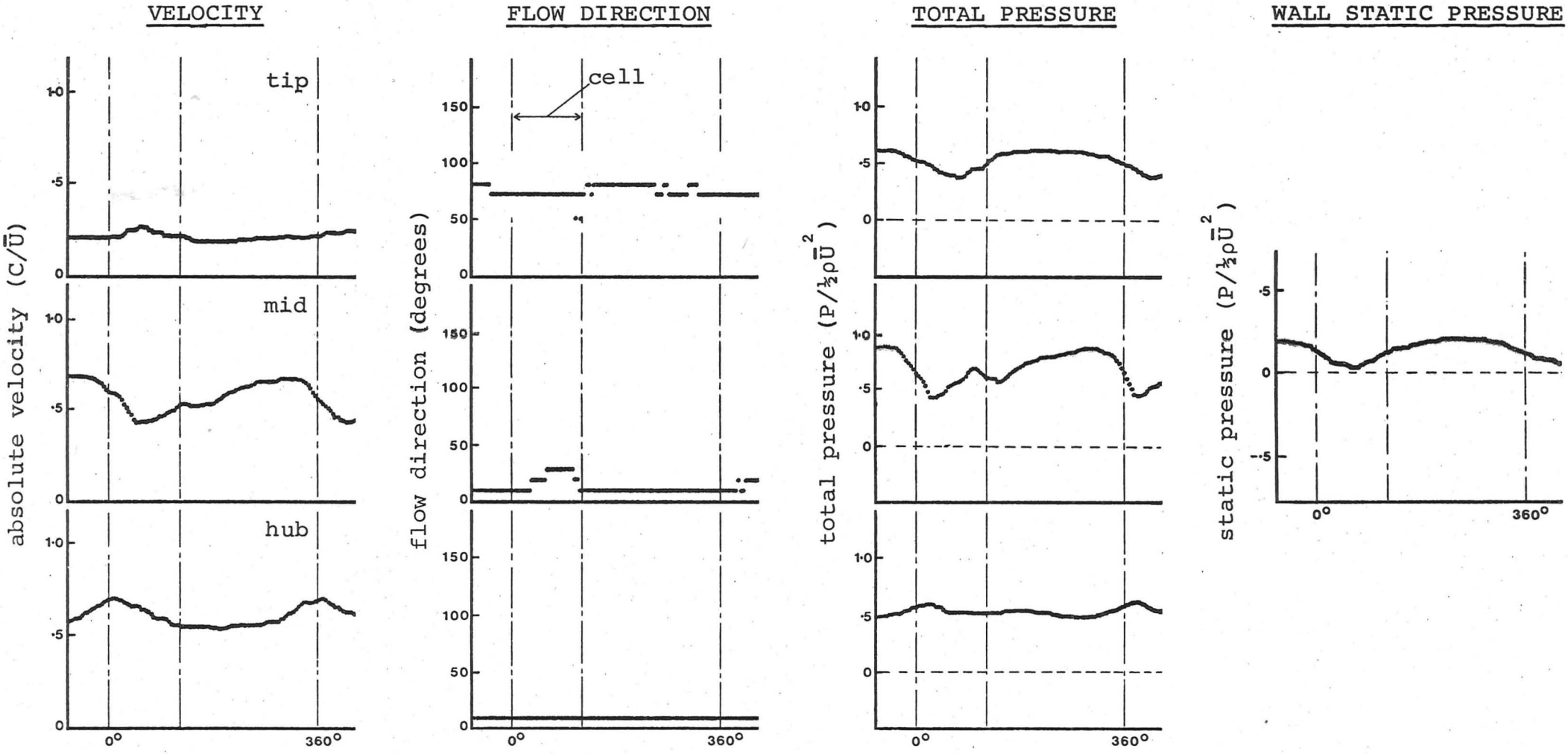

Part-span measurements at three radial positions after stator in 1-stage High Φ* compressor.

FIGURE 39c

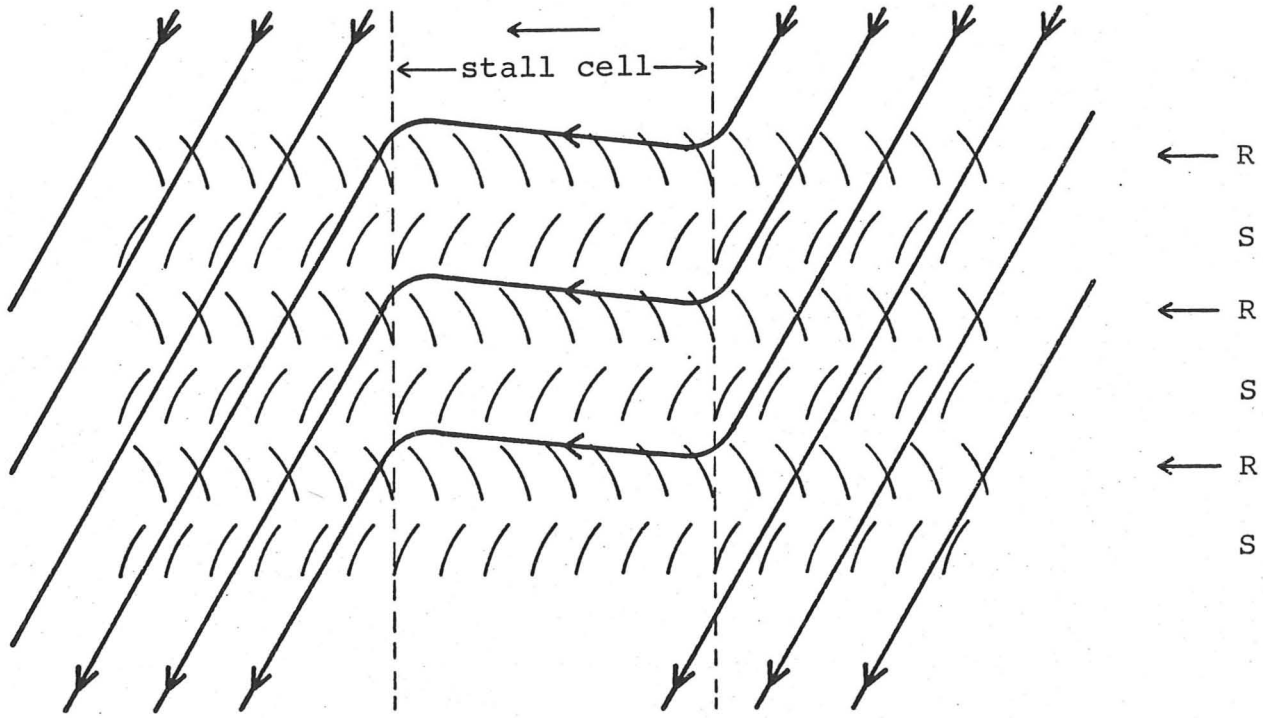

Sketch of stall cell structure showing unstalled flow being transported across the cell by the rotor blades.
(Sketch drawn in absolute reference frame).

FIGURE 40

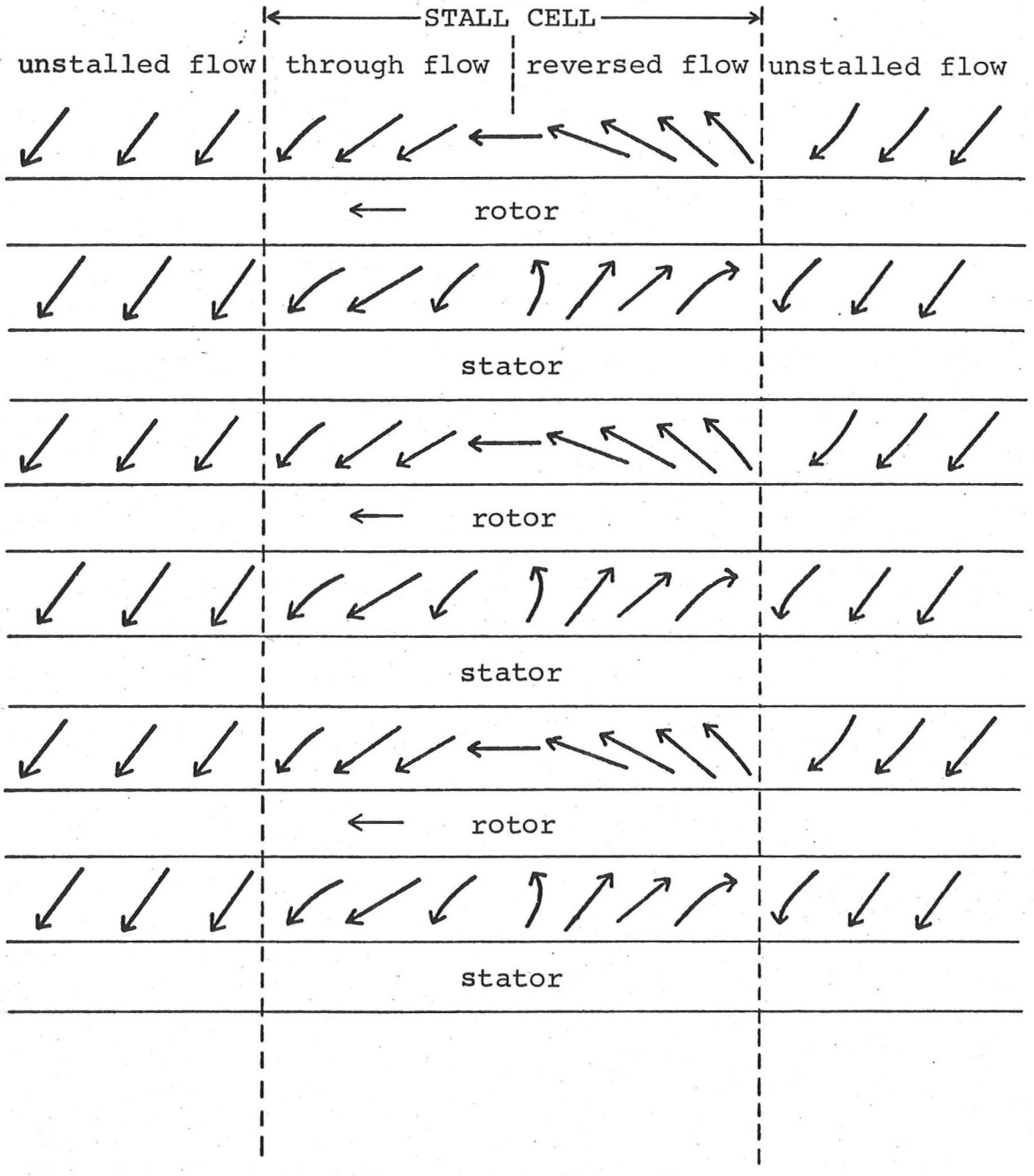

Pictorial sketch of stalled flow in 3-stage compressor of Intermediate ϕ^* build.

FIGURE 41

THREE STAGE INTERMEDIATE ϕ^* BUILD

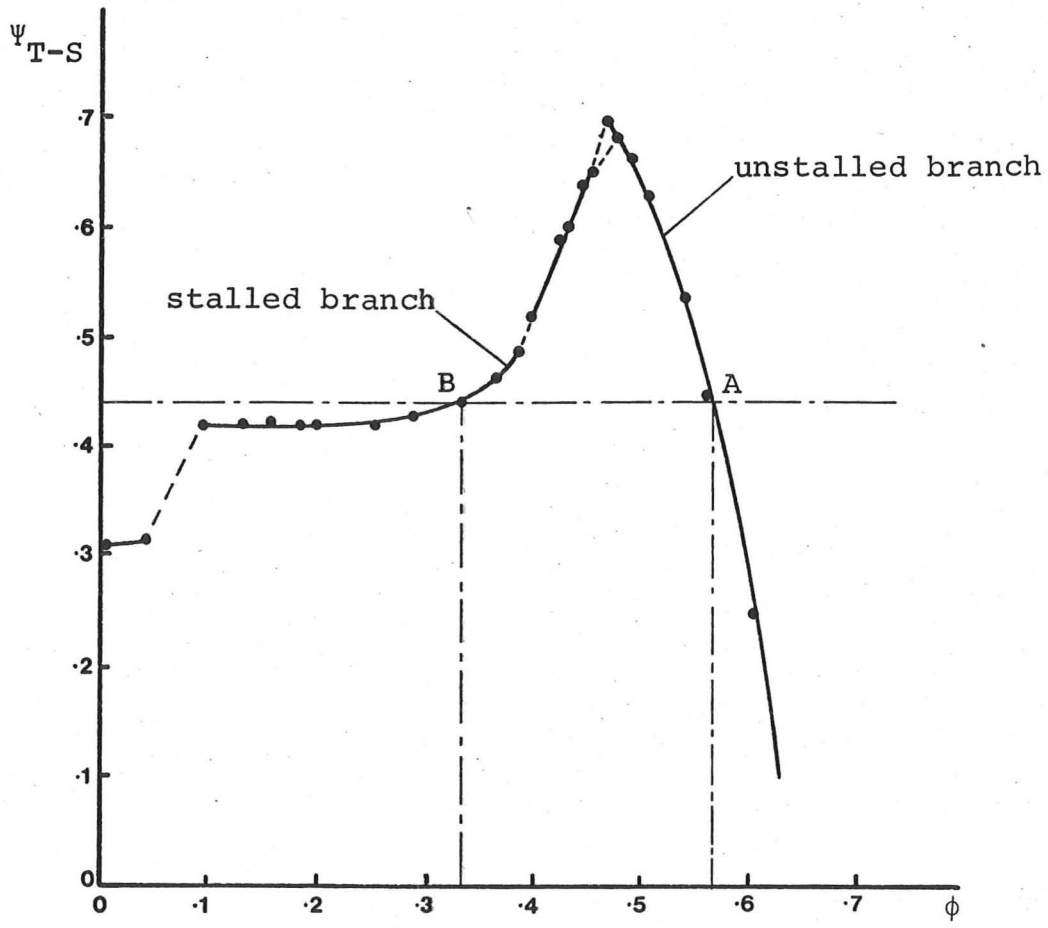

Compressor characteristic showing operating point at which measurements below were obtained.

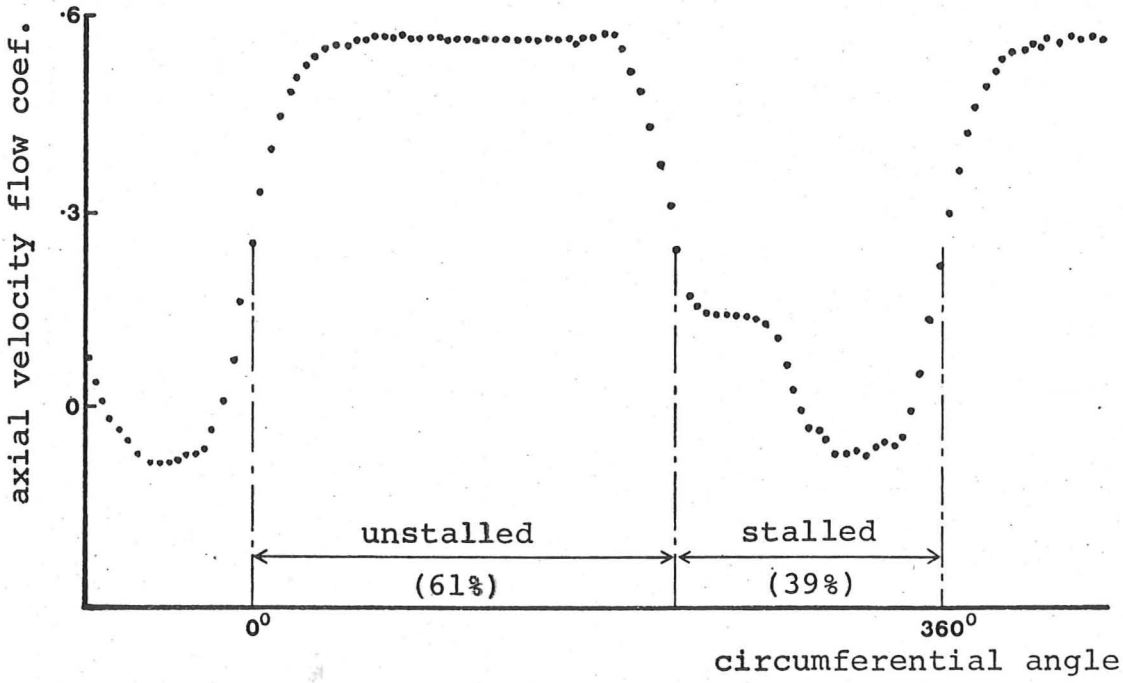

Velocity measurement at flow coefficient of 0.33.

FIGURE 42

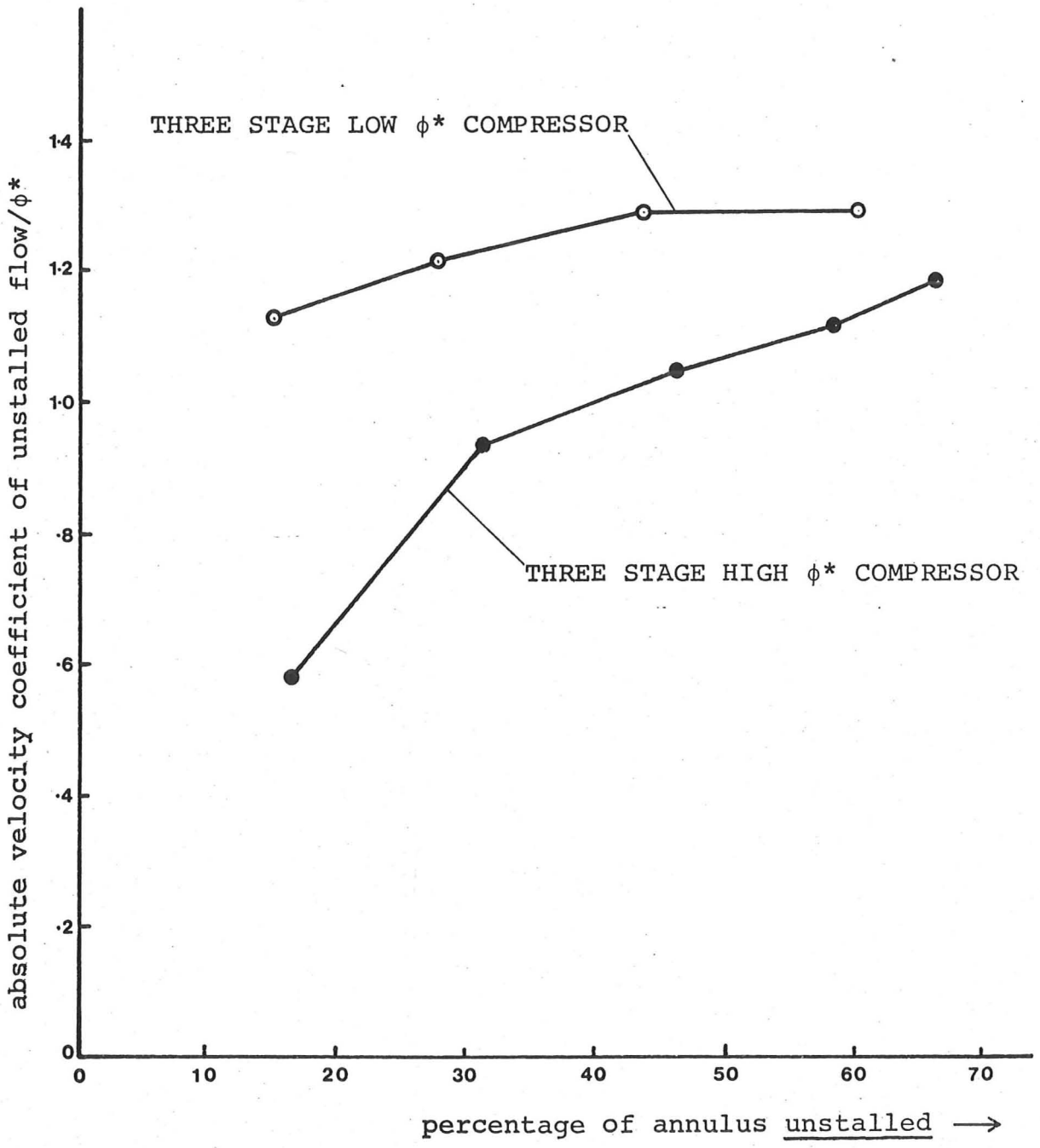

Change in unstalled flow velocity with change in size of stall cell.

FIGURE 43

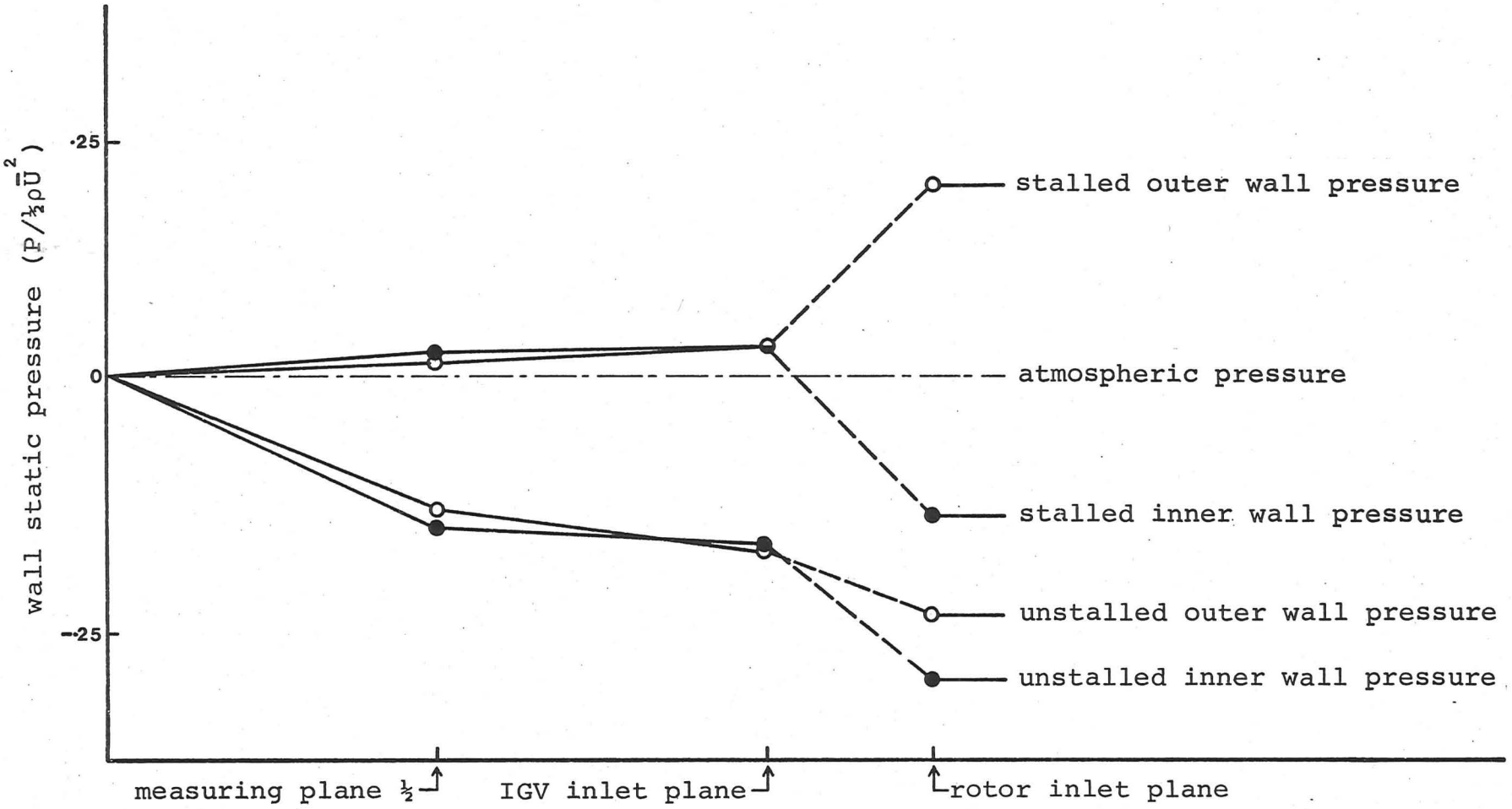

Inner and outer wall static pressure measurements during stall in inlet of 3-stage Low ϕ^* compressor.

FIGURE 44

3-STAGE LOW ϕ^* COMPRESSOR

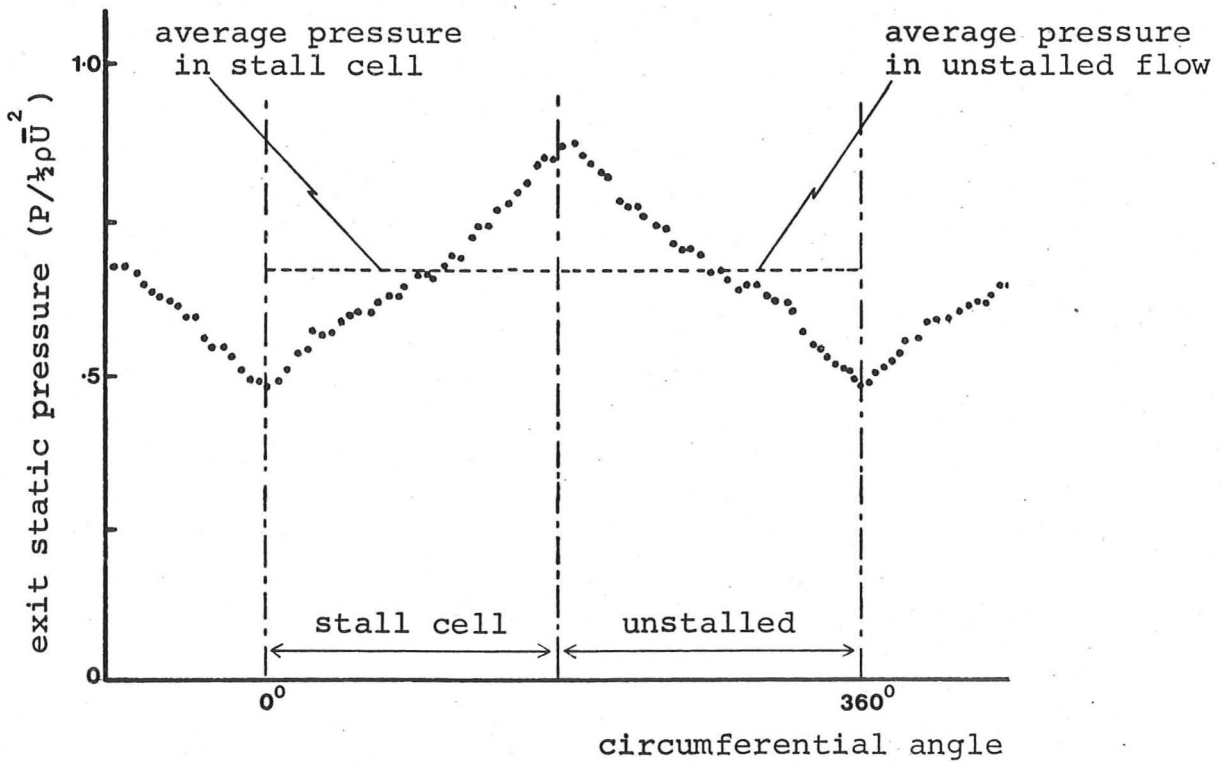

3-STAGE HIGH ϕ^* COMPRESSOR

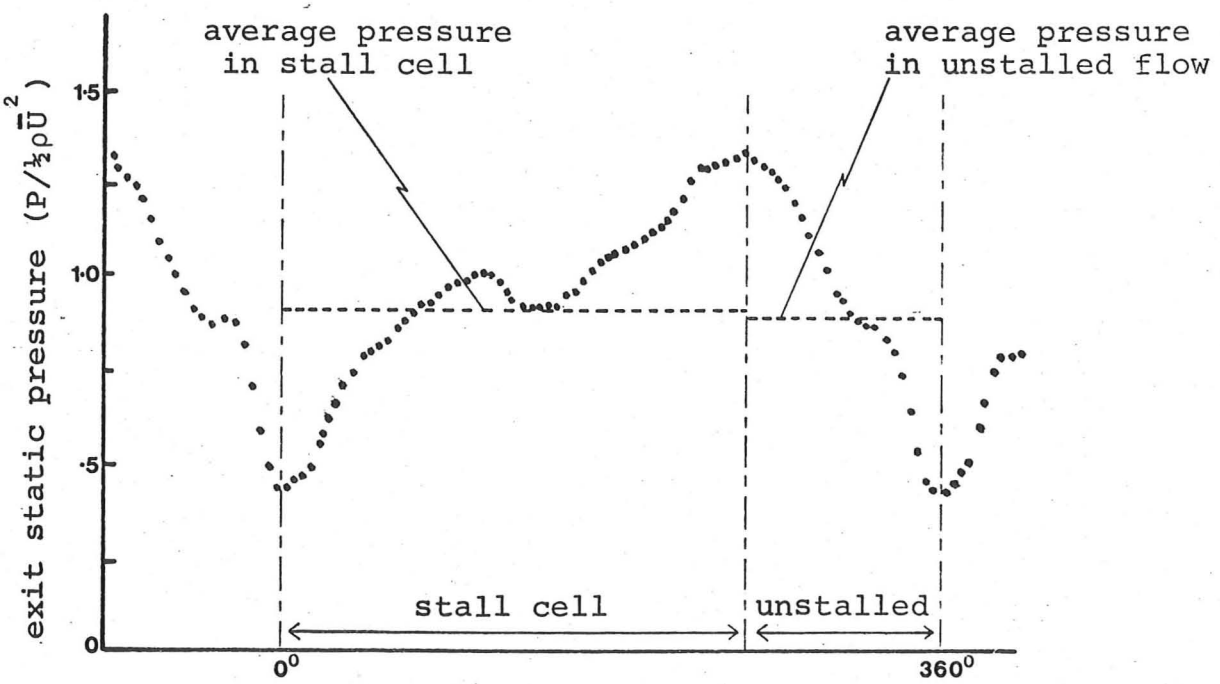

Examples of exit plane static pressure measurements.

FIGURE 45

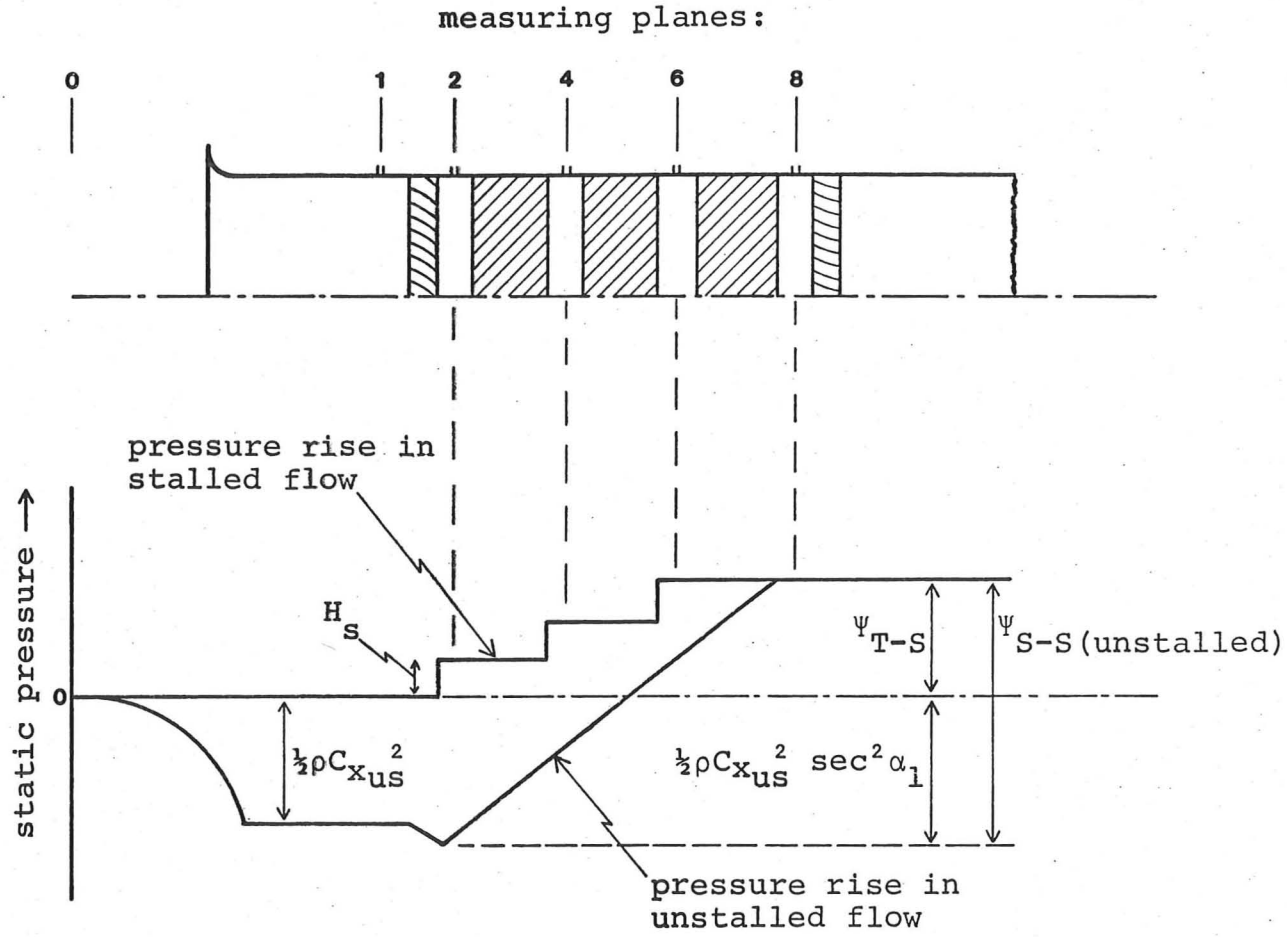

Overall model of stalled compressor performance.

FIGURE 46

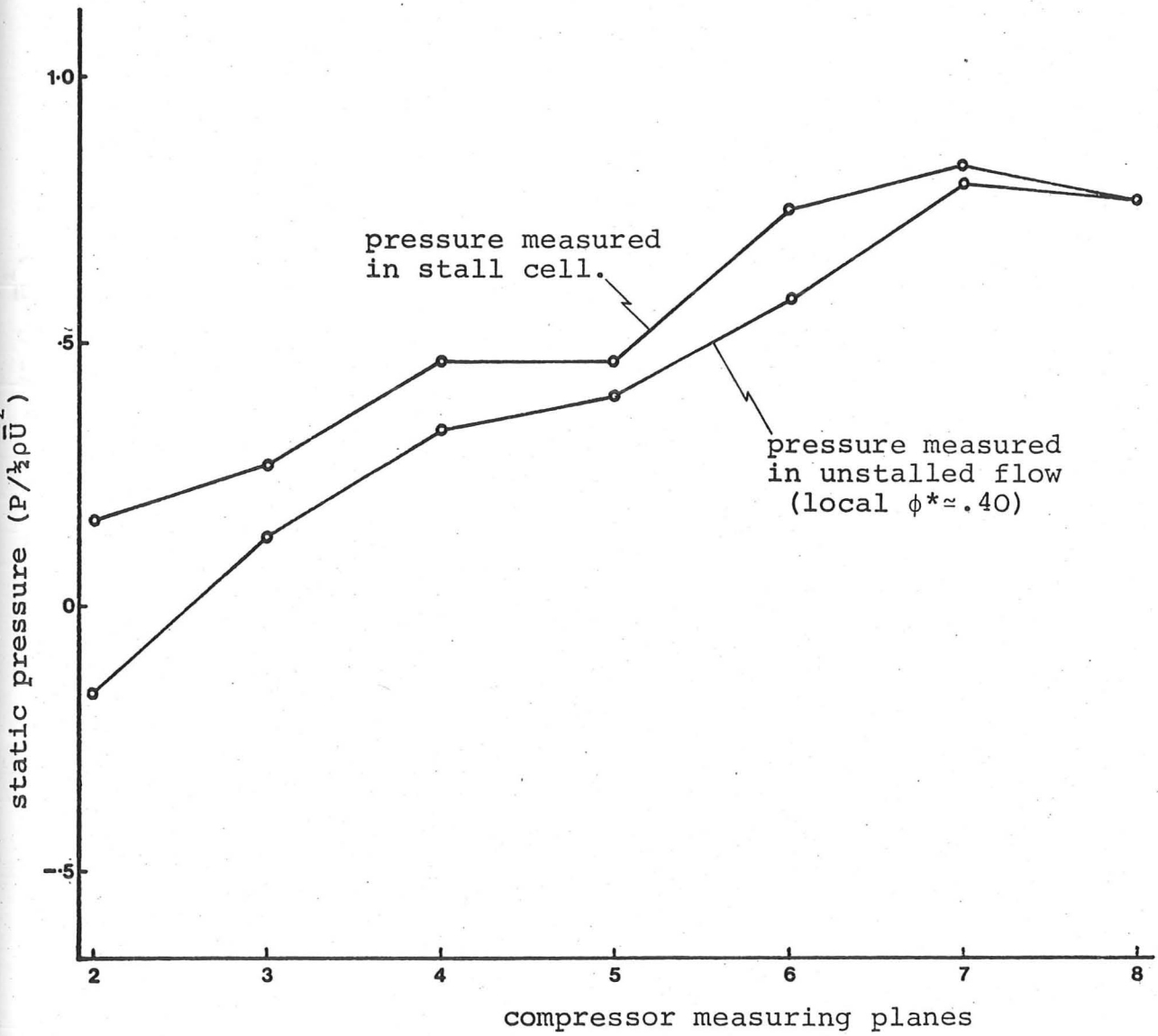

Instantaneous static pressure measurements during full-span stall in 3-stage Low ϕ^* compressor.

FIGURE 47a

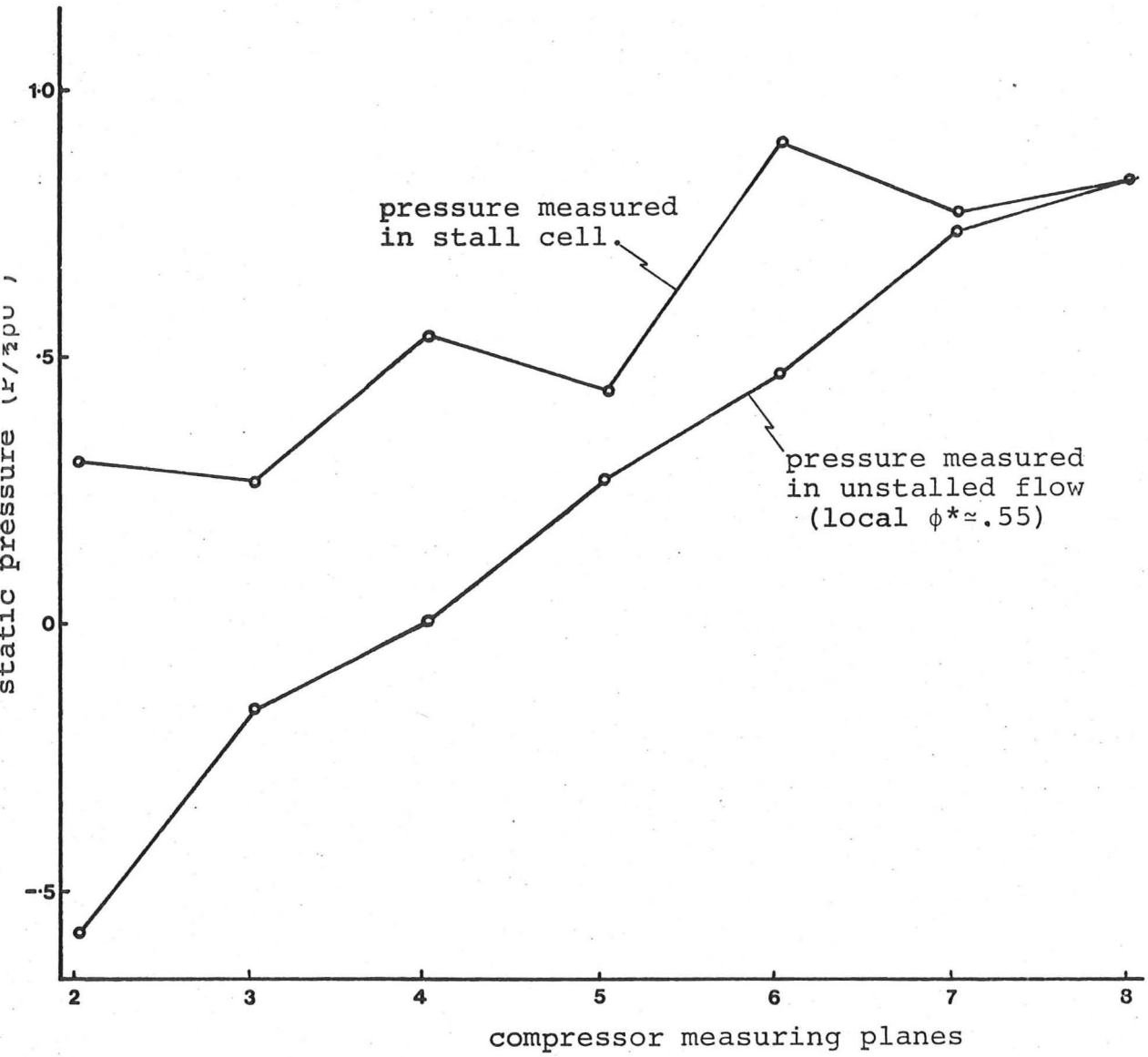

Instantanteous static pressure measurements during full-span stall in 3-stage Intermediate ϕ^* compressor.

FIGURE 47b

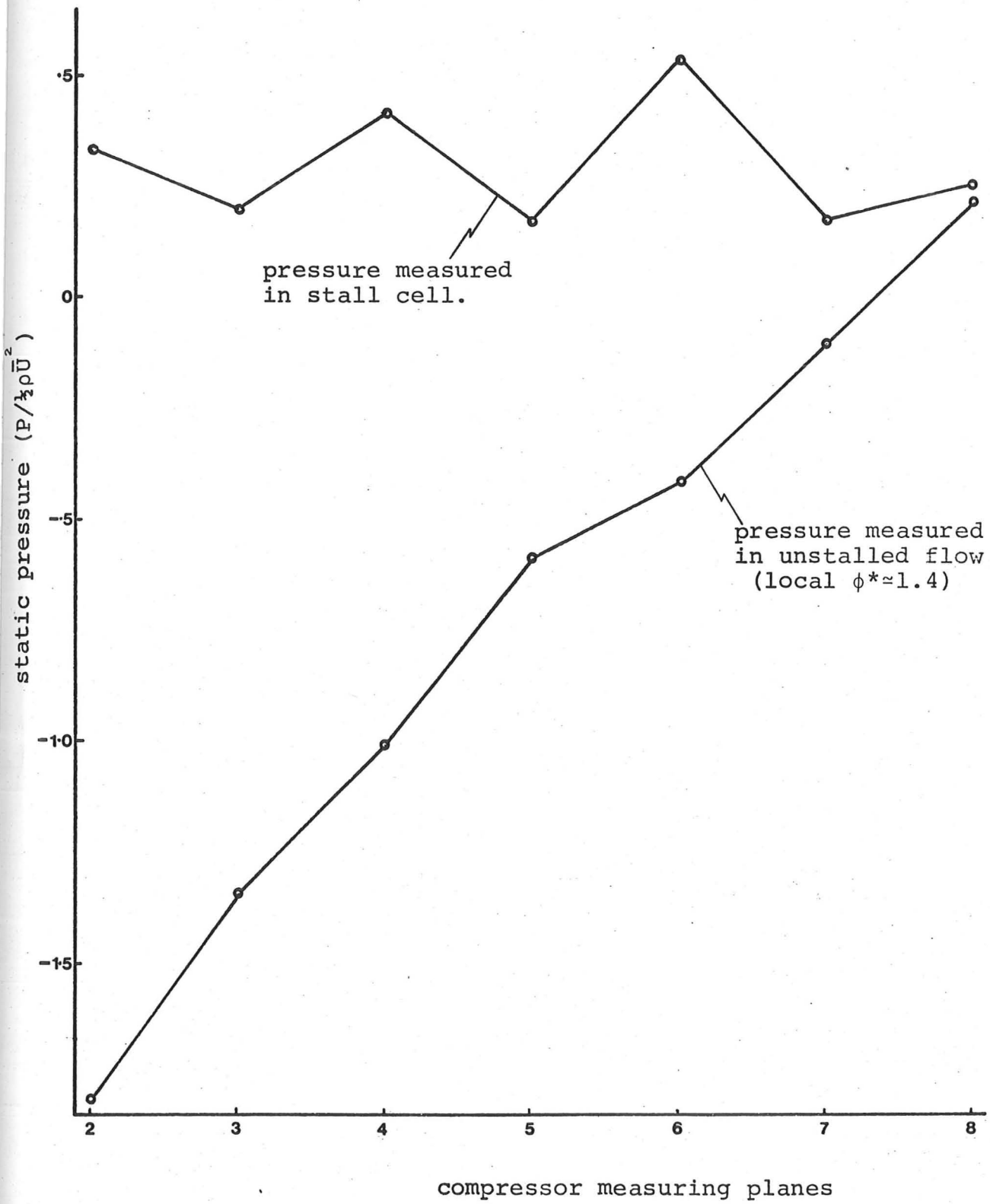

Instantaneous static pressure measurements during full-span stall in 3-stage High ϕ^* compressor.

FIGURE 47c

PROGRESSIVE STALL CHARACTERISTIC

(part-span stall)

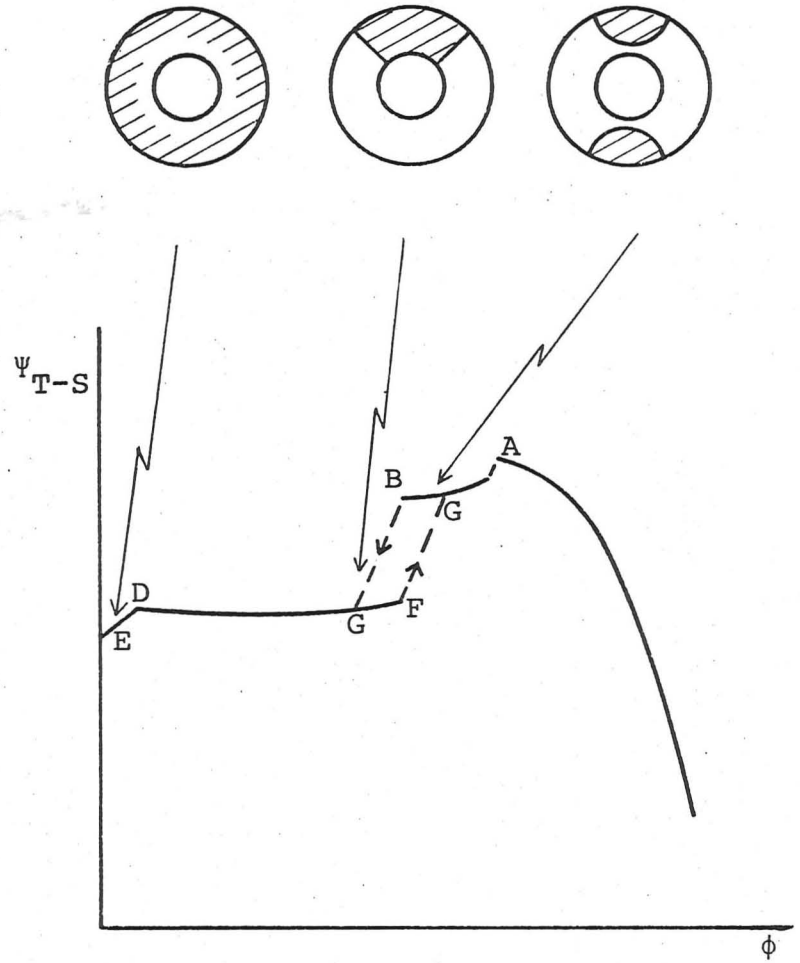

FIGURE 48a

ABRUPT STALL CHARACTERISTIC

(full-span stall)

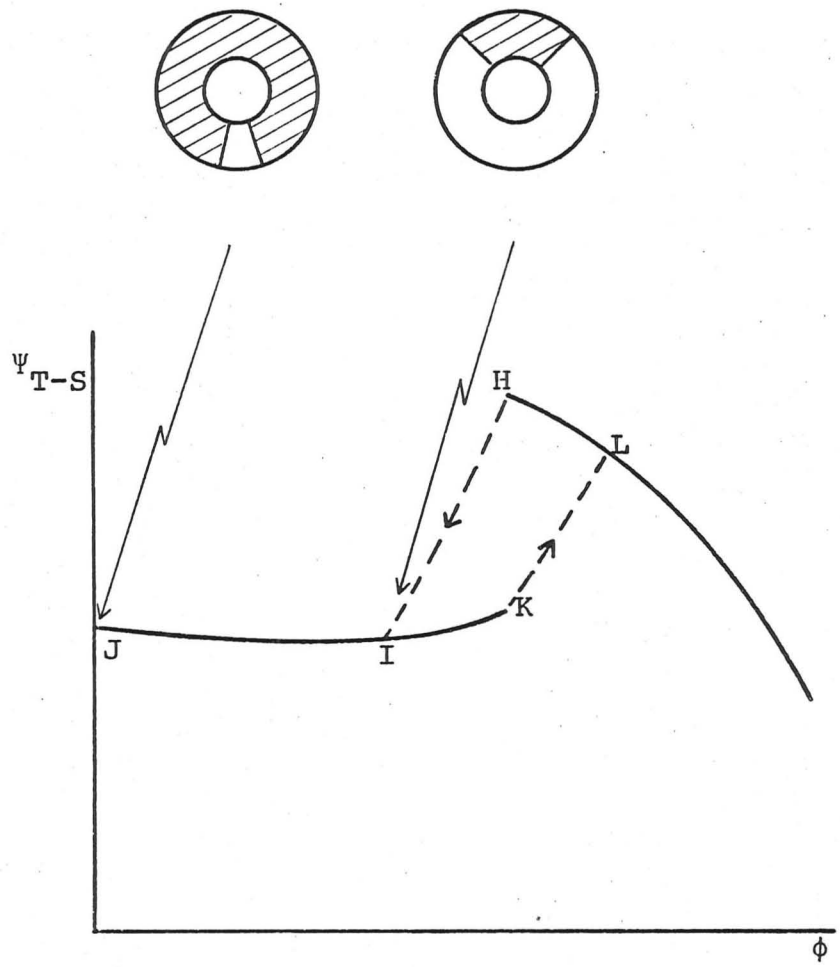

FIGURE 48b

Examples of compressor characteristics.

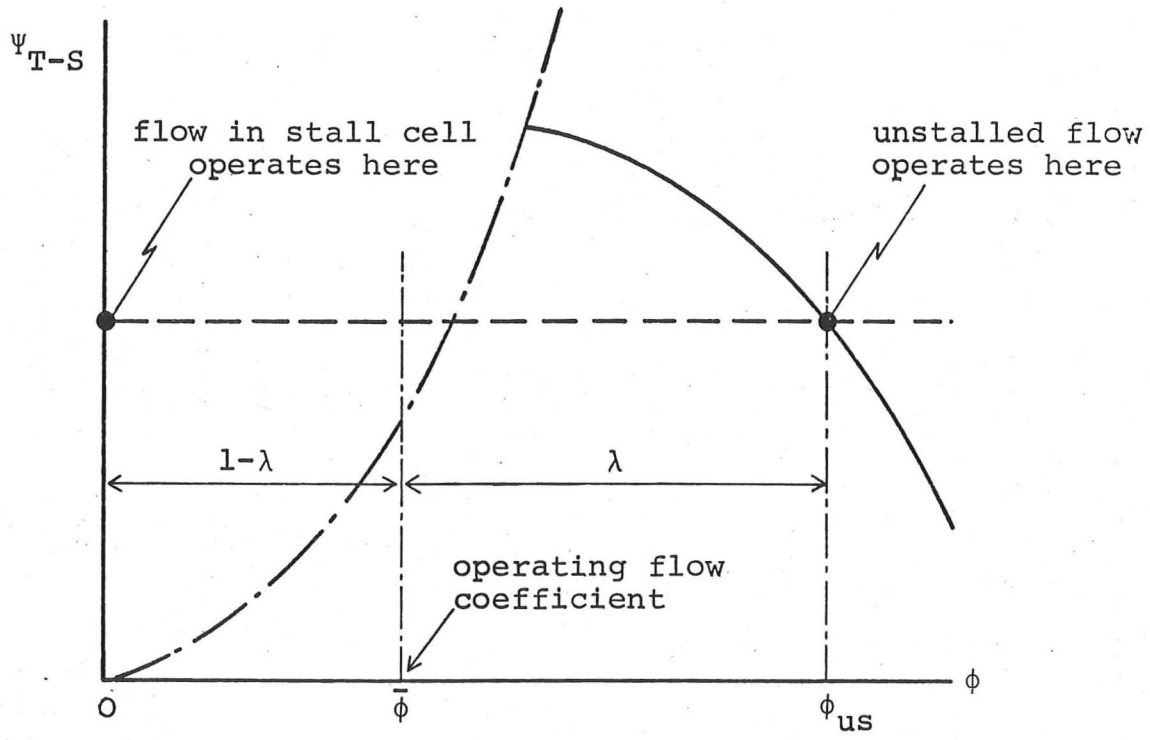

Sketch showing operating points of stalled and unstalled flow on a total-to-static characteristic.

FIGURE 49

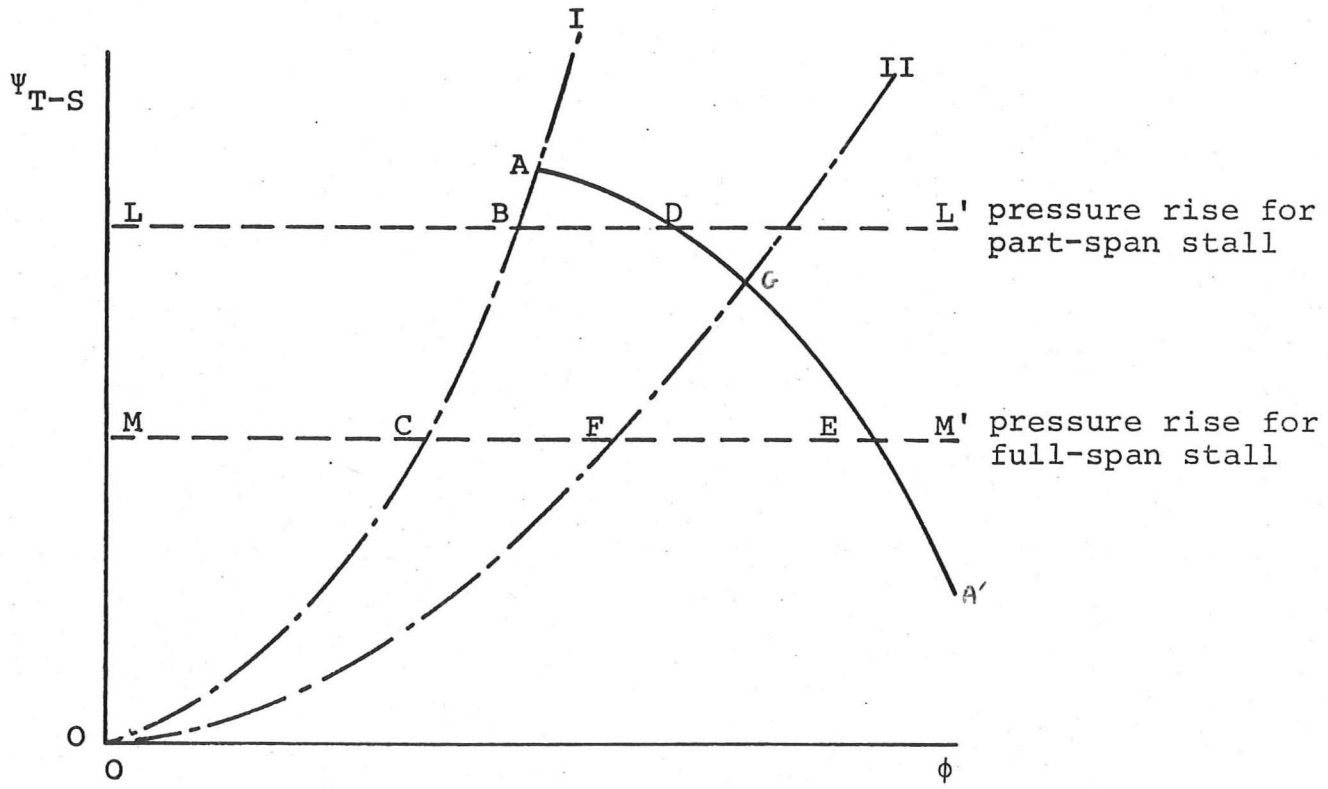

Compressor characteristic and throttle lines.

FIGURE 50

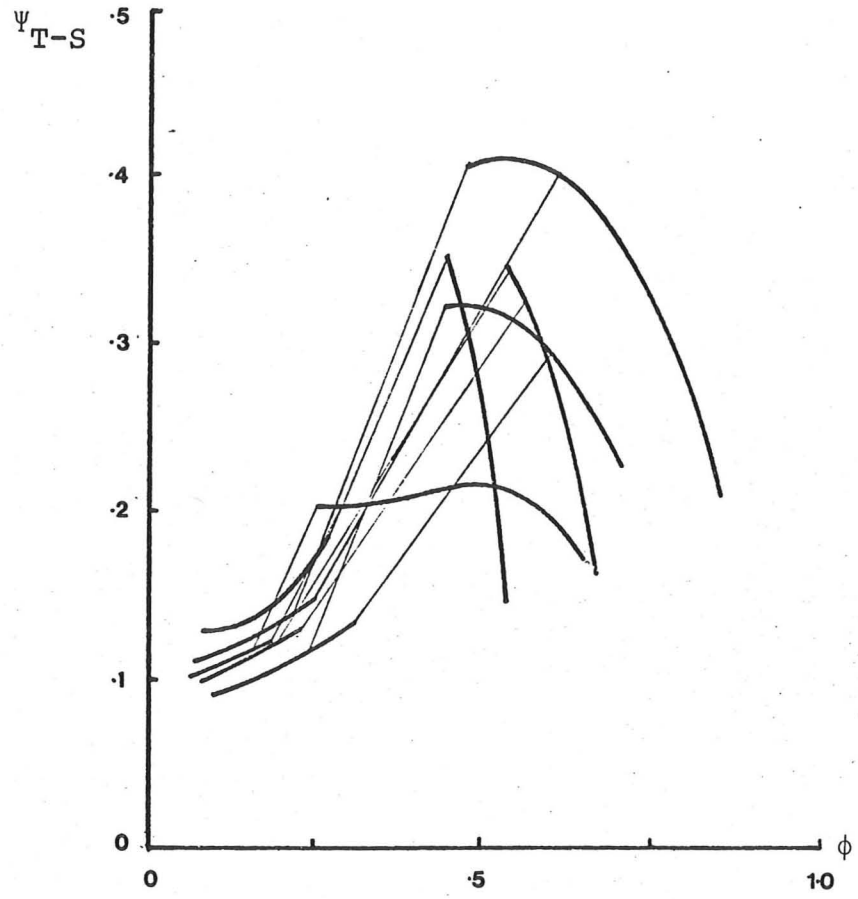

Demonstration of independence of stalled pressure rise of unstalled pressure rise (after Yershov).

FIGURE 51

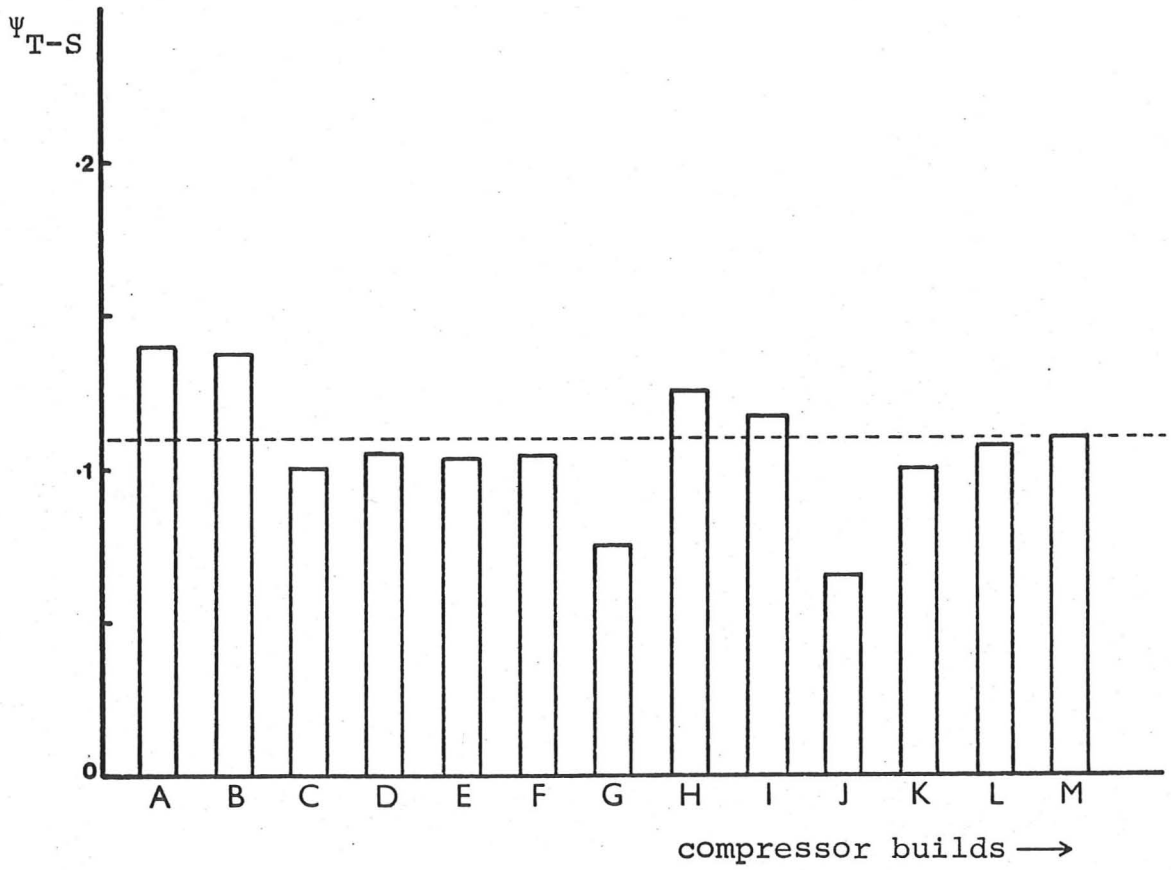

Pressure rise at shut-off for different compressor builds.

Figure 52

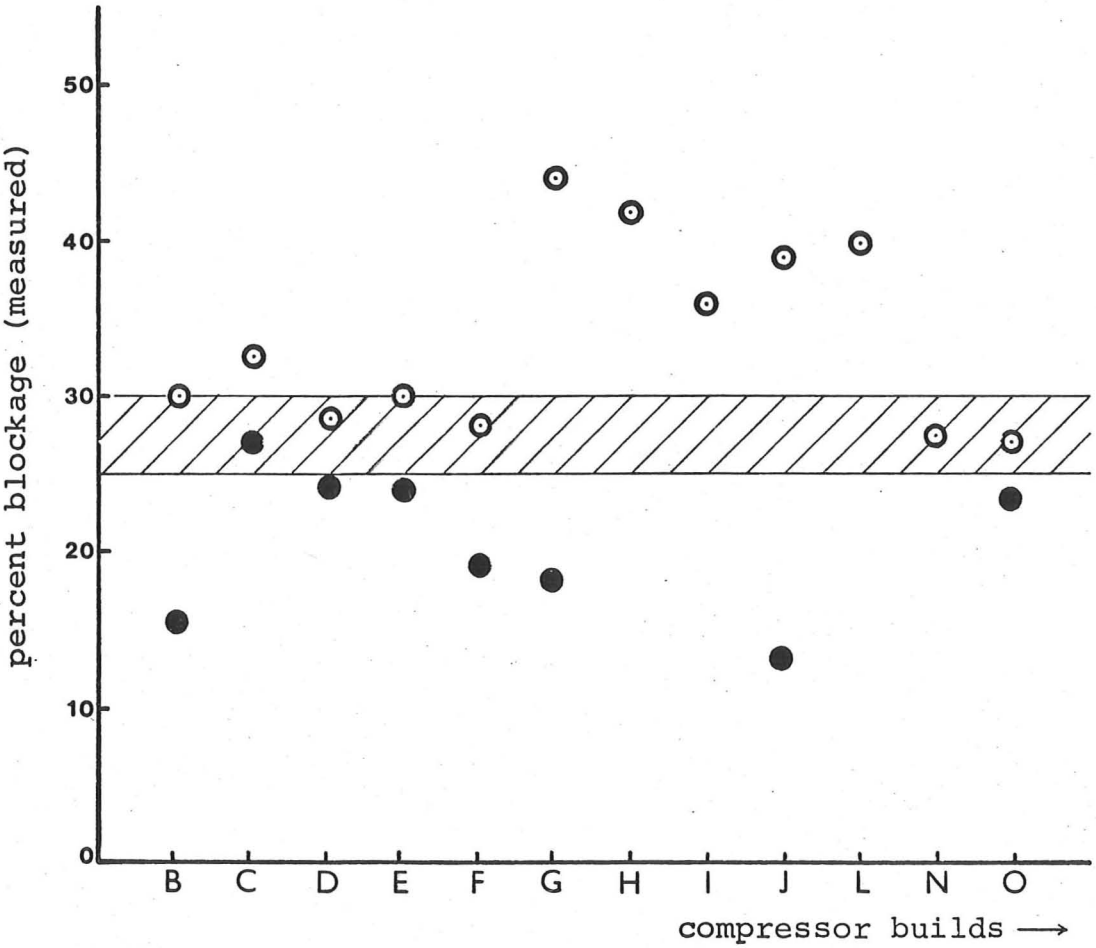

Maximum measured blockage for part-span stall and mimimum measured blockage for full-span stall.

FIGURE 53

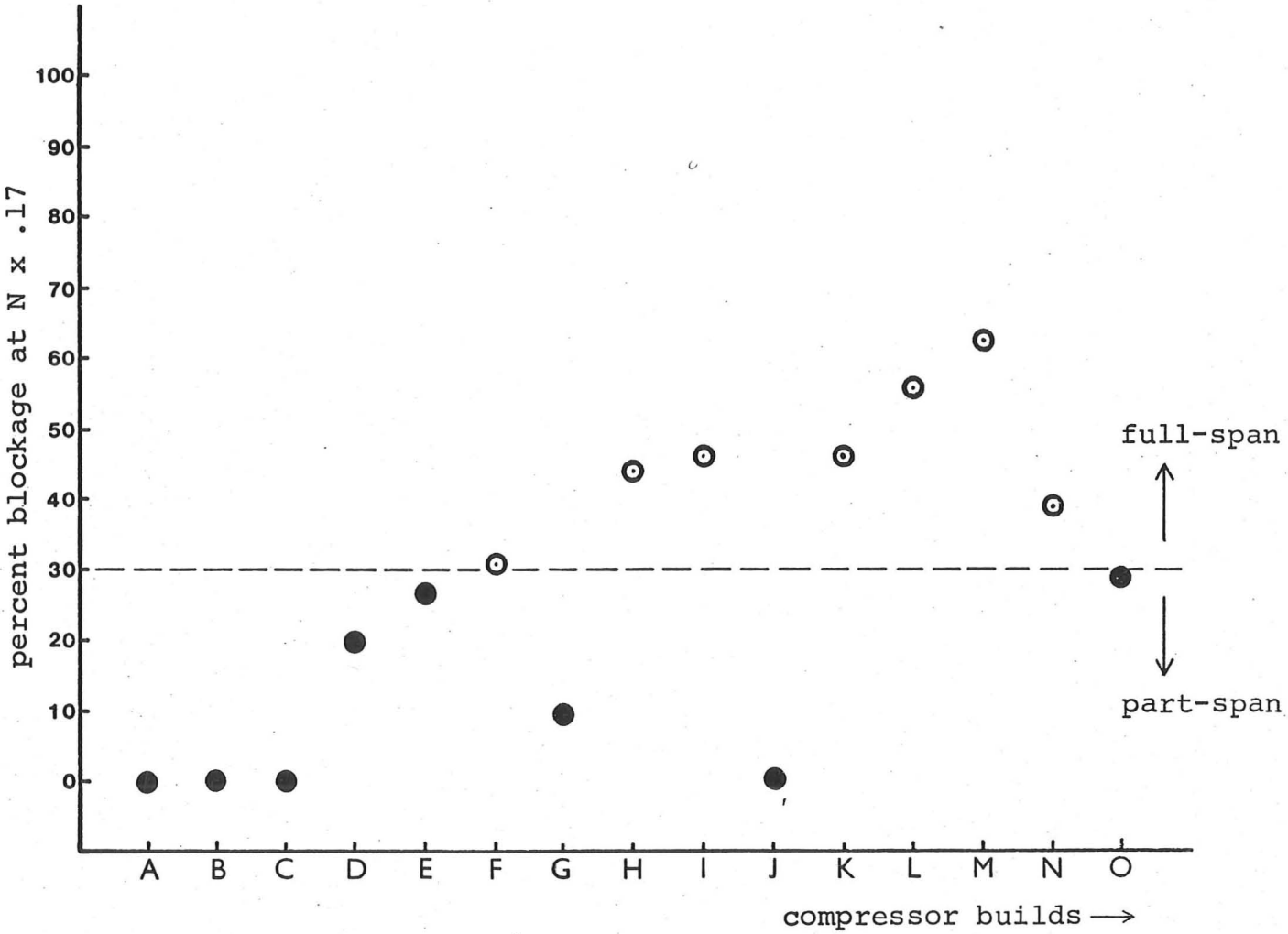

⊙—full-span stall observed at stall onset

●—part-span stall observed at stall onset

Correlation for onset of part-span or full-span stall.

Figure 54

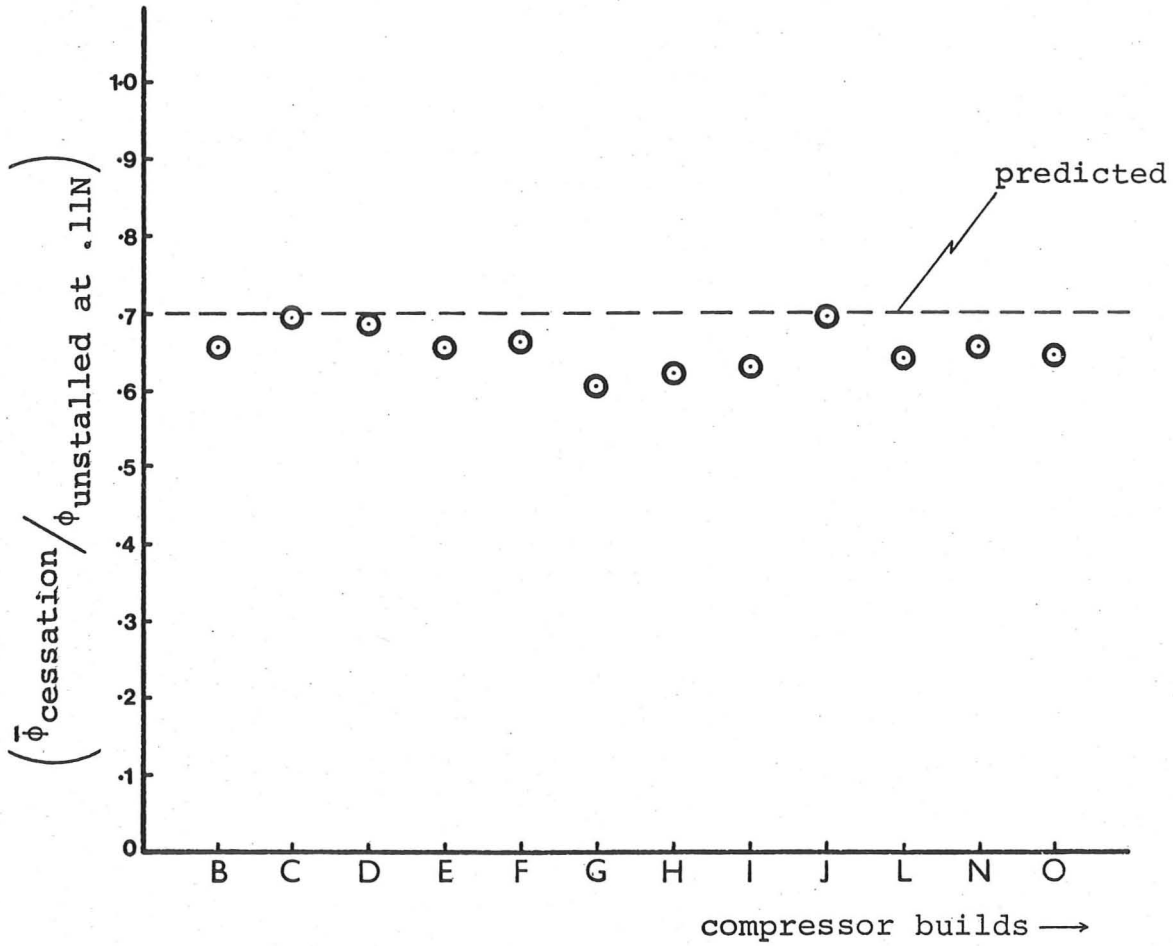

Correlation for $\bar{\phi}$ at full-span-stall cessation.

FIGURE 55

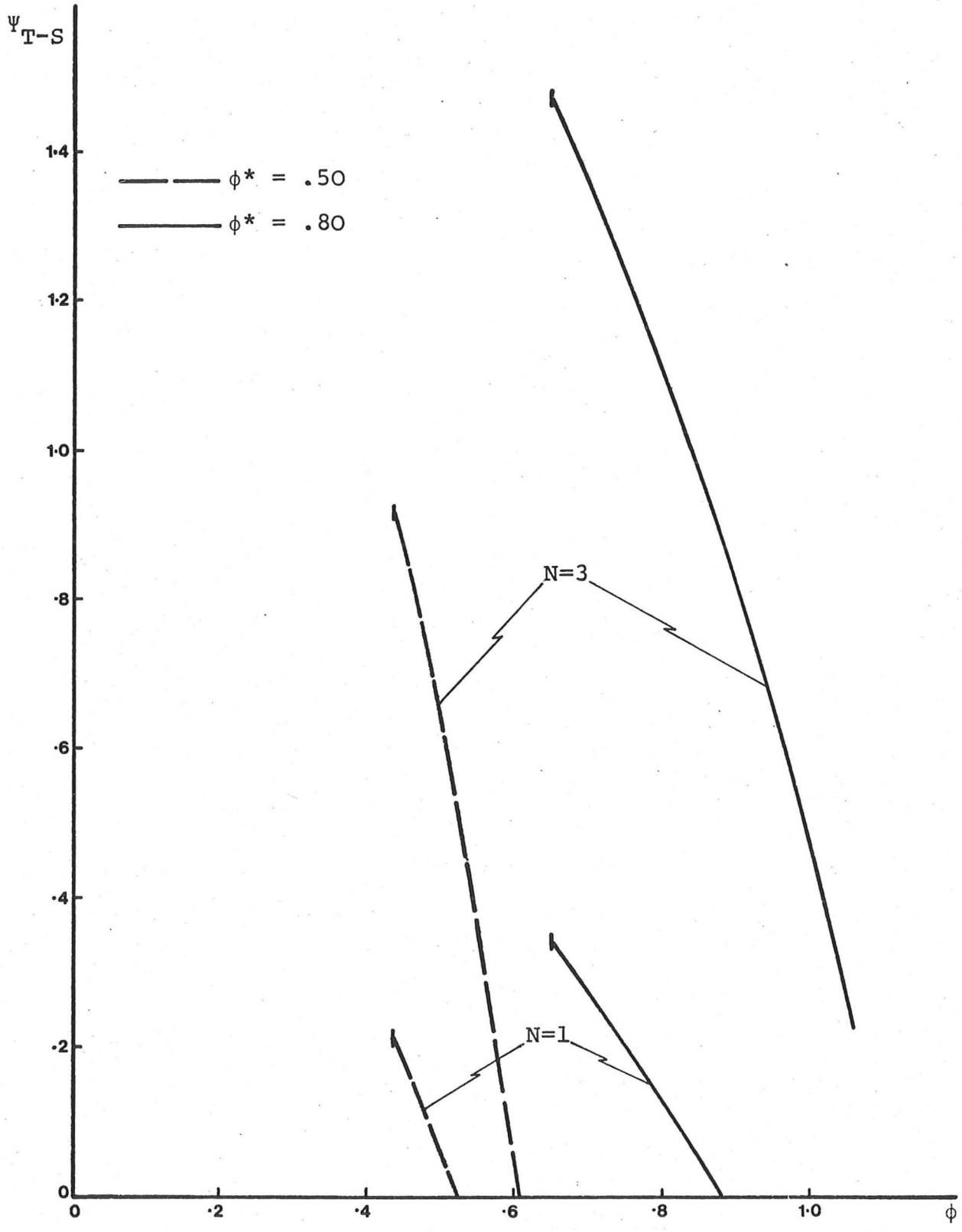

Effect of N (number of stages) and ϕ^* (design $C_x/\bar{U}$) on unstalled part of compressor performance characteristic.

FIGURE 56

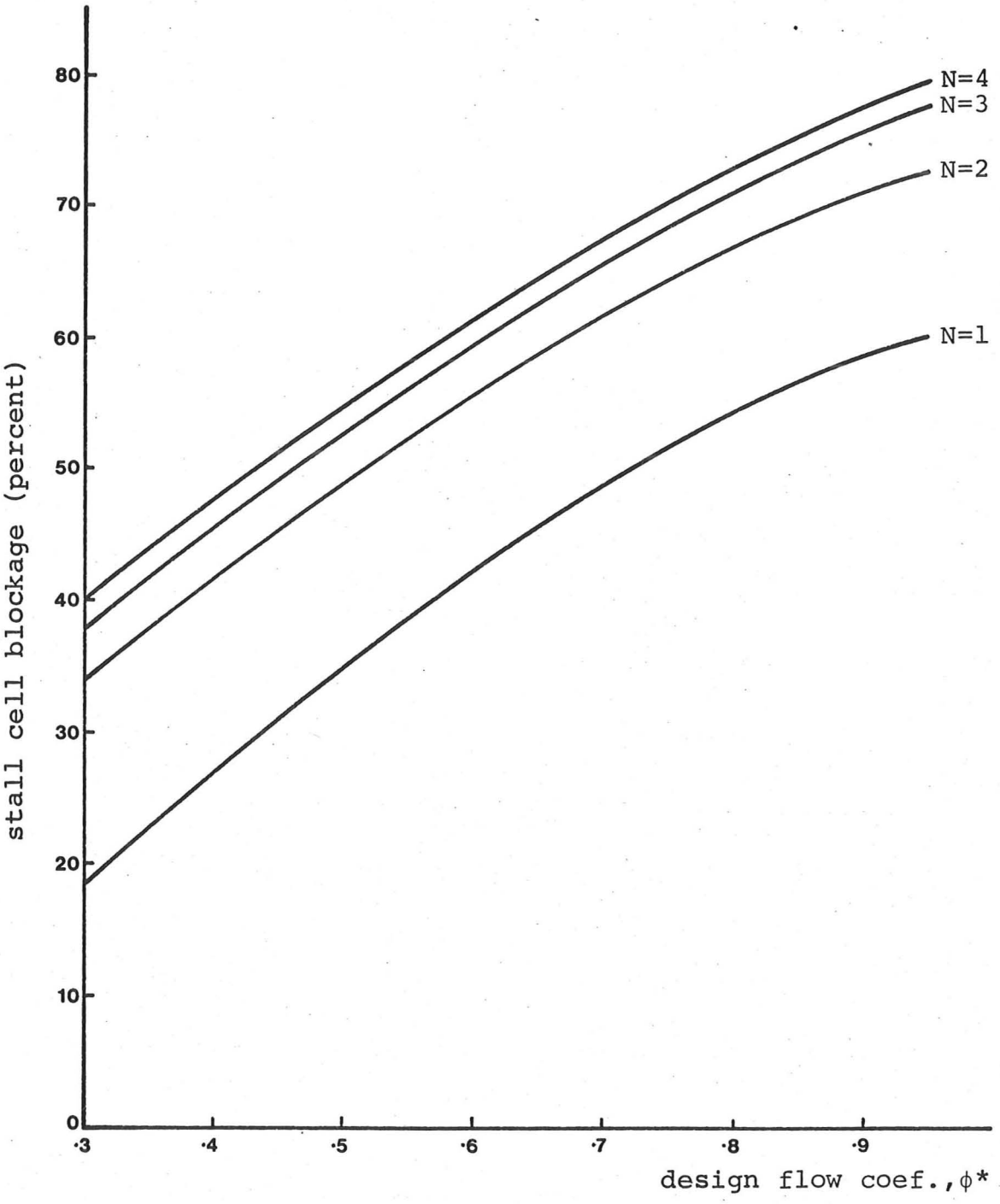

Blockage at stall inception calculated from simple analysis.

FIGURE 57

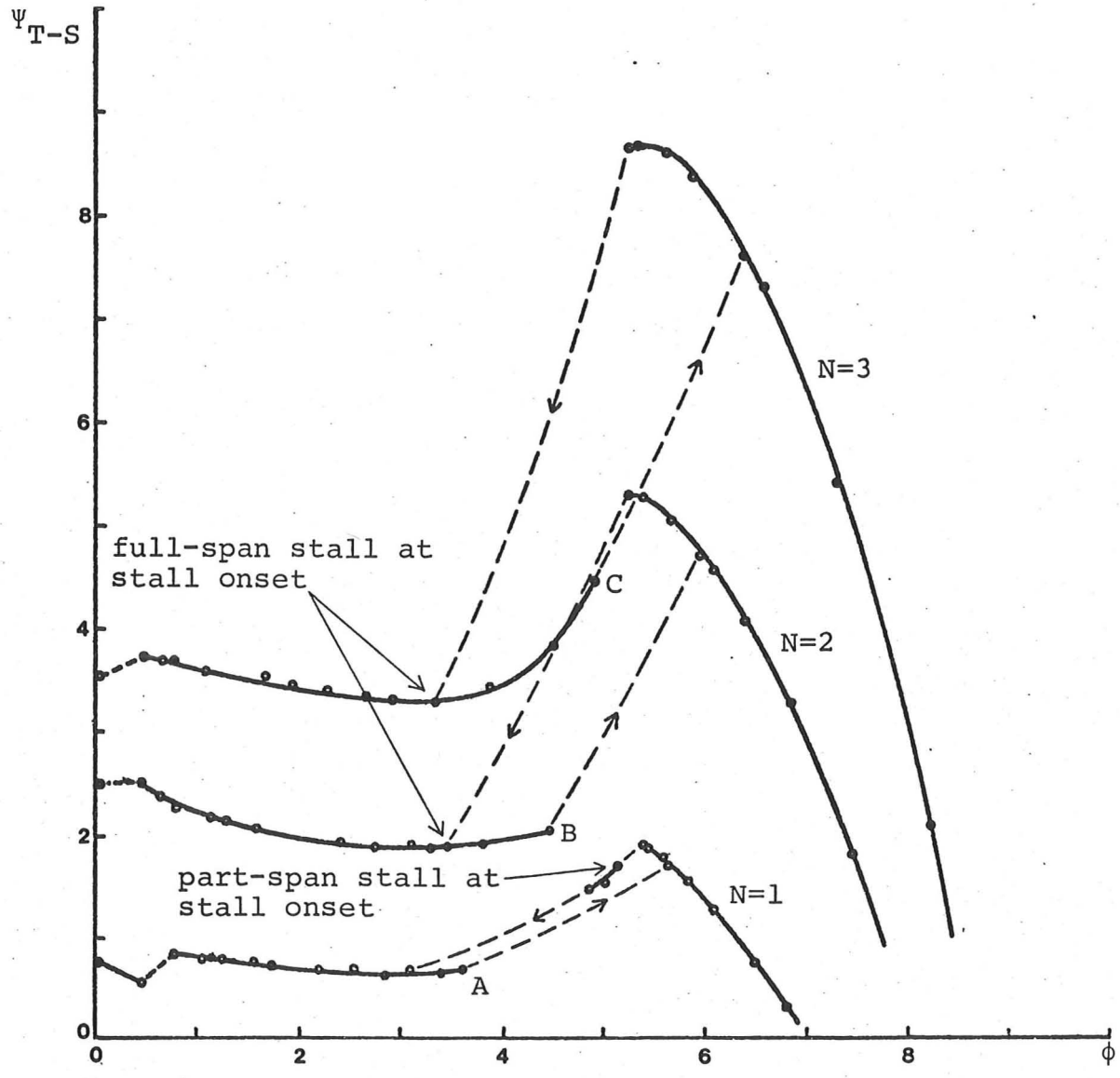

Influence of number of stages on stalled performance.

FIGURE 58

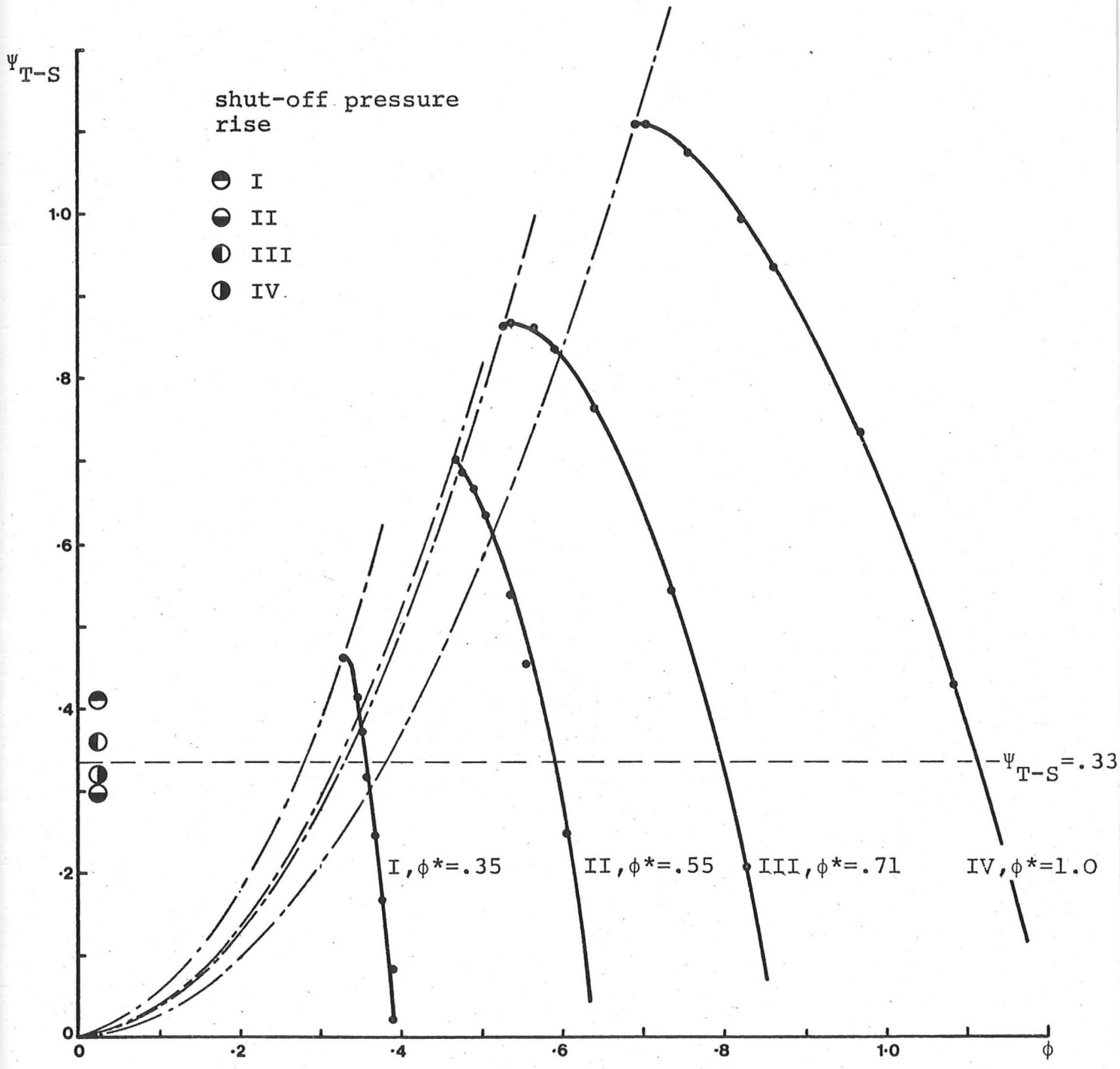

Effect of design flow rate on blockage.

FIGURE 59

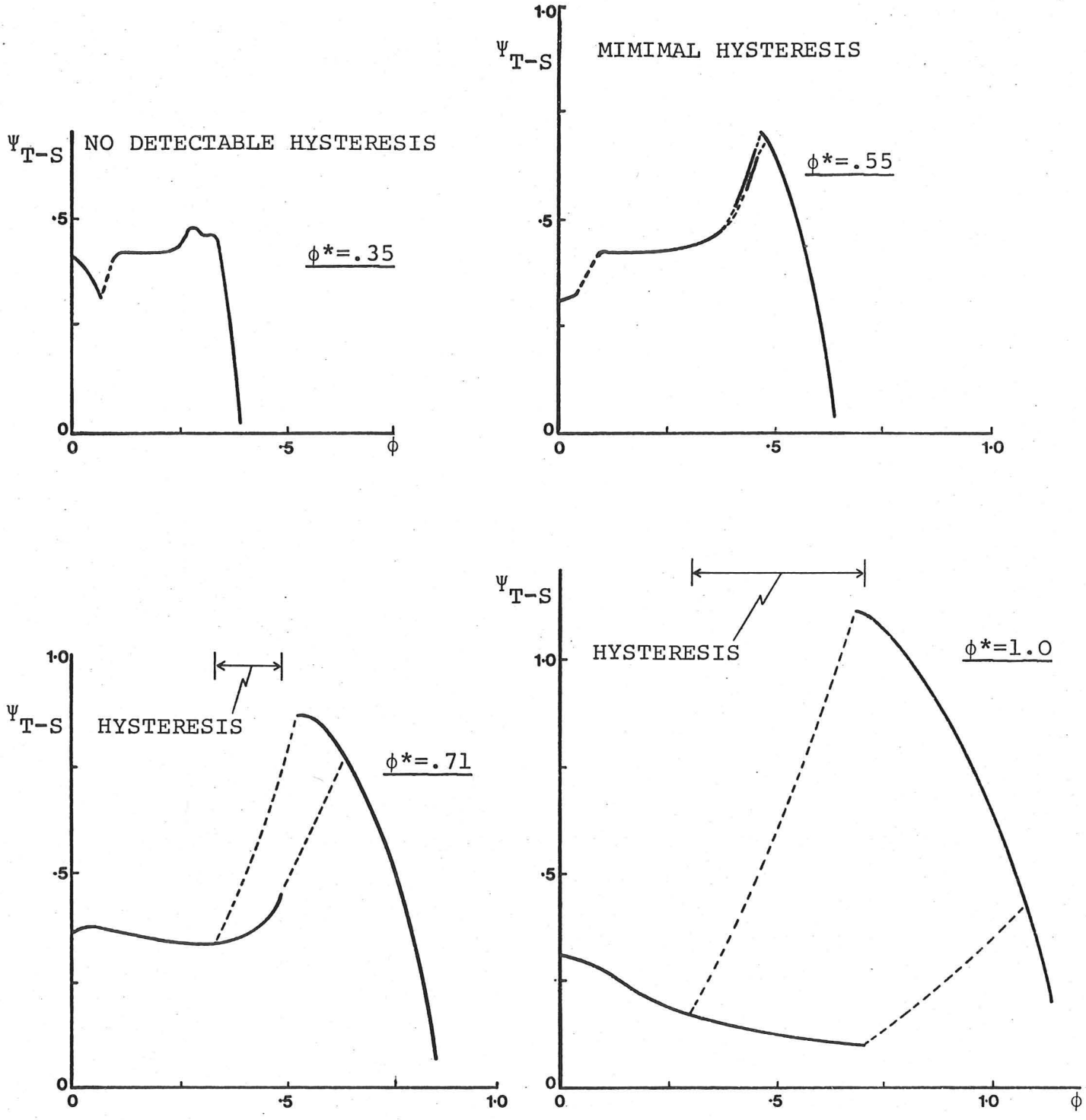

Influence of design flow rate on stall/unstall hysteresis; three stage compressor builds.

FIGURE 60

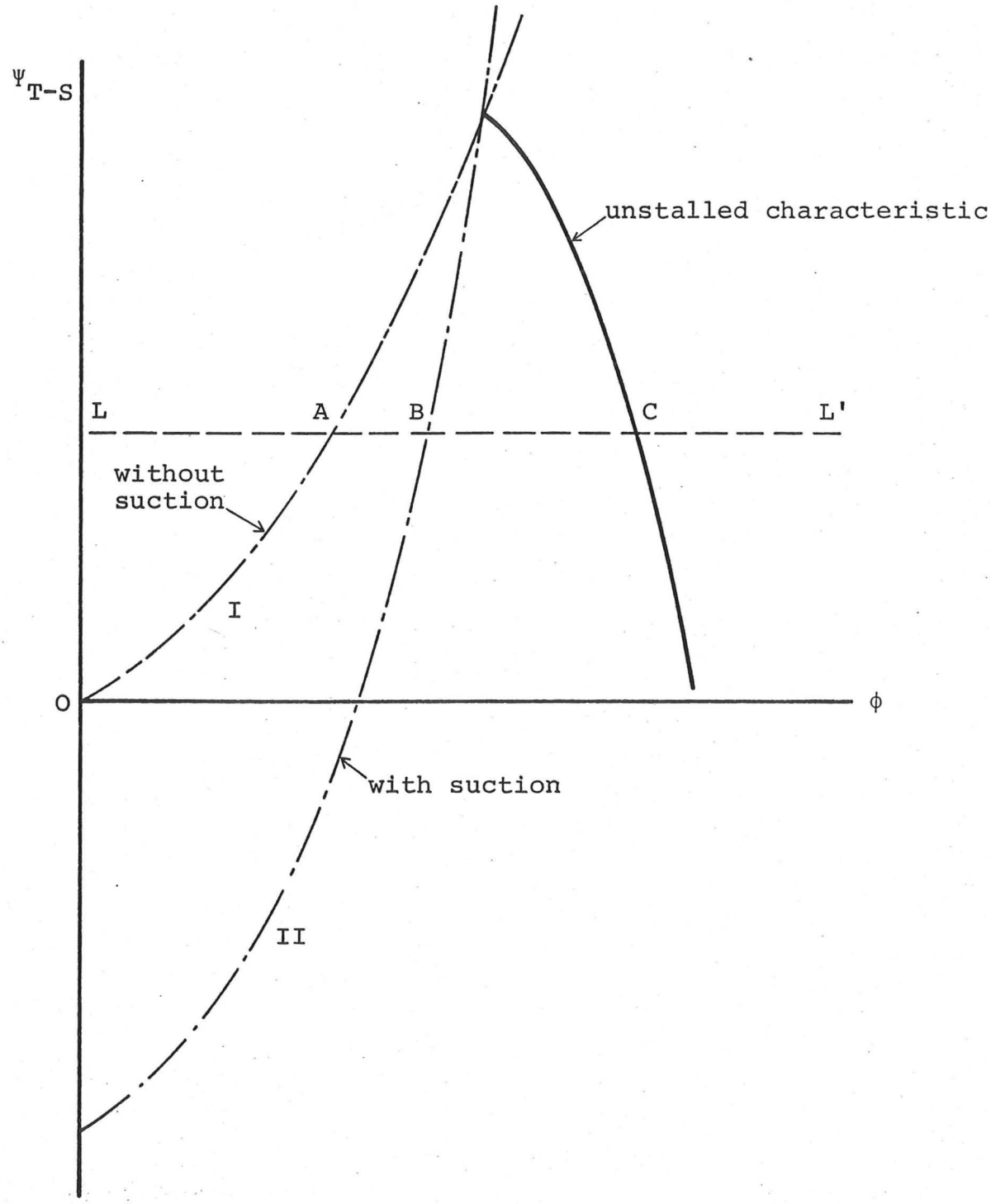

Effect of throttle line slope on stalled performance.

FIGURE 61

CHARACTERISTIC WITHOUT EXHAUST SUCTION
(normal throttle line)

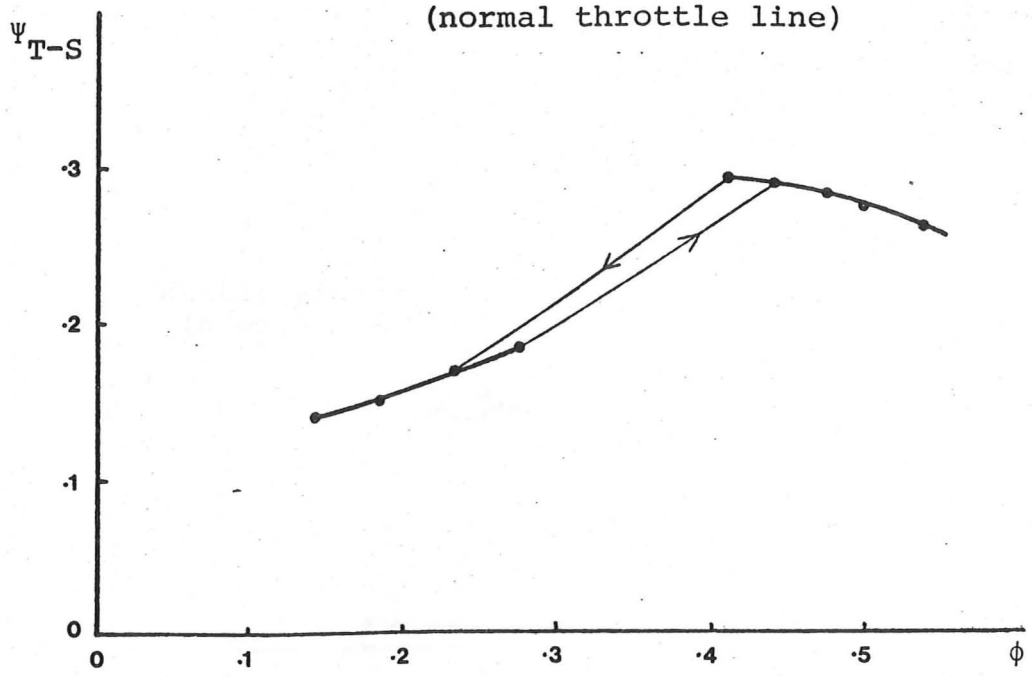

CHARACTERISTIC WITH EXHAUST SUCTION
(steeper throttle line)

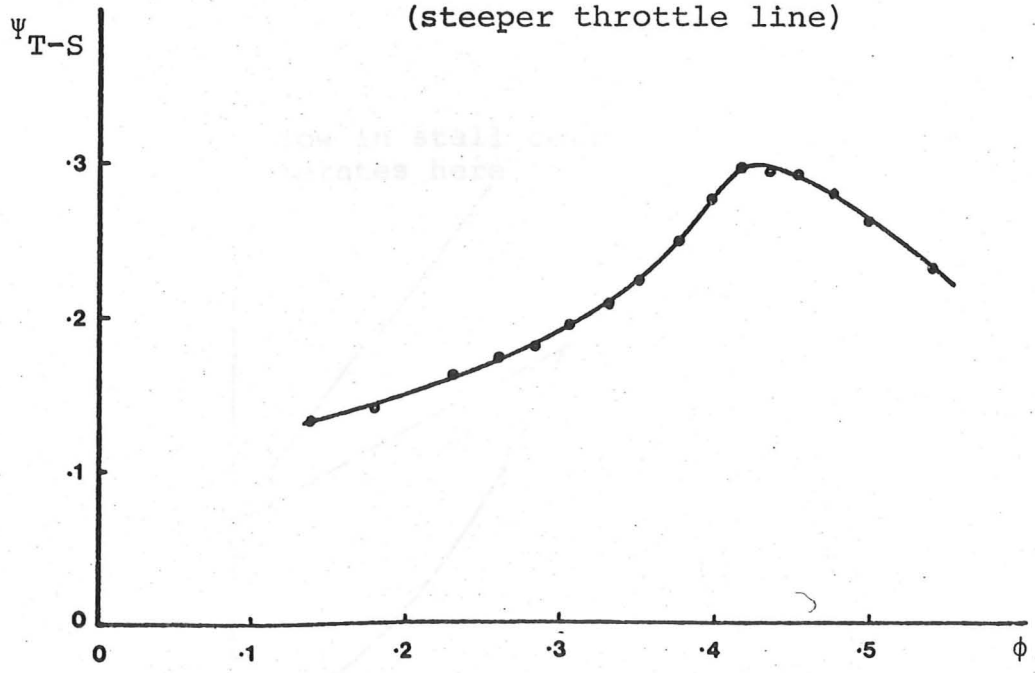

Effect of throttle line slope on stalled performance.
(after Borisov)

FIGURE 62

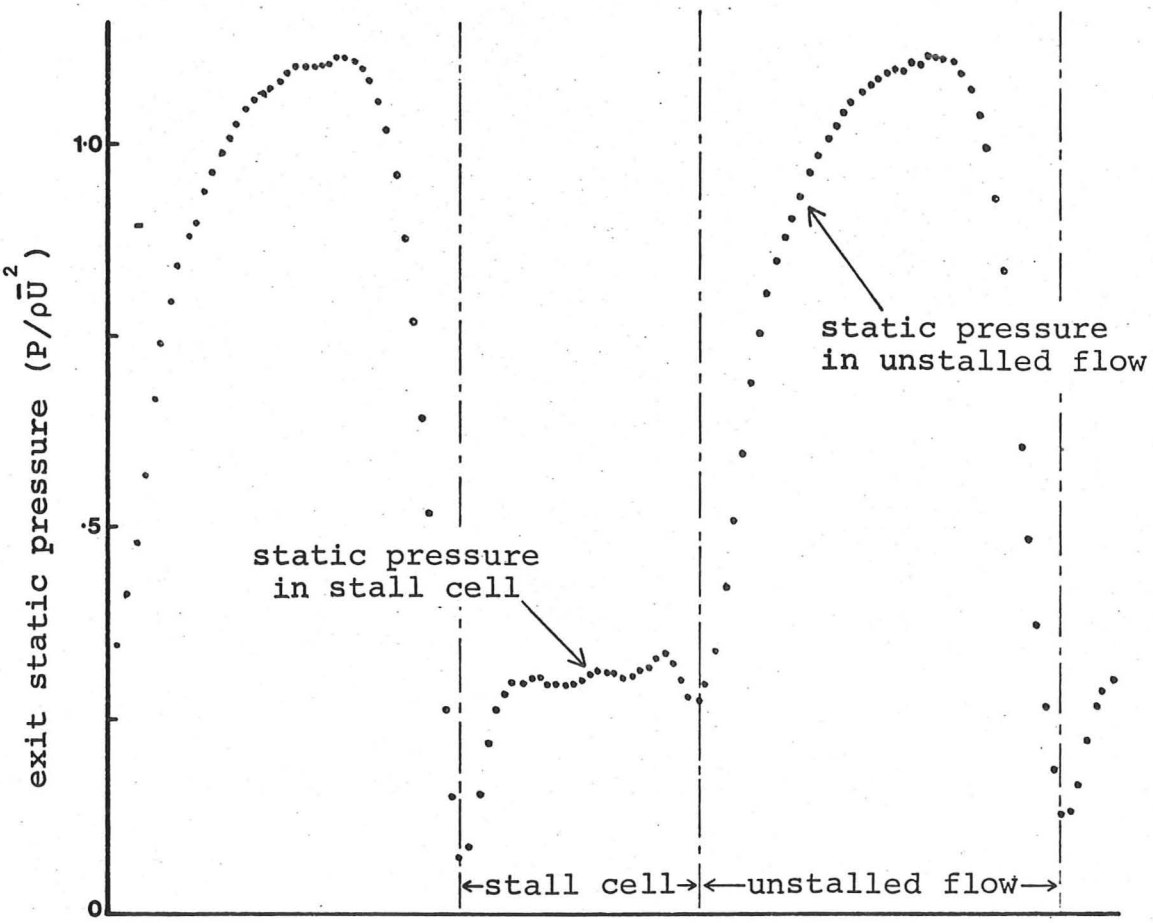

Non-uniform exit static pressure ahead of gauze.

FIGURE 63a

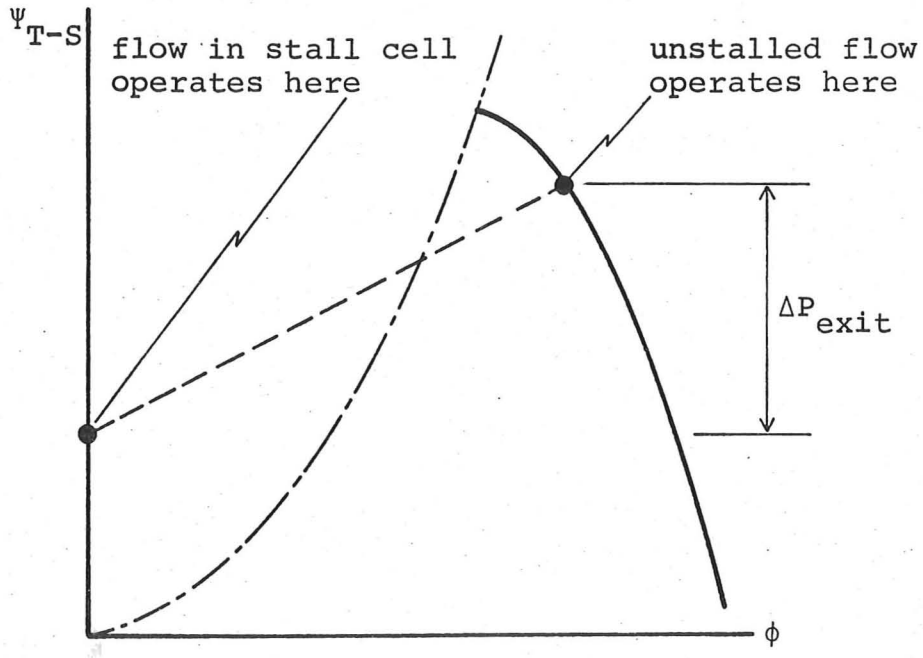

Compressor operation with non-uniform exit static pressure.

FIGURE 63b

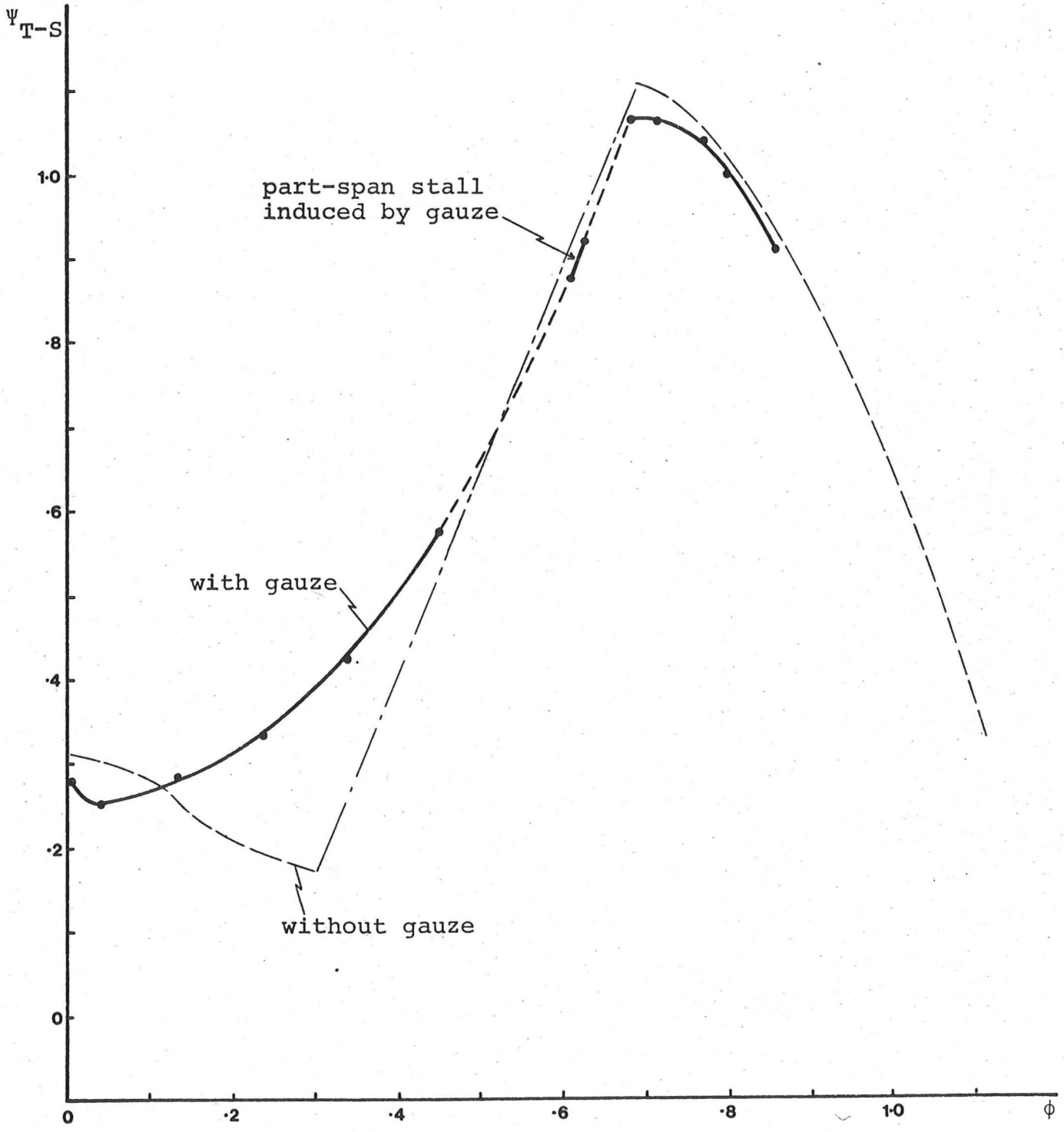

Effect of exit gause on stalled performance.
(non-uniform exit static pressure)

FIGURE 64